UNIVERSITY OF OKLAHOMA

GRADUATE COLLEGE

SYNTHESES, MOLECULAR STRUCTURES, AND FIBER-OPTIC INFRARED SPECTROELECTROCHEMISTRY OF NITROSYL METALLOPORPHYRINS CONTAINING AXIALLY BOUND ALKOXIDE, THIOLATE, IMIDAZOLE, AND IMIDAZOLATE LIGANDS.

A DISSERTATION

SUBMITTED TO THE GRADUATE FACULTY

in partial fulfillment of the requirements for the

degree of

Doctor of Philosophy

By
SHAWN M. CARTER
Norman, Oklahoma
2006

UMI Number: 3242290

ProQuest Information and Learning Company
300 North Zeeb Road
P.O. Box 1346
Ann Arbor, MI 48106-1346

SYNTHESES, MOLECULAR STRUCTURES, AND FIBER-OPTIC INFRARED SPECTROELECTROCHEMISTRY OF NITROSYL METALLOPORPHYRINS CONTAINING AXIALLY BOUND ALKOXIDE, THIOLATE, IMIDAZOLE, AND IMIDAZOLATE LIGANDS.

A DISSERTATION APPROVED FOR THE
DEPARTMENT OF CHEMISTRY AND BIOCHEMISTRY

BY

George B. Richter-Addo

Robert P. Houser

David P. Nagle, Jr.

Richard W. Taylor

Wai Tak Yip

Acknowledgements

The path that has led me to the completion of this dissertation been long and bumpy, and there have been several people who have helped me to meet my goals. First and foremost is my partner and fellow graduate student, Adam Hixson. Without his love and support (both emotionally and scientifically) none of this would have been possible. I am truly grateful for all that you have given me and am proud to share my future with you.

I am deeply indebted to my research advisor, Dr. George B. Richter-Addo for his guidance during my studies at OU. My time under your care will undoubtedly prove to be some of the most memorable and influential time of my life.

I would like to thank Drs. Richard Taylor, David Nagle, Robert Houser, Rudolf (Rudi) Wehmschulte, and Wai Tak (Ivan) Yip for serving as my advisory committee members. Your friendly help and guidance has been invaluable. I would like to extend special thanks to Drs. Masood Khan and Douglas Powell for their help with X-ray studies. I am also thankful to Dr. Susan Alguindigue not only for her help with NMR studies, but also for her friendship. I am also indebted to Dr. Michael Shaw (Southern Illinois University, Edwardsville) for his insightful help with my electrochemical studies and his friendship.

Perhaps the most influential person I have worked with in Dr. Richter-Addo's research group is Dr. Jonghyuk Lee. I've yet to meet a better scientist or a more caring soul. Thank you for your friendship and guidance. I would also like to thank my other coworkers, both present and past, in Dr. Richter-Addo's research group:

Dr. Li Chen, Dr. Lin Cheng, Keeshaloy Thompson, Naihui Guo, John Lilly, Dr. Daniel Copeland, Myron Jones, Nan Xu, Dr. Lillian Chooback, Carolina Salazar, Zaki Zahran, Yi (Eva) Jun, and Adam Warhausen. I have sincerely enjoyed being around these people and consider all of them friends.

I am appreciative for the financial support provided to me by the Department of Chemistry and Biochemistry at OU. Additionally, I am thankful to the National Institutes of Health (NIH) and National Science Foundation (NSF) for the funding that went towards the completion of this dissertation.

I am grateful for my little brother Eric Carter (who somehow, without me noticing stopped being little a long time ago). You know, I never say it but I have always felt lucky that I have you in my life.

Finally, I would like to dedicate this dissertation (and the years of work that are represented on its pages) to my Mother and Father, Jennifer and Walter Mees. There aren't any words that I could put on this paper that would even begin to describe the love I have for them. Thank you so much. All the highs and all the lows that you have shared with me over the years make this as much your work as mine.

Table of Contents

List of Tables

Appendix

List of Figures

List of Schemes

List of Graphs

Abstract

This dissertation describes the syntheses, molecular structures, and infrared spectroelectrochemistry of nitrosyl ruthenium and osmium porphyrins containing axially bound alkoxide, thiolate, imidazole, and imidazolate ligands.

Chapter 1 introduces the fundamental issues involved in the chemistry of *Group 8* Fe, Ru, and Os nitrosyl porphyrin complexes with *trans* and *O*- and *S*-bound ligands, imidazole, and pyridine and their derivatives. Additionally, this chapter introduces important aspects of the biochemistry of the relevant nitrosyl adducts of heme proteins.

Chapter 2 describes the syntheses of (OEP)Ru(NO)(XR) (XR = OEt, SEt, S-*i*-C_5H_{11}, SPh) complexes and the redox behavior of the osmium and ruthenium compounds (OEP)M(NO)(OEt) and (OEP)M(NO)(SEt) (M = Os, Ru), as determined by cyclic voltammetry and infrared spectroelectrochemistry. The (OEP)Ru(NO)(XR) complexes were prepared in 61 – 85% yields through the formal *trans* addition of RSNO to (OEP)Ru(CO) with loss of CO. These nitrosyl alkoxide and thiolate complexes were characterized by IR and ^{1}H NMR spectroscopy, and by ESI mass spectrometry. Infrared spectroelectrochemical studies revealed that the (OEP)Os(NO)(OEt) compound undergoes a single reversible oxidation process in dichloromethane. In contrast, the thiolate compound (OEP)Os(NO)(SEt) undergoes a net irreversible oxidation resulting in formal loss of the SEt ligand. Extended Hückel calculations on crystal structures of these two compounds provide insight into the nature of their HOMOs. In the case of the alkoxide compound, the HOMO is largely

metalloporphyrin centered. However, the HOMO of the thiolate compound consists of a π bonding interaction between the metal d_{xz} orbital and the p_x orbital on the sulfur, and a π antibonding interaction between the metal d orbital and a π* orbital on NO. The redox behavior of the Ru analogues have been determined, and are compared with those of the Os compounds.

Chapter 3 describes the syntheses of the neutral and cationic (por)Ru(NO)(RIm) (por = TPP, TTP, T(*p*-OMe)PP), OEP; RIm = imidazolate (Im), imidazole (HIm), 1-methylimidazole (1-MeIm), 4-methylimidazole (4-MeHIm), 5-methylimidazolate (5-MeIm), and 5-methylimidazole (5-MeHIm)) compounds. The neutral imidazolate (por)Ru(NO)(RIm) (R = nothing, 4-Me) complexes were prepared from the addition of the corresponding RHIm to (por)Ru(NO)(O-*i*-C_5H_{11}). The cationic imidazole $[(por)Ru(NO)(RIm)]^+$ complexes were prepared from the solvent-free addition of RHIm (R = nothing, 1-Me, 4-Me) to the precursor $[(por)Ru(NO)]^+$ complex. Both the neutral imidazolate and cationic imidazole complexes were characterized by IR and ^{1}H NMR spectroscopy, and by FAB or ESI mass spectrometry. The IR spectra (in CH_2Cl_2) of the neutral imidazolate complexes displayed ν_{NO} bands in the 1845 – 1855 cm^{-1} range, while the cationic imidazole complexes displayed similar bands in the 1854 – 1877 cm^{-1} range. Bands in these ranges are suggestive of linear NO ligands in these types of complexes. The ^{1}H NMR spectra of the product that resulted from addition of 4-methylimidazole to $[(OEP)Ru(NO)]^+$ resulted in two sets of peaks that were assigned to the structurally isomeric $[(OEP)Ru(NO)(4\text{-}MeHIm)]^+$ and $[(OEP)Ru(NO)(5\text{-}MeHIm)]^+$ complexes. Further, we were able to determine that the less sterically stable 4-MeHIm containing isomer undergoes a first order dissociation

of the 4-MeHIm ligand from the Ru center with the rate constant (k) of 1.44 x 10^{-5} s^{-1} with a half-life ($t_{1/2}$) of 4.81 x 10^4 s. This was followed by the rebinding of the ligand to the metal center to form the $[(OEP)Ru(NO)(5\text{-}MeHIm)]^+$ isomer. The solid-state crystal structures of the imidazolate and imidazole adducts of the (OEP)Ru(NO) complexes were determined by single-crystal X-ray crystallography.

Chapter 4 describes the electrochemistry and infrared spectroelectrochemistry of (OEP)Ru(NO)(Im) and $[(OEP)Ru(NO)(RIm)]^+$ (R = H, 1-Me). Electrochemical oxidation of the (OEP)Ru(NO)(Im) complex in CH_2Cl_2 displayed a partially reversible single electron transfer centered on the porphyrin followed by an apparent radical hydrogen extraction from the solvent by the nitrogen atom of the imidazolate ring to form the cationic $[(OEP)Ru(NO)(HIm)]^+$ derivative. The $[(OEP)Ru(NO)(HIm)]^+$ and $[(OEP)Ru(NO)(1\text{-}MeIm)]^+$ complexes, on the other-hand, exhibit porphyrin based reversible single electron transfers upon oxidation. However, the reduction of the $[(OEP)Ru(NO)(HIm)]^+$ complex proceeds through a partially reversible single electron transfer followed by an apparent $H^{\bullet}$ extraction from the nitrogen atom of the imidazole by the solvent system to form the neutral (OEP)Ru(NO)(Im) derivative. The reduction of the 1-MeIm complexes proceeds through a partially reversible single electron transfer that was followed by the loss of the bond between 1-MeIm ligand the ruthenium center of the porphyrin. Extended Hückel calculations on crystal structures of the (OEP)Ru(NO)(Im) and $[(OEP)Ru(NO)(HIm)]^+$ complexes provides insight on their redox properties. The calculated HOMOs for the isoelectronic structures show charge centered on the porphyrin, providing supporting evidence for the generation of porphyrin-centered π-

radical cations upon oxidation. The calculated LUMO of the cationic complex, however, suggests that the reduction first occurs on the metal-nitrosyl fragment of the $[(OEP)Ru(NO)(HIm)]^{+}$ complex, increasing the antibonding interaction between the metal d_{xz} and π^{*} orbital on NO. Presumably, the resulting unfavorable bent $Ru\text{-}NO^{-}$ like geometry is relieved by an electronic rearrangement that leads to the extraction of $H^{\bullet}$ from the nitrogen of the imidazole by the solvent system.

Chapter 1. Introduction

The chemistry of synthetic nitrosyl metalloporphyrins has generated intense interest over the past few decades due largely to the identification of the biological signaling molecule, Endothelial Derived Relaxing Factor (EDRF), as nitric oxide (NO). This accompanied the subsequent realization of the wealth of physiological and pathological phenomenon that occur as a result of the interaction of NO with various heme containing biomolecules such as cytochromes, peroxidases and heme-thiolate proteins like cytochrome P450 and Nitric Oxide Synthase (NOS).[1] Modeling the interaction that NO has with reactive heme centers has been accomplished primarily using synthetic metalloporphyrins to mimic the porphyrins found naturally in heme proteins and reacting them with NO gas or NO donor molecules. Indeed, modeling of the biological nitrosyl heme systems using NO or the related organic nitroso compounds (X-N=O) and synthetic metalloporphyrins has been a major focus of our research group since 1994. More recently, in 1999, we expanded our research to include studies of the chemistry of NO reactions with biologically derived heme proteins.

Synthetic metalloporphyrins containing Cr, Mo, Mn, Fe, Ru, Os, and Rh metals have been used to mimic the prosthetic iron porphyrin centers of heme containing biomolecules containing NO linkages. Further, the chemistry of ligands located *trans* to the metal nitrosyl fragment has been explored for N-donor (-NR), O-donor (-OR), S-donor (-SR), C-donor (-CR), and halide (-X) groups. In addition to synthetic, reactivity, and structural studies of nitrosyl metalloporphyrin complexes,

the electrochemistry and spectroelectrochemistry of these complexes have been examined. A review of the nitrosyl metalloporphyrin and nitrosyl heme chemistry up to 1999 can be found in *The Porphyrin Handbook*.[2]

NO is not an innocent ligand in either metalloporphyrin complexes or other metal nitrosyl complexes. When bound to metal centers NO can be redox active. Indeed, this redox activity makes assignments of formal oxidation states difficult. Hence, Enemark and Feltham formulated a notation system based on the electronic structures of metal nitrosyl complexes that better describes the trends of these complexes.[3,4] Accordingly, mononitrosyl complexes are assigned the notation $\{MNO\}^x$, where M is the metal and x is the number of electrons assigned to the fragment. The MNO triatomic group in these complexes is considered as a single unit and the NO is viewed as a neutral donor. Thus, the number of electrons are derived from the metal's group and the electron from the π^*-orbital of the NO. Five- and six-coordinate Fe porphyrin complexes display x = 6 or 7 and osmium and ruthenium porphyrin (six-coordinate)[5] complexes have only been observed for x = 6. Structural investigations of $\{MNO\}^6$ species show that they exhibit near linear to linear geometry (167° - 180°) while $\{MNO\}^7$ complexes display moderately bent M-NO geometries (137° - 149°). It should be noted that there has been an increasing deviation from the dogma associated with this notation. Group 8 complexes of Fe and Ru containing σ-bound alkyl and aryl groups of $\{MNO\}^6$ complexes have been shown to deviate from the expected MNO geometries. These complexes, presumably due to electronic contributions from the (trans) ligands, lead to structures with considerably bent M-NO groups. For reasons that are unclear, nitrosyl complexes of

iron are the only $\{MNO\}^7$ complexes of all the reported metal porphyrins. More recently, a report by our group demonstrated bending of an iron nitrosyl group in a $\{MNO\}^6$ porphyrin complex with a thiolate ligand bound *trans* to the NO group.[6] The Enemark and Feltham notation will be used throughout this dissertation, sometimes in conjunction with the "formal" oxidation state.

My research has dealt primarily with the synthetic, molecular, and electrochemical studies of the heme model complexes of ruthenium and osmium nitrosyl porphyrins containing organic *O*-, *S*-, and *imidazole* based donor ligands. As mentioned, Drs. Cheng and Richter-Addo have written a comprehensive review of the binding nitric oxide to metalloporphyrins and heme that includes references to the literature up to 1999.[2] My intent in this chapter is to provide a brief review of the literature up to September 2006 that is most relevant to my research. Hence, the following sections will focus on NO adducts of Fe, Ru, and Os metalloporphyrins that contain organic *O*, *S*, *imidazole*- and *pyridine*-based donors *trans* to the nitrosyl group. Further, the reactions of heme systems containing tyrosine, cysteine, and histidine bound iron centers by NO will be included in this review. Additionally, Table 1.1 at the end of this report is an update to a similar table previously published[2] by our group and contains a list of the nitrosyl metalloporphyrins and the spectroscopy that have been collected on these systems from 1999 to 2006. Tables 1.2 and 1.3, also at the end of this chapter, list selected geometric parameters that have been obtained from single crystal X-ray studies of Fe, Ru, and Os metalloporphyrins discussed in this chapter and the related heme systems, respectively.

I. Nitrosyl Heme and Heme Models with organic O- and S-Donors

A. Heme Models

The inherent difficulties that accompany the *in vitro* studies of proteins containing nitrosyl heme groups has led to the wide acceptance of synthetic nitrosyl-metalloporphyrins as likely structural and in some cases electronic models of the biological nitrosyl proteins. For example, nitrosyl-metalloporphyrins containing organic *S*-donor groups have been prepared as potential models of heme-thiolate proteins that are known to interact with NO like NOS and cP450.[2] Similarly, complexes containing organic *O*-donor groups have been prepared as potential models of nitrosyl-heme proteins containing the iron *O*-bound amino acid tyrosine (Tyr) like catalase (cat).[2]

Research on nitrosyl-metalloporphyrins containing organic *O*- and *S*-donor ligands has revealed striking comparisons in the synthetic, structural and reaction chemistry as well as the electrochemistry of these complexes. Additionally, with respect to nitrosyl complexes with organic *O*- and *S*-donor ligands, the collected literature shows that the chemistry and electrochemistry of ruthenium porphyrins is closely mirrored by osmium porphyrins. Hence, the following section will review the current literature pertaining to the nitrosyl-metalloporphyrins with organic *O*- and *S*-donors for the iron containing complexes followed by a section discussing the reported research related to the chemistry and electrochemistry of both the ruthenium and the osmium containing complexes.

1. Iron-nitrosyl porphyrins

{MNO}^{7}. There have been few reports of the preparation of six-coordinate iron nitrosyl porphyrin complexes with organic *O*- and *S*-donor ligands.[7,8] Yoshimura demonstrated that organic *O*- and *S*-donor groups could be added to the five-coordinate *ferrous* (PPDME) Fe(NO) at low temperatures (~77 K) to form Fe-alcohol, Fe-ether, Fe-thiol, and Fe-thioether adducts. EPR spectroscopic studies of these complexes indicated that the *O*-bound and the *S*-bound ligands were weakly coordinated, the *O*-donors more so than the *S*-donors, to the *ferrous* metal center of the complexes at low temperatures and upon warming to room temperature the complexes converted to their five-coordinate (PPDME)Fe(NO) forms.[7]. Additionally, Yoshimura suggested, based on the EPR data, that the thioether sulfur showed a stronger interaction with the iron center of the porphyrin than the thiol.

{MNO}^{6}. Recently, a series of formally *ferric* heme model complexes with mutually *trans* NO and thiolate ligands have been prepared through the addition of NO gas to a solution containing the five-coordinate (Por)Fe(III)(SR). [9,10] Nan Xu, in our laboratory, prepared X-ray quality crystals of the ferric (Por)Fe(NO)(SR) from the addition of NO gas to crystals of the five-coordinate thiolate precursor (Eq. 1.1).[6]

$$(por)Fe^{III}(SR) + NO \rightarrow (por)Fe(NO)(SR) \qquad (1.1)$$

As seen in figure 1.1, each of these complexes have unusual stabilization of the iron(III) bound thiolate ligands. In the case of the complex prepared by Suzuki et al., the thiolate located *trans* to NO is donated from one of porphyrins *meso* aryl ligands

(Fig. 1.1a) and the nitrosyl adduct of the Fe-SR complex prepared by our group shows hydrogen bonding interaction between amide hydrogen and the bound sulfur atom of the SR ligand (Fig. 1.1b).[9] The IR nitrosyl stretching frequencies for these complexes in chlorinated solvents ranged between 1826 and 1891 cm^{-1}.

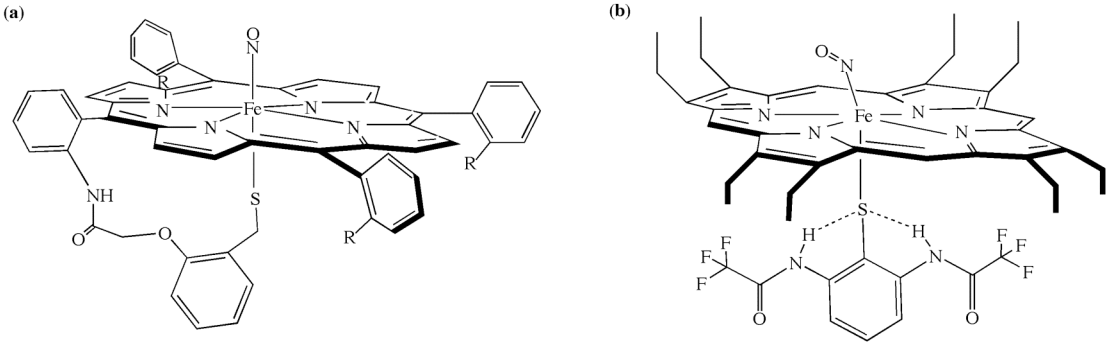

Figure 1.1: (a) (T(atpa)pivPP)Fe(NO) (R = $NHCOC(CH_3)_3$) and **(b)** (OEP)Fe(NO){S-2,6-$(CF_3CONH)_2C_6H_3$}. Adapted from references 9 and 6, respectively.

Of the nitrosyl heme thiolate model complexes, the one prepared by Nan Xu is the only structurally characterized complex reported to the literature to date (Table 1.2). The most interesting feature of the structure is the bent Fe^{III}-NO bond at 159.6(8)º. Deviation from the linear M-NO bond angle usually associated with $\{MNO\}^6$ complexes has previously only been observed in model complexes containing mutually *trans* NO and alkyl and aryl groups.[11] Similarly bent ferric-nitrosyl groups have been observed in related cP450 like heme enzymes (vide infra). This data suggests that a bent M-NO bond may be common for ferric nitrosyl thiolate heme and heme model complexes.

The isolation of the cationic *ferric* alcohol complex [(TPP)Fe(NO)(HO-*i*-C_5H_{11})]$^+$ was reported by our group and was prepared through the addition of isoamyl nitrite to [(TPP)$Fe^{III}(THF)_2$]$^+$ (Eq. 1.2).[12]

$$[(TPP)Fe(THF)_2]^+ + i\text{-}C_5H_{11}ONO \rightarrow [(TPP)Fe(NO)(HO\text{-}i\text{-}C_5H_{11})]^+ \qquad (1.2)$$

Formation of the alcohol complex was likely aided by the presence of advantageous protons in the mixture. Unlike the *ferrous* alcohol complexes discussed above, the *ferric* complex showed moderate room temperature stability in both condensed phases (solution and more so in solid state) and maintained its structural integrity over several weeks at -20 °C in solution. The molecular structure of the [(TPP)Fe(NO)(HO-*i*-C_5H_{11})]ClO_4 was obtained and the F-N-O linkage displayed the predicted linear bond angle (177.1(7)°).

The addition of the analogous RSNO to either the neutral *ferric* (TPP)$Fe(THF)_2$ or cationic analogue of the complex, however, reportedly did not produce either the thiolate or thiol complexes. In the former case, isolation of the five-coordinate nitrosyl porphyrin was verified spectroscopically, while the latter case resulted in no isolable product.

2. Ruthenium- and osmium-nitrosyl porphyrins

The lack of easily prepared synthetic nitroso iron porphyrin containing organic *O*- or *S*-donor containing complexes inspired us to study the related nitrosyl metalloporphyin complexes using the Group 8 metals ruthenium and osmium. Ruthenium and osmium porphyrins were particularly attractive as potential heme

structural model alternatives to the related synthetic iron porphyrins in the formation of six-coordinate metal-nitrosyl complexes due to their inclination to form low-spin, diamagnetic compounds that generally exhibit moderate to high stability under inert atmosphere at room temperature. Furthermore, recent discoveries that indicate S-nitroso compounds (RSNO) may play important roles in biological actions of nitric oxide have spurred interests in this area of research.[13,14] Indeed, Jonghyuk Lee's (of our group) PhD dissertation was based in part on his studies of S-nitroso compounds and their interactions with heme models.[15] A review by Lee, Chen, West, and Richter-Addo of the interaction of organic nitroso with metals including Ru and Os porphyrin complexes has been published.[16]

a. Syntheses. Preparation of ruthenium- and osmium-nitrosyl porphyrins containing a M-XR (where X = O or S) linkages have been demonstrated to generally occur through the *trans* addition of alkyl nitrites (RONO) or alkyl thionitrites (RSNO) to a metalloporphyrin carbonyl starting material (Eq. 1.3).[12,17-24]

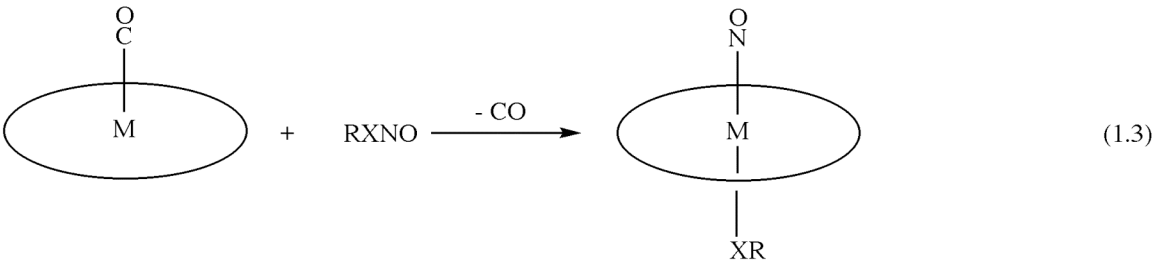

(1.3)

M = Ru or Osmium porphyrin

X = O or S

Antipas, et al. have also demonstrated in their preparation of the methoxide nitrosyl-ruthenium porphyrin complex that the alkoxide complexes can also be prepared from bubbling of NO gas into an alcohol solution of the ruthenium-carbonyl porphyrin (Eq. 1.4).[25] Dr. Jonghyuk Lee and Geun-Bae Yi, of our group, showed

$$(por)Ru(CO) + ROH + NO_g \rightarrow (por)Ru(NO)(OR) \quad (1.4)$$

that the thiolate containing complexes could also be prepared through the *trans* addition of $ONSCH_2CH_2SH$ to (por)M(CO) or from the displacement of the alkoxide ligand in a (por)Ru(NO)(OR) complex by a dithiolate ($HS(CH_2)_nSH$; n = 2 - 4) at room-temperature (Eq. 1.5 and 1.6, where M = Ru, Os and n = 2 - 4). The osmium complexes were reported to show greater stability under ambient conditions.[19]

$$(por)M(CO) + ONSCH_2CH_2SH \rightarrow (por)M(NO)(SCH_2CH_2SH) \quad (1.5)$$

$$(por)M(NO)(OR) + HS(CH_2)_nSH \rightarrow (por)M(NO)(S(CH_2)_nSH) + HOR \quad (1.6)$$

During infrared studies of the *trans* additions of alkyl nitrites and alkyl thionitrites to carbonyl porphyrins (Eq. 1.3, above) the putative alkoxide and thiolate containing the respective ruthenium- and osmium-carbonyl intermediate complexes were detected.[12,20] Further kinetic investigations of the *trans* addition of RSNO to ruthenium-carbonyl porphyrin starting materials by our group in conjunction with Peter Ford's research group suggested a mechanism of formation for the (por)M(NO)(XR) complexes to involve the attack at the sixth coordination position of

the metalloporphyrin by the RXNO molecule through the S or O (X) atom.[26] The subsequent homolysis of the X-NO bond results in the formation of the intermediate complex (por)M(CO)(XR) and the free NO interacts with the metal center on the opposite face of the porphyrin, displacing CO to produce the (por)M(NO)(XR) complex (Scheme 1.1).

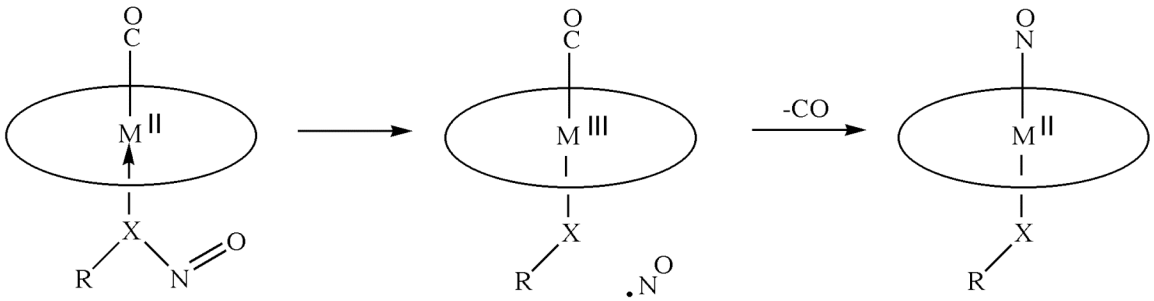

M = Ru,Os

X = O or S

Scheme 1.1: Proposed mechanism for the addition of alkyl nitrites and alkyl thionitrites to ruthenium and osmium porphyrin carbonyls (adapted from 12).

b. Spectroscopy. These complexes, as is the case with many metal-nitrosyl complexes, show intense bands in the infrared region that are attributed to a nitrosyl stretch. The infrared nitrosyl stretching frequency of the ruthenium alkoxide complexes ranges between 1780 and 1809 cm^{-1} (KBr) while those of the thiolate complexes range between 1773 and 1784 cm^{-1} (KBr). Similarly, the osmium alkoxide complexes have a ν_{NO} (KBr) ranging between 1743 and 1770 cm^{-1} and the ν_{NO} (KBr) for the thiolate complexes ranges between 1749 to 1760 cm^{-1}. These values are typical of metal-nitrosyl porphyrin complexes that have been described as containing a linear M-NO group.

To date, the structural and spectroscopic data reported for the NO adducts of alkoxide and thiolate complexes have all indicated binding of the NO ligand to the metal center through the nitrogen atom. However, our lab in conjunction with Philip Coppens research group have shown that a number of metal-NO linkage isomers are accessible to (por)Ru(NO)(XR) complexes (where X = O or S). Infrared spectroscopic data indicated that low-temperature irradiation of (OEP)Ru(NO)(O-*i*-C_5H_{11}) and (OEP)Ru(NO)(SCH_2CF_3) resulted in two nitrosyl linkage isomers. These isomers were demonstrated to contain an isonitrosyl or O-bound N(O)-Ru linkage isomer and a side-on η^2-cyclic linkage isomer of the metal-nitrosyl group (Fig. 1.2).[27] The isonitrosyl and side-on linkage isomers are both short lived and upon warming to room temperature, reform the nitrosyl isomer. Similar studies of the five-coordinate iron porphyrin analogues were reported to produce results that showed the brief formation of the isonitrosyl (ON) linkage isomer. However, the side-on isomer was not observed.[28]

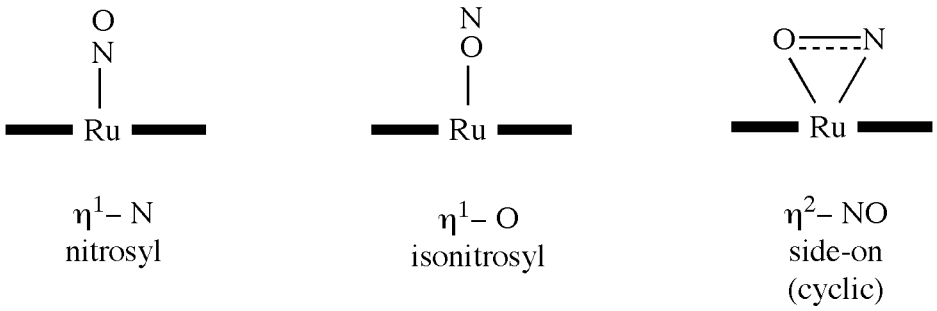

Figure 1.2. Photoinduced nitrosyl-ruthenium porphyrin linkage isomers (adapted from 27).

The characterization of these metastable isomers may provide insight into nitrosyl's approach to and leaving from iron centers of heme proteins.

c. Single crystal X-ray structures. The X-ray crystal structures have been obtained for the alkoxide complexes of (TTP)Ru(NO)(OMe), (OEP)Ru(NO)(O-*i*-C_5H_{11}) and (T(*p*-OMe)PP)Ru(NO)(O-*i*-C_5H_{11}) (Ch. 3) [27,29] and exhibit linear to near-linear Ru-NO linkages (table 1.2).

Like the alkoxide complexes, only a few X-ray molecular structures of ruthenium-NO porphyrin complexes with thiolate groups have also been obtained.[12,18,21] These complexes ((OEP)Ru(NO)($SC(Me)_2CH_2NHC(O)Me$), (OEP)Ru(NO)(NACysMe-S), and (OEP)Ru(NO)(SCH_2CH_2SH)) were reported to have near linear Ru-NO geometries ranging between 170.9(9) – 174.8(6)º (table 1.2).

d. Electrochemistry. In addition to the synthetic, spectroscopic, and solid-state molecular studies outlined above, we have examined the infrared fiber-optic spectroelectrochemistry of the dichloromethane solutions of ruthenium and osmium porphyrin complexes with alkoxide or thiolate ligands located *trans* to the M-NO group.[23] Currently, this study is the only electrochemical examination of nitrosyl metalloporphyrins containing alkoxide or thiolate linkages reported in the literature. Results from the IR spectroelectrochemistry of these complexes revealed an interesting disparity between the electrochemistry of the alkoxide and thiolate nitrosyl-metalloporphyrins. While the alkoxide complexes undergo an oxidation that is characterized by a single reversible electron removed from the porphyrin, the thiolate complexes undergo an oxidation that is chemically irreversible and based on the metal-nitrosyl axial position of the porphyrin complex resulting in the breaking of

the M-SR bond and subsequent formation of the thiol, HSR (Eqs. 1.7 and 1.8). Chapter 2 describes the IR spectroelectrochemistry study of both the Ru- and Os-NO porphyrin complexes.

$$(por)M(NO)(OR) \rightleftharpoons [(por\bullet)M(NO)(OR)]^{+} + e^{-} \quad (1.7)$$

$$(por)M(NO)(SR) \rightarrow [(por)M(NO)\bullet]^{+} + HSR + e^{-} \quad (1.8)$$

e. *Reactivity*. There have been a number of studies into the reaction chemistry of (por)M(NO)(XR) complexes (where M = Ru, Os and X = O, S). These studies have examined the consequences of proton addition to the complexes containing alkoxide and thiolate ligands and, in the case of a series of the ruthenium and osmium-nitrosyl porphyrin complexes with thiolate-thiol ligands, the coordination chemistry that occurs when the terminal –SH reacts with the metal centers of other nitrosyl-metalloporphyrins.

Protonation studies of alkoxide metal-nitrosyl porphyrin complexes were reported result in the isolation of the analogous alcohol bound complexes. However, protonation of thiolate metal-nitrosyl porphyrin complexes resulted in the cleavage of the M-SR bond. Studies, by our group, of ruthenium and osmium metal-nitrosyl porphyrin complexes with amide containing M-thiolate linkage showed that proton addition to the complex resulted in a ligand rearrangement and formation of the metal-amide form of the complex (Eq. 1.9, where M = Ru/Os and R = H/Me).[19,21]

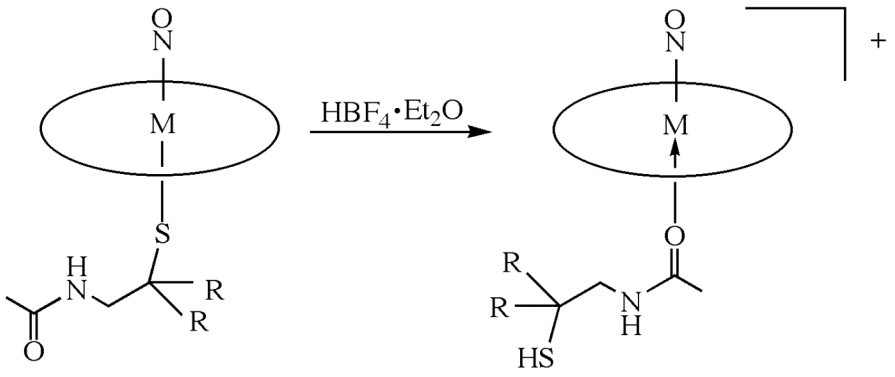

(1.9)

Dr. Lin Cheng of our group obtained spectroscopic results and solid-state molecular structures that showed that alcohol complexes of osmium-nitrosyl porphyrins could be prepared through the addition of H^+ to the related alkoxide starting materials (Eq. 1.10).[17]

$$(por)Os(NO)(OR) + H^+ \rightarrow [(por)Os(NO)(HOR)]^+ \qquad (1.10)$$

Subsequently, new alcohol complexes were reported to be prepared when the product of Eq. 1.10 was stirred in a solution containing an excess of the alcohol of interest (Eq. 1.11)

$$[(por)Os(NO)(HOR)]^+ + R'OH \rightarrow [(por)Os(NO)(HOR')]^+ + ROH \qquad (1.11)$$

Additionally, it was found that the electrophilic nature of the $[(por)Os(NO)]^+$ fragment allowed for deprotonation of the alcohol complexes with pyridine to form the alkoxide analogues (Eq. 1.12).

$$[(por)Os(NO)(HOR)]^+ + Py \rightarrow (por)Os(NO)(OR) + PyH^+ \quad (1.12)$$

Though there is evidence that ruthenium alkoxide complexes can be protonated to produce the related $[(por)Ru(NO)(HOR)]^+$ complexes[30], the addition of pyridine to the alcohol complexes, unlike the osmium analogues, has been reported to result in the replacement of the alcohol ligand with a pyridine ligand, forming the $[(por)Ru(NO)(Py)]^+$ complex.[27] It has been suggested based on this evidence that the $[(por)Ru(NO)]^+$ fragment is less electrophilic than the Os analogue, affording for the production of the cationic pyridine complex.[17]

As is evident from this report and the references herein, spectroscopic and structural studies of alkoxide (por)M(NO)(OR) and thiolate (por)M(NO)(SR) complexes (M = Ru, Os) has been extensively examined as potential models of Heme systems. In addition to the potential biomimetic value of these complexes, our group has explored the utility of the monometallic thiolate-thiol complexes (vide supra) as materials for coordination reactions in the preparation of bimetallic μ-dithiolate metalloporphyrin complexes. There have been numerous reports of the preparation of bimetallic metalloporphyrin complexes with bridging sulfido, alkyl, oxo, and other related ligands. However, prior to the studies by our group, reports of μ-dithiolate metalloporphyrins were absent from the literature. Drs. Yi and Lee isolated μ-dithiolate complexes containing symmetric phenyl-porphyrins (por/por) and asymmetric phenyl-porphyrins (por/por') through the addition of an alkoxide (por)M(NO)(OR) to the monometallic thiolate-thiol complex. An example of this can be seen in equation 1.13.[18,19] Preparation of μ-dithiolate complexes with the OEP

porphyrin and mixed Ru/Os metals was reported to be achieved from the in situ preparation of the putative nitrosyl-metalloporphyrin intermediate complex which, when in the presence of a (por)M(CO) complex, lead to the *trans* addition reaction like those previously described to form the μ-dithiolate product in low yields (Eq. 1.14).

$$(por)Ru(NO)(SCH_2CH_2SH) + (por)Ru(NO)(OR) \rightarrow [(por)Ru(NO)]_2(\mu\text{-}SCH_2CH_2S) + ROH \quad (1.13)$$

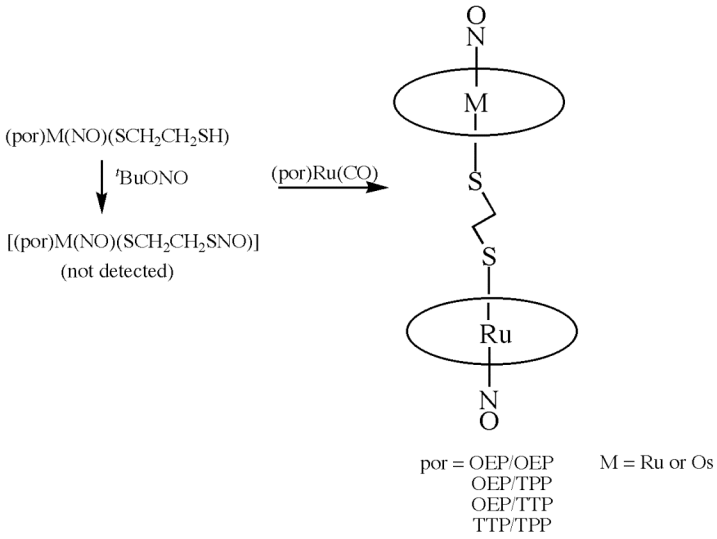

(1.14)

Of these complexes, the tetraryl porphyrin complexes were reported to exhibit the greatest stability.

B. Nitrosyl Heme with –*S*R and –*O*R donors

1. Nitric oxide synthase (NOS)

Nitric oxide synthase (NOS) is homodimeric heme enzyme with an active center composed of iron bound to the sulfur atom of cysteinate amino acid residue in

its resting state.[31,32] NOS is involved in the catabolism of L-arginine to L-citrulline and NO using NADPH and O_2 (Scheme 1.2).[33-35]

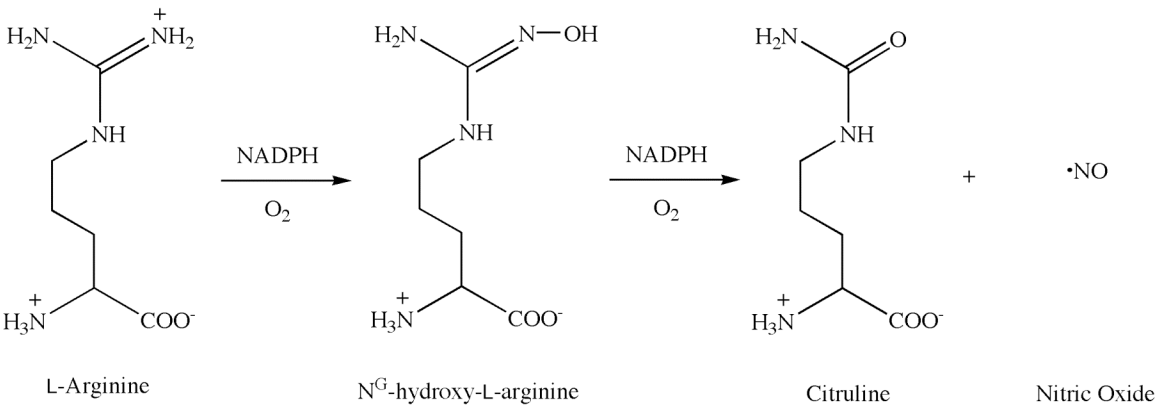

Scheme 1.2. Nitric oxide synthase (NOS) catalyzed production of NO from L-Arginine (adapted from 2).

These monooxygenase reactions have been shown to be dependent on the presence of the cofactor 5,6,7,8-tetrahydrobiopterin (H_4B).[36,37] There exist three known isoforms of the enzyme, each encoded by different genes: (1) an inducible NOS isoform (iNOS; Type II), a neuronal type (nNOS, Type I), and an isoform derived from endothial vascular cells (eNOS; Type III).[38-41] The former of these, nNOS and eNOS are constitutive and are regulated by Ca^{2+}/calmodulin, while iNOS is induced by bacterial endotoxin and inflammatory cytokines.[39,42-45]

NOS is known to form a iron-NO bond from the interaction of the heme center with catalytically NOS-generated NO in all three isoforms.[46-55] The consequence of NO binding during L-arginine catabolism is to inhibit the enzyme towards further catalysis. This form of negative feedback may serve to protect cells from being flooded with NO, which can be cytotoxic to host cells. Abu-Soud has

shown that this "suicide inhibition" of NOS by the binding of NO to the iron center is reversible in the presence of oxygen.[46,48,50] By coupling the formation of the steady state between the Fe-NO NOS and the resting NOS to O_2 levels, it is believed that it regulates NO production, allowing only the needed amounts of NO to be released while excess amounts react with dioxygen to form heavier oxides of NO like NO_2. Several reviews on the structure, function, and inhibition of NOS have been published. [56-59]

Protein crystal structures of both mammalian and bacterial NOS with iron bound NO have been obtained from exogenous addition of NO or NO donors to crystals of native NOSs.[60,61] A collaboration between Poulos and Masters resulted in the determination of the protein crystal structures for ferric-nitrosyl NOS from bovine eNOS in the presence and absence of H_4B when L-Arg is bound is bound to the active site in both structures.[60] It was revealed in both structures that the Fe(III)-NO linkage was bent at 160º at ~2.00 Å resolution. Favoring of the bent Fe(III)-NO bent geometry in the complexes over the expected linear geometry usually associated $\{MNO\}^6$ porphyrin complexes may be due to stabilization of the bent NO from hydrogen bonding between the O(NO) and guanidine group of the L-Arg co-substrate in both the H_4B and H_4B free substrates. The authors conclude from this data that H_4B has little effect on the NO geometry as long as L-Arg is present in both enzymes. Selected structural geometries for the crystals with H_4B ($+H_4B$) and without H_4B ($-H_4B$) are listed in table 1.3.

Similarly, Pant and Crane were able to obtain protein crystallographic data for the reduced form of *Bacillus subtilis* NOS with ferrous bound NOS in the presence of

L-Arg as well as the reduced form of the structure with the ezymatically catabolised N^G-hydroxyl-L-arginine (NOHA) in the active site of the enzyme.[61] Additionally, protein crystallographic geometric data was obtained for two oxidized forms of NOS Fe(III)-NO with NOHA in the active site. Each of these complexes exhibited greater than expected bends in the Fe(II)-NO and Fe(III)-NO geometries of the crystal structures. The reduced ferrous-NO—L-Arg and ferrous-NO—NOHA structures showed Fe(II)-NO angles of 132º and 126° at 1.9 Å resolution, respectively. The variation in the bond angles for the two complexes was credited to refinement problems in the NOHA containing complex. Despite the differences in the two angles, both complexes show a surprising deviation from the expected linearity found in other $\{MNO\}^6$ porphyrin complexes. The difference in the structures include hydrogen-bonding between the nitrogen of the nitrosyl group and the guanidinium nitrogen of in the L-Arg complex found in the ferrous-NO—L-Arg structure, while, in the ferrous-NO—NOHA the nitrogen of the nitrosyl group forms a tight hydrogen bond with the N^G of NOHA (2.86 Å vs 2.55 Å).

Ferric-NO—NOHA NOS complex was reported to crystallize with two molecules per asymmetric symmetry, one exhibiting a moderately bent Fe(III)-NO geometry (161°) and another with a severally bent ferric-nitrosy group (101°). The unexpectedly small angle exhibited by the latter Fe-NO group was attributed to possible nitrosylation of NOHA molecule in the structure.[61]

More recent work has suggested that the binding of NO to the heme center may induce monomerization of the NOS homodimer. Further, the monomeric form of NOS can be converted back into the dimeric form with the addition of arginine and

H_4B. Thereby, the initiation of monomerization by binding NO may be another regulatory response of the enzyme.[62]

2. Cytochrome P450

Cytrochrome P450 (cP450) is a heme enzyme with an iron(III) active site covalently linked to the sulfur in cysteine (Cys) in the resting state. In anaerobes, cP450 is primarily responsible for catalyzing the insertion of oxygen into substrates (S) (Eq. 1.15).

$$S + O_2 + 2e^-_{(NADPH)} + 2H^+ \rightarrow SO + H_2O \qquad (1.15)$$

An excellent review of the reactions catalyzed by cP450 was prepared by Meunier, Visser, and Shaik.[63]

Numerous spectroscopic studies have suggested that NO binds to the iron-heme center of cP50 trans to Cys and is believed to inhibit the function of the enzyme.[31,64-79] Binding of NO to the ferric $P450_{cam}$ has been predicted to be linear in the absence of substrate but otherwise bent when substrate is present.[71] Mutation of the conserved Glu318 in P450 1A2 to Ala resulted in the reduction of NO ferric complex to the ferrous analogue.[80] The authors of this study suggest that hydrogen bonding interactions between the carboxyl group of Glu318 and NO are crucial for stabilization the ferric nitrosyl structure.

To date, there have not been any reports of single-crystal protein structures of the six-coordinate cP450-NO.

3. Fungal nitric oxide reductase

Fungal nitric oxide reductase ($P450_{nor}$) is part of the global denitrification cycle and catalyzes the conversion of NO to N_2O at the cost of NADH. Fungal NOR, unlike the bacterial analogue (vide infra), is a cytochrome P450-like enzyme that binds NO through the ferric center of the heme trans to Cys during catalytic reduction of the substrate.[81-84] It, however, is unable to catalyze cP450 oxygen insertions into substrates. There have been numerous spectroscopic studies comparing $P450_{nor}$ from various sources to cP450.[81-85] Spectroscopic and computational evidence has led to the suggestion that a nitroxyl species (HNO) is formed from the reduction of NO.[85,86]

Recently, Shiro and co-workers have prepared an X-ray quality crystal of Fe(III)-NO fungal NOR from the reaction of crystalline *Furasarium oxysporum* NOR with NO gas under anaerobic conditions.[87] The Fe^{III}-NO bond was shown to have a bend (161°) and was in agreement with earlier predictions of the bond angle based on EXAFS studies. The ferric-nitrosyl bond angle reported for this heme complex is similar to the M-NO bond angle (159.6(8)°) for the related Fe(III)-NO thiolate complex [(OEP)Fe(NO)(S-2,6-$(CF_3CONH)_2C_6H_3$}] reported by Nan Xu (vide supra).[6] The authors conclude that the bent Fe(III)-NO is due to trans electronic effects from the cysteinate (S^-) ligand rather than steric effects from the amino acid residues surrounding the active site since it is relatively not crowded.

4. Chloroperoxidase

Chloroperoxidase is a heme enzyme that contains a five-coordinate iron center bound to the sulfur atom of Cys and is responsible for catalyzing the H_2O_2-dependent chlorination of substrates.[88] Preparations of NO adducts of chloroperoxidase using

exogenous NO sources were done with the intent of using the diatomic molecule as a ligand probe of the reactive center of the enzyme.[69,89-91] Such probes are often used in heme proteins that have traits which make them spectroscopically difficult to characterize and/or are difficult to crystallize for single-crystal X-ray studies.[92] The biological significance of nitrosylated chloroperoxidase is unknown.

5. Catalase

Catalase is responsible for catalyzing the disproportionation of peroxide to water and dioxygen (Eq. 1.16) and the ferric metal center of the heme enzyme contains *O*-bound tyrosine (Tyr) and water.[93]

$$2H_2O_2 \rightarrow 2H_2O + O_2 \qquad (1.16)$$

Several studies have been published that describe the formation of ferrous-NO catalase complex upon the exposure of catalase to low concentrations of NO, NH_2OH, or hydrazine[94-100] Further, the reactions of azide with catalase has been suggested to result in NO release[98,101-103] and may form an NO-catalase complex[104]. Brown has shown that exposure of catalase to physiological levels of NO results in the formation of Fe(II)-NO bond and inhibits enzymes catalytic activity.[96] The nitrosyl-catalase complex is stable in inert atmospheres, however, the five-coordinate catalase is reformed when the nitroso catalase is exposed to oxygen.[103]

Recently King, et al. have published a report that details the formation of nitrosyl catalase from the reaction of hyroxyurea with catalase in the presence of hydrogen peroxide.[105] The ferric catalase oxidation of hyroxyurea to form NO

catalase is significant due to the recent approval of the use of hydroxyurea as a treatment in the reduction of "painful crises" in patients with sickle cell disease.[105] Trials have shown that patients who have been administered hydroxyurea have an increase in NO metabolites and, as suggested by Brown, may be due to the catalase-mediated oxidation of the hydroxyurea medication.

II. Nitrosyl Heme and Heme Models with Pyridine and Imidazole Based N-Donors

A. Heme Models

1. Iron-nitrosyl porphyrins

Unlike the six-coordinate iron-nitrosyl porphyrin complexes with organic *O*- and *S*-donor ligands, reports of the similar complexes containing pyridine and imidazole based ligands are numerous.[106-129] Interest in imidazole and pyridine bound metalloporphyrin complexes arises partly from the high percentage of metal bound, imidazole containing, histidine (His) residues that are found in biological heme proteins. Of all the Heme proteins, those with *N*-bound His are most prevalent. Further, an abundance of these biological macromolecules are believed to interact with NO. A general review of the published data related to the chemistry of nitrosyl-iron porphyrins will be presented in this section.

a. Syntheses. The six-coordinate $\{MNO\}^7$, formally ferrous, (por)Fe(NO)(L) (L = imidazole- or pyridine-base) are generally prepared through addition of NO or *N*-base to the corresponding five-coordinate precursor (Eqs. 1.17 and 1.18).

(por)Fe(NO) + *N*-base → (por)Fe(NO)(*N*-base) (1.17)

(por)Fe(*N*-base) + NO → (por)Fe(NO)(*N*-base) (1.18)

Scheidt and co-workers have also prepared similar complexes of $\{MNO\}^6$ (ferric) $[(OEP)Fe(NO)(N\text{-base})]^+$ bubbling NO gas through a solution containing $[(OEP)Fe(OClO_3)]$ and the *N*-base (Eq. 1.19).[126] Preparation of the $\{MNO\}^6$ complexes required special preparation techniques that involve precise addition of the neutral *N*-donor ligand due to the highly labile MNO fragment. Addition of too much ligand quickly results in the denitrosylation of the complex resulting in the formation the *bis*-N_{ligand} complexes. This is in contrast to the formation of the analogues $\{MNO\}^7$ complexes, which generally require and excess of ligand to form the six-coordinate nitrosyl complexes. Clearly, the binding affinities of the ligands are very different in neutral and cationic complexes (vide infra).

$[(OEP)Fe(OClO_3)]$ + *N*-base + NO → $[(por)Fe(NO)(N\text{-base})]ClO_4$ (1.19)

b. Spectroscopy. An arsenal of spectroscopic techniques (IR, resonance Raman (RR), UV/Vis, electron paramagnetic resonance (EPR), and magnetic circular dichroism (MCD)) have been used to better understand the ligand binding in the nitrosyl adducts of the iron porphyrin complexes [(por)Fe(NO)(L)] (L = imidazole-, pyridine-based ligands) of both the $\{MNO\}^6$ and $\{MNO\}^7$. Universally, the data indicate that binding of imidazole- and pyridine-based ligands to the metal centers of these complexes is weak; the more acidic pyridine-based ligands have weaker bonds

than the imidazole-based ligands and the cationic ("ferrous") $\{MNO\}^6$ $[(por)Fe(NO)(N(L))]^+$ have much weaker Fe-N(L) bonds than the analogues neutral ferric complexes. The difference in NO binding for the $\{MNO\}^7$ and $\{MNO\}^6$ complexes is reflected in the respective nitrosyl stretching frequencies.

{MNO}^{7}. Kon[109] and Wayland[111], independently using EPR studies suggest that the unpaired electron from NO is significantly delocalized away from the NO into the d_{z^2} orbital of the Fe. According to Scheidt, this leads to an antibonding orbital combination upon addition of a neutral *N*-based ligand and contributes to low binding constants of the *trans* ligand that are estimated between 0.1 and 10.[130] Further, this explains the weakening of the Fe-N(MeIm) bond in (TPP)Fe(NO)(1-MeIm) (2.180(4) Å) when compared to the six-coordinate *bis*-1-MeIm analogue (2.00 Å).[130 131 132] Recently, Lehnert and coworkers reported, based on NMR and computational data, that upon binding the neutral imidazole base the Fe^{II}-NO bond is weakened.[127]

Interestingly, the activation of soluble guanylate cyclase (sGC) by NO shows a similar *trans* effect on iron bound histidine. Once NO binds to the five-coordinate heme center, the Fe-His bond breaks, activating sGC to catalyze the cyclization of 5'-triphospate (GTP) to guanosine 3',5'-cyclic monophosphate (cGMP). cGMP has been shown to be the biomolecule that is responsible for physiological events like vasodilation.

{MNO}^{6}. As mentioned above, formation of the Fe(III)-NO complexes is more dependent on precise additions of the neutral *N*-donor ligand than the analogous Fe(II)-NO complexes. This suggests that the stability of the $[(por)Fe(NO)(N(L))]^+$ is

low in comparison to the similar *neutral* analogues. This assumption agrees with the results obtained from laser photolysis studies by Ford and coworkers on water soluble hexacoordinate $\{MNO\}^7$ and $\{MNO\}^6$ nitrosyl heme proteins where the NO binding constants were reported to be ca. 10^{11} and $10^3 - 10^5$, respectively.[133,134] This is, to a degree, a reflection of the high (k_{off}) unit in the ferric system.[130]

c. Single crystal X-ray structures. Single crystal X-ray data have been obtained for the six-coordinate nitrosyl adduct of ferrous $\{MNO\}^7$ and ferric $\{MNO\}^6$ metalloporphyrins containing imidazole and pyridine derived metal linkages. However, due to exceptionally weak coordination of the neutral bases to the formally ferric metal center, few of these structures are of the $\{MNO\}^6$ type (table 1.2). An excellent review by Wyllie and Scheidt of the molecular structures of iron-nitrosyl porphyrin complexes and other nitrosyl metalloporphyrin complexes has been published.[130]

$\{MNO\}^7$. As is evident from table 1.2, the X-ray derived geometric parameters of a few ferrous porphyrin complexes containing mutually *trans* nitrosyl and imidazole/pyridine derived ligands have been reported. These complexes contain the bent M-NO groups (131.8(12) – 143.7(6) º). In line with the apparent weak binding of the neutral donor ligand to the metal *trans* of NO, there is no significant deviation from the geometry of the Fe-NO group in the five-coordinate nitrosyl complex upon binding of the neutral *N*-donor ligand.[130] Additionally, comparison of the six-coordinate *bis*-MeIm complex to the related (por)Fe(NO)(MeIm) reveals a lengthening of the Fe(II)-N(Im) bond in the NO complex (2.014(5) vs. 2.180(4) Å,

respectively)[131,132,135] This relatively long Fe(II)-N(Im) bond is due to weak coordination of the ligand to the Fe-NO group in the complex.

{MNO}^{6}. As mentioned above, the labile nature of the Fe(III)-NO fragment in the [(por)Fe(NO)(*N*-donor)]$^+$ complexes leads to easy, rapid denitrosylation. In fact, the few {MNO}^{6} crystal structures reported by Scheidt for these complexes were solved only after specialized equipment was constructed for the growth of X-ray quality crystals.[126] These complexes displayed nearly linear Fe-NO geometries (~177°).

d. Electrochemistry. Choi and Ryan have reported the cyclic voltammograms of (por)Fe(NO)(Py) complexes (por = TPP, PPDME; Py = pyridine-based ligand).[123] Not surprisingly, considering the weak interaction between neutral *N*-donor ligands and the ferric centers of the metal-nitrosyl complexes reported above, the reversible one-electron reduction of these complexes were reported to result in the loss of the pyridine-substituted bases (Eq. 1.20; site of reduction is not specified).

$$\text{(por)Fe(NO)(L)} + e^- \rightleftharpoons \text{(por)Fe(NO)}\bullet^- + \text{L} \qquad (1.20)$$

There have been no other reports of electrochemical studies of {MNO}^{7} or {MNO}^{6} iron porphyrin complexes with imidazole- or pyridine-based ligands.

2. Ruthenium- and osmium-nitrosyl porphyrins

There have been only a few reports of the preparation of ruthenium-nitrosyl complexes with either metal bound imidazole- or pyridine-based ligands, and of these reports only one contains full synthetic and spectral data for the complexes. There

have been no reports of the preparation of osmium-nitrosyl porphyrin complexes with either imidazole- or pyridine-based ligands.

In the interest of expanding knowledge of Group 8 metalloporphyrin nitroso complexes with imidazole- and pyridine-based ligands, we have studied the synthesis, X-ray crystal structures, and electrochemistry of the ruthenium analogues of these complexes. This data will be presented and discussed in Chapter 3 and 4 of this thesis.

a. Syntheses

Bohle was able to obtain the TTP derivative of (por)Ru(NO)(Im) through the solvent free reaction of the nitrosyl porphyrin alkoxide precursor complex with imidazole (Eq. 1.21)

$$(TTP)Ru(NO)(OR) + HIm \rightarrow (TTP)Ru(NO)(Im) + HOR \qquad (1.21)$$

The preparation of a pyridine containing ruthenium nitrosyl porphyrin complex has been reported, however, neither the details of the synthesis or spectroscopic elucidation were provided.

3. Myoglobin

Myoglobin (Mb) is a monomeric heme protein that, in its resting state, is composed of a pentacoordinate prosthetic group with an iron porphyrin attached through the nitrogen atom of His. The primary function of Mb is generally regarded as a dioxygen storage protein in muscles.

NO adducts of myoglobin are perhaps the most studied of the heme proteins containing iron-NO groups since the wild-type (wt) protein is known to interact with NO through the iron heme center and mutated versions of the protein are used to

model the reactions of other, less understood heme enzyme interactions with NO.[106,107,136-164] Indeed, Dan Copeland of our group recently completed his thesis entitled "Structural Studies of the Interactions of Nitric Oxide and Nitric Oxide Containing Molecules with Heme Proteins." Reviews of the NO adducts of Mb have been published.[2,165] For brevity and in keeping with the scope of this work, only a general review of the interactions of NO with Mb will be presented. More specific details can be obtained from the sources listed here.

Recent studies have brought the role of Mb as a dioxygen storage protein as its *primary* function into question. Research by Flögel et al. suggests that oxymyoglobin ($Mb^{II}O_2$) may act as a molecular scavenger of NO in the presence of elevated NO synthase activity, protecting the inhibition of cytochromes by NO binding.[166] Further, it was postulated that oxymyoglobin reacts with NO, forming an MbFe(II)NO intermediate that reacts with dioxygen forming metMb and releasing NO_3^-.

This, however, is not the first report of NO binding to the iron in Mb(II). It has been known for over 100 years that the coloration in cured meat is due to the formation of pentacoordinate Mb(II)NO.[2,141,161] The addition of nitrite to uncooked meat reacts to form N_2O_3 that, when reduced, forms the NO that binds to the iron center of Mb. This process is commonly believed to be aided by bacterical or enzymatic actions as well as chemical curing agents like sodium chloride. It has been proposed that the addition of nitrite to meat results in the oxidation of $Mb(II)O_2$ forming Mb(III)NO. Reduction in the meat matrix powered by NADH results in the

formation of the penatcoordinate Mb(II)NO that is associated with the blood red color of cured meat.[167]

The binding of NO to Mb(II) has been extensively studied. It has been suggested that there is a charge transfer from Fe(II) to NO when bound in Mb that results in NO being nitroxyl (NO^-) in character. The single crystal protein X-ray structures of sperm whale MbNO (swMbNO)[168] and horse heart MbNO (hhMbNO)[169,170] have been reported and selected geometric data for these complexes can be found in table 1.3. The former sperm whale structure exhibited a Fe(II)-NO bond angle of 112°. The Fe-NO angle is more acute than what is generally associated with $\{MNO\}^7$ complexes but agrees with M-NO angles derived previously from EPR data (108º-110º).[162,163] The authors of this work attributed this to electrostatic interactions between the ligand and a distal His residue in the swMbNO. Three different crystal structures of hhMbNO were prepared; two of the structures were prepared from the addition of nitrite/dithionitrite to a hhMb crystal while a third complex was prepared from the addition of NO gas to crystalline hhMb. The Fe-NO geometry for the structures prepared from the nitrite/dithionitrite soak were essentially the same (147° and 144°), while, surprisingly, the Fe-NO bond angle in the structure that was prepared from the addition of NO gas showed a Fe-NO bond angle of 120°. Copeland and coworkers explain the discrepancy in these geometries as occurring from constraints placed on the formation of the different hhMbNO structures from the "pre-formed distal pocket" of the protein. Presumably the reactions occur through different pathways, which result in formation of intermediates whose structures are dependent on stabilization by the distal pocket.

The end result reflects the minimized structures afforded by the distal pocket interactions.

In addition to the Mb(II) nitrosyl complexes, there have been reports of nitrosyl adducts of the oxidized ferric Mb.[140,142,144,147,150,152,155] The binding affinity of NO for Mb(III) have been shown to be significantly lower than for Mb(II).[140] The bond angle of the Fe^{III}-NO group is predicted to be near linear via EPR studies and is similar to the angle predicted for other $\{MNO\}^6$ heme model complexes.[146] The biological importance of the in vivo binding of NO to Mb(III) has been questioned.[167]

There have been reports that also describe the weakening of the ferrous-nitrogen bond in the *trans* His of MbFe(II) upon binding NO.[164] The bond between the proximal base and the Fe(II) center of Mb is further weakened in low pH solutions of MbFe(II)NO complexes.[139,148,154,157]

In addition to studies of the binding of NO in wild type (wt) Mb, there have also been studies of the binding of NO to the ferrous centers of Mb that have had amino acid residues changed through mutation.[142,153] Similarly, metal-substitution MbNO has been studied.[136-138,155,156] While this research supplies important information about mechanistic and stabilization aspects of the addition and formation of NO adducts of Mb, it lies outside the scope of this work and will not be further reviewed here.

4. Cytochrome c Oxidase

Cytochrome *c* oxidase (C*c*O) reduces molecular oxygen to water through a series of electron transfers which in-turn provides energy to pump protons across the mitochondrial membrane in eukaryotic cells.[171-173] C*c*O is composed of two hemes,

heme *a* and a_3, a dimeric copper center, Cu_A, and a mononuclear Cu_B.[174,175] Reduction of dioxygen occurs at the heme-copper binuclear center, where heme a_3 and Cu_B are in close proximity (Fig. 1.3). The structural features of various C*c*O enzymes have been extensively explored. The heme a_3 contains an Fe center axially linked with a His, whereas the Cu_B site is linked to three His residues, one of which is covalently bound to a tyrosine (Tyr) residue.

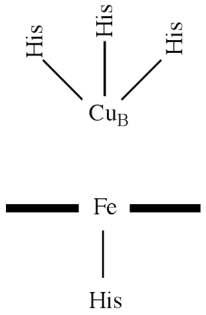

Figure 1.3: Binuclear center in *CcO*.

Evidence has shown that NO reversibly binds to the iron center of C*c*O competitively with oxygen.[176-199] It is believed that the binding of NO to the heme center plays a role in oxygen sensing and the cell's response to hypoxia.[200] Additionally, interaction of a NO molecule with the Cu_B site reversibly induces limited inhibition of the dioxygen reduction.[179,180,188-190,192-195,197-199,201]

A series of studies comparing the reactions of NO with oxidized and reduced forms of CcO in both the presence and absence of azide have resulted in spectroscopic evidence that suggests highly conditional forms of NO binding to the iron center and the Cu_B binuclear site of the protein.[176,178-180] In the case of the oxidized complex (a_3^+, Cu_B^{2+}) in the absence of azide NO reversibly binds to the Cu_B.

Interestingly, in the presence of azide, NO reacts with the oxidized CcO to form a bridged isonitrosyl structure (a_3^{2+}-NO-Cu_B^{2+}) that was reported to be stable.[180] When NO was introduced to reduced forms of CcO (a_3^{+}, Cu_B^{+}), a_3^{+}-NO and Cu_B^{+}-NO where observed. [178]

5. Soluble Guanylyl Cyclase

Soluble guanylyl cyclase (sGC) is a heterodimeric heme enzyme consisting of a pentacoordinate high-spin ferrous metal center bound to histidine and a hexacoordinate low-spin iron heme center (likely consisting of His ligands bound in a *trans* fashion across the face of the porphyrin) in the resting state.[202,203] sGC is activated by NO binding to the iron heme center which in-turn catalyzes the cyclization of guanosine 5'-triphosphate (GTP) to guanosine 3',5'-cyclic monophosphate (cGMP). cGMP is the biological molecule that initiates a series of physiological events like vasodilation.

The NO adducts of ferrous sGC have been studied[204-217] and it is generally accepted that upon binding NO to the ferrous heme center the proximal His is liberated leaving the pentacoordinate (por)Fe(NO) heme complex[206,207,209-212,214,217]. Indeed, Burstyn et al. concluded from studies on sGC proteins that had been reconstituted with (PPIX)Mn^{II} and (PPIX)Co^{II} that the loss of the metal-His bond upon binding NO is required to activate sGCs enzymatic activity.[206] Further, Marletta and co-workers have shown from their studies of the loss of the ferrous-His bond upon the binding of NO to sGC that a conformational change in the proximal pocket of the enzyme occurs and have speculated that this may have important implications to the mechanism of sGC activation by NO. [210]

6. Nitrite Reductase

Nitrite reductase (NiR) enzymes are another important member of the denitrification cycle and are responsible for the reduction of nitrite (NO_2^-) to NO. There are two major classes of NiR enzymes. The first is the heme containing cytochrome cd_1 NiR and the second is the non-heme copper nitrite reductase.[2]

The cyt cd_1 NiR, as the name implies, is composed of a heme *c* and heme d_1 in each subunit of the enzyme. Both hemes have iron centers bound to His. Heme d_1 has been shown to bind NO_2^- whereas heme *c* has been proposed to the location of the initial electron donation and provides the needed reductive energy through a series of steps to heme d_1 for reduction of the bound NO_2^- to NO.[218-224] Heme d_1 has been shown crystollographically (from *Thiosphaera pantotropha* (NiR-Pd)) to have two histidine residues (His345 and His388) and a tyrosine residue (Tyr25) in the distal pocket.[225,226] The His residues are believed to be involved in the reduction NO_2^- to NO while the Tyr residue is believed to be involved in the removal of NO from the Fe(III) heme d_1 center. Reviews of the proposed mechanism of reduction of nitrite to NO have been published.[222,227]

The single crystal protein structures for the NO adduct of cyt cd_1 NiRs have been reported from *Thiosphaera pantotropha*[225] (NiR-Tp) as well as *Pseudomonas aeruginosa*[228] (NiR-Pa). Both structures contain a bent Fe(III)-NO angles (131° and 135°, respectively). The bending of these $\{MNO\}^7$ complexes is proposed to arise due to interactions between the oxygen atom of NO and His in the distal pocket of the

enzyme. The NO adducts of cyt cd_1 NiR are believed to form just prior to the release of the ligand from the metal center during the catalytic path of reduction of nitrite.

7. Bacterial Nitric Oxide Reductase

Like the fungal nitric oxide reductase discussed above, bacterial nitric oxide reductase (NOR) catalyzes the reduction of NO to N_2O. There have been a number of reports describing the composition of the enzyme as cytochrome *bc* complex, however, more recent data suggests that the enzyme may be composed of two heme *b* centers and a heme *c* center (denoted as cytochrome *cbb*).[177,229-231]

The current belief is that the catalytic site of the enzyme is composed of a five-coordinate low-spin heme *b* bound to a His through the ferric iron and a non-heme iron(II) located next to the heme center in the distal pocket. EPR studies by Saraste and coworkers suggest that both the heme and non-heme iron(II) active centers each bind an NO during the catalytic reduction to N_2O.[232]

8. Other Heme-proteins

There have been reports of the interaction of NO with the iron centers of a number of other heme proteins. The binding and activation of NO to these heme proteins has been reviewed[2] and will not be discussed further in this work.

Table 1.1: Fe, Ru, and Os nitrosyl-porphyrins with organic *S*-, *O*-donors and imidazole- and pyridine-based axial ligands reported from 1999-2006.

Compound	{MNO}^{x}	ν_{NO} (cm^{-1}) (medium) (ref)	Raman ($\nu_{Fe-N(O)}$ cm^{-1}) (ref)	EPR (ref)	UV-Vis (ref)	Electrochemistry (ref)	Other (ref)
Iron							
Organic *S*-donor							
(OEP)Fe(NO){S-2,6-$(CF_3CONH)_2C_6H_3$}	6	1850 (Nujol) (6)					
[(TPP)Fe(NO)(L′)](TBA)							
L′ = 1-SPh	7			(8)			
1-SPh^{OMe}	7			(8)			
1-SPh^{F}	7			(8)			
***N*-donor**							
(TPP)Fe(NO)(L′)							
L′ = 1-MeIm	7	1625 (KBr) (132) 1630 (KBr) (127) 1628 (Nujol) (233)	440 (127)	(117,233)	(127)		Mössbauer (233)

Compound	{MNO}^{x}	ν_{NO} (cm^{-1}) (medium) (ref)	Raman ($\nu_{Fe-N(O)}$ cm^{-1}) (ref)	EPR (ref)	UV-Vis (ref)	Electrochemistry (ref)	Other (ref)
Py	7				(127)		
4-NMe_2Py	7	1653 (Nujol) (233)		(233)			
Pip	7						NMR (127)
4-MePip	7	1642 (Nujol) (233)		(233)			Mössbauer (233)
(TMP)Fe(NO)(L′)							
L′ = Py	7				(127)		
Pip	7						NMR (127)
1-MeIm	7	1624 (KBr) (127)			(127)		
(To-F_2PP)Fe(NO)(L′)							
L′ = Py	7				(127)		
Pip	7						NMR (127)
1-MeIm	7	1624 (KBr) (127)			(127)		NMR (127)

Compound	{MNO}^{x}	ν_{NO} (cm^{-1}) (medium) (ref)	Raman ($\nu_{Fe-N(O)}$ cm^{-1}) (ref)	EPR (ref)	UV-Vis (ref)	Electrochemistry (ref)	Other (ref)
(TpivPP)Fe(NO)(py)	7	1635 (pyridine) (233)					
Ruthenium							
***O*-donor**							
(OEP)Ru(NO)(OEt)	6	1801 (CH_2Cl_2) (23) 1791 (KBr) (23)				(23, Ch. 4)	NMR (23)
(OEP)Ru(NO)(O-i-C_5H_{11})	6	1800 (CH_2Cl_2) (18) 1791 (KBr) (27) 1788 (KBr) (18)					NMR (18)
(TPP)Ru(NO)(O-i-C_5H_{11})	6	1809 (CH_2Cl_2) (18) 1800 (CH_2Cl_2) (18)					NMR (18)

Compound	{MNO}^{x}	ν_{NO} (cm^{-1}) (medium) (ref)	Raman ($\nu_{Fe-N(O)}$ cm^{-1}) (ref)	EPR (ref)	UV-Vis (ref)	Electrochemistry (ref)	Other (ref)
(T(p-OMe)PP)Ru(NO)(O-i-C_5H_{11})	6	1808 (CH_2Cl_2) (Ch. 3) 1801 (KBr) (CH. 3)					NMR (Ch. 3)
***S*-donor**							
(OEP)Ru(NO)(L′)							
L′ = SEt	6	1788 (CH_2Cl_2) (23, Ch. 2) 1773 (KBr) (23, Ch. 2)				(23, Ch. 2)	NMR (23, Ch. 2)
S-i-C_5H_{11}	6	1786 (CH_2Cl_2) (Ch. 2) 1775 (KBr) (Ch.2)					NMR (Ch. 2)
$S(CH_2)_2SH$	6	1803 (CH_2Cl_2) (18) 1792 (KBr) (18)					NMR (18)

Compound	{MNO}^{x}	ν_{NO} (cm^{-1}) (medium) (ref)	Raman ($\nu_{Fe-N(O)}$ cm^{-1}) (ref)	EPR (ref)	UV-Vis (ref)	Electrochemistry (ref)	Other (ref)
SPh	6	1793 (CH_2Cl_2) (Ch. 2) 1783 (KBr) (Ch. 2)					NMR (Ch. 2)
(TPP)Ru(NO)($S(CH_2)_2SH$)	6	1803 (CH_2Cl_2) (18) 1792 (KBr) (18)					NMR (18)
(TTP)Ru(NO)(L′)							
L′ = $S(CH_2)_2SH$	6	1793 (CH_2Cl_2) (18) 1770 (KBr) (18)					NMR (18)
$S(CH_2)_3SH$	6	1799 (CH_2Cl_2) (18) 1779 (KBr) (18)					NMR (18)

Compound	{MNO}^{x}	ν_{NO} (cm^{-1}) (medium) (ref)	Raman ($\nu_{Fe-N(O)}$ cm^{-1}) (ref)	EPR (ref)	UV-Vis (ref)	Electrochemistry (ref)	Other (ref)
$S(CH_2)_4SH$	6	1794 (CH_2Cl_2) (18) 1770 (KBr) (18)					NMR (18)
$[(OEP)Ru(NO)]_2(\mu$-edt-S,S′)	6	1786 (CH_2Cl_2) (18) 1770 (KBr) (18)					NMR (18)
$[(TPP)Ru(NO)]_2(\mu$-edt- S,S′)	6	1802 (CH_2Cl_2) (18) 1779 (KBr) (18)					NMR (18)
$[(TTP)Ru(NO)]_2(\mu$-edt- S,S′)	6	1788 (CH_2Cl_2) (18) 1770 (KBr) (18)					NMR (18)

Compound	{MNO}^{x}	ν_{NO} (cm^{-1}) (medium) (ref)	Raman ($\nu_{Fe-N(O)}$ cm^{-1}) (ref)	EPR (ref)	UV-Vis (ref)	Electrochemistry (ref)	Other (ref)
$[(TTP)Ru(NO)]_2(\mu$-pdt- S,S′)	6	1790 (CH_2Cl_2) (18) 1772 (KBr) (18)					NMR (18)
[(TPP)Ru(NO)](μ-edt- S,S′)[Ru(NO)(OEP)]	6	1786 (CH_2Cl_2) (18) 1770 (KBr) (18)					NMR (18)
***N*-donor**							
(OEP)Ru(NO)(L′)							
L′ = Im	6	1848 (CH_2Cl_2) (Ch. 3) 1828 (KBr) (Ch. 3)				(Ch. 4)	NMR (Ch. 3)
5-MeIm	6	1845 (CH_2Cl_2) (Ch. 3)					NMR (Ch. 3)
(TPP)Ru(NO)(Im)	6	1854 (CH_2Cl_2) (Ch. 3)					NMR (Ch. 3)

Compound	{MNO}^{x}	ν_{NO} (cm^{-1}) (medium) (ref)	Raman ($\nu_{Fe-N(O)}$ cm^{-1}) (ref)	EPR (ref)	UV-Vis (ref)	Electrochemistry (ref)	Other (ref)
(T(p-OMe)PP)Ru(NO)(Im)	6	1855 (CH_2Cl_2) (Ch. 3) 1846 (KBr) (Ch. 3)					NMR (Ch. 3)
[(OEP)Ru(NO)(L')]$^+$							
L' = HIm	6	1870 (CH_2Cl_2) (Ch. 3) 1852 (KBr) (Ch. 3)				(Ch. 4)	NMR (Ch. 3)
1-MeIm	6	1872 (CH_2Cl_2)				(Ch. 4)	NMR (Ch. 3)
5(4)-MeHIm	6	1871 (CH_2Cl_2)					NMR (Ch. 3)
Py	6	1877 (CH_2Cl_2) (Ch. 3) 1855 (KBr) (Ch. 3)					NMR (Ch. 3)

Compound	{MNO}^{x}	ν_{NO} (cm^{-1}) (medium) (ref)	Raman ($\nu_{Fe-N(O)}$ cm^{-1}) (ref)	EPR (ref)	UV-Vis (ref)	Electrochemistry (ref)	Other (ref)
$[(TTP)Ru(NO)(HIm)]^+$	6	1866 (KBr) (Ch. 3)					NMR (Ch. 3)
Osmium							
O-donor							
(OEP)Os(NO)(L′)							
L′ = OEt	6	1759 (CH_2Cl_2) (17) 1756 (KBr) (17)			(17)	(23, Ch. 2)	NMR (17)
O-i-C_5H_{11}	6	1757 (CH_2Cl_2) (17) 1754 (KBr) (17)					NMR (17)

Compound	{MNO}^{x}	ν_{NO} (cm^{-1}) (medium) (ref)	Raman ($\nu_{Fe-N(O)}$ cm^{-1}) (ref)	EPR (ref)	UV-Vis (ref)	Electrochemistry (ref)	Other (ref)
OC_6H_{11}-cyclo	6	1755 (CH_2Cl_2) (17) 1751 (KBr) (17)					NMR (17)
$[(OEP)Os(NO)(L')]^+$							
L′ = HOMe	6	1828 (CH_2Cl_2) (17) 1813 (KBr) (17)			(17)		NMR (17)
HOEt	6	1828 (CH_2Cl_2) (17) 1814 (KBr) (17)			(17)	(23, Ch. 2)	NMR (17)
HO^{i}Pr	6	1828 (CH_2Cl_2) (17) 1814 (KBr) (17)			(17)		NMR (17)

Compound	{MNO}^{x}	ν_{NO} (cm^{-1}) (medium) (ref)	Raman ($\nu_{Fe-N(O)}$ cm^{-1}) (ref)	EPR (ref)	UV-Vis (ref)	Electrochemistry (ref)	Other (ref)
HO-i-C_5H_{11}	6	1828 (CH_2Cl_2) (17) 1816 (KBr) (17)			(17)		NMR (17)
HOC_6H_{11}-cyclo	6	1828 (CH_2Cl_2) (17) 1816 (KBr) (17)			(17)		NMR (17)
HOC_6H_4F	6						NMR (17)
O=C(Me)$NHCH_2CH_2SH$	6	1826 (CH_2Cl_2) (19) 1814 (KBr) (19)			(19)		NMR (19)
O=C(Me)$NHCH_2C(Me)_2SH$	6	1826 (CH_2Cl_2) (19) 1816 (KBr) (19)			(19)		NMR (19)
***S*-donor**							

Compound	{MNO}^{x}	ν_{NO} (cm^{-1}) (medium) (ref)	Raman ($\nu_{Fe-N(O)}$ cm^{-1}) (ref)	EPR (ref)	UV-Vis (ref)	Electrochemistry (ref)	Other (ref)
(OEP)Os(NO)(L′)							
L′ = SMe	6	1759 (CH_2Cl_2) (19) 1755 (KBr) (19)			(19)		NMR (19)
SEt	6	1758 (CH_2Cl_2) (19) 1753 (KBr) (19)			(19)		NMR (19)
L′ = S^{i}Pr	6	1754 (CH_2Cl_2) (19) 1751 (KBr) (19)			([19])		NMR (19)

Compound	{MNO}^{x}	ν_{NO} (cm^{-1}) (medium) (ref)	Raman ($\nu_{Fe-N(O)}$ cm^{-1}) (ref)	EPR (ref)	UV-Vis (ref)	Electrochemistry (ref)	Other (ref)
S^tBu	6	1758 (CH_2Cl_2) (19) 1754 (KBr) (19)			([19])		NMR (19)
$S(CH_2)_2SH$	6	1764 (CH_2Cl_2) (19) 1756 (KBr) (19)			(19)		NMR (19)
$S(CH_2)_2NHC(O)Me$	6	1765 (CH_2Cl_2) (19) 1756 (KBr) (19)			(19)		NMR (19)
$L' = SC(Me)_3CH_2NHC(O)Me$	6	1773 (CH_2Cl_2) (19) 1764 (KBr) (19)			(19)		NMR (19)

Compound	{MNO}^{x}	ν_{NO} (cm^{-1}) (medium) (ref)	Raman ($\nu_{Fe-N(O)}$ cm^{-1}) (ref)	EPR (ref)	UV-Vis (ref)	Electrochemistry (ref)	Other (ref)
[(OEP)Os(NO)](μ-SCH_2CH_2S-S,S′)[Ru(NO)(TTP)]	6						NMR (19)

Table 1.2: X-Ray geometric parameters from Group 8 synthetic nitrosyl porphyrins with organic *S*- and *O*-donors and imidazole- and pyridine-based axial ligands reported from 1999 - 2006.

	{M(NO)}^{n}	M–N_{NO} (Å)	N–O (Å)	∠MNO (°)	M–X_{lig} (Å)	∠MXY (°)	ref
Iron							
[(TPP)Fe(NO)(HO–*i*–C_5H_{11})]ClO_4[a]	6	1.776(5)	0.925(6)	177.1(7)	2.063(3)	127.8(6), 131.8(6)	12
[(OEP)Fe(NO){S–2,6–$(CF_3CONH)_2C_6H_3$}]	6	1.671(9)	1.187(9)	159.6(8)	2.356(3)	110.6(3)	6
[(OEP)Fe(NO)(1–MeIm)]ClO_4	6	1.6465(17)	1.135(2)	177.28(17)	1.9889(16)	128.09(13), 125.74(13)	126
[(OEP)Fe(NO)(Iz)]ClO_4	6	1.996(4)	1.136(4)	177.6(3)	2.010(3)	130.0(2) (FeNC), 123.71(18) (FeNN)	126
(T*o*–F_2PP)Fe(NO)(1–MeIm)[b]	7	1.752(2)	1.202(2)	131.8(12)[i, j]	2.188(2)	105.02(17)[j], 127.10(14)[j]	127
(TPP)Fe(NO)(1–MeIm)•$CHCl_3$[b]	7	1.743(4)	1.121(8)	142.1(6)	2.180(4)	126.6(4)[j], 130.4(4)[j]	131,132
(TPP)Fe(NO)(1–MeIm)•$CHCl_3$[b,k]	7	1.750(2)	1.182(3)	137.7(2), 137.0(8)	2.173(2)	127.9(2), 126.8(2)	233
(TPP)Fe(NO)(4–MePip)[b]	7	1.7210(10)	1.141(13)	138.5(11)	2.328(10)	112.5(5), 113.1(6)	234
(TPP)Fe(NO)(4–MePip)•$CHCl_3$	7	1.740(7)	1.112(9)	143.7(6)	2.463(7)	113.6(8), 113.3(9)	234
(TPP)Fe(NO)(4–MePip)•$CHCl_3$[k]	7	1.7517(19)	1.171(2)	138.04(17)	2.2851(19)	115.10(13)[j], 113.65(13)[j]	233
(TPP)Fe(NO)(4–NMe_2Py)[b]	7	1.7577(13)	1.1700(13)	139.79(12)	2.2783(13)	123.77(11)[j], 118.91(11)[j]	233
(TpivPP)Fe(NO)(NO)(Py)•C_6H_5Cl	7	1.742(5)	1.194(9)	133.4(5)	2.260(5)	121.0(3), 121.0(3)	233
Ruthenium							
(TTP)Ru(NO)(OMe)[a, c]	6	1.84(4)		180.0	1.80(5)		29
[(OEP)Ru(NO){O=C(Me)$NHCH_2C(Me)_2SH$}]BF_4	6	1.708(6)	1.141(7)	177.8(5)	2.049(4)	143.8(5)	21
(OEP)Ru(NO)($SC(Me)_2CHNHC(O)Me$)	6	1.769(3)	1.114(4)	172.8(3)	2.390(1)	121.74(13)	21
(OEP)Ru(NO)(O–*i*–C_5H_{11})[b]	6	1.780(10)	1.191(14), 1.191(14)	170.2(11), 137(3)	1.908(11)	133.853[l]	27
(T(*p*–OMe)PP)Ru(NO)(O–*i*–C_5H_{11})[y]	6	1.754(4)	1.172(5)	176.9(3)	1.932(3)	129.1(9), 128.0(8), 161.1(12)	Ch. 3

	{M(NO)}^{n}	M–N_{NO} (Å)	N–O (Å)	∠MNO (°)	M–X_{liq} (Å)	∠MXY (°)	ref
(OEP)Ru(NO)(S-NACysMe)	6	1.790(5)	1.123(8)	174.8(6)	2.362(2)	107.1(3)	12,20
(OEP)Ru(NO)(SCH_2CH_2SH)•CH_2Cl_2[c]	6	1.802(9)	1.166(11)	170.9(9)	2.316(4)	111.0(4)	18
(OEP)Ru(NO)(SCH_2CF_3)[c]	6	1.758(9), 1.773(9)	1.162(15), 1.187(14)	161(2), 157(2)	2.394(7), 2.390(8)	128.8(13), 164(3)	27
(OEP)Ru(NO)(Im)•HIm•CH_2Cl_2	6	1.748(3)	1.148(4)	174.9(3)	2.063(3)	127.9(2), 128.0(2)	Ch. 3
(OEP)Ru(NO)(5-MeIm)•4-MeHIm	6	1.740(4)	1.145(5)	171.2(4)	2.059(4)	128.1(4), 127.9(3)	Ch. 3
[(OEP)Ru(NO)(HIm)]SbF_6[d]	6	1.695(9)	1.131(12)	175.3(7)	2.069(8)	128.9(6), 128.2(8)	Ch. 3
[(OEP)Ru(NO)(4-MeHIm)]SbF_6/ [(OEP)Ru(NO)(5-MeHIm)]SbF_6[e]	6	1.7305(17)	1.144(2)	176.94(18)	2.1036(17)	122.49(16), 130.93(13)	Ch. 3
Osmium							
(OEP)Os(NO)(O-*n*-Bu)[c]	6	1.833(8)	1.173(11)	172.8(8)	1.877(7)	130.8(9)	22
(OEP)Os(NO)(OEt)[c]	6	1.81(2)	1.33(2)	156.1(17)	1.89(2)	123.7(15)	17
(OEP)Os(NO)(OEt)[c, f]	6	1.880(7)	1.165(9)	172.4(10)	1.849(7)	128.0(8)	23
[(OEP)Os(NO)(HOEt)]BF_4•HOEt	6	1.720(4)	1.167(5)	178.5(3)	2.062(3)	130.5(4)	17
[(OEP)Os(NO)(HO^{i}Pr)]BF_4•^{i}PrOH[g]	6	1.709(4)	1.186(5)	176.6(3)	2.075(3)	129.1(6)	17
[(OEP)Os(NO)(HOhexyl)]BF_4	6	1.740(6)	1.159(9)	174.4(6)	2.097(5)	127.3(4)	17
[(OEP)Os(NO)(HOhexyl)]BF_4[h]	6	1.728(7)	1.174(9)	176.8(7)	2.073(5)	126.3(5)	17
(OEP)Os(NO)(SEt)•CH_2Cl_2[c]	6	1.994(10)	1.136(11)	172.7(8)	2.227(2)	112.8(4)	23
(OEP)Os(NO)($SC(Me)_2CH_2NC(O)Me$	6	1.781(5)	1.126(6)	176.8(5)	2.415(2)	121.8(2)	19
(TTP)Os(NO)(S-*i*-C_5H_{11})[a]	6	2.041(7)	1.086(10)	170.0(9)	2.209(3)	111.8(5)	12

[a]Disorder in ligand *trans* NO. [b]Two positions of NO ligand observed. [c]Disorder of the axial ligands across the face of the porphyrin required by an inversion center. [d]Crystal was reported to be weakly diffracting. [e]Isomeric disorder. [f]Second molecule from different crystallization. [g]Mixture of EtOH and ^{i}PrOH structures observed in the crystal. [h]Second crystal. [i]Conflicting values were provided for the ∠MNO angle in the publication (138°) and in the author's supplementary material (131.8(12)°). [j]Data taken from author's supporting information.[k]Low temperature (100 K) data collection. [l]Calculated by inputting x, y, z coordinates into the CrystalMaker software.

Table 1.3: Selected geometric parameters for nitrosyl Heme biomolecules.

Nitrosyl heme proteins	res (Å)	pdb	O.S.	Fe-N_{NO} (Å)	N-O (Å)	∠FeNO (°)	Fe-L_{ax} (Å)	∠FeXC (°)	ref
Cys-ligated									
prokaryotic NOS from *Bacillus subtilis*									
with L-Arg cofactor	1.9	1FC1	II	1.68	1.15[a]	132	2.31[a]	107[a]	61
with NOHA cofactor	1.9	2FBZ	II	1.86	1.16[a]	126	2.45[a]	104[a]	61
with NOHA cofactor	2.2	2FC2	III	1.69	1.14[a]	161	2.44[a]	111[a]	61
with NOHA cofactor	2.2	2FC2	III	2.29	1.13[a]	103	2.56[a]	106[a]	61
eukaryotic eNOS									
with L-Arg cofactor	2.0	1FOP	II	1.79	1.14	160	2.26	110[a]	60
				1.79	1.15	160	2.27	116[a]	60
with L-Arg + H_4B cofactors	2.3	1FOO	II	1.79	1.15	160	2.26	112[a]	60
	2.3	1FOO	II	1.79	1.13	160	2.27	111[a]	60
Fungal NOR									
WT	1.7	1CL6	III	1.63	1.16	161	2.31	115[a]	87
S286V mutant	1.7	1CMN	III	1.62	1.13	162	2.37	115[a]	87
S286T mutant	1.7	1CMJ	III	1.65	1.13	165	2.33	112[a]	87
His-ligated									
sw Mb	1.7		II	1.89	1.15	112	2.18	121[a, b], 130[a, c]	168
L29F/D122 sw Mb	1.9		II	1.86[a]	1.14[a]	127[a]	2.31[a]	125[a, b], 123[a, c]	168
hh Mb	1.30	2FRJ	II	1.87	1.20	144	2.08	126[a, b], 126[a, c]	170
hh Mb	1.30	2FRK	II	2.13	1.17	120	2.15	127[a, b], 125[a, c]	170
NP1 from *Rhodnius prolixus*	2.3	4NP1	II	2.06[a]	1.34[a]	119.5[a]	2.10[a]	123[a, b], 131[a, c]	235
			III	2.02[a]	1.32[a]	146[a]	2.0[a]	118[a, b], 135[a, c]	
NP2	1.45	1T68		1.93[a]	1.38[a]	134[a]	2.10[a]	124[a, b], 128[a, b]	236

Nitrosyl heme proteins	res (Å)	pdb	O.S.	Fe-N_{NO} (Å)	N-O (Å)	∠FeNO (°)	Fe-L_{ax} (Å)	∠FeXC (°)	ref
NP4 from *Rhodnius proxilus*									
WT (pH 7.4)	1.08	1X8N	II	1.74(2)	1.20(2)	143.8(1.6)	2.06(1)	127[a, b, c], 126[a, c]	237
WT (pH 5.6)	1.01	1X8O	III	1.69(1)	1.09(1)	159.1(1.1)	1.994(7)	126[a, b, c], 127[a, c]	237
D129A/L130A mutant	1.0	1SXX	III	1.60(2)	1.35[a]	155(2)	2.05[a]	126[a, b, c], 125[a, c]	238
T121V mutant	1.0	1SY1	III	1.62(2)	1.29[a]	158(2)	2.03[a]	125[a, b, c], 126[a, c]	238
D30N mutant	1.0	1SY3	II	1.78(2)	1.38[a]	132(2)	2.06[a]	126[a, b, c], 125[a, c]	238
D30A mutant	1.05	1SXW	II	1.71(3)	1.35[a]	139(2)	2.09[a]	125[a, b, c], 126[a, c]	238
HO from *Neisseriae meningitides*	1.75	1P3U	II	1.58 [a]	1.17 [a]	147 [a]	2.13 [a]	128[a, b, c], 123[a, c]	239
HO-1 from rat	1.7	1J02	II	2.10 [a]	1.14 [a]	125 [a]	2.17 [a]	128[a, b, c], 122[a, c]	240
Human HO-1									
WT	1.55	1OZW	II	1.64 [a]	1.14 [a]	138 [a]	2.12 [a]	123[a, b, c], 126[a, c]	241
D140A mutant	2.59	1OZL	II	1.49 [a]	1.16 [a]	148 [a]	2.12 [a]	127[a, b, c], 123[a, c]	241
Verdoheme	2.10	1TWR		1.83 [a]	1.15 [a]	150.9 [a]	2.54 [a]	89[a, b], 155[a, c]	242
				1.98 [a]	1.16 [a]	150.4 [a]	2.36 [a]	100[a, b, c], 145[a, c]	
Lupin legHb	1.8	1GDL	II	1.97 [a]	1.35 [a]	145 [a]	2.19 [a]	118[a, b, c], 133[a, c]	243
FixL from *Bradyrhizobium japonicum*	2.5	1DP8	II	1.76 [a]	1.14 [a]	154 [a]	2.10 [a]	124[a, b, c], 127[a, c]	244
cyt *c'* from *Alcaligenes xylosoxidans*	1.35	1E85	II	2.03 [a]	1.16 [a]	125 [a]	5-coor		245
				1.92 [a]	1.16 [a]	132 [a]			
cyt cd_1 NiR from *Paracoccus pantotropha*	1.8	1AOM	II	2.0	1.37 [a]	128 [a]	1.99 [a]	116[a, b, c], 138[a, c]	225
cyt cd_1 from *Pseudomonas*	2.65	1NNO	II	1.80	1.15	140 [a]	2.04 [a]	124[a, b, c], 124[a, c]	228

Nitrosyl heme proteins	res (Å)	pdb	O.S.	Fe-N_{NO} (Å)	N-O (Å)	∠FeNO (°)	Fe-L_{ax} (Å)	∠FeXC (°)	ref
aeruginosa									
cyt *c* peroxidase from yeast	1.85			1.82		125, 135	2.04		246
cyt *c* from *Rhodobacter sphaeroides*	2.20	1DW2	II	1.76 [a]	1.43 [a]	112 [a]	2.23 [a]	123[a, b], 130[a, c]	247
				1.83 [a]	1.37 [a]	112 [a]	2.16 [a]	126[a, b], 125[a, c]	247
Horse Hb	2.8			1.74	1.11	~145			248
Hb (βcysSNOH)		1BUW							
α heme	1.8		II	1.75	1.13	131	2.28	125[a, b], 125[a, c]	249
β heme	1.8		II	1.74	1.11	123	2.28	127[a, b], 124[a, c]	249
T-state human Hb		1RPS							
α heme	2.15		II	1.72	1.13	138	5-coor		250
β heme	2.15		II	1.75	1.15	128	2.25	123[a, b], 129[a, c]	250
T-state human Hb (βcysSOH)		1RQ4							
α heme	2.11			1.72[a]	1.15[a]	138	5-coor		250
β heme	2.11			1.75	1.15	128	2.19	121[a, b], 130[a, c]	250
T-state human Hb βW37E mutant		1RQA							
α heme	2.11			1.71	1.16	135	2.24	116[a, b], 135[a, c]	250
β heme	2.11			1.76	1.18	126	2.19	120[a, b], 130[a, c]	250

[a]Geometric data obtained from PDB. [b]Fe-N-C(α) angle. [c]Fe-N-C(β) angle

III. Abbreviations

HIm	imidazole
1-MeIm	1-methylimidazole
4-MeHIm	4-methylimidazole
4-MePip	4-methylpiperidine
5-MeHIm	5-methylimidazole
Cat	catalase
CcO	cytochrome *c* oxidase
CD	circular dichroism
cGMP	guanosine 3′,5′-cyclic monophosphate
$Cp_2Fe^{0/+}$	Ferrocene/ferrocenium couple
cyt	cytochrome
ENDOR	electron-nuclear double resonance
eNOS	endothelial nitric oxide synthase
EPR	electron paramagnetic resonance
EXAFS	extended X-ray absorption fine structure
FTIR	Fourier transform IR
H_4B	5,6,7,8-tetrahydrobiopterin
Hb	hemoglobin
hh	horse heart
HRP	Horseradish peroxidase
Im	imidazolate
iNOS	inducible nitric oxide synthase
Iz	indazole
Lb	leghemoglobin
Mb	myoglobin
MCD	magnetic circular dichroism
NACysMe	*N*-acetyl-L-cysteinate methyl ester
NADPH	reduced nicotinamide adenine denuleotide
NiR	nitrite reductace
nNOS	neuronal nitric oxide reductase
NO	nitric oxide
NOHA	N-hydroxyarginine
NOR	nitric oxide reductase
NOS	nitric oxide synthase
NOS	nitric oxide synthase
NP	nitrophorin
OEP	dianion of 2,3,7,8,12,13,17,18-octaethylporphyrin
Por	dianion of porphyrin
pdb	Protein data base
Pip	piperidine
PPDME	dianion of propotporphyrin IX
Prz	pyrazine
py	pyridine
Pz	Pyrazole
res	Resolution
RR	resonance Raman
sGC	soluble guanylyl cyclase
sw	sperm whale
T(*p*-OMe)PP	dianion of *meso*-tetrakis(*p*-methoxy-phenyl)porphyrin
TMP	dianion of *meso*-tetrakis(2,4,6-trimethylphenyl)porphyrin
To-F_2PP	Dianoin of tetrakis(*o*-diflurophenyl)porphyrin
TpivPP	dianion of *meso*-$\alpha,\alpha,\alpha,\alpha$-tetrakis-(*o*-pivalamidophenyl)porphyrin
T(atpa)pivPP	dianion of *meso*-$\alpha,\alpha,\alpha,\alpha$-[*o*[[*o*-[(acetylthio)methyl]phenoxy]acetamido]phenyl]tris(*o*-pivalamidophenyl)porphyrin

TPP	dianion of tetraphenylporphyrin
TTP	dianion of tetratolylporphyrin
UV	ultra violet
Vis	visible
WT	wild type
XAFS	X-ray absorption fine structure
XANES	X-ray absorption near-edge spectroscopy

IV. References

(1) Palmer, R. M. J.; Ferrige, A. G.; Moncada, S. *Nature (London)* **1987**, *327*, 524-526.

(2) Cheng, L.; Richter-Addo, G. B. In *The Porphyrin Handbook*; Guilard, R., Smith, K., Kadish, K. M., Eds.; Academic Press: New York, 2000; Vol. 4, p Ch. 33.

(3) Feltham, R. D.; Enemark, J. H. *Top. Stereochem.* **1981**, *12*, 155-215.

(4) Enemark, J. H.; Feltham, R. D. *Coord. Chem. Rev.* **1974**, *13*, 339-406.

(5) Nitrosyl adducts of ruthenium and osmium porphyrins have only been reported for the six-coordinate complexes.

(6) Xu, N.; Powell, D. R.; Cheng, L.; Richter-Addo, G. B. *Chem. Commun.* **2006**, 2030-2032.

(7) Yoshimura, T. *Inorg. Chim. Acta* **1982**, *57*, 99-105.

(8) Praneeth, V. K. K.; Haupt, E.; Lehnert, N. *J. Inorg. Biochem.* **2005**, *99*, 940-948.

(9) Suzuki, N.; Higuchi, T.; Urano, Y.; Kikuchi, K.; Uchida, T.; Mukai, M.; Kitagawa, T.; Nagano, T. *J. Am. Chem. Soc.* **2000**, *122*, 12059-12060.

(10) Franke, A.; Stochel, G.; Suzuki, N.; Higuchi, T.; Okuzono, K.; vanEldik, R. *J. Am. Chem. Soc.* **2005**, *127*, 5360-5375.

(11) Richter-Addo, G. B.; Wheeler, R. A.; Hixson, C. A.; Chen, L.; Khan, M. A.; Ellison, M. K.; Schulz, C. E.; Sheidt, W. R. *J. Amer. Chem. Soc.* **2001**, *123*, 6314-6326.

(12) Yi, G.-B.; Chen, L.; Khan, M. A.; Richter-Addo, G. B. *Inorg. Chem.* **1997**, *36*, 3876-3885.

(13) Mathews, W. R.; Kerr, S. W. *J Pharmacol Exp Ther* **1993**, *267*, 1529-1537.

(14) Upchurch, G. R. J.; Welch, G. N.; Loscalzo, J. *Adv. Pharmacol.* **1995**, *34*, 343.

(15) Lee, J., University of Oklahoma, 2002.

(16) Lee, J.; Chen, L.; West, A. H.; Richter-Addo, G. B. *Chem. Rev.* **2002**, *102*, 1019-1065.

(17) Cheng, L.; Powell, D. R.; Khan, M. A.; Richter-Addo, G. B. *Inorg. Chem.* **2001**, *40*, 125-133.

(18) Lee, J.; Yi, G.-B.; Khan, M. A.; Richter-Addo, G. B. *Inorg. Chem.* **1999**, *38*, 4578-4584.

(19) Lee, J.; Yi, G.-B.; Powell, D. R.; Khan, M. A.; Richter-Addo, G. B. *Can. J. Chem.* **2001**, *79*, 830-840.

(20) Yi, G.-B.; Khan, M. A.; Richter-Addo, G. B. *Chem. Commun.* **1996**, 2045-2046.
(21) Yi, G.-B.; Khan, M. A.; Powell, D. R.; Richter-Addo, G. B. *Inorg. Chem.* **1998**, *37*, 208-214.
(22) Chen, L.; Khan, M. A.; Richter-Addo, G. B. *Inorg. Chem.* **1998**, *37*, 533-540.
(23) Carter, S. M.; Lee, J.; Hixson, C. A.; Powell, D. R.; Wheeler, R. A.; Shaw, M. J.; Richter-Addo, G. B. *Dalton Trans.* **2006**, *10*, 1338-1346.
(24) Andreasen, L. V.; Lorkovic, I. M.; Richter-Addo, G. B.; Ford, P. C. *Nitric Oxide* **2002**, *6*, 228-235.
(25) Antipas, A.; Buchler, J. W.; Gouterman, M.; Smith, P. D. *J. Amer. Chem. Soc.* **1978**, *100*, 3015-3024.
(26) Andreasen, L. V.; Lorkovic, I. M.; Richter-Addo, G. B.; Ford, P. C. *Nitric Oxide* **2002**, *6*, 228-235.
(27) Formitchev, D. V.; Coppens, P.; Li, T.; Bagley, K. A.; Chen, L.; Richter-Addo, G. B. *Chem. Commun.* **1999**, 2013-2014.
(28) Cheng, L.; Novozhilova, I.; Kim, C.; Kovalevsky, A.; Bagley, K. A.; Coppens, P.; Richter-Addo, G. B. *J. Amer. Chem. Soc.* **2000**, *122*, 7142-7143.
(29) Bohle, D. S.; Goodson, P.; Smith, B. *Polyhedron* **1996**, *15*, 3147-3150.
(30) Richter-Addo, unpublished data
(31) Sono, M.; Stuehr, D. J.; Ikeda-Saito, M.; Dawson, J. H. *J. Biol. Chem.* **1995**, *270*, 19943-19948.
(32) Ortiz de Montellano, P. R.; Nishida, C.; Rodriguez-Crespo, I.; Gerber, N. *Drug Metabol. Disp.* **1998**, *26*, 1185-1189.
(33) White, K. A.; Marletta, M. A. *Biochemistry* **1992**, *31*, 6627-6631.
(34) Marletta, M. A. *J. Biol. Chem.* **1993**, *268*, 12231-12234.
(35) Masters, B. S. S.; McMillan, K.; Sheta, E. A.; Nishimura, J. S.; Roman, L. J.; Martasek, P. *FASEB J.* **1996**, *10*, 552-558.
(36) Sato, H.; Nomura, S.; Sagami, I.; Ito, O.; Daff, S.; Shimizu, T. *FEBS Lett.* **1998**, *430*, 377-380.
(37) Perry, J. M.; Marletta, M. A. *Proc. Natl. Acad. Sci. U.S.A.* **1998**, *95*, 11101-11106.
(38) Bredt, D. S.; Hwang, P. M.; Glatt, C. E.; Lowenstein, C.; Reed, R. R.; Snyder, S. H. *Nature (London)* **1991**, *351*, 714-718.
(39) Klatt, P.; Schmidt, K.; Mayer, B. *Biochem. J.* **1992**, *288*, 15-17.
(40) Pollock, J. S.; Forstermann, U.; Mitchell, J. A.; Warner, T. D.; Schmidt, H. H. H. W.; Nakane, M.; Murad, F. *Proc. Natl. Acad. Sci. U.S.A.* **1991**, *88*, 10480-10484.
(41) Förstermann, U.; Closs, E. I.; Pollock, J. S.; Nakane, M.; Schwarz, P.; Gath, I.; Kleinert, H. *Hypertension* **1994**, *23*, 1121-1131.
(42) Bredt, D. S.; Snyder, S. H. *Proc. Natl. Acad. Sci. U.S.A.* **1990**, *87*, 682-685.
(43) Pufahl, R. A.; Wishnok, J. S.; Marletta, M. A. *Biochemistry* **1995**, *34*, 1930-1941.
(44) Wu, G.; Morris, S. M., Jr. *Biochem. J.* **1998**, *336*, 1-17.
(45) Hurshman, A. R.; Marletta, M. A. *Biochemistry* **1995**, *34*, 5627-5634.

(46) Abu-Soud, H. M.; Ichimori, K.; Nakazawa, H.; Stuehr, D. J. *Biochemistry* **2001**, *40*, 6876-6881.
(47) Abu-Soud, H. M.; Wang, J.; Rousseau, D. L.; Fukuto, J. M.; Ignarro, L. J.; Stuehr, D. J. *J. Biol. Chem.* **1995**, *270*, 22997-23006.
(48) Abu-Soud, H. M.; Rousseau, D. L.; Stuehr, D. J. *J. Biol. Chem.* **1996**, *271*, 32515-32518.
(49) Wang, J.; Rousseau, D. L.; Abu-Soud, H. M.; Stuehr, D. J. *Proc. Natl. Acad. Sci. U.S.A.* **1994**, *91*, 10512-10516.
(50) Abu-Soud, H. M.; Wu, C.; Ghosh, D. K.; Stuehr, D. J. *Biochemistry* **1998**, *37*, 3777-3786.
(51) Griscavage, J. M.; Hobbs, A. J.; Ignarro, L. J. *Adv. Pharmacol.* **1995**, *34*, 215-234.
(52) Griscavage, J. M.; Rogers, N. E.; Sherman, M. P.; Ignarro, L. J. *J. Immunol.* **1993**, *151*, 6329-6337.
(53) Griscavage, J. M.; Fukuto, J. M.; Komori, Y.; Ignarro, L. J. *J. Biol. Chem.* **1994**, *269*, 21644-21649.
(54) Migita, C. T.; Salerno, J. C.; Masters, B. S. S.; Martasck, P.; McMillan, K.; Ikeda-Saito, M. *Biochemistry* **1997**, *36*, 10987-10992.
(55) Marletta, M. A. *J. Med. Chem.* **1994**, *37*, 1899-1907.
(56) Knowles, R. G.; Moncada, S. *Biochem. J.* **1994**, *298*, 249-258.
(57) Rosen, G. M.; Tsai, P.; Pou, S. *Chem. Rev.* **2002**, *102*, 1191-1199.
(58) Alderton, W. K.; Cooper, C. E.; Knowles, R. G. *Biochem. J.* **2001**, *357*, 593-615.
(59) Roman, L. J.; Martasek, P.; Masters, B. S. S. *Chem. Rev.* **2002**, *102*, 1179-1189.
(60) Li, H.; Raman, C. S.; Martasek, P.; Masters, B. S. S.; Poulos, T. L. *Biochemistry* **2001**, *40*, 5399-5406.
(61) Pant, K.; Crane, B. R. *Biochemistry* **2006**, *45*, 2537-2544.
(62) Li, D.; Hayden, E. Y.; Panda, K.; Stuehr, D. J.; Deng, H.; Rousseau, D. L.; Yeh, S.-R. *J. Biol. Chem.* **2006**, *281*, 8197-8204.
(63) Meunier, B.; de Visser, S. P.; Shaik, S. *Chem. Rev.* **2004**, *104*, 3947-3980.
(64) Punta, K. D.; Charreau, E. H.; Pignataro, O. P. *Endocrinology* **1996**, *137*, 5337-5343.
(65) Stadler, J.; Trockfeld, J.; Schmalix, W. A.; Brill, T.; Siewert, J. R.; Greim, H.; Doehmer, J. *Proc. Natl. Acad. Sci. U.S.A.* **1994**, *91*, 3559-3563.
(66) Khatsenko, O. G.; Gross, S. S.; Rifkind, A. B.; Vane, J. R. *Proc. Natl. Acad. Sci. U.S.A.* **1993**, *90*, 11147-11151.
(67) Alonso-Galicia, M.; Drummond, H. A.; Reddy, K. K.; Falck, J. R.; Roman, R. J. *Hypertension* **1997**, *29*, 320-325.
(68) Sono, M.; Dawson, J. H. *J. Biol. Chem.* **1982**, *257*, 5496-5502, and references therein.
(69) Sono, M.; Eble, K. S.; Dawson, J. H.; Hager, L. P. *J. Biol. Chem.* **1985**, *260*, 15530-15535.
(70) Hu, S.; Kincaid, J. R. *J. Am. Chem. Soc.* **1991**, *113*, 9760-9766.
(71) Hu, S.; Kincaid, J. R. *J. Am. Chem. Soc.* **1991**, *113*, 2843-2853.

(72) Tsubaki, M.; Hiwatashi, A.; Ichikawa, Y.; Fujimoto, Y.; Ikekawa, N.; Hori, H. *Biochemistry* **1988**, *27*, 4856-4862.
(73) Tsubaki, M.; Hiwatashi, A.; Ichikawa, Y.; Hori, H. *Biochemistry* **1987**, *26*, 4527-4534.
(74) Hori, H.; Masuya, F.; Tsubaki, M.; Yoshikawa, S.; Ichikawa, Y. *J. Biol. Chem.* **1992**, *267*, 18377-18381.
(75) Tsubaki, M.; Ichikawa, Y.; Fujimoto, Y.; Yu, N.-T.; Hori, H. *Biochemistry* **1990**, *29*, 8805-8812.
(76) Masuya, F.; Tsubaki, M.; Makino, R.; Hori, H. *J. Biochem.* **1994**, *116*, 1146-1152.
(77) Hill, H. A. O.; Röder, A.; Williams, R. J. P. *Biochem. J.* **1969**, *115*, 59P-60P.
(78) O'Keeffe, D. H.; Ebel, R. E.; Peterson, J. A. *J. Biol. Chem.* **1978**, *253*, 3509-3516.
(79) Ebel, R. E.; O'Keeffe, D. H.; Peterson, J. A. *FEBS Lett.* **1975**, *55*, 198-201.
(80) Nakano, R.; Sato, H.; Watanabe, A.; Ito, O.; Shimizu, T. *J. Biol. Chem.* **1996**, *271*, 8570-8574.
(81) Obayashi, E.; Tsukamoto, K.; Adachi, S.-i.; Takahashi, S.; Nomura, M.; Iizuka, T.; Shoun, H.; Shiro, Y. *J. Am. Chem. Soc.* **1997**, *119*, 7807-7816.
(82) Shiro, Y.; Fujii, M.; Isogai, Y.; Adachi, S.-i.; Iuzuka, T.; Obayashi, E.; Makino, R.; Nakahara, K.; Shoun, H. *Biochemistry* **1995**, *34*, 9052-9058.
(83) Nakahara, K.; Tanimoto, T.; Hatano, K.-I.; Usuda, K.; Shoun, H. *J. Biol. Chem.* **1993**, *268*, 8350-8355.
(84) Shiro, Y.; Fujii, M.; Iizuka, T.; Adachi, S.-I.; Tsukamoto, K.; Nakahara, K.; Shoun, H. *J. Biol. Chem.* **1995**, *270*, 1617-1623.
(85) Obayashi, E.; Takahashi, S.; Shiro, Y. *J. Am. Chem. Soc.* **1998**, *120*, 12964-12965.
(86) Nicolai Lehnert, V. K. K. P. F. P. *J. Comput. Chem.* **2006**, *27*, 1338-1351.
(87) Shimizu, H.; Obayashi, E.; Gomi, Y.; Arakawa, H.; Park, S.-Y.; Nakamura, H.; Adachi, S.-i.; Shoun, H.; Shiro, Y. *J. Biol. Chem.* **2000**, *275*, 4816-4826.
(88) Omura, T. *Biochemical and Biophysical Research Communications* **2005**, *338*, 404-409.
(89) Hu, S.; Kincaid, J. R. *J. Biol. Chem.* **1993**, *268*, 6189-6193.
(90) Chiang, R.; Makino, R.; Spomer, W. E.; Hager, L. P. *Biochemistry* **1975**, *14*, 4166-4171.
(91) Sono, M.; Dawson, J. H.; Hall, K.; Hager, L. P. *Biochemistry* **1986**, *25*, 347-356.
(92) Anderson, J. L. R.; Chapman, S. *Dalton Transactions* **2005**, 13-24.
(93) Grzegorz, B. *Superoxide Dismutases and Catalase*, 2005.
(94) Keilin, D.; Hartree, E. F. *Nature (London)* **1943**, *152*, 626.
(95) Hoshino, M.; Ozawa, K.; Seki, H.; Ford, P. C. *J. Am. Chem. Soc.* **1993**, *115*, 9568-9575.
(96) Brown, G. C. *Eur. J. Biochem.* **1995**, *232*, 188-191.

(97) Kalyanaraman, B.; Janzen, E. G.; Mason, R. P. *J. Biol. Chem.* **1985**, *260*, 4003-4006.
(98) Craven, P. A.; DeRubertis, F. R.; Pratt, D. W. *J. Biol. Chem.* **1979**, *254*, 8213-8222.
(99) Lemberg, R.; Foulkes, E. C. *Nature (London)* **1948**, *161*, 131-132.
(100) Keilin, D.; Hartree, E. F. *Proc. R. Soc. London, Ser. B* **1936**, *121*, 173-191.
(101) Keilin, D.; Hartree, E. F. *Nature (London)* **1954**, *173*, 720-723.
(102) Keilin, D.; Hartree, E. F. *Biochem. J.* **1955**, *60*, 310-325.
(103) Nicholls, P. *Biochem. J.* **1964**, *90*, 331-343.
(104) Foulkes, E. C.; Lemberg, R. *Enzymologia* **1949**, *13*, 302-312.
(105) Huang, J.; Kim-Shapiro, D. B.; King, S. B. *J. Med. Chem.* **2004**, *47*, 3495-3501.
(106) Stong, J. D.; Burke, J. M.; Daly, P.; Wright, P.; Spiro, T. G. *J. Am. Chem. Soc.* **1980**, *102*, 5815-5819.
(107) Bracete, A. M.; Kadkhodayan, S.; Sono, M.; Huff, A. M.; Zhuang, C.; Cooper, D. K.; Smith, K. M.; Chang, C. K.; Dawson, J. H. *Inorg. Chem.* **1994**, *33*, 5042-5049.
(108) Hüttermann, J.; Burgard, C.; Kappl, R. *J. Chem. Soc., Faraday Trans.* **1994**, *90*, 3077-3087.
(109) Kon, H.; Kataoka, N. *Biochemistry* **1969**, *8*, 4757-4762.
(110) Maxwell, J. C.; Caughey, W. S. *Biochemistry* **1976**, *15*, 388-396.
(111) Wayland, B. B.; Olson, L. W. *J. Am. Chem. Soc.* **1974**, *96*, 6037-6041.
(112) Morse, R. H.; Chan, S. I. *J. Biol. Chem.* **1980**, *255*, 7876-7882.
(113) Yoshimura, T. *Inorg. Chem.* **1986**, *25*, 688-691.
(114) Suzuki, S.; Yoshimura, T.; Nakahara, A.; Iwasaki, H.; Shidara, S.; Matsubara, T. *Inorg. Chem.* **1987**, *26*, 1006-1008.
(115) Yoshimura, T. *Bull. Chem. Soc. Jpn.* **1983**, *56*, 2527-2528.
(116) Yoshimura, T. *Bull. Chem. Soc. Jpn.* **1987**, *60*, 1375-1378.
(117) Yoshimura, T. *Bull. Chem. Soc. Jpn.* **1991**, *64*, 2819-2828.
(118) Yoshimura, T. *Bull. Chem. Soc. Jpn.* **1990**, *63*, 3689-3691.
(119) Yoshimura, T.; Ozaki, T. *Arch. Biochem. Biophys.* **1984**, *229*, 126-135.
(120) Yoshimura, T.; Ozaki, T.; Shintani, Y.; Watanabe, H. *Arch. Biochem. Biophys.* **1979**, *193*, 301-313.
(121) Yoshimura, T. *Arch. Biochem. Biophys.* **1983**, *220*, 167-178.
(122) Yoshimura, T. *Inorg. Chim. Acta* **1980**, *46*, 69-76.
(123) Choi, I.-K.; Ryan, M. D. *Inorg. Chim. Acta* **1988**, *153*, 25-30.
(124) Ohba, Y.; Yokoyama, Y.; Iwaizumi, M. *Inorg. Chim. Acta* **1983**, *78*, L57-L59.
(125) Addison, A. W.; Stephanos, J. J. *Biochemistry* **1986**, *25*, 4104-4113.
(126) Ellison, M. K.; Scheidt, W. R. *J. Amer. Chem. Soc.* **1999**, *121*, 5210-5219.
(127) Praneeth, V. K. K.; Nather, C.; Peters, G.; Lehnert, N. *Inorg. Chem.* **2006**, *45*, 2795-2811.

(128) Praneeth, V. K. K.; Neese, F.; Lehnert, N. *Inorg. Chem.* **2005**, *44*, 2570-2572.
(129) Bohle, D. S.; Hung, C.-H. *J. Amer. Chem. Soc.* **1995**, *117*, 9584-9585.
(130) Wyllie, G. R. A.; Scheidt, W. R. *Chem. Rev.* **2002**, *102*, 1067-1090.
(131) Piciulo, P. L.; Rupprecht, G.; Scheidt, W. R. *J. Amer. Chem. Soc.* **1974**, *96*, 5293-5295.
(132) Scheidt, W. R.; Piciulo, P. L. *J. Amer. Chem. Soc.* **1976**, *98*, 1913-1919.
(133) Hoshino, M.; Ozawa, K.; Seki, H.; Ford, P. C. *J. Amer. Chem. Soc.* **1993**, *115*, 9568-9575.
(134) Laverman, L. E.; Wanat, A.; Oszajca, J.; Stochel, G.; Ford, P. C.; van Eldik, R. *J. Am. Chem. Soc.* **2001**, *123*, 285-293.
(135) Safo, M. K.; Scheidt, W. R.; Gupta, G. P. *Inorg. Chem.* **1990**, *29*, 626-633.
(136) Hori, H.; Ikeda-Saito, M.; Leigh, J. S., Jr.; Yonetani, T. *Biochemistry* **1982**, *21*, 1431-1437.
(137) Ikeda-Saito, M.; Dou, Y.; Yonetani, T.; Olson, J. S.; Li, T.; Regan, R.; Gibson, Q. H. *J. Biol. Chem.* **1993**, *268*, 6855-6857.
(138) Parthasarathi, N.; Spiro, T. G. *Inorg. Chem.* **1987**, *26*, 2280-2282.
(139) Trittelvitz, E.; Sick, H.; Gersonde, K. *Eur. J. Biochem.* **1972**, *31*, 578-584.
(140) Hoshino, M.; Maeda, M.; Konishi, R.; Seki, H.; Ford, P. C. *J. Am. Chem. Soc.* **1996**, *118*, 5702-5707.
(141) Andersen, H. J.; Skibsted, L. H. *J. Agric. Food Chem.* **1992**, *40*, 1741-1750.
(142) Sharma, V. S.; Isaacson, R. A.; John, M. E.; Waterman, M. R.; Chevion, M. *Biochemistry* **1983**, *22*, 3897-3902.
(143) Olson, J. S.; Phillips, G. N., Jr. *J. Biol. Chem.* **1996**, *271*, 17593-17596.
(144) Blyth, D. J.; Aylott, J. W.; Richardson, D. J.; Russell, D. A. *Analyst* **1995**, *120*, 2725-2730.
(145) Upmacis, R. K.; Hajjar, D. P.; Chait, B. T.; Mirza, U. A. *J. Am. Chem. Soc.* **1997**, *119*, 10424-10429.
(146) Rich, A. M.; Armstrong, R. S.; Ellis, P. J.; Lay, P. A. *J. Am. Chem. Soc.* **1998**, *120*, 10827-10836.
(147) Benko, B.; Yu, N.-T. *Proc. Natl. Acad. Sci. U.S.A.* **1983**, *80*, 7042-7046.
(148) Walters, M. A.; Spiro, T. G. *Biochemistry* **1982**, *21*, 6989-6995.
(149) Tsubaki, M.; Yu, N.-T. *Biochemistry* **1982**, *21*, 1140-1144.
(150) Miller, L. M.; Pedraza, A. J.; Chance, M. R. *Biochemistry* **1997**, *36*, 12199-12207.
(151) Höhn, M.; Hütterman, J.; Chien, J. C. W.; Dickinson, L. C. *J. Am. Chem. Soc.* **1983**, *105*, 109-115.
(152) DiFeo, T. J.; Addison, A. W.; Stephanos, J. J. *Biochem. J.* **1990**, *269*, 739-747.

(153) Dou, Y.; Admiraal, S. J.; Ikeda-Saito, M.; Krzywda, S.; Wilkinson, A. J.; Li, T.; Olson, J. S.; Prince, R. C.; Pickering, I. J.; George, G. N. *J. Biol. Chem.* **1995**, *270*, 15993-16001.
(154) Duprat, A. F.; Traylor, T. G.; Wu, G.-Z.; Coletta, M.; Sharma, V. S.; Walda, K. N.; Magde, D. *Biochemistry* **1995**, *34*, 2634-2644.
(155) Hori, H.; Ikeda-Saito, M.; Lang, G.; Yonetani, T. *J. Biol. Chem.* **1990**, *265*, 15028-15033.
(156) Ikeda-Saito, M.; Lutz, R. S.; Shelley, D. A.; McKelvey, E. J.; Mattera, R.; Hori, H. *J. Biol. Chem.* **1991**, *266*, 23641-23647.
(157) Ascenzi, P.; Giacometti, G. M.; Antonini, E.; Rotillo, G.; Brunori, M. *J. Biol. Chem.* **1981**, *256*, 5383-5386.
(158) Flores, M.; Wajnberg, E.; Bemski, G. *Biophys. J.* **1997**, *73*, 3225-3229.
(159) Bartnicki, D. E.; Mizukami, H.; Romero-Herrera, A. E. *J. Biol. Chem.* **1983**, *258*, 1599-1602.
(160) Muench, P. J.; Stapleton, H. J. *J. Chem. Phys.* **1985**, *82*, 2828-2830.
(161) Kamarei, A. R.; Karel, M. *Int. J. Radiat. Biol.* **1983**, *44*, 135-142.
(162) Hori, H.; Ikeda-Saito, M.; Yonetani, T. *J. Biol. Chem.* **1981**, *256*, 7849-7855.
(163) Dickinson, L. C.; Chien, J. C. W. *J. Am. Chem. Soc.* **1971**, *93*, 5036-5040.
(164) Decatur, S. M.; Franzen, S.; DePillis, G. D.; Dyer, R. B.; Woodruff, W. H.; Boxer, S. G. *Biochemistry* **1996**, *35*, 4939-4944.
(165) Moller, J. K. S.; Skibsted, L. H. *Chem. Rev.* **2002**, *102*, 1167-1178.
(166) Flogel, U.; Merx, M. W.; Godecke, A.; Decking, U. K. M.; Schrader, J. *PNAS* **2001**, *98*, 735-740.
(167) Moller, J. K. S.; Skibsted, L. H. *Chem. Rev.* **2002**, *102*, 1167-1178.
(168) Eric Allen Brucker, J. S. O. M. I.-S. G. N. P., Jr. *Proteins: Struct., Funct., Genet.* **1998**, *30*, 352-356.
(169) Daniel M. Copeland, A. H. W. G. B. R.-A. *Proteins: Struct., Funct., Genet.* **2003**, *53*, 182-192.
(170) Copeland, D. M.; Soares, A. S.; West, A. H.; Richter-Addo, G. B. *J. Inorg. Biochem.* **2006**, *100*, 1413-1425.
(171) Ferguson-Miller, S.; Babcock, G. T. *Chem. Rev.* **1996**, *96*, 2889-2907.
(172) Namslauer, A.; Brzezinski, P. *FEBS Letters* **2004**, *567*, 103-110.
(173) Popović, D. M.; Quenneville, J.; Stuchebrukhov, A. A. *J. Phys. Chem., B* **2005**, *109*, 3616-3626.
(174) Scholes, C. P.; Janakiraman, R.; Taylor, H.; King, T. E. *Biophys. J.* **1984**, *45*, 1027-1030.
(175) Malmström, B. G. *Chem. Rev.* **1990**, *90*, 1247-1260.
(176) Brudvig, G. W.; Stevens, T. H.; Chan, S. I. *Biochemistry* **1980**, *19*, 5275-5285.
(177) Fujiwara, T.; Fukumori, Y. *J. Bacteriol.* **1996**, *178*, 1866-1871.
(178) Blair, D. F.; Bocian, D. F.; Babcock, G. T.; Chan, S. I. *Biochemistry* **1982**, *21*, 6928-6935.

(179) Torres, J.; Cooper, C. E.; Wilson, M. T. *J. Biol. Chem.* **1998**, *273*, 8756-8766.
(180) Stevens, T. H.; Brudvig, G. W.; Bocian, D. F.; Chan, S. I. *Proc. Natl. Acad. Sci. U.S.A.* **1979**, *76*, 3320-3324.
(181) Yoshida, S.; Hori, H.; Orii, Y. *J. Biochem.* **1980**, *88*, 1623-1627.
(182) LoBrutto, R.; Wei, Y.-H.; Yoshida, S.; Camp, H. L. V.; Scholes, C. P.; King, T. E. *Biophys. J.* **1984**, *45*, 473-479.
(183) Rousseau, D. L.; Singh, S.; Ching, Y.-c.; Sassaroli, M. *J. Biol. Chem.* **1988**, *263*, 5681-5685.
(184) Ohnishi, T.; LoBrutto, R.; Salerno, J. C.; Bruckner, R. C.; Frey, T. G. *J. Biol. Chem.* **1982**, *257*, 14821-14825.
(185) Mascarenhas, R.; Wei, Y.-H.; Scholes, C. P.; King, T. E. *J. Biol. Chem.* **1983**, *258*, 5348-5351.
(186) LoBrutto, R.; Wei, Y.-H.; Mascarenhas, R.; Scholes, C. P.; King, T. E. *J. Biol. Chem.* **1983**, *258*, 7437-7448.
(187) Sharpe, M. A.; Cooper, C. E. *J. Biol. Chem.* **1998**, *273*, 30961-30972.
(188) Giuffrè, A.; Sarti, P.; D'Itri, E.; Buse, G.; Soulimane, T.; Brunori, M. *J. Biol. Chem.* **1996**, *271*, 33404-33408.
(189) Torres, J.; Darley-Usmar, V.; Wilson, M. T. *Biochem. J.* **1995**, *312*, 169-173.
(190) Cooper, C. E.; Torres, J.; Sharpe, M. A.; Wilson, M. T. *FEBS Lett.* **1997**, *414*, 281-284.
(191) Stevens, T. H.; Bocian, D. F.; Chan, S. I. *FEBS Lett.* **1979**, *97*, 314-316.
(192) Cleeter, M. W. J.; Cooper, J. M.; Darley-Usmar, V. M.; Moncada, S.; Schapira, A. H. V. *FEBS Lett.* **1994**, *345*, 50-54.
(193) Brown, G. C. *FEBS Lett.* **1995**, *369*, 136-139.
(194) Brown, G. C.; Cooper, C. E. *FEBS Lett.* **1994**, *356*, 295-298.
(195) Borutaitė, V.; Brown, G. C. *Biochem. J.* **1996**, *315*, 295-299.
(196) Giuffrè, A.; Stubauer, G.; Brunori, M.; Sarti, P.; Torres, J.; Wilson, M. T. *J. Biol. Chem.* **1998**, *273*, 32475-32478.
(197) Brown, G. C.; Foxwell, N.; Moncada, S. *FEBS Lett.* **1998**, *439*, 321-324.
(198) Giulivi, C. *Biochem. J.* **1998**, *332*, 673-679.
(199) Torres, J.; Cooper, C. E.; Sharpe, M.; Wilson, M. T. *J. Bioenerg. Biomem.* **1998**, *30*, 63-69.
(200) Clementi, E.; Nisoli, E. *Comp. Biochem. Physiol., A* **2005**, *142*, 102-110.
(201) Mason, M. G.; Nicholls, P.; Wilson, M. T.; Cooper, C. E. *Proc. Natl. Acad. Sci. U.S.A.* **2006**, *103*, 708-713.
(202) Stone, J. R.; Marletta, M. A. *Biochemistry* **1995**, *34*, 14668-14674.
(203) Stone, J. R.; Marletta, M. A. *Biochemistry* **1996**, *35*, 1093-1099.
(204) Dierks, E. A.; Burstyn, J. N. *Arch. Biochem. Biophys.* **1998**, *351*, 1-7.
(205) Kim, S.; Deinum, G.; Gardner, M. T.; Marletta, M. A.; Babcock, G. T. *J. Am. Chem. Soc.* **1996**, *118*, 8769-8770.

(206) Dierks, E. A.; Hu, S.; Vogel, K. M.; Yu, A. E.; Spiro, T. G.; Burstyn, J. N. *J. Am. Chem. Soc.* **1997**, *119*, 7316-7323.
(207) Yu, A. E.; Hu, S.; Spiro, T. G.; Burstyn, J. N. *J. Am. Chem. Soc.* **1994**, *116*, 4117-4118.
(208) Brandish, P. E.; Buechler, W.; Marletta, M. A. *Biochemistry* **1998**, *37*, 16898-16907.
(209) Kharitonov, V. G.; Sharma, V. S.; Magde, D.; Koesling, D. *Biochemistry* **1997**, *36*, 6814-6818.
(210) Zhao, Y.; Hoganson, C.; Babcock, G. T.; Marletta, M. A. *Biochemistry* **1998**, *37*, 12458-12464.
(211) Stone, J. R.; Sands, R. H.; Dunham, W. R.; Marletta, M. A. *Biochemistry* **1996**, *35*, 3258-3262.
(212) Stone, J. R.; Marletta, M. A. *Biochemistry* **1994**, *33*, 5636-5640.
(213) Fan, B.; Gupta, G.; Danziger, R. S.; Friedman, J. M.; Rousseau, D. L. *Biochemistry* **1998**, *37*, 1178-1184.
(214) Burstyn, J. N.; Yu, A. E.; Dierks, E. A.; Hawkins, B. K.; Dawson, J. H. *Biochemistry* **1995**, *34*, 5896-5903.
(215) Tomita, T.; Ogura, T.; Tsuyama, S.; Imai, Y.; Kitagawa, T. *Biochemistry* **1997**, *36*, 10155-10160.
(216) Craven, P. A.; DeRubertis, F. R. *J. Biol. Chem.* **1978**, *253*, 8433-8443.
(217) Deinum, G.; Stone, J. R.; Babcock, G. T.; Marletta, M. A. *Biochemistry* **1996**, *35*, 1540-1547.
(218) Silvestrini, M. C.; Colosimo, A.; Brunori, M.; Walsh, T. A.; Barber, D.; Greenwood, C. *Biochem. J.* **1979**, *183*, 701-709.
(219) Johnson, M. K.; Thomson, A. J.; Walsh, T. A.; Barber, D.; Greenwood, C. *Biochem. J.* **1980**, *189*, 285-294.
(220) Costa, C.; Moura, J. J. G.; Moura, I.; Liu, M. Y.; Peck, H. D., Jr.; LeGall, J.; Wang, Y.; Huynh, B. H. *J. Biol. Chem.* **1990**, *265*, 14382-14387.
(221) Garber, E. A. E.; Hollocher, T. C. *J. Biol. Chem.* **1982**, *257*, 8091-8097.
(222) Aerssens, E.; Tiedje, J. M.; Averill, B. A. *J. Biol. Chem.* **1986**, *261*, 9652-9656.
(223) Huynh, B. H.; Lui, M. C.; Moura, J. J. G.; Moura, I.; Ljungdahl, P. O.; Münck, E.; Payne, W. J.; Peck, H. D., Jr.; DerVartanian, D. V.; LeGall, J. *J. Biol. Chem.* **1982**, *257*, 9576-9581.
(224) Muhoberac, B. B.; Wharton, D. C. *J. Biol. Chem.* **1980**, *255*, 8437-8442.
(225) Williams, P. A.; Fulop, V.; Garman, E. F.; Saunders, N. F. W.; Ferguson, S. J.; Hajdu, J. *Nature (London)* **1997**, *389*, 406-412.
(226) Fülöp, V.; Moir, J. W. B.; Ferguson, S. J.; Hajdu, J. *Cell* **1995**, *81*, 369-377.
(227) Averill, B. A. *Chem. Rev.* **1996**, *96*, 2951-2964.
(228) Nurizzo, D.; Cutruzzola, F.; Arese, M.; Bourgeois, D.; Brunori, M.; Cambillau, C.; Tegoni, M. *Biochemistry* **1998**, *37*, 13987-13996.
(229) Sakurai, N.; Sakurai, T. *Biochemistry* **1997**, *36*, 13809-13815.

(230) Cheesman, M. R.; Zumft, W. G.; Thomson, A. J. *Biochemistry* **1998**, *37*, 3994-4000.
(231) Moënne-Loccoz, P.; de_Vries, S. *J. Am. Chem. Soc.* **1998**, *120*, 5147-5152.
(232) Hendriks, J.; Warne, A.; Gohlke, U.; Haltia, T.; Ludovici, C.; Lübben, M.; Saraste, M. *Biochemistry* **1998**, *37*, 13102-13109.
(233) Wyllie, G. R. A.; Schulz, C. E.; Scheidt, W. R. *Inorg. Chem.* **2003**, *42*, 5722-5734.
(234) Scheidt, W. R.; Brinegar, A. C.; Ferro, E. B.; Kirner, J. F. *J. Amer. Chem. Soc.* **1977**, *99*, 7315-7322.
(235) Ding, X. D.; Weichsel, A.; Andersen, J. F.; Shokhireva, T. K.; Balfour, C.; Pierik, A. J.; Averill, B. A.; Montfort, W. R.; Walker, F. A. *J. Am. Chem. Soc.* **1999**, *121*, 128-138.
(236) Weichsel, A., Montfort, W.R. structure deposited with PDB (1T68).
(237) Kondrashov, D. A.; Roberts, S. A.; Weichsel, A.; Montfort, W. R. *Biochemistry* **2004**, *43*, 13637-13647.
(238) Maes, E. M.; Weichsel, A.; Andersen, J. F.; Shepley, D.; Montfort, W. R. *Biochemistry* **2004**, *43*, 6679-6690.
(239) Friedman, J.; Lad, L.; Deshmukh, R.; Li, H.; Wilks, A.; Poulos, T. L. *J. Biol. Chem.* **2003**, *278*, 34654-34659.
(240) Sugishima, M.; Sakamoto, H.; Noguchi, M.; Fukuyama, K. *Biochemistry* **2003**, *42*, 9898-9905.
(241) Lad, L.; Wang, J.; Li, H.; Friedman, J.; Bhaskar, B.; Ortiz de Montellano, P. R.; Poulos, T. L. *J. Mol. Biol.* **2003**, *330*, 527-538.
(242) Lad, L.; Ortiz de Montellano, P. R.; Poulos, T. L. *J. Inorg. Biochem.* **2004**, *98*, 1686-1695.
(243) Harutyunyan, E. H.; Safonova, T. N.; Kuranova, I. P.; Popov, A. N.; Teplyakov, A. V.; Obmolova, G. V.; Vainshtein, B. K.; Dodson, G. G.; Wilson, J. C. *J. Mol. Biol.* **1996**, *264*, 152-161.
(244) Gong, W.; Hao, B.; Chan, M. K. *Biochemistry* **2000**, *39*, 3955-3962.
(245) Lawson, D. M.; Stevenson, C. E. M.; Andrew, C. R.; Eady, R. R. *EMBO Journal* **2000**, *19*, 5661-5671.
(246) Edwards, S. L.; Kraut, J.; Poulos, T. L. *Biochemistry* **1988**, *27*, 8074-8081.
(247) Leys, D.; Backers, K.; Meyer, T. E.; Hagen, W. R.; Cusanovich, M. A.; Van Beeumen, J. J. *J. Biol. Chem.* **2000**, *275*, 16050-16056.
(248) Deatherage, J. F.; Moffat, K. *J. Mol. Biol.* **1979**, *134*, 401-417.
(249) Chan, N.-L.; Rogers, P. H.; Arnone, A. *Biochemistry* **1998**, *37*, 16459-16464.
(250) Chan, N. L.; Kavanaugh, J. S.; Rogers, P. H.; Arnone, A. *Biochemistry* **2004**, *43*, 118-132.

Chapter 2. Synthesis and fiber-optic infrared reflectance spectroelectrochemical studies of osmium and ruthenium nitrosyl porphyrins containing alkoxide and thiolate ligands*

Introduction

Nitric oxide (NO) is known to interact with metals. Several review articles[1] and a book[2] have been published containing details of the preparation, characterization, and reaction chemistry of metal-NO compounds. NO is important in bioinorganic chemistry; it reacts with many heme-containing biomolecules[3,4] and iron sulfur clusters[5] to result in the formation of Fe-NO bonds. Related reactions with the cobalt-containing vitamin B_{12} have also been studied.[6,7] We are interested in the reactions of NO with group 8 synthetic metalloporphyrins as models for the interactions of NO with heme. Buchler and Smith were the first to report the syntheses of the osmium nitrosyl porphyrins (OEP)Os(NO)X (X = OMe, F).[8] Other neutral (por)Os(NO)X compounds (X = halide,[9] alkoxide,[10,11] thiolate,[11,12] ONO,[13] $OClO_3$,[14] O_2PF_2,[11] alkyl/aryl[9]) have since been described, including the μ-oxo dimer $[(OEP)Os(NO)]_2(\mu\text{-}O)$.[9] Several related ruthenium compounds (por)Ru(NO)X (X = halide, O-donor, S-donor, N-donor, C-donor) have also been reported.[14-31]

---

* This Chapter was taken in part from "Fiber-optic infrared reflectance spectroelectrochemical studies of osmium and ruthenium nitrosyl porphyrins containing alkoxide and thiolate ligands." Carter, S.M.; Lee, J.; Hixson, C.A.; Powell, D.R.; Wheeler, R.A.; Shaw, M.J.; Richter-Addo, G.B. *Dalton Trans*. **2006**, 10, 1338-1346, with permission from RSC Publishing at http://www.rsc.org/AboutUs/Copyright/RightsRetainedbyJournalsauthors.asp in August 2006.

As part of our studies on the class of Os and Ru nitrosyl porphyrins containing alkoxide and thiolate *trans* ligands, we investigated the redox behavior of a representative set of these species. Infrared spectroelectrochemistry[32] is a very useful tool for identifying the products resulting from electron removal or addition in metal nitrosyl and carbonyl compounds. We recently developed a relatively simple apparatus for infrared spectroelectrochemistry based on fiber-optic infrared reflectance spectroscopy,[33] and we have also extended this methodology to low-temperature work with manganese nitrosyl porphyrins.[34]

In this chapter, we report the preparation of the (OEP)Ru(NO)(XEt) (X = O, S) and (OEP)Ru(NO)(SR) (R = *i*-C_5H_{11}, Ph) complexes. Additionally, we report on the comparative electrochemistry and infrared spectroelectrochemistry of the set of (OEP)M(NO)(OEt) and (OEP)M(NO)(SEt) compounds, where M = Os and Ru. Prior to the publication of this work[35], only a few other studies of the electrochemistry of ruthenium nitrosyl porphyrins had been reported,[15,26,28,36] including the infrared spectroelectrochemistry of (TPP)Ru(NO)(ONO).[26]

Experimental Section

All reactions were performed under an atmosphere of prepurified nitrogen using standard Schlenk techniques and/or in an Innovative Technology Labmaster 100 Dry Box unless stated otherwise. Dichloromethane and hexane were distilled from CaH_2 under nitrogen just prior to use.

Chemicals. Ethyl nitrite (10-20 wt.% in ethanol), *t*-butyl nitrite (95%), ethanethiol (97%), 3-methyl-1-butanethiol (isoamylthiol) (97%), thiophenol (97%),

methanol (anhydrous, 99.8%) were purchased from Aldrich Chemical Company and used as received. NBu_4PF_6 (98%; Aldrich Chemical Company) was recrystallized from hot ethanol. (OEP)Ru(CO)(MeOH) was purchased from Midcentury Chemicals. Chloroform-*d* (99.8 %) was obtained from Cambridge Isotope Laboratories, subjected to three freeze-pump-thaw cycles, and stored over Linde 4 Å molecular sieves. Ferrocene (Cp_2Fe; Cp = η^5-cyclopentadienyl anion) was sublimed prior to use.

Instrumentation. Electrochemical measurements were recorded using a BAS CV50W instrument (Bioanalytical Systems, West Lafayette, IN, USA). For all electrochemical experiments, a 3.0 mm diameter Pt disk electrode was used as the working electrode, a silver wire coated with silver chloride acted as the reference electrode, and a platinum wire served as the auxiliary electrode. All experiments were performed at room temperature unless otherwise noted, and were performed under an atmosphere of pre-purified nitrogen in a 0.1 M NBu_4PF_6 solution of the analyte (1.0 mM) in CH_2Cl_2. Ferrocene served as an internal standard, and potentials are referenced to the $Cp_2Fe^{0/+}$ couple set at 0.00 V (+0.44 V vs. Ag/AgCl).[37] Typical solvent system windows with our configuration were +1.2 to +1.5 V for the oxidation limit, and –1.8 to –2.1 V for the reduction limit (vs. the $Cp_2Fe^{0/+}$ couple).

Infrared spectroscopic measurements for the synthetic work were performed using a BioRad FT-155 FT-IR spectrometer. For the spectroelectrochemical experiments, the infrared spectroscopic measurements were performed using a Bruker Vector 22 FTIR spectrometer equipped with a mid-IR fiber-optic dip probe and liquid nitrogen cooled MCT detector (Remspec Corporation, Sturbridge, MA, USA) as

described previously.[33] The same electrode configuration was used for both cyclic voltammetry and infrared spectroelectrochemical experiments. The fiber-optic infrared reflectance spectroelectrochemical experiments were performed in a specially designed cell and in a manner that was previously reported.[33] For the low-temperature work we jacketed the cell with a dry ice/acetone bath as described in our complementary studies on manganese nitrosyl porphyrins.[34]

NMR measurements were performed on a Varian 300 MHz instrument, and the signals referenced to that of $CDCl_3$ (at 7.24 ppm). All couplings are in Hz. Electrospray-ionization mass spectra were obtained on a Micromass Q-TOF spectrometer.

Preparation of (OEP)Ru(NO)(OEt). To a stirred pink solution of (OEP)Ru(CO)(MeOH) (20 mg, 0.029 mmol) in CH_2Cl_2 (15 mL) was added ethyl nitrite (0.55 mL, ~6 mmol). The resulting mixture was refluxed for 45 min resulting in a change of color to dark red. An IR spectrum of the solution showed the disappearance of the ν_{CO} of the starting material at 1921 cm^{-1} and the appearance of a new band at 1801 cm^{-1} assigned to ν_{NO}. The solution was taken to dryness in vacuo. The residue was redissolved in CH_2Cl_2 (5 mL), and hexane was added (2 mL). The resulting solution was subjected to slow solvent evaporation at room temperature to yield microcrystals of the product (12 mg, 0.018 mmol, 61% isolated yield). IR (KBr, cm-1): ν_{NO} = 1791. ^{1}H-NMR ($CDCl_3$ ppm): 10.29 (s, 4H, *meso*-H of OEP); 4.15 (q, 16H of OEP, J = 8 Hz), 1.98 (t, 24H of OEP, J = 7 Hz), –2.78 (q, 2H of OEt, J = 7 Hz), –3.02 (t, 3H of OEt, J = 7 Hz). ESI-MS (*m/z*): 664.3 $[(OEP)Ru(NO)]^+$ (100%).

Preparation of (OEP)Ru(NO)(SEt). To a stirred CH_2Cl_2 solution (15 mL) of (OEP)Ru(CO)(MeOH) (20 mg, 0.029 mmol) was added a previously prepared red mixture of ethanethiol and *t*-BuONO (1:1 v/v, 0.20 mL; in 4 mL of CH_2Cl_2; 10 min mixing time). The mixture was stirred for 10 min, during which time it turned from pink to dark red. The solvent was removed in vacuo, and the product isolated as for the ethoxide derivative (20 mg, 0.028 mmol, 97% isolated yield). IR (CH_2Cl_2, cm-1): ν_{NO} = 1788. IR (KBr, cm-1): ν_{NO} = 1773. ^{1}H NMR($CDCl_3$, ppm): 10.26 (s, 4H, *meso*-H of OEP), 4.14 (m, 16H of OEP, *J* = 8 Hz), 1.99 (t, 28H of OEP, *J* = 8 Hz), –1.84 (t, 3H of SEt, *J* = 8 Hz), –3.09 (q, 2H of SEt, *J* = 8 Hz). ESI-MS (*m/z*): 664.3 $[(OEP)Ru(NO)]^+$ (87%).

Preparation of (OEP)Ru(NO)(S-*i*-C_5H_{11}). (OEP)Ru(NO)(S-*i*-C_5H_{11}) was prepared in a manner similar to what was described for the preparation of (OEP)Ru(NO)(SEt) except isoamylthiol was used in place of ethanethiol and vacuum was applied while heating at 85° C for 4.15 hr in order to remove excess isoamyl thiol, which under standard conditions, boils at ~118 ºC (18 mg, 0.024 mmol, 81% isolated yield). IR (CH_2Cl_2, cm^{-1}): ν_{NO} = 1786. IR (KBr, cm^{-1}): ν_{NO} = 1775. ^{1}H-NMR ($CDCl_3$, ppm): 10.27 (s, 4H, *meso*-H of OEP), 4.15 (m, *J* = 4, 16H of OEP), 2.00 (t, *J* = 8, 28H of OEP), -0.32 (d, *J* = 5, 6H of S-*i*-C_5H_{11}), -0.39 (m, *J* = 7, 1H of S-*i*-C_5H_{11}), -1.88 (q, *J* = 6, 2H of S-*i*-C_5H_{11}), -3.18 (t, *J* = 8, 2H of S-*i*-C_5H_{11}). ESI-MS (*m/z*): 664.3 $[(OEP)Ru(NO)]^+$ (100%).

Preparation of (OEP)Ru(NO)(SPh). (OEP)Ru(NO)(SPh) was prepared in a manner similar to that described above except thiophenol was mixed with *t*-BuONO to make the putative thionitrite and the excess thiol precursor was removed by

washing three times with MeOH (anhydrous, 15 mL total), followed by drying under vacuum (19 mg, 0.025 mmol, 85% isolated yield). IR (CH_2Cl_2, cm^{-1}): ν_{NO} = 1793. IR (KBr, cm^{-1}): ν_{NO} = 1783. ^{1}H-NMR ($CDCl_3$, ppm): 10.15 (s, 4H, *meso*-H of OEP), 6.28 (t, J = 8, 1H of SC_6H_5), 5.85 (t, J = 8, 2H of SC_6H_5), 4.11(q, J = 8, 16H of OEP), 2.87 (d, J = 8, 2H of SC_6H_5), 1.96 (t, J = 8, 24H of OEP). ESI-MS (*m/z*): 664.3 $[(OEP)Ru(NO)]^+$ (70%).

Preparation of (OEP)Os(NO)(OEt). The (OEP)Os(NO)(OEt) was prepared as previously described.[10] A suitable crystal of (OEP)Os(NO)(OEt) was grown from a CH_2Cl_2/hexane mixture by slow evaporation of the solvent under inert atmosphere.[†] The molecular structure is displayed in Fig. 2.1a.

Preparation of (OEP)Os(NO)(SEt). The (OEP)Os(NO)(SEt) complex was prepared as previously described.[12] A suitable crystal of (OEP)Os(NO)(SEt)·0.5(CH_2Cl_2) was grown from a CH_2Cl_2/hexane mixture by slow evaporation of the solvent under inert atmosphere.[†] The molecular structure is displayed in Fig. 2.1b.

Extended Hückel Calculations.[‡] Extended Hückel calculations, as implemented in the YAeHMOP suite of programs,[38] were performed on the six-coordinate osmium nitrosyl complexes (OEP)Os(NO)(OEt) and (OEP)Os(NO)(SEt) using geometries obtained from the crystal structures included in this work. Calculations on the five-coordinate complex $[(OEP)Os(NO)]^+$ were also performed

---

[†] Jonghyuk Lee, of our group, obtained the (OEP)Os(NO)(OEt) and (OEP)Os(NO)(SEt) crystals. Structural data will be included in this report to aid in the discussion.

[‡] Extended Hückel calculations were performed in collaboration with Dr. Ralph Wheeler and C. Adam Hixson of this Department.

using a geometry derived from the crystal structure of (OEP)Os(NO)(SEt) by removing the thiolate ligand. Initial images of the molecular orbitals were produced using the viewkel application distributed in the YAeHMOP suite.[38] Adobe Photoshop® was used to add color to the figures.

Results and Discussion

Synthesis and Structural Characterization. The osmium compounds used in this study have been reported previously,[10,12] and the ruthenium compounds were synthesized using procedures similar to those used for the osmium compounds. Thus, the nitrosyl ethoxide compound (OEP)Ru(NO)(OEt) was prepared in 61% isolated yield from the reaction of ethyl nitrite with the ruthenium carbonyl precursor as shown in Eq. 2.1.

$$(OEP)Ru(CO)(MeOH) + EtONO \rightarrow (OEP)Ru(NO)(OEt) + CO + MeOH \quad (2.1)$$

The thiolate analogue (OEP)Ru(NO)(SEt) was prepared in 97% isolated yield in an analogous manner using *in situ* generated EtSNO. Similarly, the isoamylthiolate complex (OEP)Ru(NO)(S-*i*-C_5H_{11}) and the phenolthiolate analogue (OEP)Ru(NO)(SC_6H_5) were prepared in 81 and 85% isolated yields, respectively. All the compounds (OEP)M(NO)(XR) (M = Os, Ru; X = O, S; R = Et, *i*-C_5H_{11}, or Ph) contain mutually *trans* nitrosyl and XR groups and exhibit similar spectroscopic features for their (OEP)M(NO) units; they are diamagnetic with strong NO stretches in the infrared spectra.

Tables 2.1 and 2.2 list the infrared nitrosyl stretching frequencies of selected osmium and ruthenium porphyrin complexes containing alkoxide and thiolate linkages and linear metal nitrosyl groups. As is evident from the data listed in the tables, the complexes reported here exhibit nitrosyl stretching frequencies characteristic of synthetic metalloporphyrin compounds with linear metal-nitrosyl linkages.[3] The thiolate substituted (OEP)Ru(NO)(SR) complexes prepared by us, for example, exhibit ν_{NO}s of 1773 cm^{-1} (SEt), 1775 cm^{-1} (S-*i*-C_5H_{11}), and 1783 cm^{-1} (SPh). The (OEP)Ru(NO)(SPh) has the highest reported ν_{NO} stretch of the ruthenium complexes reported here and is among the highest reported for similar ruthenium porphyrin thiolate complexes, suggesting that the phenolthiol ligand is a poor contributor of charge to the metal due to the electron withdrawing aromatic group contained in the ligand. The high frequency ν_{NO}, thus, results from the decreased charge otherwise available to the π-backbonding NO ligand from the metal center.

It is interesting to note that a similar effect by the phenolthiolate ligand on the *meso* protons of the OEP macrocycle is revealed in the ^1H NMR spectra of the thiolate and alkoxide complexes. The *meso* (porphyrin) proton peaks in the (OEP)Ru(NO)(X) complexes containing the *trans* axial ligands OEt, SEt, S-*i*-C_5H_{11}, and SPh resonate at 10.29, 10.26, 10.27, and 10.15 ppm, respectively.

Similar to the aforementioned '*trans* effect', the substitution around the porphyrin periphery also affects the NO stretching frequency, as is evidenced in Tables 2.1 and 2.2. Of the substituted porphyrins reported for (por)M(NO)(XR) complexes (where por = porphyrin; M = Os, Ru; XR = alkoxide or thiolate ligand), the ethyl substituted porphyrins tend to have lower nitrosyl stretches in the infrared

frequency when compared to their analogous aryl substituted porphyrin complexes. The delocalized aryl groups around the porphyrin periphery pull electrons away from the metal core of the porphyrin center whereas the ethyl groups are electron donors. In the later case, the increased charge is contributed to the metal where it is incorporated in the M→NO electron donation, strengthening the π bond and leading to lower nitrosyl stretching frequencies. Buchler et al. have reviewed the *trans* and *cis* effects on metalloporphyrins.[39]

The infrared data listed in the two tables indicates that alkoxide and thiolate ligands containing hydrocarbon chains tend to donate more charge to the ruthenium and osmium metal centers and that the longer, unbranched chains are the best electron donors as evidenced by the lower ν_{NO}s exhibited by the compounds with hydrocarbon chains. Further, the complexes containing alkoxide and thiolate ligands with aromatic groups or electronegative atoms are poor donors of charge to the metal centers and, hence, have relatively higher nitrosyl stretching frequencies. Surprisingly, these trends are not clearly reflected in the IR data for the thiolate containing osmium-nitrosyl porphyrin complexes.

In this case the aromatic phenolthiolate (-SPh) complex exhibits the lowest IR nitrosyl stretching frequency of the complexes listed in Table 2.2 indicating that it contributes more charge to the metal center than related complexes with thiolates containing hydrocarbon chains. This data suggests that the electronic interaction between the osmium and the axial ligands in the (OEP)Os(NO)(SR) complexes is more complex than the model used above to explain the trends.

The mass spectra of the (OEP)Ru(NO) alkoxide and thiolate complexes shows that the complexes are easily fragmented at the Ru-O or Ru-S portion of the molecule resulting in the appearance of the $[(OEP)Ru(NO)]^+$ moiety as a major component in the spectrum. This data indicates that, relative to the Ru-NO bond, the Ru-alkoxide and Ru-thiolate bonds are weaker and under the conditions of the mass spectrometry experiment are easy to break.

We have obtained the X-ray crystal structures of (OEP)Os(NO)(OEt) and (OEP)Os(NO)(SEt), and their molecular structures are shown in Figure 2.1. Selected bond angles and lengths are listed in Table 2.3. A full list of the bond lengths and bond angles for the molecular structures are included in the Appendix (Tables 2.5 – 2.9).

The compounds contain nearly linear OsNO groups, and the axial ligands are disordered over the two faces of the porphyrin macrocycle. In our earlier report on the crystal structure of (OEP)Os(NO)(OEt),[10] we proposed a bent OsNO geometry for the axially-disordered structure based on the refinement statistics for the earlier data. However, the spectroscopic and spectroelectrochemical data for this compound are more consistent with a linear OsNO geometry as favored in our re-refined structure.[35]

Table 2.1. Infrared nitrosyl stretching frequencies of select ruthenium nitrosyl porphyrins with alkoxide and thiolate ligands.

Compound	ν_{NO} (KBr, cm^{-1})	Reference
Alkoxide complexes		
(OEP)Ru(NO)(OMe)	1780	40
(OEP)Ru(NO)(O-*i*-C_5H_{11})	1788	*28*
(OEP)Ru(NO)(OEt)	1791	*This work*
(TPP)Ru(NO)(O-*i*-C_5H_{11})	1800	28
(T(*p*-OMe)PP)Ru(NO)(O-*i*-C_5H_{11})	1801	*Chapter 3*
(TTP)Ru(NO)(O-*i*-C_5H_{11})	1809	16
Thiolate complexes		
(OEP)Ru(NO)(SEt)	1773	*This work*
(OEP)Ru(NO)(S-*i*-C_5H_{11})	1775	*This work*
(OEP)Ru(NO)(SCH_2CF_3)	1782	*18*
(OEP)Ru(NO)(SPh)	1783	*This work*
(OEP)Ru(NO)($SC(Me)_2CH_2NHC(O)Me$)	1789	19
(OEP)Ru(NO)(SC_6F_4H)	1798	18
(TTP)Ru(S-*p*-tolyl)	1784	*27*

Table 2.2. Infrared nitrosyl stretching frequencies of select osmium nitrosyl porphyrins with alkoxide and thiolate ligands.

Compound	**ν_{NO} (KBr, cm^{-1})**	**Reference**
Alkoxide complexes		
(OEP)Os(NO)(O-*n*-Bu)	1743	11
(OEP)Os(NO)(OMe)	1745	41
(OEP)Os(NO)(O-*i*-C_5H_{11})	1747	11
(OEP)Os(NO)(OEt)	1756	10
(TTP)Os(NO)(O-*i*-C_5H_{11})	1770	17
Thiolate complexes		
(OEP)Os(NO)(SPh)	1749	11
(OEP)Os(NO)(S-*i*-C_5H_{11})	1751	11
(OEP)Os(NO)(S-*i*-Pr)	1751	12
(OEP)Os(NO)(SEt)	1753	12
(OEP)Os(NO)(S-*t*-Bu)	1754	12
(OEP)Os(NO)(SMe)	1755	12
(TTP)O(NO)(S-*i*-C_5H_{11})	1760	17

Table 2.3. Selected bond lengths and angles for (OEP)Os(NO)(XEt) (X = O, S).

	(OEP)Os(NO)(OEt)	**(OEP)Os(NO)(SEt)**
Os-N(NO) (Å)	1.880(7)	1.994(10)
N-O (Å)	1.165(9)	1.136(11)
Os-X (Å)	1.849(7)	2.227(2)
Os-N(por) (Å)	2.059(4), 2.066(4)	2.048(3), 2.054(2)
Os-N-O (º)	172.4(10)	172.7(8)
Os-X-C (º)	128.0(8)	112.8(4)
X-Os-N(NO) (º)	168.4(6)	172.0(3)

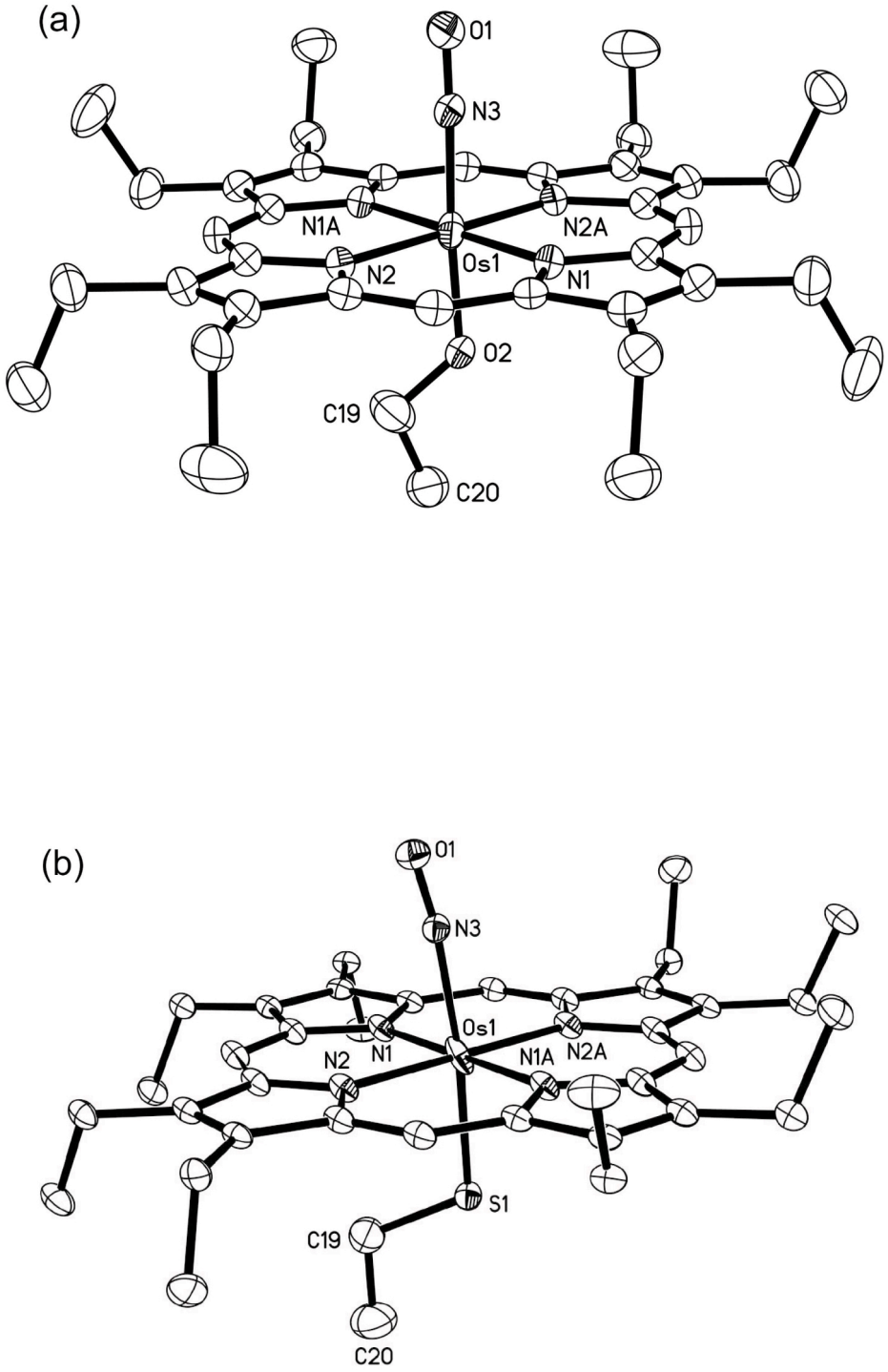

Figure 2.1. Molecular structure of (a) (OEP)Os(NO)(OEt), and (b) (OEP)Os(NO)(SEt). Hydrogen atoms have been omitted for clarity.

Cyclic Voltammetry and Infrared Spectroelectrochemistry. The redox properties of the related four compounds (OEP)M(NO)(XEt) (M = Os, Ru; X = O, S) were examined by cyclic voltammetry, and the electrochemical data are summarized in Table 2.4. We will consider the alkoxide and thiolate compounds in turn.

Alkoxide Compounds. The single response feature in the cyclic voltammogram of (OEP)Os(NO)(OEt) is shown in Figure 2.2. No other features for oxidation or reduction were observed within the solvent limit.

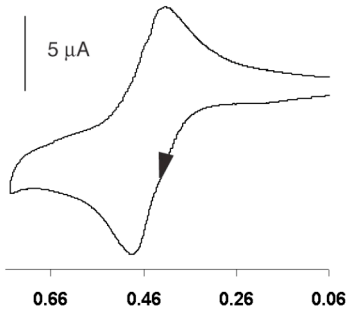

Figure 2.2. Cyclic voltammogram of (OEP)Os(NO)(OEt) in CH_2Cl_2 containing 0.1 M NBu_4PF_6. Potentials are referenced to the $Cp_2Fe^{0/+}$ couple at $E°' = 0.00$ V. Scan rate of 200 mV/s.

Table 2.4. Electrochemical data for the (OEP)M(NO)(XEt) (M = Os, Ru; X = O, S) compounds in CH_2Cl_2.[a]

	Oxidations			Reductions
Compound	$E^{\circ\prime}_1$	$E^{\circ\prime}_2$	E_{pa3}	$E^{\circ\prime}$
(OEP)Os(NO)(OEt)	0.42 (72)			
(OEP)Ru(NO)(OEt)	0.43 (117)	0.67 (93)	1.01	–1.83 (240)
(OEP)Os(NO)(SEt)	0.42[b]	0.66 (144)	0.84	–2.02 (129)
(OEP)Ru(NO)(SEt)	0.37[b]	0.66 (120)		–1.64 (195)

[a] Potentials are in volts, and are referenced to the ferrocene-ferrocenium couple set at 0.00 V. Conditions: 1 mM analyte, 200 mV/s, 0.1 M NBu_4PF_6. The numbers are in brackets represent the ΔE values (in mV) for the redox couples.
[b] These peaks are irreversible.

The compound (OEP)Os(NO)(OEt) exhibits a single well-defined reversible oxidation at +0.42 V versus the ferrocene-ferricenium couple. The ΔE_p for this redox couple is 72 mV and its value is independent of scan rate over the 50 to 500 mV/s range. The cathodic to anodic peak current ratio (i_{pc}/i_{pa}) is 0.9 at 200 mV/s, and approaches unity at higher scan rates, suggesting that the oxidation is chemically reversible. The plot of i_{pa} vs (scan rate)$^{1/2}$ is linear and indicative of a diffusion-controlled reversible one-electron transfer process (Eq. 2.2; site of oxidation not specified).

$$(OEP)Os(NO)(OEt) \rightleftharpoons [(OEP)Os(NO)(OEt)]^+ + e^- \qquad (2.2)$$

The cyclic voltammogram of the Ru analogue (OEP)Ru(NO)(OEt) is shown in Figure 2.3. The redox behavior is characterized by three oxidations and one reduction. When the potential scan is reversed just after the first oxidation, a coupled reduction becomes clearly evident, suggesting reversibility for this first oxidation as shown in Figure 3b ($E°'$ = +0.43 V; i_{pc}/i_{pa} = 0.9; ΔE = 117 mV). When the potential scan (oxidation) is continued until the solvent limit, two other oxidations are observed; a reversible couple at +0.67 V and an irreversible peak at +1.01 V. Follow-up electrochemical processes at –1.00 and –1.50 V as a result of these latter oxidations are observed (Figure 2.3a). Since we were primarily interested in detailing the first oxidation (and first reduction) of the ruthenium compounds, the other oxidation processes were not investigated further.

An irreversible reduction peak at E_{pc} = –1.90 V is observed at 50 mV/s, and reversibility for this reduction process ($E°'$ = –1.83 V) first becomes apparent at scan rates close to 200 mV/sec (Figure 2.3a). Even at 1.0 V/s, i_{pa}/i_{pc} for this redox couple was 0.6, indicative of considerable reactivity of the reduction product; consistent with this conclusion is the appearance of a daughter peak at –1.32 V. Based on infrared spectroscopic evidence (vide infra), we believe that the lack of complete reversibility is due to the loss of NO from the reduction product.

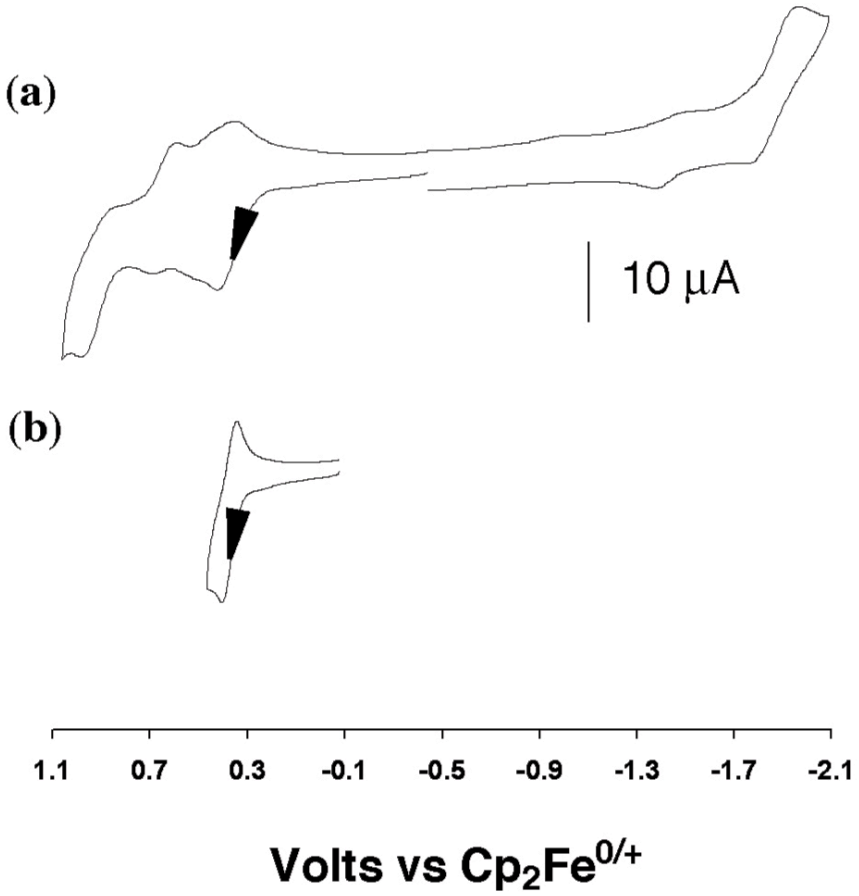

Figure 2.3. Cyclic voltammograms of (OEP)Ru(NO)(OEt) in CH_2Cl_2 containing 0.1 M NBu_4PF_6. Potentials are referenced to the $Cp_2Fe^{0/+}$ couple at $E°' = 0.00$ V. Scan rate of 200 mV/s. (a) Complete cyclic voltammogram. (b) Cyclic voltammogram showing only the first oxidation.

The IR difference spectrum which shows product formation after the oxidation of (OEP)Os(NO)(OEt) is presented in Figure 2.4. The electrogenerated product of the oxidation has a ν_{NO} band at 1789 cm^{-1}, which is shifted by +30 cm^{-1} from that of the starting compound. Such a relatively small shift in ν_{NO} is attributed to an oxidation site that is somewhat remote from the OsNO fragment. Indeed, evidence for a porphyrin-centered oxidation is provided by the appearance in the spectrum of a new band at 1530 cm^{-1} due to an OEP-containing π-radical cation.

Diagnostic bands at 1520-1570 cm^{-1} have been reported for OEP-containing π-radical cations and have been proposed to arise from a combination of carbon-carbon and carbon-nitrogen stretches in the macrocycle.[42] Thus, the oxidation process may best be represented by Eq. 2.3 (i.e., a slight modification of Eq. 2.2), where the electrooxidation occurs at the porphyrin ring.

$$(OEP)Os(NO)(OEt) \rightleftharpoons [(OEP^{\bullet})Os(NO)(OEt)]^{+} + e^{-} \qquad (2.3)$$

As noted earlier, no reduction process was observed by cyclic voltammetry for (OEP)Os(NO)(OEt) within the solvent limit.

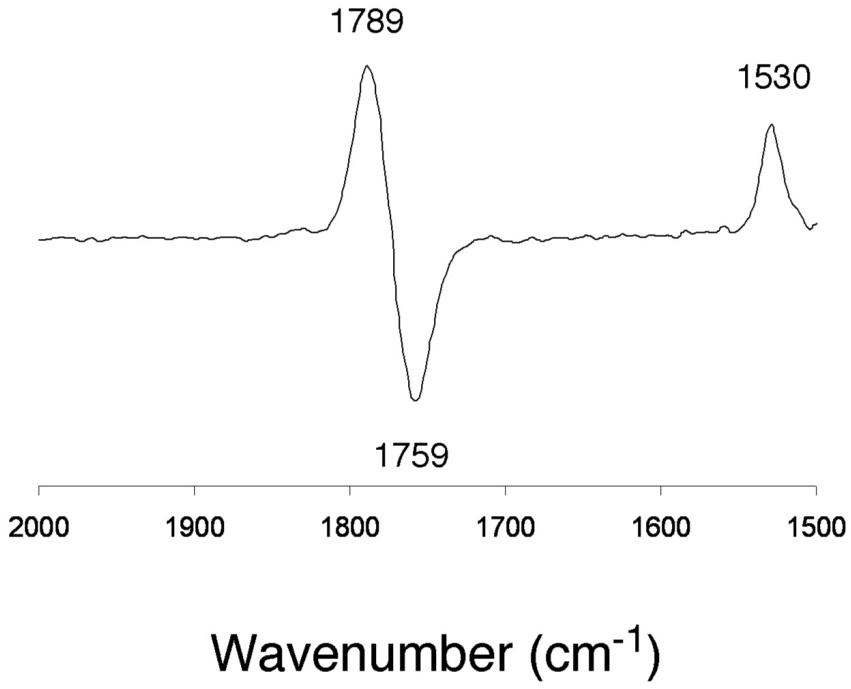

Figure 2.4. Difference FTIR spectrum showing the formation of product from the first oxidation of (OEP)Os(NO)(OEt) in CH_2Cl_2 containing 0.1 M NBu_4PF_6, with the potential held at +0.60 V vs. the $Cp_2Fe^{0/+}$ couple.

The IR spectroelectrochemistry result obtained during the first oxidation of the related (OEP)Ru(NO)(OEt) compound is similar to that of the Os analogue (i.e., Eq. 2.4). Thus, a new ν_{NO} band at 1855 cm^{-1} ($\Delta\nu_{NO}$ = +50 cm^{-1}) is observed to form when the potential is held at +0.58V, positive of the *E*°' for the first oxidation (Figure 2.5). In addition, a small band at 1530 cm^{-1} is also evident in the IR difference spectrum

$$(OEP)Ru(NO)(OEt) \rightleftharpoons [(OEP^{\bullet})Ru(NO)(OEt)]^{+} + e^{-} \qquad (2.4)$$

indicative of a porphyrin-based first oxidation. Such porphyrin-based first oxidations have been observed and proposed for other six-coordinate (por)Ru(NO)-containing compounds.[15,26,28,36] Holding the electrode potential at values higher than that sufficient for the second oxidation of (OEP)Ru(NO)(OEt) led to ill-defined product υ_{NO} bands in the 1857-1900 cm^{-1} region, indicative of multiple new RuNO oxidation species that were not examined further.

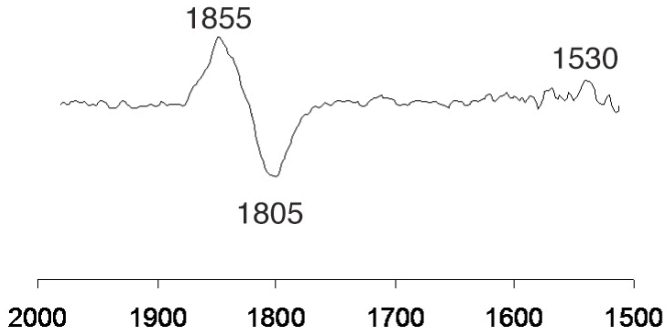

Figure 2.5. Difference FTIR spectrum showing formation of product from the first oxidation of (OEP)Ru(NO)(OEt) in CH_2Cl_2 containing 0.1 M NBu_4PF_6, with the potential held at +0.58 V vs. the $Cp_2Fe^{0/+}$ couple.

The reduction behavior for (OEP)Ru(NO)(OEt) was also examined by IR spectroelectrochemistry. As noted earlier in Figure 2.3a, this complex displays a somewhat reversible reduction process at higher scan speeds. As seen in Figure 2.6, the spectroelectrochemical reduction of (OEP)Ru(NO)(OEt) results in loss of ν_{NO} at 1803 cm^{-1} due to the consumption of the (OEP)Ru(NO)(OEt) compound at the electrode surface without formation of a new RuNO-containing species, suggesting rapid loss of the NO ligand after reduction (Eqs 2.5 and 2.6).

$$(OEP)Ru(NO)(OEt) + e^- \rightleftharpoons [(OEP)Ru(NO)(OEt)]^- \quad (2.5)$$

$$[(OEP)Ru(NO)(OEt)]^- \rightarrow [(OEP)Ru(OEt)]^- + NO \quad (2.6)$$

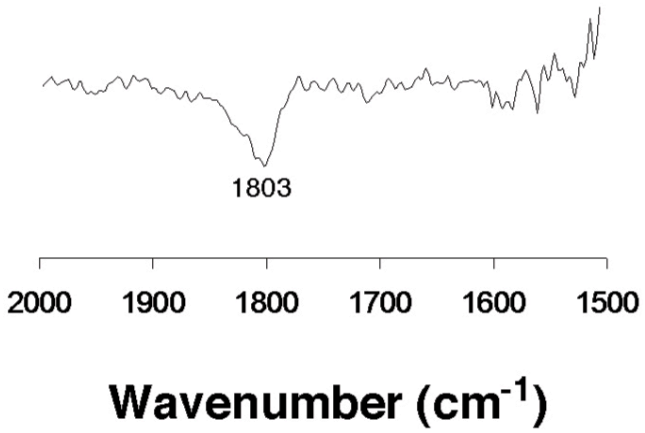

Figure 2.6. Difference FTIR spectrum showing the consumption of (OEP)Ru(NO)(OEt) during its reduction in CH_2Cl_2 containing 0.1 M NBu_4PF_6, with the potential held at –2.00 V vs. the $Cp_2Fe^{0/+}$ couple.

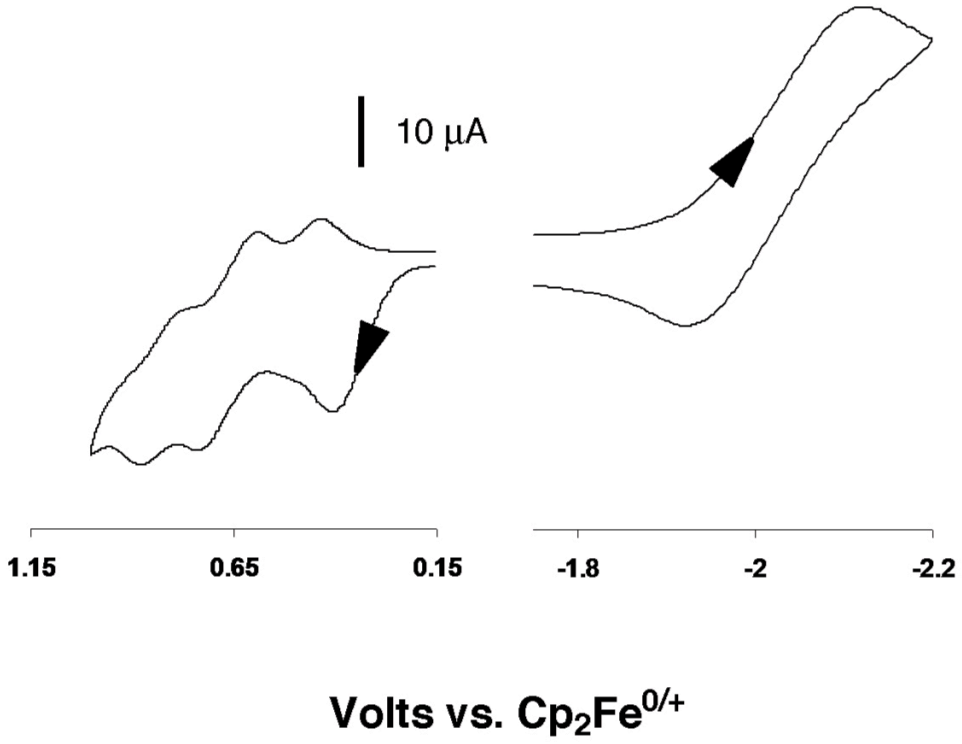

Figure 2.7. Cyclic voltammogram of (OEP)Os(NO)(SEt) in CH_2Cl_2 containing 0.1 M NBu_4PF_6. Potentials are referenced to the $Cp_2Fe^{0/+}$ couple at $E°' = 0.00$ V. Scan rate of 200 mV/s.

Thiolate Complexes. The response features of the cyclic voltammogram of (OEP)Os(NO)(SEt) are shown in Figure 2.7. The first oxidation occurs at E_{pa1} = +0.42 V,

and is irreversible up to 500 mV/s. The $|E_p\text{-}E_{p/2}|$ value of 83 mV (at 200 mV/s) suggests a reversible oxidation followed by a rapid chemical reaction. A second oxidation process is evident which is partially reversible ($E°'_2$ at +0.66 V; ΔE = 144 mV) with an associated cathodic peak at +0.44 V. A third oxidation at E_{pc3} = +0.84 V is also observed, which we assign to the oxidation of ethanethiol generated in solution (vide infra). In addition, a reduction peak is observed at –2.02 V, which is partially reversible at scan speeds >100 mV/sec. This peak becomes more reversible at higher scan speeds. This reduction peak is close to the solvent limit, hence we are uncertain if the apparent increased peak height is due to a two-electron reduction process or interference from the electrolyzed solvent system.

The cyclic voltammogram of the related (OEP)Ru(NO)(SEt) is shown in Figure 2.8.

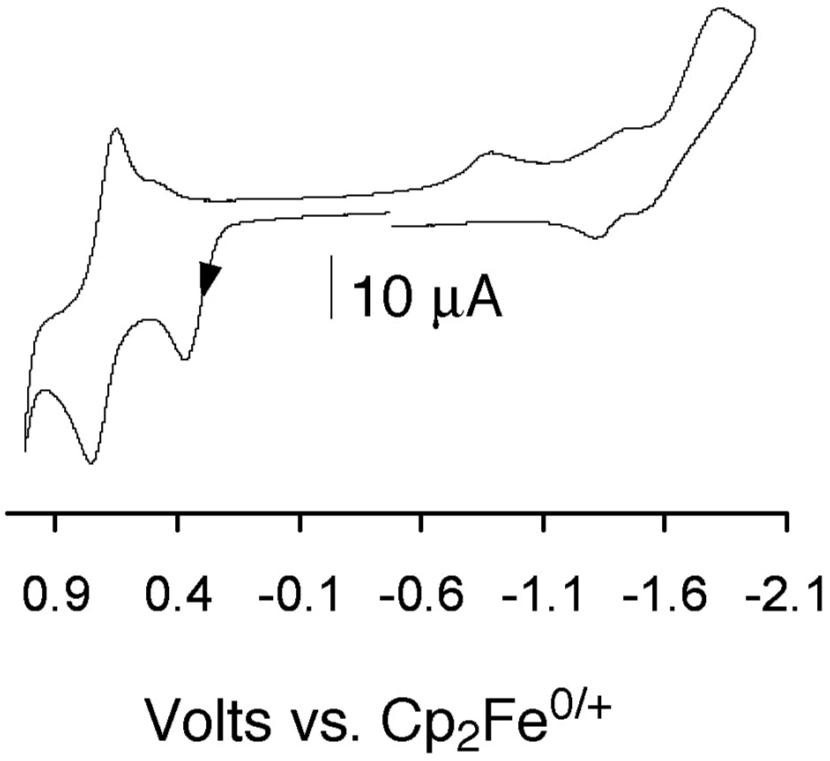

Figure 2.8. Cyclic voltammogram of (OEP)Ru(NO)(SEt) in CH_2Cl_2 containing 0.1 M NBu_4PF_6. Potentials are referenced to the $Cp_2Fe^{0/+}$ couple at $E°' = 0.00$ V. Scan rate of 200 mV/s.

The first oxidation of (OEP)Ru(NO)(SEt) occurs at +0.37 V, and is irreversible with an $|E_p\text{-}E_{p/2}|$ value of 79 mV at 200 mV/s. This is indicative of a reversible electron transfer followed by a fast chemical reaction; two daughter peaks at –0.91 and –1.45 V are also observed after the first oxidation.

Interestingly, the second oxidation of (OEP)Ru(NO)(SEt) is reversible (Figure 2.8), and occurs at $E°' = +0.66$ V. Unlike the case for Os, there is only a small daughter peak at +0.45 V associated with this redox couple. This daughter peak is virtually absent in the low-temperature (–78 °C) cyclic voltammogram of the compound (Figure 2.9).

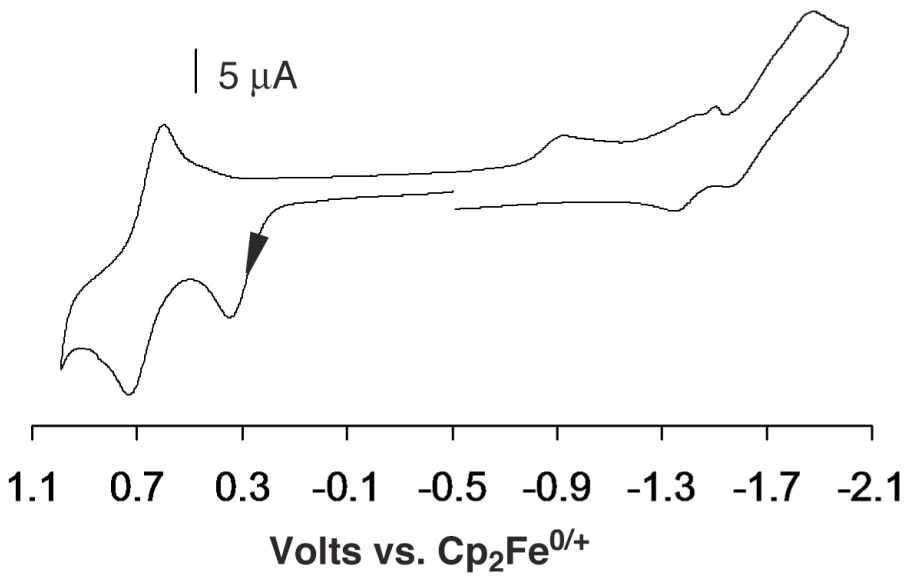

Figure 2.9. Low temperature (-78 °C) cyclic voltammogram of (OEP)Ru(NO)(SEt) in CH_2Cl_2 containing 0.1 M NBu_4PF_6. Potentials are referenced to the $CpFe^{0/+}$ couple at $E°' = 0.00$ V. Scan rate of 200 mV/s.

A single cathodic peak at –1.64 V is observed at room temperature upon scanning to negative potentials (Figure 2.8), and this peak has an associated daughter peak at –1.37 V. At a scan rate of 500 mV/s, the i_{pa}/i_{pc} ratio of this couple is 0.8 indicative of increased reversibility for this process at higher scan rates.

The IR difference spectrum demonstrating the formation of the product from the first oxidation of (OEP)Os(NO)(SEt) is shown in Figure 2.10a.

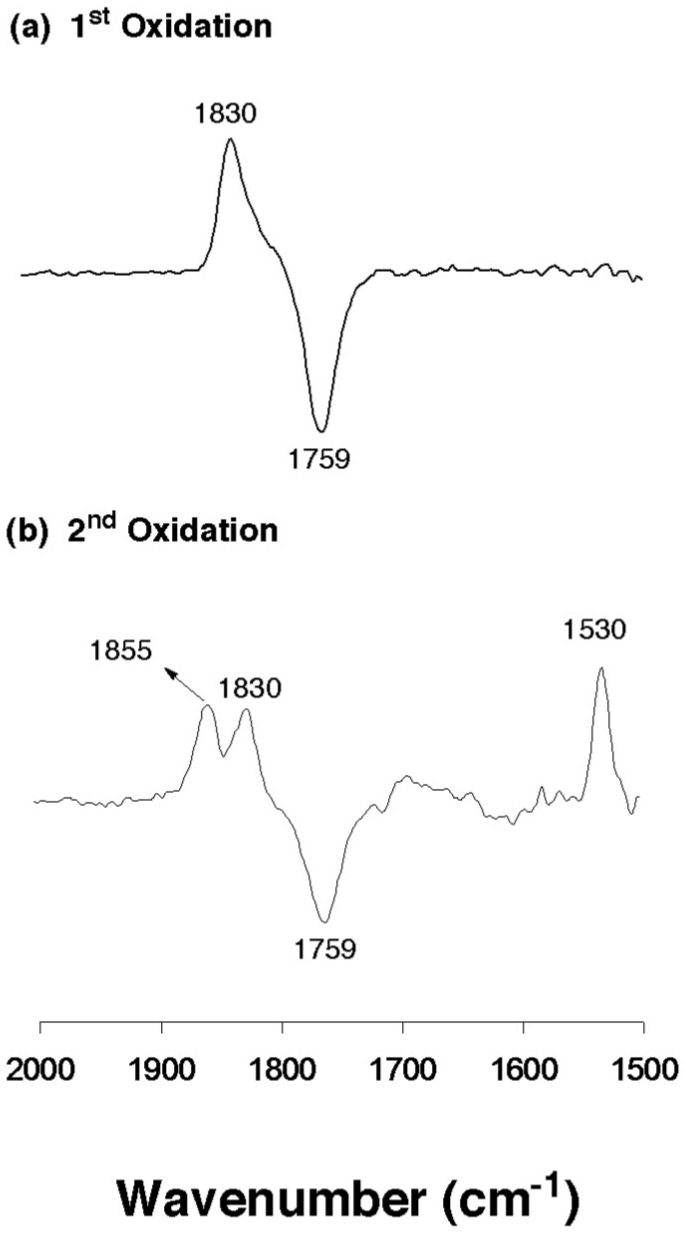

Figure 2.10. Difference FTIR spectra showing formation of products during (a) the first oxidation of (OEP)Os(NO)(SEt), and (b) the second oxidation of (OEP)Os(NO)(SEt). The potentials were held at +0.50 V and +0.80 V (vs. the $Cp_2Fe^{0/+}$ couple) for the first and second oxidations, respectively.

As can be seen in the Figure, the ν_{NO} of 1759 cm^{-1} due to the starting (OEP)Os(NO)(SEt) is consumed at an applied potential just slightly positive of E_{pa1}, and a new product with ν_{NO} at 1830 cm^{-1} is formed. This relatively large shift of ν_{NO} ($\Delta\nu_{NO}$ = 71 cm^{-1}) is indicative of a change in electron density close to the Os-NO fragment of the complex. Based on the electrochemical and IR spectroelectrochemical results, the net irreversible first oxidation of (OEP)Os(NO)(SEt) can be described as consisting of a reversible oxidation process followed by a fast irreversible structural change that does not involve the loss of NO from the metal center, but rather involves cleavage of the Os-SEt bond (Eq. 2.7 and 2.8).

$$(OEP)Os(NO)(SEt) \rightleftharpoons [(OEP)Os(NO)(SEt)]^{\bullet+} + e^- \quad (2.7)$$

$$[(OEP)Os(NO)(SEt)]^{\bullet+} \rightarrow [(OEP)Os(NO)]^+ + {\bullet}SEt \quad (2.8)$$

Examination of the second oxidation by spectroelectrochemistry reveals a further shift in υ_{NO} to 1855 cm^{-1} and the appearance of a new band at 1530 cm^{-1} due to an OEP-radical cation species. The relative small shift of υ_{NO} ($\Delta\nu_{NO}$ = 25 cm^{-1}) is characteristic for a porphyrin-ring centered oxidation for this compound *after* the first oxidation. The second oxidation can thus be described by Eq. 2.9, which involves the formation of the π-radical species in the dicationic product. In this experiment, the monocationic product

$$[(OEP)Os(NO)]^{+} \rightleftharpoons [(OEP^{\bullet})Os(NO)]^{2+} + e^{-} \quad (2.9)$$

was not entirely consumed at the electrode surface as evidenced by presence of the peak of the monocation (υ_{NO} 1830 cm^{-1}) in the IR spectrum.

We assign the third oxidation in Figure 2.7 to the oxidation of EtSH, since a cyclic voltammogram of authentic EtSH shows an oxidation at +0.84 V, which is coincident with E_{pa3} in Figure 2.7. It may then be possible that hydrogen-atom abstraction by the ·SEt radical produced in Eq. 2.8 occurs in the presence of the solvent system. We do not have experimental evidence to support the formation of the disulfide, although it may be present as well.

The reduction (OEP)Os(NO)(SEt) results in the loss of the NO ligand, as demonstrated by the IR difference spectrum shown in Figure 2.11a. However, when the difference spectrum is recorded while the electrode potential is cycled between –1.8 V and –2.2 V at 400 mV/sec for 1 min (to allow for a build-up, and better detection, of this short-lived OsNO-containing species near the electrode surface), a new ν_{NO} band is observed at 1709 cm^{-1} (Figure 2.11b). This relatively small shift of ν_{NO} ($\Delta\nu_{NO} = -50$ cm^{-1}) suggests a porphyrin-centered reduction process. Thus, the IR data suggests that the (OEP)Os(NO)(SEt) undergoes a fast electron transfer centered on the porphyrin (Eq. 2.10) followed by a structural change that involves loss of the NO from the metal center (Eq. 2.11).

$$(OEP)Os(NO)(SEt) + e^{-} \rightleftharpoons [(OEP)Os(NO)(SEt)]^{-} \quad (2.10)$$

$$[(OEP)Os(NO)(SEt)]^{-} \rightarrow [(OEP)Os(SEt)]^{-} + NO \quad (2.11)$$

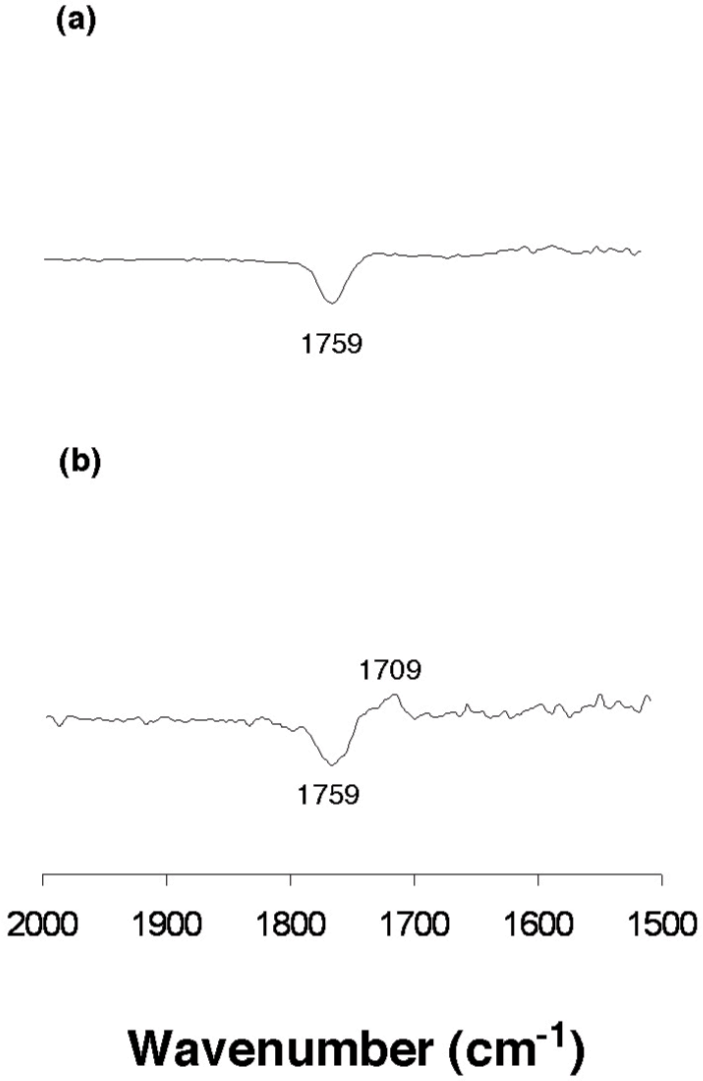

Figure 2.11. Difference FTIR spectra showing the consumption (OEP)Os(NO)(SEt) during its reduction (a) without buildup of product, and (b) with buildup of product on the electrode surface. The potential was held at –2.10 V vs. the $Cp_2Fe^{0/+}$ couple. The build-up of the reduction product was achieved by cycling the potential between –1.80 and –2.20 V at 400 mV/s for 1 min.

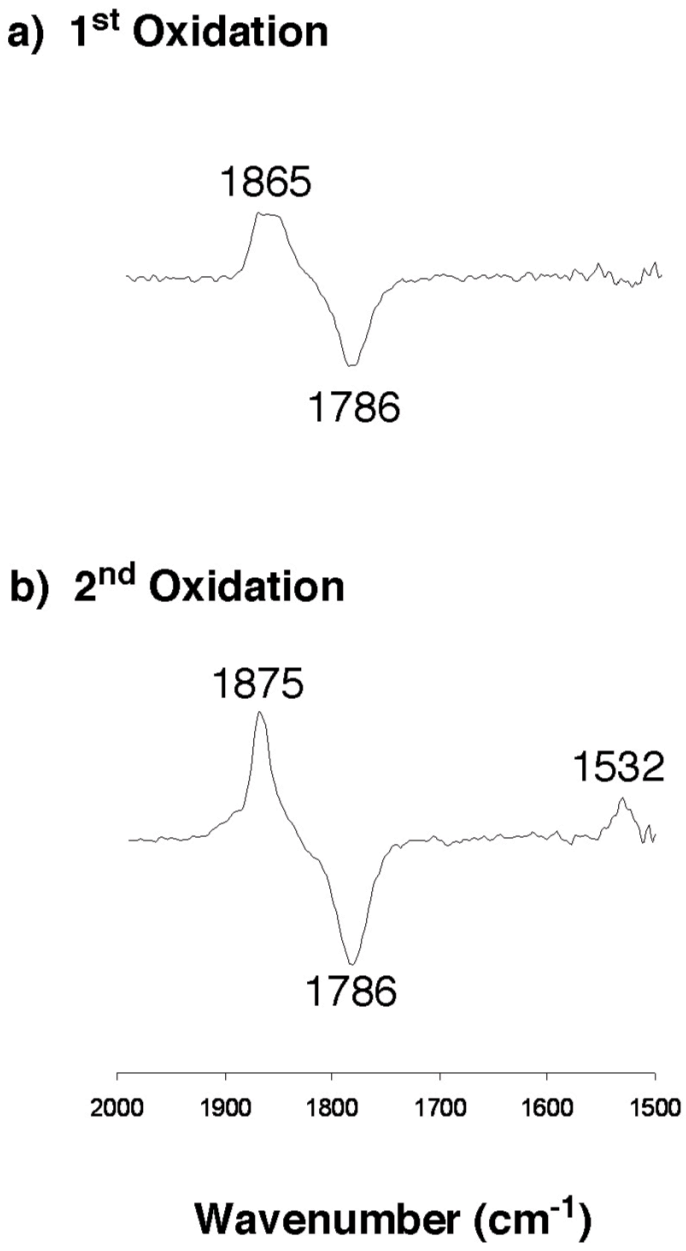

Figure 2.12. Difference FTIR spectra showing formation of products during (a) the first oxidation of (OEP)Ru(NO)(SEt), and (b) the second oxidation of (OEP)Ru(NO)(SEt).

The IR difference spectrum which reveals the consumption of the (OEP)Ru(NO)(SEt) complex upon oxidation is shown in Figure 2.12a. The band geometry for the new product suggests that perhaps more than one cationic species are produced in the timescale of our experiment. Upon the second oxidation (Figure 10b), however, the product peak sharpens considerably, consistent with the presence of a single nitrosyl-containing dicationic species with ν_{NO} = 1875 cm^{-1}. Similar to that seen in the Os analogue, a new band at 1532 cm^{-1} is also evident in the difference spectrum after the second oxidation, which suggests that a π-radical cation is produced during the second oxidation. The spectroelectrochemical results upon reduction of (OEP)Ru(NO)(SEt) show consumption of the complex, and will not be discussed further.

Extended Hückel Calculations. We were interested in the electronic structures of the osmium alkoxide and thiolate complexes, since both (OEP)Os(NO)(OEt) and (OEP)Os(NO)(SEt) display an identical ν_{NO} value of 1759 cm^{-1} in CH_2Cl_2. In contrast, the (OEP)Ru(NO)(OEt) (ν_{NO} = 1801 cm^{-1}) and the (OEP)Ru(NO)(SEt) (ν_{NO} = 1788 cm^{-1}) compounds display ν_{NO}s that are consistent with the increased electron density of the thiolate complex.

The highest occupied molecular orbitals (HOMOs) of (OEP)Os(NO)(OEt), (OEP)Os(NO)(SEt), and $[(OEP)Os(NO)]^+$ are displayed in Figure 2.13. The HOMO of (OEP)Os(NO)(OEt) is largely centered on the (OEP)Os fragment as shown in Figure 2.13a, with 70% of its charge in the metal d orbitals, ~25% concentrated on the porphyrin ring, and small contributions from the axial ligands. The infrared spectroelectrochemical results for the oxidation of (OEP)Os(NO)(OEt), described

earlier, reveal a net formation of a porphyrin-based π-radical cation as the primary observable product. The axial ligands are not affected much by the oxidation of (OEP)Os(NO)(OEt), consistent with the HOMO of (OEP)Os(NO)(OEt) having only small axial ligand contributions and significant contributions from the (OEP)Os moiety. The LUMO of (OEP)Os(NO)(OEt) (Figure 2.14a) involves antibonding interactions between the metal d_{xz} orbital and both the π* orbital of NO (major) and the ethoxy O-atom's p_x orbital (minor). In the electrochemical experiment with (OEP)Os(NO)(OEt), however, this LUMO is not accessed since the compound's reduction potential apparently falls outside the solvent limit. The HOMO of (OEP)Os(NO)(SEt) is shown in Figure 2.13b. It consists of a π bonding interaction between the metal d_{xz} orbital and the p_x orbital on the sulfur (46% of the electron density is localized on sulfur, 10% on the metal), and a π antibonding interaction between the metal d_{yz} orbital and a π* orbital on NO (25% of the electron density is located on the nitrosyl N-atom, 8% on the O-atom). This implies that oxidation of this compound should weaken the Os-sulfur bond and strengthen the OsNO link. Indeed, our cyclic voltammetry and infrared spectroelectrochemical results support this conclusion.

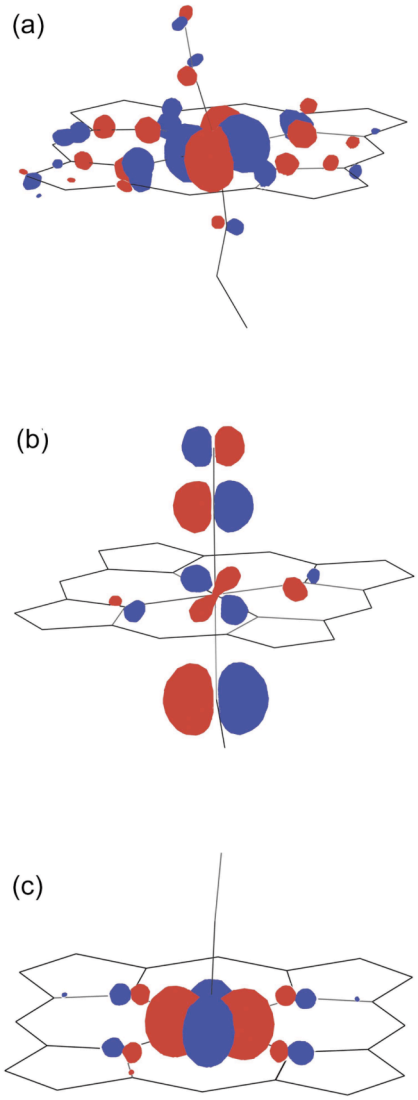

Figure 2.13. Highest occupied molecular orbitals of (a) (OEP)Os(NO)(OEt), (b) (OEP)Os(NO)(SEt), and (c) the model compound $[(OEP)Os(NO)]^+$ as determined by extended Hückel calculations. The eight ethyl groups on the porphyrin ring and all hydrogen atoms were included in the calculations, but are not shown for clarity.

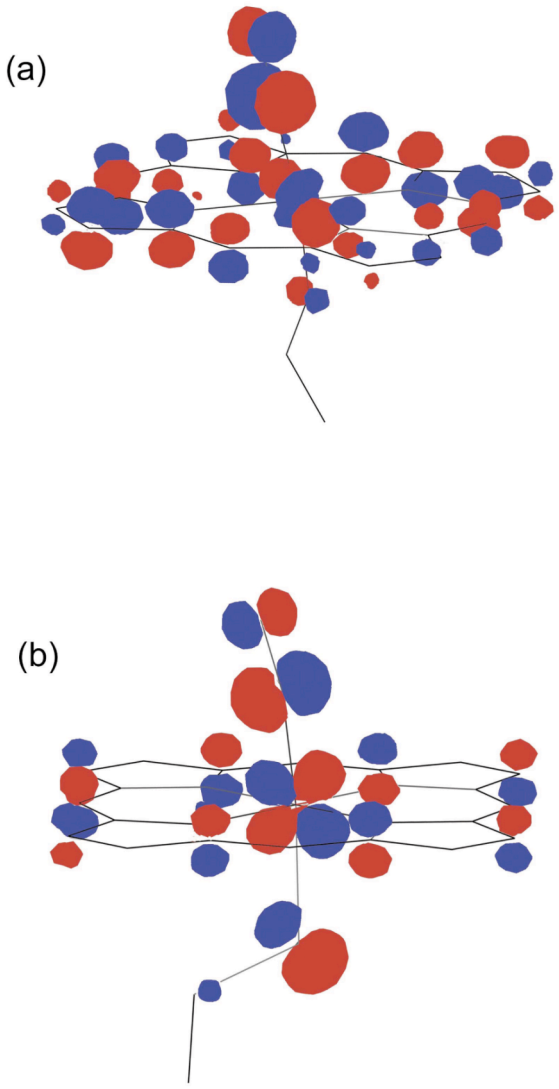

Figure 2.14. Lowest unoccupied molecular orbitals of (a) (OEP)Os(NO)(OEt), and (b) (OEP)Os(NO)(SEt) as determined by extended Hückel calculations. The eight ethyl groups on the porphyrin ring and all hydrogen atoms were included in the calculations, but are not shown for clarity.

Upon oxidation, both the υ_{NO} increase ($\Delta\nu_{NO}$ = 71 cm^{-1}) and Os-SEt bond cleavage (Eq. 2.8) occur. In fact, the result is the generation of $[(OEP)Os(NO)]^+$ as shown in Eq. 2.8. We thus computed the HOMO of the cation $[(OEP)Os(NO)]^+$, depicted in Figure 2.13c. The HOMO is largely centered on the (OEP)Os fragment (88% of its electron density on the metal), similar to that described for (OEP)Os(NO)(OEt) and shown in Figure 2.13a. We have shown that the second oxidation of (OEP)Os(NO)(SEt) results in the generation of a porphyrin π-radical cationic species $[(OEP^{\bullet})Os(NO)]^{2+}$ (Eq. 2.9), which is consistent with the calculated orbital using similar reasoning to that shown in the (OEP)Os(NO)(OEt) case.

The LUMO of (OEP)Os(NO)(SEt) (Figure 2.14b) involves antibonding interactions between the metal d_{xz} orbital and both the S-atom and a π* orbital on NO. Thus, reduction of the thiolate complex will be expected to result in a weakening of the Os-NO bond and an increase in the antibonding character of the N-O bond, with a weakening of the Os-SEt bond. Our experimental observation of a partially reversible reduction resulting in loss of the NO ligand (Eq. 2.11 and Figure 2.11) during the reduction of (OEP)Os(NO)(SEt) ($\Delta\upsilon_{NO}$ = –50 cm^{-1}) is consistent with the increased occupation of this LUMO.

Conclusion

We have shown that within the class of (OEP)M(NO)(XEt) compounds (M = Os, Ru; X = O, S), differences exist in their redox behaviors that can be readily explained by extended Hückel calculations. In the case of (OEP)Os(NO)(OEt), only

one electrochemical response was observed in its cyclic voltammogram in CH_2Cl_2, and this was a reversible oxidation centered on the porphyrin ring. A different redox behavior was observed for the thiolate analogue (OEP)Os(NO)(SEt), where the first oxidation results in a net removal of the SEt ligand. The calculations on (OEP)Os(NO)(SEt) reveal a HOMO with significant π bonding character between Os and S, consistent with loss of SEt in the oxidation process. Further, the calculated LUMO shows an antibonding interaction between the metal and the NO ligand, consistent with the observation that reduction of (OEP)Os(NO)(SEt) results in denitrosylation.

References

(1) Richter-Addo, G. B.; Legzdins, P.; Burstyn, J. *Chem. Rev.* **2002**, *102*, 857-860.
(2) Richter-Addo, G. B.; Legzdins, P. *Metal Nitrosyls*; Oxford Unversity Press: New York, 1992.
(3) Cheng, L.; Richter-Addo, G. B. In *The Porphyrin Handbook*; Guilard, R., Smith, K., Kadish, K. M., Eds.; Academic Press: New York, 2000; Vol. 4, p Ch. 33.
(4) Ford, P. C.; Laverman, L. E.; Lorkovic, I. M. *Adv. Inorg. Chem.* **2003**, *51*, 203-257.
(5) Butler, A. R.; Glidewell, C.; Li, M.-H. *Adv. Inorg. Chem.* **1988**, *32*, 335-393.
(6) Sharma, V. S.; Pilz, R. B.; Boss, G. R.; Magde, D. *Biochemistry* **2003**, *42*, 8900-8908, and references therein.
(7) Selçuki, C.; van Eldik, R.; Clark, T. *Inorg. Chem.* **2004**, *43*, 2828-2833, and references therein.
(8) Buchler, J. W.; Smith, P. D. *Chem. Ber.* **1976**, *109*, 1465-1476.
(9) Cheng, L.; Chung, H.-S.; Khan, M. A.; Young, V. G.; Richter-Addo, G. B. *Organometallics* **1998**, *17*, 3853-3864.
(10) Cheng, L.; Powell, D. R.; Khan, M. A.; Richter-Addo, G. B. *Inorg. Chem.* **2001**, *40*, 125-133.
(11) Chen, L.; Khan, M. A.; Richter-Addo, G. B. *Inorg. Chem.* **1998**, *37*, 533-540.
(12) Lee, J.; Yi, G.-B.; Powell, D. R.; Khan, M. A.; Richter-Addo, G. B. *Can. J. Chem.* **2001**, *79*, 830-840.

(13) Leal, F. A.; Lorkovic, I. M.; Ford, P. C.; Lee, J.; Chen, L.; Torres, L.; Khan, M. A.; Richter-Addo, G. B. *Can. J. Chem.* **2003**, *81*, 872-881.
(14) Antipas, A.; Buchler, J. W.; Gouterman, M.; Smith, P. D. *J. Am. Chem. Soc.* **1980**, *102*, 198-207.
(15) Leung, W.-H.; Chim, J. L. C.; Lai, W.; Lam, L.; Wong, W.-T.; Chan, W. H.; Yeung, C. H. *Inorg. Chim. Acta* **1999**, *290*, 28-35.
(16) Bohle, D. S.; Goodson, P.; Smith, B. *Polyhedron* **1996**, *15*, 3147-3150.
(17) Yi, G.-B.; Chen, L.; Khan, M. A.; Richter-Addo, G. B. *Inorg. Chem.* **1997**, *36*, 3876-3885.
(18) Yi, G.-B.; Khan, M. A.; Richter-Addo, G. B. *Chem. Commun.* **1996**, 2045-2046.
(19) Yi, G.-B.; Khan, M. A.; Richter-Addo, G. B. *Inorg. Chem.* **1996**, *35*, 3453-3454.
(20) Yi, G.-B.; Khan, M. A.; Powell, D. R.; Richter-Addo, G. B. *Inorg. Chem.* **1998**, *37*, 208-214.
(21) Bohle, D. S.; Hung, C.-H.; Powell, A. K.; Smith, B. D.; Wocadlo, S. *Inorg. Chem.* **1997**, *36*, 1992-1993.
(22) Hodge, S. J.; Wang, L.-S.; Khan, M. A.; Young, V. G.; Richter-Addo, G. B. *Chem. Commun.* **1996**, 2283-2284.
(23) Pandey, D. S.; Saini, S. K.; Agarwala, U. C. *Bull. Chem. Soc. Jpn.* **1987**, *60*, 3031-3033.
(24) Miranda, K. M.; Bu, X.; Lorkovic, I.; Ford, P. C. *Inorg. Chem.* **1997**, *36*, 4838-4848.
(25) Srivastava, T. S.; Hoffman, L.; Tsutsui, M. *J. Am. Chem. Soc.* **1972**, *94*, 1385-1386.
(26) Kadish, K. M.; Adamian, V. A.; Caemelbecke, E. V.; Tan, Z.; Tagliatesta, P.; Bianco, P.; Boschi, T.; Yi, G.-B.; Khan, M. A.; Richter-Addo, G. B. *Inorg. Chem.* **1996**, *35*, 1343-1348.
(27) Massoudipour, M.; Pandey, K. K. *Inorg. Chim. Acta* **1989**, *160*, 115-118.
(28) Bohle, D. S.; Hung, C.-H.; Smith, B. D. *Inorg. Chem.* **1998**, *37*, 5798-5806.
(29) Lee, J.; Yi, G.-B.; Khan, M. A.; Richter-Addo, G. B. *Inorg. Chem.* **1999**, *38*, 4578-4584.
(30) Richter-Addo, G. B.; Wheeler, R. A.; Hixson, C. A.; Chen, L.; Khan, M. A.; Ellison, M. K.; Schulz, C. E.; Sheidt, W. R. *J. Amer. Chem. Soc.* **2001**, *123*, 6314-6326.
(31) Patterson, J. C.; Lorkovic, I. M.; Ford, P. C. *Inorg. Chem.* **2003**, *42*, 4902-4908.
(32) Ashley, K.; Pons, S. *Chem. Rev.* **1988**, *88*, 673-695.
(33) Shaw, M. J.; Henson, R.; Houk, S. E.; Westhoff, J. W.; Jones, M. W.; Richter-Addo, G. B. *J. Electroanal. Chem* **2002**, *534*, 47-53.
(34) Zahran, Z. N.; Shaw, M. J.; Khan, M. A.; Richter-Addo, G. B. *Inorg. Chem.* **2006**, *45*, 2661-2668.
(35) Carter, S. M.; Lee, J.; Hixson, C. A.; Powell, D. R.; Wheeler, R. A.; Shaw, M. J.; Richter-Addo, G. B. *Dalton Transactions* **2006**, *10*, 1338-1346.

(36) Xu, N.; Lee, J.; Powell, D. R.; Richter-Addo, G. B. *Inorg. Chim. Acta* **2005**, *358*, 2855-2860.
(37) Connelly, N. G.; Geiger, W. E. *Chem. Rev.* **1996**, *96*, 877-910.
(38) Landrum, G. A.; Glassey, W. V. 2004.
(39) Buchler, J. W.; Kokisch, W.; Smith, P. D. *Struct. Bonding* **1978**, *34*, 79-134.
(40) Antipas, A.; Buchler, J. W.; Gouterman, M.; Smith, P. D. *J. Amer. Chem. Soc.* **1978**, *100*, 3015-3024.
(41) Johann W. Buchler, P. D. S. *Chem. Ber.* **1976**, *109*, 1465-1476.
(42) Shimomura, E. T.; Phllippi, M. A.; Goff, H. M. *J. Amer. Chem. Soc.* **1981**, 103, 6778-6780.

Chapter 3. Syntheses, spectroscopy, and solid-state molecular structures of ruthenium nitrosyl porphyrin complexes containing imidazolate and imidazole ligands.

Introduction

Nitric oxide (NO) is known to be a biologically important signaling molecule that interacts with the iron centers of heme proteins resulting in both pathological and physiological consequences. In many cases, the exact nature of this interaction is not well defined and over the past three decades has been the subject of intense worldwide study. While biochemists have scrutinized the overall interaction of NO with the prosthetic heme center and the surrounding protein, chemists have taken the more fundamental approach of studying the binding of the free radical to the metal center using metalloporphyrin models of the reactive heme prosthetic group. In some cases, as with our group, a combination of biomimetic modeling and examination of NO binding in natural and mutated heme proteins has been used in conjunction to better understand this interaction.

Of the biologically abundant heme proteins, those with the imidazole containing histidine (His) residue bound to the iron center of the porphyrin prosthetic group are most prevalent. In enzymatic heme proteins, the cytochrome and peroxidase classes of enzymes are the largest groups containing iron bound histidine. Cytochromes are membrane bound proteins that facilitate electron transfers in and out of the membrane and catalyze various redox reactions while peroxidases catalyze the oxidation of

substrates using peroxide as an electron acceptor. In both cases, NO is believed to interact with the heme iron centers under physiological conditions.[1-7]

Recently, the importance of the protonation state of histidine in heme proteins has been questioned.[8] It has been suggested that the protonation state of the imidazole containing proximal His residue in heme proteins may influence the binding of both the substrate and the proximal His to the iron center of the heme pocket. Additionally, strong hydrogen bonding between the N-H segment of His with other amino acid residues in proteins essentially causes the His residue to have more of a deprotonated like charge and may effect the reactivity of some heme proteins. The known crystal structures of many of the peroxidases, for example, show putative hydrogen bonding between the proximal His and a conserved asparagine (Asn) residue (Fig. 3.1). These studies suggests that not only is the question of if the imidazole group of the His contains a protonated nitrogen is important, but also that the strength of the N-H bond may be significant in the reactive properties of heme containing peroxidases and some cytochromes.

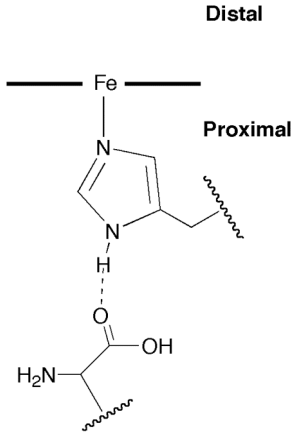

Figure 3.1: Hydrogen bonding between a heme bound histidine and an asparagine amino acid residue inside the proximal pocket of a heme enzyme.

Despite the abundance of heme proteins with iron histidine bonds and their known interactions with nitric oxide, there have been few modeling studies involving a metalloporphyrin containing both NO and imidazole linkages.[9,10] Scheidt and coworkers have obtained single crystal molecular structural data for an ferric metalloporphyrin containing *trans* 1-methylimidazole and NO groups, however, specially developed synthetic and crystallization techniques were required due to the ease in which this complex underwent reductive nitrosylation which results in the loss of the NO group from the six-coordinate complex.[10] The instability of this complex severely limits synthetic and chemical studies. The few reports of nitrosyl-heme model complexes with imidazole linkages in the literature and the previously mentioned importance of the protonation state of the imidazole containing histidine ligand, interested us in preparing stable *Group 8* nitrosyl metalloporphyrin complexes containing metal bound imidazole ligands with emphasis on synthetic, reactivity, spectroscopic, and structural comparison of imidazolate with cationic imidazole complexes.

Previously, our group has extensively explored the synthesis, solid-state molecular structures, and reaction chemistry of *Group 8* nitrosyl-metalloporphyrins containing alkoxides (-OR) and thiolate (-SR) linkages *trans* to the NO.[11-20] Studies of the infrared-spectroelectrochemistry of some of these complexes have been published and were presented in Chapter 2.[21] In these studies, we have shown that osmium and ruthenium porphyrin complexes readily react in the presence of organic nitrite (ONOR) and organic thionitrite (ONSR) complexes to form osmium and ruthenium porphyrins containing alkoxides and thiolates, respectively, *trans* to a nitrosyl group.

Interestingly, while the alcohol analogues of the alkoxide complexes can be prepared without difficulty from protonation of (por)Os(NO)(OR) to give the $[(por)Os(NO)(HOR)]^+$ cationic derivatives[18], attempts at the preparation of the thiol complexes of the nitrosyl-metalloporphyrins have been unsuccessful to date. This difference in reactivity of *Group 8* osmium and ruthenium nitrosyl-metalloporphyrins towards the formation of alcohol and thiol metal bound complexes is still under investigation. The discrepancies in these *Group 8* nitrosyl-metalloporphyrins towards the formation of the alcohol vs. thiol complexes has further compelled us into examining the chemistry of imidazolate- and imidazole-containing ruthenium low-spin nitrosyl porphyrins.

In this chapter, we examine the synthesis, structure and reactivity of neutral (por)Ru(NO)(RIm) and the analogues cationic $[(por)Ru(NO)(RIm)]^+$ complexes (where por = TPP, TTP, T(*p*-OMe)PP, and OEP and RIm = imidazolate (Im), imidazole (HIm), 1-methylimidzole (1-MeIm), 5-methylimidazolate (5-MeIm) or 4- and 5-methylimidazole (4(5)-MeHIm)) (Scheme 3.1).

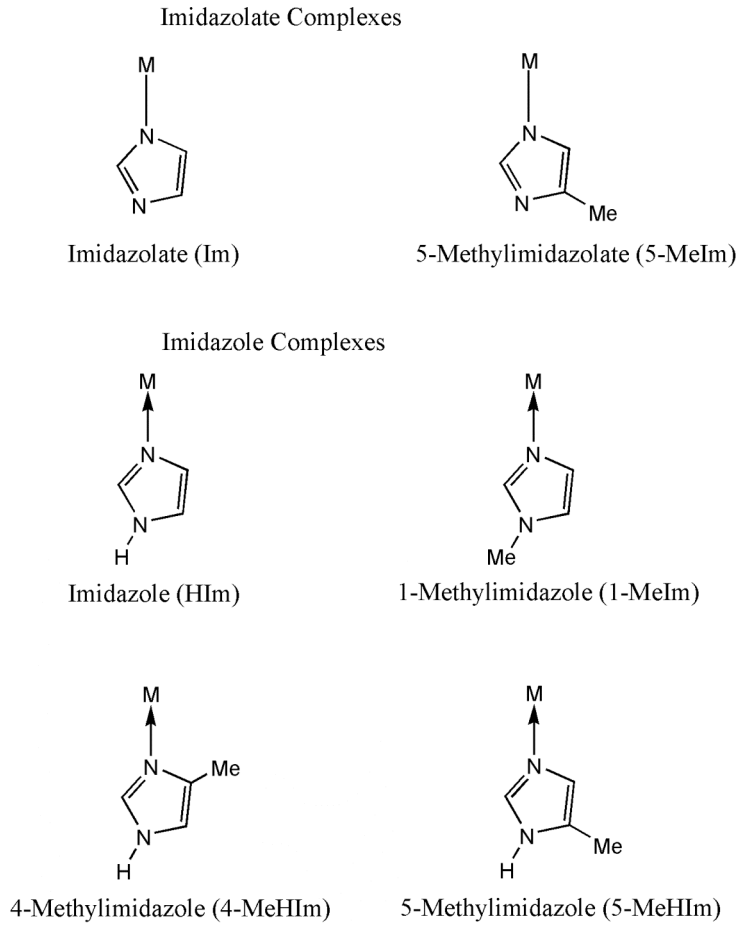

Scheme 3.1. Imidazolate and imidazole ligands used in this study.

Experimental Section

All reactions were performed under an atmosphere of prepurfied nitrogen gas in standard Schlenk glassware and/or a Labmaster 100 Dry Box. All samples for spectral studies were also prepared under a nitrogen atmosphere. All solvents were distilled from appropriate drying agents under an atmosphere of nitrogen just prior to use: CH_2Cl_2 (CaH_2), hexanes (CaH_2).

The (Por)Ru(CO) compounds were prepared by published procedures (TTP, TPP, T(*p*-OMe)PP).[22] (OEP)Ru(CO) and (OEP)Ru(CO)·HOMe were purchased from

Mid-Century Chemicals and Aldrich Chemical Company, respectively. Isoamyl nitrite (*i*-$C_5H_{11}ONO$, 97%), imidazole (HIm, 99+%), 1-methylimidazole (1-MeIm, ≥99%, purified by redistillation), 4-methylimidazole (4-MeHIm, 98%), and pyridine (Py, anhydrous, 99.8%) were purchased from Aldrich Chemical Co. and used as received. Nitrosonium hexafluoroantimonate (99%) and nitrosonium tetrafluoroborate (98%) were purchased from Strem Chemicals and Alfa Aesar Chemicals, respectively. Chloroform-*d* (99.8%, Cambridge Isotope Laboratories) was subject to three freeze-pump-thaw cycles and stored over molecular sieve (type 4A) under nitrogen prior to use. (OEP)Ru(NO)(O-*i*-C_5H_{11}) and (TPP)Ru(NO)(O-*i*-C_5H_{11}) where prepared as described in the literature.[16]

Infrared spectra were recorded using a Bio-Rad FT-155 FTIR spectrometer. Proton NMR spectra were obtained on Varian 400 or 300 MHz spectrometers and the signals were referenced to the residual proton signal of $CDCl_3$ (7.24 ppm). All coupling constants are in Hz. FAB mass spectra were obtained on a VG-ZAB-E mass spectrometer. ESI mass spectra were obtained on a TOF-MS-ES mass spectrometer.

Preparation of (T(*p*-OMe)PP)Ru(NO)(O-*i*-C_5H_{11}). (T(*p*-OMe)PP)Ru(NO)(O-*i*-C_5H_{11}) was prepared using methods similar to those previously reported for the related (TPP)Ru(NO)(O-*i*-C_5H_{11}) complex[16] but with slight modifications. A stirred red mixture of (T(*p*-OMe)PP)Ru(CO) (14.6 mg, 0.0169 mmol) and isoamyl nitrite (2.5 μL, 0.0169 mmol, 98%) in CH_2Cl_2 (15 mL) was refluxed under N_2 for 40 min. The color changed to a dark red-brown and the IR spectrum of an aliquot showed the disappearance of υ_{CO} at 1937 cm^{-1} and the appearance of υ_{NO} at 1808 cm^{-1}. The sample was dried in vacuo leaving a purple

microcrystalline residue. The crude yield prior to recrystallization was ca. 90 %. ^{1}H NMR, prior to recrystallization, showed that an unidentified (T(*p*-OMe)PP)Ru complex (~10%) remained with the nitrosyl product. Purple crystals suitable for single crystal X-ray crystallographic analysis were obtained from the slow evaporation under N_2 of a CH_2Cl_2/hexanes (1:1, 6 mL total) mixture of the reaction product. IR (KBr): υ_{NO} = 1801 cm^{-1}. ^{1}H NMR ($CDCl_3$, 7.24 ppm, δ): 8.98 (s, 1.6 H, unidentified β-H porphyrin), 8.94 (s, 8 H, β-H of T(*p*-OMe)PP), 8.15 (m, 8H, *J* = 2 Hz, phenyl H of T(*p*-OMe)PP), 7.29 (d, 8 H, 8H, *J* = 8 Hz, phenyl H of T(*p*-OMe)PP), 4.09 (s, 12 H, H of OMe), 0.054 (s, grease), -0.573 (d, 6 H, *J* = 7 Hz, H of O-*i*-C_5H_{11}), -1.00 (m, 1 H, *J* = 7 Hz, , H of O-*i*-C_5H_{11}), -2.34 (t, 2 H, *J* = 8 Hz, , H of O-*i*-C_5H_{11}), -2.80 (q, 2 H, *J* = 8 Hz, , H of O-*i*-C_5H_{11}). ESI Mass Spec: 864.0 m/z (100%, (T(*p*-OMe)PP)Ru(NO)$^+$), 952.1 m/z (31%, [(T(*p*-OMe)PP)Ru(NO)(O-*i*-C_5H_{11}) + H]).

Preparation of (OEP)Ru(NO)(Im). This procedure is a slight modification of a published procedure for the preparation of the analogous (TTP)Ru(NO)(Im).[9] (OEP)Ru(NO)(O-*i*-C_5H_{11})[16] (0.0505 g, 0.0672 mmol) and excess HIm (0.0241 mg, 0.354 mmol) were loaded into a Schlenk tube, the bottom three-quarters of which was wrapped in aluminum foil. The stirred solid mixture was heated under nitrogen between 85 and 100 °C in an oil bath. During 2 hr of heating, white, crystalline HIm sublimed onto the upper portion of the Schlenk tube that was not wrapped with aluminum foil. The white imidazole crystals were removed from the top of the Schlenk tube by carefully syringing hexanes over the crystals while the Schlenk tube was inverted. The crude product contained ca. 3% of the unbound HIm ligand (as

evidenced by ^{1}H NMR spectroscopy) and was removed by heating to 90 ºC with stirring under vacuum for 1 hr. Free HIm was once again washed out with hexanes from the top of the Schlenk tube. Recrystallization of the residue from a 1:2 mixture of CH_2Cl_2:hexanes (9 mL total) resulted in the generation of dark red brown microcrystals of the (OEP)Ru(NO)(Im) product (0.0439 g, 0.585 mmol, 87% isolated yield). A suitable brownish red crystal of (OEP)Ru(NO)(Im)·Im·0.25 CH_2Cl_2 was grown from the slow evaporation of a CH_2Cl_2:hexanes mixture of the crude mixture containing free imidazole. IR (CH_2Cl_2, cm^{-1}): ν_{NO} = 1848 cm^{-1}. IR (KBr, cm^{-1}): ν_{NO} = 1828 s; also 2963 s, 2927 s, 2870 m, 1465 m, 1446 m, 1371 w, 1315 w, 1263 w, 1228 w, 1151 m, 1106 m, 1080 m, 1058 m, 1019 m, 993 m, 961 m, 904 w, 843 w, 811 w, 742 w, 709 w, 664 w, 621 w, 574 w. ^{1}H NMR ($CDCl_3$, δ): 10.36 ppm (s, 4H, *meso*-H of OEP), 5.27 ppm (s, CH_2Cl_2), 4.16 ppm (m, 16 H, J = 7, CH_2CH_3 of OEP), 1.99 ppm (t, J = 8, 24 H, CH_2CH_3 of OEP), 0.073 ppm (sharp s, 1H, bound Im), -0.03 ppm (broad s, 1H, bound Im), -0.52 ppm (broad s, 1H, bound Im). ESI mass spectrum: *m/z* 732 (100 %) $[(OEP)Ru(NO)(Im) + H]^+$.

Preparation of (por)Ru(NO)(Im) (por = TPP and T(p-OMe)PP). [†]

(TPP)Ru(NO)(O-*i*-C_5H_{11})[16] (0.091 g, 0.108 mmol) and imidazole (0.04 g, 0.588 mmol) were loaded into a Schlenk tube and heated with an oil bath at 90-95 °C for 3h as described for the OEP analogue. Excess imidazole was removed under high vacuum. IR (CH_2Cl_2, cm^{-1}): ν_{NO} = 1854 cm^{-1}. ^{1}H-NMR ($CDCl_3$, δ): 8.98 (s, 8H, *pyr*-H of TPP), 8.26 (d, *J* = 6, 4H, *o*-H of TPP), 8.13 (d, *J* = 7, 4H, *o*'-H of TPP), 7.79 (m, 12H, *p*, *m*-H of TPP), 4.36 (s, 1H, imidazole), 0.48 (s, 1H, imidazole), -

[†] These complexes were originally prepared by Dr. Li Chen in our group.

0.045 (s, 1H, imidazole). ESI mass spectrum: *m/z* 812.1725 (100%) $[(TPP)Ru(NO)(Im) + H]^+$.

The new (T(*p*-OMe)PP)Ru(NO)(Im) compound was also generated by this method quantitatively as judged by ^1H NMR spectroscopy.

(T(p-OMe)PP)Ru(NO)(Im). IR (CH_2Cl_2, cm^{-1}): ν_{NO} = 1855 cm^{-1}. IR (KBr, cm^{-1}): ν_{NO} = 1846 s, also 2834 w , 1605 s, 1574 w, 1526 w, 1511 s, 1493 m, 1462 m, 1439 m, 1411 w, 1349 m, 1304 m, 1288 m, 1244 s, 1175 s, 1152 w, 1107 m, 1074 m, 1043 w, 1018 s, 1009 s, 905 w, 885 w, 867 w, 848 w, 811 m, 798 m, 788 m, 713 m, 664 w, 639 w, 600 w, 556 w, 537w, and 508 w. ^1H NMR ($CDCl_3$, δ): 9.02 (s, 8 H, pyrrole H), 8.11 (d of doublets, *J* = 42, 8 H, *m*-H), 7.30 (t, *J* = 9, 8 H, *o*-H), 4.37 (s, 1 H, Im), 4.10 (s, 12 H, OMe H), 0.49 (s, 1 H, Im), -0.049 (s, 1 H, Im). ESI mass spectrum: *m/z* 932 (80 %) $[(T(p\text{-}OMe)PP)Ru(NO)(Im) + H]^+$, 864 (100 %) $[(T(p\text{-}OMe)PP)Ru(NO) + H]^+$.

Preparation of (OEP)Ru(NO)(5-MeIm). (OEP)Ru(NO)(5-MeIm) was prepared using methods similar to those described in the preparation of (OEP)Ru(NO)(Im) except 4-MeHIm was used in place of HIm and the mixture was heated to just above the melting point of 4-MeHIm, between 82 and 100 °C for 2 hr. Peaks corresponding to free 4-MeHIm were observed in the ^1H NMR spectrum of the product mixture and further separation from the product was not attempted. A dark red single crystal of (OEP)Ru(NO)(5-MeIm)·4-MeHIm suitable for X-ray crystallographic analysis was grown from the slow evaporation of a 1:1 CH_2Cl_2:hexanes mixture containing the product. IR (CH_2Cl_2, cm^{-1}): ν_{NO} = 1845. ^1H NMR ($CDCl_3$, δ): 10.36 ppm (s, 4H, *meso*-H of OEP), 7.20 ppm (s, free 4-

MeHIm), 6.54 ppm (s, free 4-MeIm), 5.29 ppm (s, CH_2Cl_2), 4.17 ppm (m, J = 8 Hz, 16 H, CH_2CH_3 of OEP), 2.06 ppm (s, 3H, free 4-MeHIm), 2.01 ppm (t, *J* = 8, 24 H, CH_2CH_3 of OEP), 0.36 ppm (s, 3H, bound 5-MeIm) 0.08 ppm (sharp s, grease), -0.11 ppm (s, 1H, bound 5-MeIm), -0.84 ppm (s, 1H, bound 4-MeIm). ESI mass spectrum: *m/z* 746.4 (100 %) $[(OEP)Ru(NO)(5\text{-}MeIm) + H]^+$.

Preparation of $[(por)Ru(NO)(HIm)]^+$ ($[(OEP)Ru(NO)(HIm)]SbF_6$, and $[(TTP)Ru(NO)(HIm)]BF_4$). (OEP)Ru(CO)•(MeOH) (12.3 mg, 1.76 x 10^{-5} mol) and HIm (2.1 mg, 3.09 x 10^{-5} mol) were stirred together in freshly distilled CH_2Cl_2 (20 mL). $NOSbF_6$ (~10.2 mg, ~3.940 x 10^{-5} mol) was added to the light red solution, resulting immediately in a darkening of the solution. IR spectroscopic monitoring of the reaction solution showed that the ν_{CO} at 1936 cm^{-1} was replaced by a ν_{NO} at 1870 cm^{-1}. The solvent was removed in vacuo leaving a red-purple crystalline solid. Excess HIm was sublimed at the top of the Schlenk tube after heating the tube (the bottom ¾ of which was wrapped in aluminum foil) at 100 ºC for 1 hr. The white crystalline solid was removed as described above. This red-purple solid was washed with hexanes (3x10 mL) and redissolved in CH_2Cl_2. Microcrystals of the $[(OEP)Ru(NO)(HIm)]SbF_6$ product were obtained from slow evaporation of a 1:2 mixture of CH_2Cl_2:hexanes (9 mL total) (84% yield, 14.6 mg). A dark red single crystal of $[(OEP)Ru(NO)(HIm)]SbF_6$ suitable for X-ray crystallographic analysis was grown from the slow evaporation of a 1:1 chlorobenzene:hexanes mixture (8 mL total) under nitrogen. IR (CH_2Cl_2, cm^{-1}): ν_{NO} = 1870. IR (KBr, cm^{-1}): 1852. ^1H NMR ($CDCl_3$, δ): 10.47 ppm (s, 4H, *meso*-H of OEP), 5.28 ppm (s, CH_2Cl_2), 4.21 ppm (m, *J* = 8, 16 H, Et of OEP), 2.02 ppm (t, *J* = 8, 24 H, Et of OEP), 0.22 ppm (s, 1

H, bound HIm), 0.06 ppm (s, 1 H, bound HIm), -0.63 ppm (s, 1 H, bound HIm). ESI mass spectrum: *m/z* 732.3120 (100 %) [(OEP)Ru(NO)(HIm) + H].

The new [(TTP)Ru(NO)(HIm)]BF_4 compound was generated using this method except $NOSbF_6$ was substituted with $NOBF_4$. ^{1}H NMR spectroscopy showed quantitative conversion of the reagents to product.

[(TTP)Ru(NO)(HIm)]BF_4. IR (CH_2Cl_2, cm^{-1}): ν_{NO} = 1854. ^{1}H NMR ($CDCl_3$, δ): 9.13 (s, 8 H, pyrrole H), 8.12 (d , *J* = 8, 4 H, *o*-H), 8.08 (d, *J* = 7, 4 H, *o'*-H), 7.61 (t, *J* = 7, 8 H, *m*-H), 4.62 (s, 1 H, Im), 2.72 (s, 12 H, CH_3 of TTP), -0.09 (s, 1H, Im). ESI mass spectrum: *m/z* 868.2338 (100 %) [(TTP)Ru(NO)(HIm) + H]$^+$.

Preparation of [(OEP)Ru(NO)(Py)]BF_4. Preparation of [(OEP)Ru(NO)(Py)]$^+$ was previously reported, however, the synthetic details and spectroscopy were not given.[17] The [(OEP)Ru(NO)(Py)]BF_4 complex was prepared in a Schlenk tube by mixing $NOBF_4$ (4.3 mg, 0.037 mmol) with a bright pink solution of (OEP)Ru(CO)•(MeOH) (20 mg, 0.029 mmol) in CH_2Cl_2 (15 mL). The resulting dark red-brown solution was stirred for 15 min. Pyridine (2.3 μL, 0.029 mmol) was syringed into the solution. The mixture was stirred for 30 min resulting in a deep crimson solution. Removal of solvent under vacuum resulted in red-purple microcrystals of the [(OEP)Ru(NO)(Py)]BF_4 complex. IR (CH_2Cl_2): ν_{NO} = 1877 cm^{-1}. IR (KBr): ν_{NO} = 1859 cm^{-1}. ^{1}H NMR ($CDCl_3$, δ): 10.51 (s, 4 H, *meso*-H of OEP), 6.18 (t, *J* = 8 Hz, 1 H, Py), 4.98 (t, *J* = 8 Hz, 2 H, Py), 4.22 (m, *J* = 8 Hz, 16 H, CH_2CH_3 of OEP), 2.01 (t, *J* = 8 Hz, 32 H, CH_2CH_3 of OEP), -0.28 (d, *J* = 5 Hz, 2 H, Py). FAB mass spectrum: *m/z* 743.32 (100%) [(OEP)Ru(NO)(Py)]$^+$.

Preparation of [(OEP)Ru(NO)(1-MeIm)]BF_4. The [(OEP)Ru(NO)(1-MeIm)]BF_4 complex was prepared by the addition of $NOBF_4$ (4.0 mg, 0.034 mmol) to a Schlenk tube containing a bright pink (OEP)Ru(CO)(MeOH) (20 mg, 0.029 mmol) solution in CH_2Cl_2 (15 mL). After an immediate darkening of the solution to red-brown, the mixture was stirred for 15 min. Excess 1-MeIm (5.7 μL, 0.072 mmol) was syringed into the stirred solution and the reaction proceeded at room temperature for 30 min. The solution was dried in vacuo. Excess 1-methylimidazole was removed from the mixture by heating the Schlenk at ~120 °C for 1 hr followed by washing with hexanes as described above, followed by redissolving the microcrystals in a 2:1 mixture of CH_2Cl_2:hexanes (3 mL total) and recrystallizing, resulting in a dark red [(OEP)Ru(NO)(1-MeIm)]BF_4 complex which contained (as evident by ^{1}H NMR spectroscopy) ca. 1% free 1-MeIm. IR (CH_2Cl_2): ν_{NO} = 1872 cm^{-1}. ^{1}H NMR ($CDCl_3$, δ): 10.48 (s, 8 H, *meso*-H of OEP), 7.58 (s, free 1-MeIm), 7.05 (s, free 1-MeIm), 6.92 (s, free 1-MeIm), 4.46 (t, *J* = 2 Hz, 1 H, 1-MeIm), 4.21 (m, *J* = 8 Hz, 16 H, CH_2CH_3 of OEP), 3.79 (s, free 1-MeIm), 2.01 (t, *J* = 8 Hz, 32 H, CH_2CH_3 of OEP), 1.81 (s, 3 H, CH_3 of 1-MeIm), -0.32 (s, 1 H, 1-MeIm), -0.681 (t, *J* = 2 Hz, 1 H, 1-MeIm). FAB mass spectrum: *m/z* 746.3 (100%) [(OEP)Ru(NO)(1-MeIm)]$^+$.

Preparation of [(OEP)Ru(NO)(5-MeHIm)]SbF_6/[(OEP)Ru(NO)(4-MeHIm)]SbF_6[*]. [(OEP)Ru(NO)(5-MeHIm)]SbF_6 was prepared in a manner similar to that described above for the imidazole complexes except HIm was substituted with 4-MeHIm. Repeated preparations consistently resulted in the observation of a second set of ^{1}H NMR peaks, which were assigned to the structural isomer [(OEP)Ru(NO)(4-

[*] The mixture containing the ruthenium bound 4-MeHIm and 5-MeHIm isomers is represented by the notation 5(4)-MeHIm.

MeHIm)]SbF_6. A dark red single crystal of [(OEP)Ru(NO)(5-MeHIm)]SbF_6 suitable for X-ray crystallographic analysis was grown from the slow evaporation of a 1:1 CH_2Cl_2:hexanes mixture containing the dissolved product. IR (CH_2Cl_2, cm^{-1}): ν_{NO} = 1871. ^{1}H-NMR ($CDCl_3$, δ): 10.44 (s, 4H, *meso*-H of OEP for 5-MeHIm isomer), 10.40 (s, 1.6H, *meso*-H of OEP for 4-MeHIm isomer), 7.34 (s, free 4-MeHIm), 6.58 (s, free 4-MeHIm), 4.19 (m, 8Hz, 23H, CH_2CH_3 of OEP for 5(4)-MeHIm isomeric mixture), 2.09 (s, free 4-MeHIm), 1.99 (m, 8Hz, 36H, CH_2CH_3 of OEP for 5(4)-MeHIm isomeric mixture), 0.23 (s, 3H, 5-MeHIm), -0.40 (s, 0.76 H, 4-MeHIm), -1.01 (s, 1H, 5-MeHIm), -2.63 (s, 1.4H, 4-MeHIm).

High-Temperature ^{1}H NMR Spectrum of [(OEP)Ru(NO)(5(4)-MeHIm)]SbF_6. All experiments were performed using a J. Young NMR tube containing $CDCl_3$ solution of the [(OEP)Ru(NO)(5-MeHIm)]$^+$/[(OEP)Ru(NO)(4-MeHIm)]$^+$ isomers sealed under N_2. The temperature of the sample in the ^{1}H NMR probe was determined to be 58.6 ºC using an ethylene glycol NMR solution and standard NMR temperature calibration techniques. An ^{1}H NMR spectrum obtained just after the initial preparation of the 5(4)-MeHIm isomeric mixture revealed distinct peaks for the porphyrin *meso*-Hs of [(OEP)Ru(NO)(5-MeHIm)]SbF_6 and [(OEP)Ru(NO)(4-MeHIm)]SbF_6 at 10.47 and 10.43 ppm with peak integrations of 2.49 and 2.46 H, respectively. Similarly, the peaks assigned to CH_3 protons of the methyl imidazoles for the 5-MeHIm and 4-MeHIm isomers at 0.33 and -2.65 ppm. These peaks, the porphyrin *meso* and methyl imidazole protons, were considered spectroscopic handles and were followed throughout the experiment as a means to measure the relative ratios of the isomers in solution. The additional porphyrin and

ligand peaks mentioned above were also observed but are not listed here for clarity. In addition to the peaks assigned to the isomeric mixture, there was a small, unidentified porphyrin *meso*-H peak at 10.57 ppm (~5%) that remained unaffected throughout the kinetics study. An arrayed ^{1}H NMR experiment at 58.6 °C with a total of 30 discrete transient sets, with a 0.5 hr rest time between the sets (15 hr total), was acquired for the isomeric mixture.

Results and Discussion

Synthesis. Several ruthenium porphyrin complexes containing an imidazole-derived ligand, [(por)Ru(NO)(RIm)]$^+$, or a imidazolate-derived ligand, (por)Ru(NO)(RIm) (where R is vacant, 1-Me, 4-Me, or 5-Me), *trans* to the nitrosyl ligand have been synthesized and characterized.

The neutral imidazolate derived complexes were prepared from the addition of an alkoxide complex (por)Ru(NO)(O-*i*-C_5H_{11}) to RIm. The alkoxide served as a convenient starting material that deprotonated the imidazole starting material, forming the imidazolate product, (por)Ru(NO)(Im), and presumably isoamyl alcohol (eq 3.1, where por = TPP, T(*p*-OMe)PP or OEP and RIm = imidazole(reagent)/imidazolate(product) or 4-methylimidazole(reagent)/5-methylimidazole(product)).

$$\text{(por)Ru(NO)(O-}i\text{-C}_5\text{H}_{11}\text{)} + \text{RIm} \rightarrow \text{(por)Ru(NO)(RIm)} + \text{HO-}i\text{-C}_5\text{H}_{11} \quad (3.1)$$

Syntheses of these compounds were carried out under solvent free conditions similar to that reported by Bohle et al., in the preparation of the analogous (TTP)Ru(NO)(Im) complex[9] and showed quantitative or near quantitative conversion to products.

The preparation of the cationic compounds $[(por)Ru(NO)(HIm)]^+$, was achieved through the reaction of the in situ generated cationic $[(por)Ru(NO)]^+$ complex with pyridine or an imidazole derivative (eq 3.2, where por = TTP or OEP and HR = pyridine, imidazole, 5(4)-methylimidazole, or 1-MeIm).

$$[(por)Ru(NO)]^+ + HR \rightarrow [(por)Ru(NO)(HR)]^+ \quad (3.2)$$

The addition of 4-methylimidazole to $[(OEP)Ru(NO)]^+$ resulted in a 3:1 tautomeric mixture of the $[(OEP)Ru(NO)(5\text{-MeHIm})]^+$ and $[(OEP)Ru(NO)(4\text{-MeHIm})]^+$, which was determined by the ^1H NMR spectroscopy and from an X-ray crystal structure analysis. Compounds containing similar mixtures of the 4- and 5-methylimidazole structural isomers have been reported non-porphyrin ruthenium compounds.[23-25] Clarke et al. for example, reported that the addition of 4-MeHIm to $[H_2O(NH_3)_5Ru]^{2+}$ resulted in the formation of a $[(5\text{-MeHIm})(NH_3)_5Ru]^{3+}$ and its isomeric 4-MeHIm analogue in a 20:1 ratio.[25] Similar, ^1H NMR spectroscopy data showed the formation of the $[Ru(5\text{-MeHIm})_6]^{2+}$ complex and the isomeric $[Ru(5\text{-MeHIm})_5(4\text{-MeHIm})]^{2+}$ analogue.[23] In this case, the authors reported that X-ray crystallographic data showed conversion to the sterically less hindered $[Ru(5\text{-MeHIm})_6]^{2+}$ isomer upon recrystallization. However, the rate of isomeric conversion was not reported.

Spectroscopy.

a. Infrared (IR). All of the NO species display intense nitrosyl bands in their infrared spectra. Table 3.1 lists the nitrosyl stretching frequencies for the imidazole, imidazolate, and the pyridine complexes, as well as for the previously reported (TTP)Ru(NO)(Im) complex.[9]

Table 3.1. Nitrosyl stretching frequencies of imidazole, imidazolate, and pyridine ruthenium-nitrosyl porphyrins.

	ν_{NO} (cm^{-1})[a]	Reference
Neutral Complexes		
(OEP)Ru(NO)(L′)		
L′ = Im	1848	*This work*
5-MeIm	1845	*This work*
(TPP)Ru(NO)(Im)	1854	*This work*
(TTP)Ru(NO)(Im)	1846 (KBr)	*9*
(T(*p*-OMe)PP)Ru(NO)(Im)	1855	*This work*
Cationic complexes		
[(OEP)Ru(NO)(L′)]SbF_6		
L′ = HIm	1868	*This work*
5(4)-MeHIm	1868	*This work*
[(OEP)Ru(NO)(L′)]BF_4		
L′ = 1-MeIm	1872	*This work*
Py	1877	*This work*
[(TTP)Ru(NO)(HIm)]BF_4	1854	*This Work*

[a] All ν_{NO}s were recorded for complexes in CH_2Cl_2 unless otherwise noted.

Neutral complexes. The υ_{NO}s for the imidazolate complexes ranged between 1845 and 1855 cm^{-1}, which is typical of ruthenium porphyrins containing linear NO linkages.[26] The compounds containing the electron donating OEP macrocycle had lower υ_{NO} (1848 and 1845 cm^{-1} for the Im and 5-MeIm derivatives, respectively) than the complexes with the tetraarylporphyrin macrocycle as a result of the increased Ru→NO backbonding afforded by the increased electron density around the metal center.

Cationic complexes. The ν_{NO}s for the cationic complexes ranged between 1866 – 1877 cm^{-1}. Of these complexes, the 1-MeIm and Py analogues exhibit the highest ν_{NO}s in their infrared spectra. Presumably the higher nitrosyl stretches in the IR spectra reflect poor electron donation of the bases when compared to the HIm and 5(4)-MeHIm analogues.

The cationic imidazole complexes ([(TTP)Ru(NO)(HIm)]BF_4, [(OEP)Ru(NO)(HIm)]SbF_6, and the [(OEP)Ru(NO)(5(4)-MeHIm)]SbF_6 isomeric mixture) exhibit the same characteristic linear ν_{NO}s as their neutral analogues, however, the nitrosyl stretches are ~20 cm^{-1} higher. This indicates decreased Ru→NO back-bonding in the cationic imidazole complexes and follows the trend observed for the υ_{NO}s of the *group 8* cationic osmium-porphyrin-nitrosyl alcohol and neutral alkoxide complexes ($\Delta\nu_{NO}$ = ~70 cm^{-1}) previously reported by us.[18]

b. ^{1}H NMR. *Neutral complexes*. ^{1}H NMR spectra of the low-spin diamagnetic neutral ruthenium nitrosyl complexes in $CDCl_3$ confirmed the near quantitative to quantitative conversion of precursor compounds to the desired

product. The OEP macrocycles and the tetraarylporphyrin macrocycles exhibited the expected proton peaks for the macrocycles and imidazolate-derived ligands. The protons of the imidazolate ligands tended to exhibit resonances downfield (~0 ppm) due to influence from the aromatic macrocycle.

Cationic complexes. Like the neutral analogues, the cationic complexes exhibited ^{1}H NMR spectra that were typical of low-spin, diamagnetic ruthenium nitrosyl porphyrin complexes.[27] Similarly, the proton resonances associated with the imidazole and pyridine peaks were located downfield (~0 ppm) in the NMR spectra. No peaks were observed for the imidazole (N-H) protons for any of the cationic complexes. The reaction of $[(OEP)Ru(NO)]^{+}$ with 4-MeHIm that yielded $[(OEP)Ru(NO)(5\text{-}MeHIm)]^{+}$, consistently resulted in a second set of ^{1}H NMR peaks. This second set of peaks was assigned to the linkage isomer $[(OEP)Ru(NO)(4\text{-}MeHIm)]^{+}$. X-Ray crystallographic analysis confirmed presence of the linkage isomers of the bound 5-MeHIm to 4-MeHIm complexes in the crystalline state (vide infra). The formation of the isomeric mixture of $[(OEP)Ru(NO)(5\text{-}MeHIm)]^{+}$ and $[(OEP)Ru(NO)(4\text{-}MeHIm)]^{+}$ complexes is not surprising, considering that when 4-methylimidazole is added to solutions it tautomerizes to form an equilibrium with 5-methylimidazole (1:2 ratio, respectively) (fig. 3.2).[28,29] Hence, the existence of the tautomeric ligands in the reaction mixture allows for the formation of the nitrosyl ruthenium isomeric products.

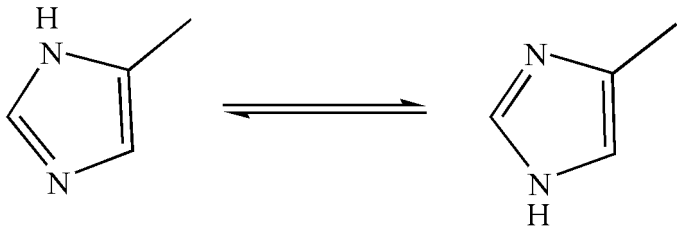

5-Methylimidazole 4-Methylimidazole

Figure 3.2. Tautomeric mixture of 5- and 4-methylimidazole.

Over time, the peaks assigned to the sterically bulky 4-MeHIm isomer decreased in intensity while those peaks assigned to the 5-MeHIm isomer showed growth in their intensities, indicating that the 4-MeHIm isomer was converted to the less sterically hindered 5-MeHIm isomer, likely through the disassociation of the 4-MeHIm ligand followed by the binding of 5-MeHIm ligand to the metal center. To measure the rate of conversion of the 4-MeHIm complex to the 5-MeHIm, we performed high temperature (58.6 °C) ^{1}H NMR spectroscopy experiments. As outlined in the experimental section of this chapter, at this elevated temperature the *meso*-H of [(OEP)Ru(NO)(5-MeHIm)]SbF_6 and [(OEP)Ru(NO)(4-MeHIm)]SbF_6 displayed resonances at 10.47 and 10.43 ppm with relative intensities of 3.60 and 4 H, respectively. Similarly, the peaks assigned to CH_3 of the methyl imidazoles for the 5-MeHIm and 4-MeHIm isomers displayed resonances at 0.33 and -2.65 ppm with relative intensities of 3.39 and 3.00 H, respectively. In addition to the peaks assigned to the isomeric mixture, there was a small unidentified *meso*-H (OEP)Ru peak at 10.57 ppm (~5%) that remained unaffected throughout the kinetics study. Conveniently, the frequencies of the *meso*-H and the methyl-Hs peaks assigned to the 4-methylimidazole and 5-methylimidazole complexes remained unaffected

throughout the NMR experiment, however, the (porphyrin) *meso*-peak associated with the 4-MeHIm derivative showed significant reduction while the peak associated with the 5-MeHIm showed significant enhancement (Fig. 3.3). The same trend was reflected in the peaks associated with the methyl protons of the 5-MeHIm and 4-MeHIm derivatives.

The decrease of the peaks associated with the [(OEP)Ru(NO)(4-MeHIm)]SbF_6 isomer exhibited first order kinetics with a rate constant, $k = 1.44 \times 10^{-5}\ s^{-1}$ and a half-life, $t_{1/2} = 4.81 \times 10^4$ s (Graph 3.1). The rate of growth for the peaks associated with the 5-MeHIm isomer was more complex and did not fit the criteria for zero, first, or second order. Though the compound was prepared in a different solvent, CH_2Cl_2, than what the ^{1}H NMR experiments were performed in ($CDCl_3$) we expect that the result of ligand isomerization to be qualitatively the same.

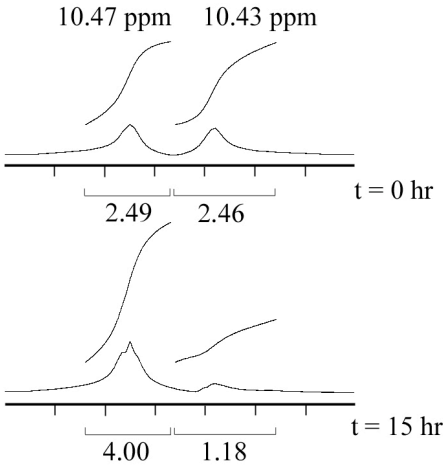

Figure 3.3. ^{1}H NMR spectra of the *meso*-H porphyrin peaks assigned to the isomers [(OEP)Ru(NO)(5-MeHIm)]SbF_6 (10. 47 ppm) and [(OEP)Ru(NO)(4-MeHIm) (10.43 ppm) in $CDCl_3$ at (a) time = 0 and the integration of the peaks at 10.47 and 10.43 ppm are 2.49 and 2.46, respectively, and (b) time = 15 hr and the integration of the peaks at 10.47 and 10.43 ppm change to 4.00 and 1.18, respectively. The spectra were recorded at 58.6 °C.

In order to better understand the nature of the dissociation of the 4-MeHIm ligand and subsequent binding of the 5-MeHIm ligand in the isomeric mixture of the nitrosyl ruthenium porphyrins, ~3.5 molar excess of unsubstituted imidazole (HIm) was added to the freshly prepared $[(OEP)Ru(NO)(5(4)\text{-}MeHIm)]^+$ mixture. Addition of the external imidazole ligand provided us with a more detailed spectroscopic glimpse into the plausible pathway by which the 4-MeHIm isomer was converted to the 5-MeHIm isomer. There are two likely ways in which this conversion occurs: (1) both the 4-MeHIm and the 5-MeHIm ligands are released from the ruthenium forming an equilibrium with the five-coordinate complex (Scheme 3.2a) or (2) the 4-MeHIm dissociates from the metal center and the 5-MeHIm tautomer binds to the 5-coordinate nitrosyl ruthenium porphyrin to form the sterically favored product, which is stable and does not undergo bond dissociation (Scheme 3.2b).

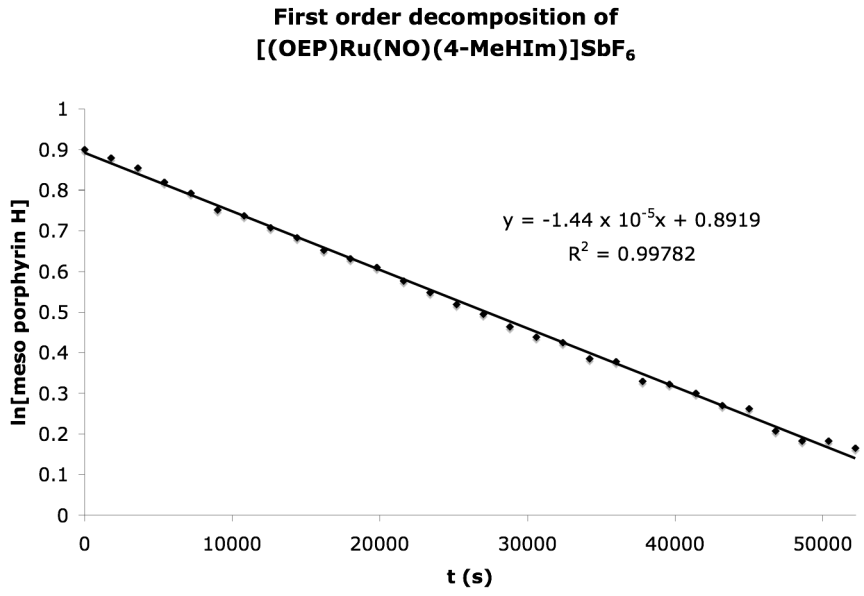

Graph 3.1. First order decomposition of the peak at δ 10.43 ppm assigned to the porphyrin *meso*-Hs of the $[(OEP)Ru(NO)(4\text{-}MeHIm)]SbF_6$ isomer.

In the first scenario, we would expect to observe decreases in the concentrations of both the 5-MeHIm and 4-MeHIm isomers since abundant free imidazole ligand would have a higher probability of interacting with the five-coordinate equilibrium product, diminishing both the 5-MeHIm and 4-MeHIm complexes and forming the $[(OEP)Ru(NO)(HIm)]^+$ complex. The second scenario would reveal diminishing peaks for the 4-MeHIm isomer with growth of new peaks associated with the HIm complex, while the concentration of the 5-MeHIm remained unaffected.

When an excess amount of imidazole (ca. 3.5 molar) was added to a freshly prepared mixture of the $[(OEP)Ru(NO)(5(4)\text{-}MeHIm)]^+$ isomers in $CDCl_3$, high temperature ^1H NMR revealed a gradual decrease in the resonance peaks associated with the porphyrin *meso*- and methyl-protons associated with the 4-MeHIm ring (10.43 and -2.65 ppm, respectively). In addition to the disappearance of the peaks associated with the 4-MeHIm complex, new resonances were observed for the appearance of the $[(OEP)Ru(NO)(HIm)]^+$ complex. There was no observed change in the resonances for the $[(OEP)Ru(NO)(5\text{-}MeHIm)]^+$ complex. The ^1H NMR data suggests that the 4-MeHIm dissociates from the metal center followed by the binding of the tautomeric 5-MeHIm ligand to form the $[(OEP)Ru(NO)(5\text{-}MeHIm)]^+$ complex. The $[(OEP)Ru(NO)(5\text{-}MeHIm)]^+$ complex is stable and undergoes no ligand dissociation (Scheme 3.2b).

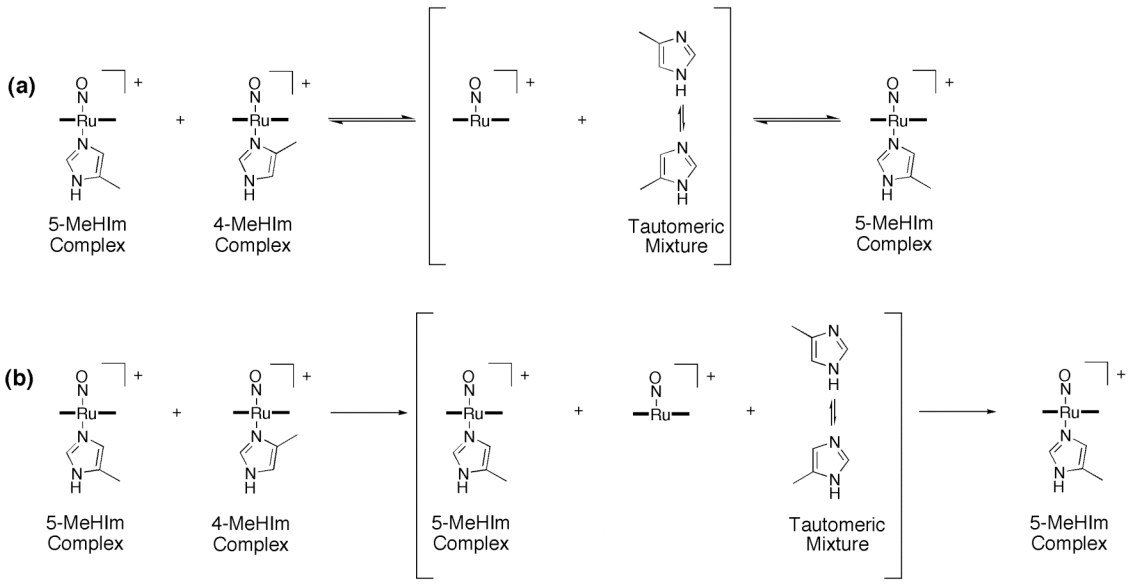

Scheme 3.2. Plausible pathway of ligand dissociation in the [(OEP)Ru(NO)(5(4)-MeHIm]$^{+}$ isomeric complexes. **(a)** The methylimidazole ligands dissociate from the ruthenium centers of both isomeric complexes, forming the 5-coordinate nitrosyl complex and a tautomeric mixture of ligands, prior to the formation of the 5-MeHIm complex. **(b)** The 4-MeHIm ligand dissociates from the ruthenium center of the [(OEP)Ru(NO)(4-MeHIm)]$^{+}$ isomer forming the 5-coordinate nitrosyl complex and a tautomeric mixture of ligands, prior to the formation of the 5-MeHIm complex.

c. X-ray crystallography. Isolated crystalline solids were obtained for the imidazole, imidazolate, 5(4)-methylimidazole mixture and 5-methylimidazolate complexes containing the (OEP)Ru(NO) fragment.

The structure for the (T(*p*-OMe)PP)Ru(NO)(O-*i*-C_5H_{11}) starting complex was obtained (Fig 3.3). The C_5H_{11} portion of the alkoxide ligand showed disorder over three positions in the X-ray structure. The geometric parameters for the related (OEP)Ru(NO)(O-*i*-C_5H_{11}) complex was obtained previously in a collaboration with the Coppens laboratory.[17] Besides these complexes, there have been no reports of solid-state molecular structure for any of the metal-nitrosyl porphyrin complexes containing isoamyl alkoxide linkages in the literature.[11,16,19,20] There has only been one other report of a solid state crystal of a metalloporphyrin complex containing

mutually *trans* nitrosyl and methoxy ligands.[30] Table 3.2 compares selected solid-state structural parameters for the related alkoxide complexes whose X-ray structures are known. A complete list of the bond lengths and bond angles obtained from single crystal X-ray crystallographic structure reported here can be found in Tables 3.4 through 3.12 of the Appendix. However, beyond acknowledging the geometric similarities between this complex and the similar (TTP)Ru(NO)(OMe) complexes obtained by Bohle, this structure will not be further discussed in the context of the imidazolate and imidazole complexes that are the focus of this chapter.

Table 3.2. Selected structural data (in Å and º) for ruthenium-nitrosyl complexes containing alkoxides.

	Ru-N(O) (Å)	N-O (Å)	∠RuNO (º)	Ru-O(R) (Å)	∠RuOC (º)	*ref*
(OEP)Ru(NO)(O-*i*-C_5H_{11})[a]	1.780(10)	1.191(14), 1.191(14)	170.2(11), 137(3)	1.908(11)	133.853	17 and personal communication
(T(*p*-OMe)PP)Ru(NO)(O-*i*-C_5H_{11})[b]	1.754(4)	1.172(5)	176.9(3)	1.932(3)	129.1(9), 128.0(8), 161.1(12)	This work
(TTP)Ru(NO)(OMe)	1.84(4)	Not reported	180	1.80(5)		30

[a]Two positions of NO ligand observed. [b]Alkoxide ligand was disordered over three positions.

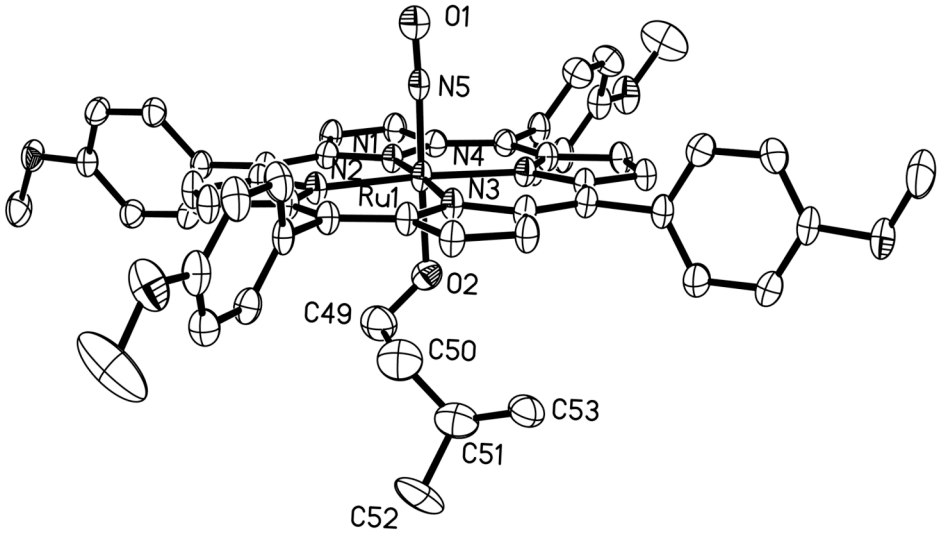

Figure 3.4. Molecular structure of (T(*p*-OMe)PP)Ru(NO)(O-*i*-C_5H_{11}). The disordered C_5H_{11} groups of the alkoxide and the hydrogen atoms have been omitted for clarity.

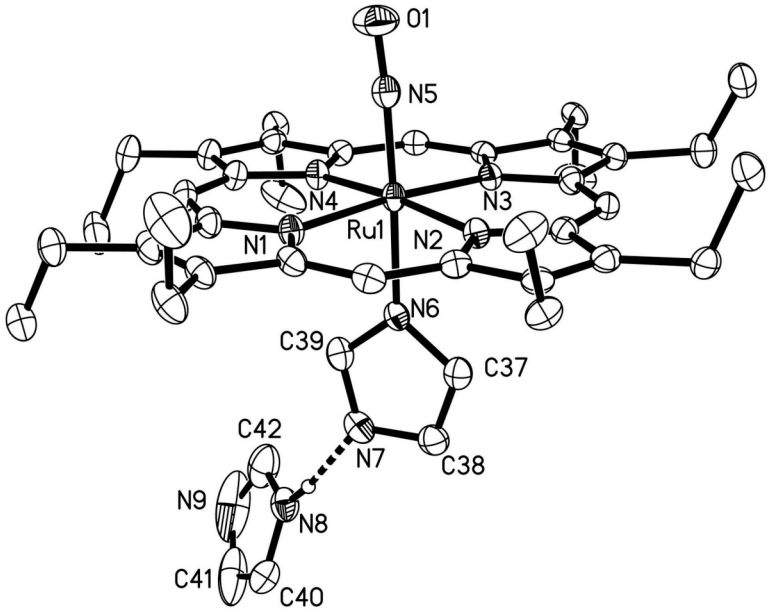

Figure 3.5. Solid-state structure of (OEP)Ru(NO)(Im)•HIm. Hydrogen atoms have been omitted for clarity, except that of the uncomplexed HIm.

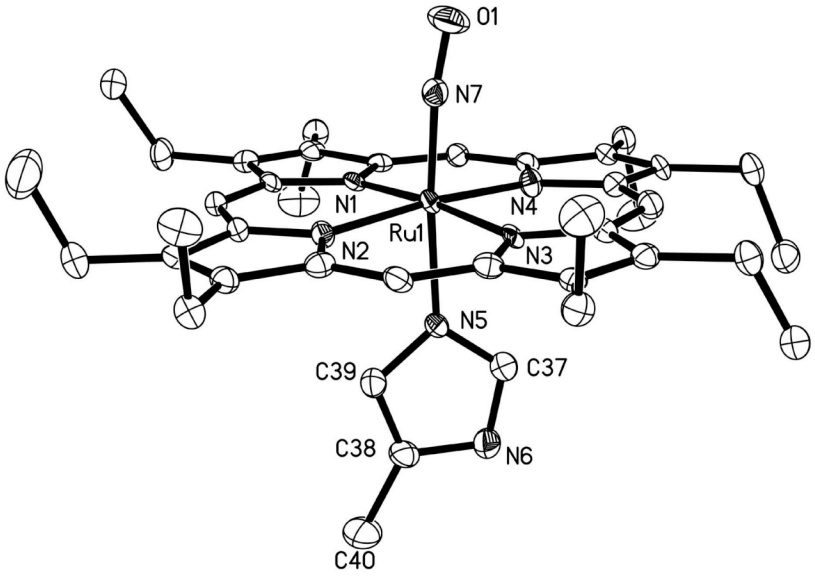

Figure 3.6. Molecular structure of (OEP)Ru(NO)(5-MeIm). Hydrogen atoms have been omitted for clarity.

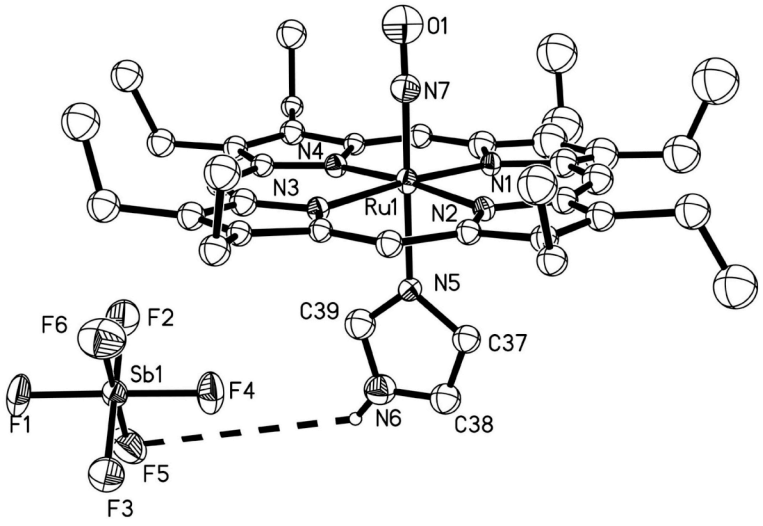

Figure 3.7. Crystal structure of [(OEP)Ru(NO)(HIm)]SbF_6. Hydrogen atoms have been omitted for clarity.

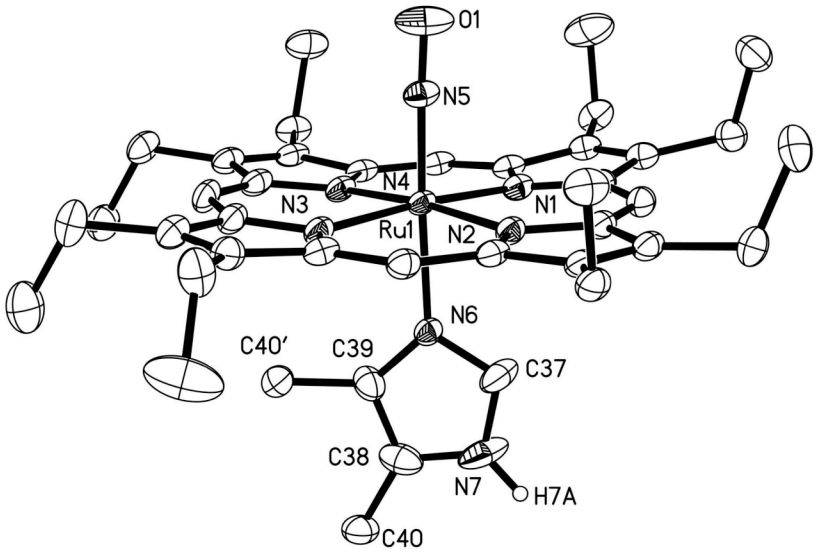

Figure 3.8. Crystal structure of the cation of [(OEP)Ru(NO)(5-MeHIm)]SbF_6/[(OEP)Ru(NO)(4-MeHIm)]SbF_6. Hydrogen atoms and the SbF_6 anion have been omitted for clarity.

Table 3.3. Selected structural data (in Å and °) for ruthenium complexes containing imidazolate and imidazole ligands.

	Ru-N(O)	**N-O**	**Ru-N-O**	**Ru-L(ax)**	***ref***
Imidazolate					
$[Ru(bpy)_2(Im)_2][BF_4]_2$				2.093(6), 2.096(7)	*3*
(OEP)Ru(NO)(Im)	1.748(3)	1.148(4)	174.9(3)	2.063(3)	*This work*
(OEP)Ru(NO)(5-MeIm)	1.740(4)	1.145(5)	171.2(4)	2.059(4)	*This work*
Imidazole					
$[Ru(2,2'\text{-bipy})_2(HIm)_2]SO_4$				2.096(11), 2.093(11)	*32*
Na[*trans*-$RuCl_4$(DMSO)(HIm)]				2.081(2)	*33*
$[P(C_6H_5)_4][RuCl_4(5\text{-}NO_2HIm)_2]$				2.081(5)	*34*
$[Ru(bipy)(terpy)(HIm)](PF_6)_2$				2.072(8)	*35*
$[Ru(bipy)(terpy)(Ph_2HIm)](PF_6)_2$				2.124(3)	*35*
$[Ru(HIm)_6][CF_3SO_3]_2$				2.105(2), 2.095(2), 2.098(2)	*23*
$[Ru(HIm)_6]CO_3 \cdot H_2O$				2.102(2)	*36*
$[Ru(OH)_2HIm_4][RuCl_4\text{-}HIm_2]$				2.075(5), 2.080(5), 1.313(9)	*36*
trans-$[(HIm)_2(NH_3)_4Ru]Cl_3$				2.046(4), 2.051(4)	*37*
cis-$[(HIm)_2(NH_3)_4Ru]Br_3$				2.05(1), 2.051(9)	*38*
[*trans*-$(NH_3)_4Ru(HIm)(^i\text{Nic})](CF_3CO_2)_3$				2.049(7)	*39*
$[RuCl_2(DMSO\text{-}d_6)_2HIm_2$				2.105(4)	*40*
$(HIm)_2[RuHImCl_5]$				2.044(12)	*41*
HIm[*trans*-$RuHIm_2Cl_4$]				2.079(3)	*42*
4-MeHIm[*trans*-Ru(5-MeHIm)Cl_4]				2.087(6), 2.088(5)	*42*
$[(Im)_2H]$[*trans*-$RuCl_4$(HIm)(NO)]	1.740(3)	1.128(4)	177.7(3)	2.091(2)	*43*
$[Ru_2O(O_2CMe)_2(HIm)_6](ClO_4)_2$				2.076(6), 2.128(5), 2.087(5), 2.065(6), 2.119(4), 2.073(3)	*44*
[(OEP)Ru(NO)(HIm)]SbF_6	1.695(9)	1.131(12)	175.3(7)	2.069(8)	*This work*
[(OEP)Ru(NO)(5-MeHIm)]SbF_6	1.7305(17)	1.144(2)	176.94(18)	2.1036(17)	*This work*

Prior to this study, there have only been a few reports containing geometric parameters for complexes containing the imidazole or imidazolate Ru-L_N linkages and none for those containing the porphyrin ON-Ru-L_N axial group.[6,7,12-24] Selected bond lengths and angles for the structures reported here and other related crystalline solids containing either a Ru-imidazole or Ru-imidazolate linkage can be found in Table 3.3. Tables listing complete bond distances and angles for all structures obtained in this work are provided in the Appendix.

Neutral complexes. The crystal structures for the neutral (OEP)Ru(NO)(Im) and (OEP)Ru(NO)(5-MeIm) are shown in Figures 3.5 and 3.6, respectively. Figure 3.9 a and b displays the torsional angles between the four nitrogen core of the porphyrin and the six-membered ring of the axial ligand for the neutral complexes. Also shown in Figure 3.9 are the deviations of the atoms from the 24-atom mean plane; positive values, in units of 0.01 Å, are toward the nitrosyl ligand.

The imidazolate solid-state structures, (OEP)Ru(NO)(Im) and (OEP)Ru(NO)(5-MeIm), exhibited nearly linear Ru-N-O groups (174.9(3) and 171.2(4)º, respectively) with M-N(O) and N-O bond lengths that are comparable to solid-state structures that have been reported for other $\{RuNO\}^6$ complexes (Table 3.3). [26] The Ru-N_{Im} bond lengths displayed in the crystal structures for the Im and the 5-MeIm complexes were 2.063(3) and 2.059(4) Å, respectively. The crystal structure of the imidazolate complex exhibited a moderate hydrogen bonding interaction between the basal nitrogen of the bound imidazolate and the N-H of an unbound

imidazole (N8-H---N7 in Figure 3.5) with a 1.89 Å H-N7 bond length and an angle of 169.4º between N8-H-N7.

Both of solid-state structures of the neutral complexes showed moderate ruffled distortions of the 24-atom porphyrin planes and the Ru atom in both complexes are displaced by ~0.1 Å from the porphyrin cores towards the NO ligands (Fig. 3.9). The imidazolate ligands in both of the crystal structures (as can been seen in Fig. 3.9) bisect the nitrogen core of the porphyrin at ~25.5°.

Cationic complexes. The solid state crystal structures of the cationic imidazole complexes $[(OEP)Ru(NO)(HIm)]^+$ and $[(OEP)Ru(NO)(5(4)\text{-}MeHIm)]^+$ are shown in Figures 3.7 and 3.8, respectively. Figure 3.9 c and d displays the torsional angles between the four nitrogen core of the porphyrin and the six-membered ring of the axial ligand for the neutral complexes. An interesting feature of the 5(4)-MeHIm crystal structure was the presence of isomeric disorder in the 5-MeHIm ligand in the form of ~25% of the methyl groups in the unit cell positioned on C39 of the ring (Fig. 3.8). This value agrees well with the ^{1}H NMR data showing a 3:1 ratio of the 5-MeHIm to 4-MeHIm linkage isomers of $[(OEP)Ru(NO)]^+$, suggesting that the linkage isomers have similar stabilities in both the solid state and $CDCl_3$ mixture.

(a) (OEP)Ru(NO)(Im)

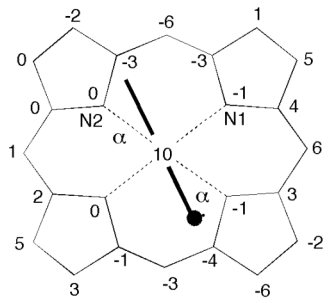

α = 26.5(3)°

(b) (OEP)Ru(NO)(5-MeIm)

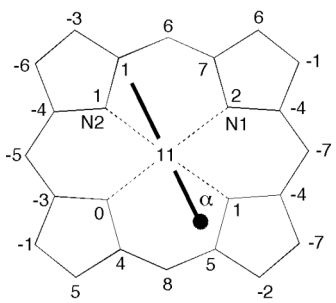

α = 25.1(5)°

(c) [(OEP)Ru(NO)(HIm)]SbF_6

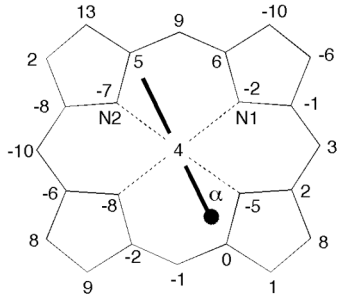

α = 29.0(8)°

(d) [(OEP)Ru(NO)(5(4)-MeHIm)]SbF_6

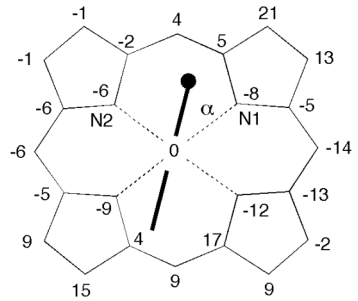

α = 36.75(17)°

Figure 3.9. Formal diagrams of the porphinato cores of (a) (OEP)Ru(NO)(Im), (b) (OEP)Ru(NO)(5-MeIm), (c) [(OEP)Ru(NO)(HIm)]SbF_6, and (d) [(OEP)Ru(NO)(5(4)-MeHIm)]SbF_6 displaying displacements from the 24-atom porphinato plane of each unique atom in units of 0.01 Å. Positive values are towards the nitrosyl ligand. The torsional angles between the nitrogen cores of the porphyrins and the six-membered imidazole/imidazolate ring of the axial ligands (i.e., N_P-Ru-N_{Im}-C(37)) are shown.

Similar to the neutral complexes, the solid-state structures of the cationic complexes $[(OEP)Ru(NO)(HIm)]^+$ and $[(OEP)Ru(NO)(5(4)\text{-}MeHIm)]^+$ display nearly linear Ru-N-O groups (175.3(7) and 176.94(18)º, respectively) with little difference in the Ru-N(O) and N-O bond lengths reported above for the neutral analogues (Table

3.3). The Ru-N_{Im} bond length in the HIm complex shows no real difference from the neutral analogue (2.063(3) vs. 2.069(8) Å, respectively); however, the 5(4)-MeHIm structure displays moderate lengthening of Ru-N_{Im} when compared to the neutral analogue (2.103(17) vs 2.059(4) Å, respectively). The lengthening of the Ru-N_{Im} bond in the cationic complex is likely due to the presence of the 4-MeHIm structural linkage isomer in the crystal structure. The methyl group (denoted C40' in Fig. 3.8) of this isomer is directed toward the OEP macrocycle. The increased steric stress that would otherwise result from this is minimized by the elongation of the Ru-N_{Im} bond length. It is interesting to note that the only other reported six-coordinate linear $\{MNO\}^6$ structural analogue, namely [(OEP)Fe(1-MeIm)(NO)]ClO_4, displays axial bond geometries similar to the protonated complexes with the exception of a shorter M-N_{Im} bond length (Fe-N(O) = 1.6465(17) Å, N-O = 1.135(2), Fe-N_{Im} = 1.9889(16) Å).[10]

A hydrogen bonding interaction between the hydrogen atom attached to the basal nitrogen of the bound imidazole to F(5) of SbF_6 (N6-H6a---F(5) in Fig. 3.6) is observable in the crystal structure of [(OEP)Ru(NO)(HIm)]SbF_6 (H6a-F5 = 2.45 Å and ∠N6-H6a-F5 = 123.1º). This interaction is significantly weaker than the hydrogen bonding interaction discussed above in the neutral Im complex.

The crystal of $[(OEP)Ru(NO)(HIm)]^+$ shows a moderate wave distortion of the 24-atom porphyrin plane, while the 5(4)-MeHIm structure displays more of a ruffled distortion. Of both the neutral and cationic structures, the $[(OEP)Ru(NO)(5(4)\text{-}MeHIm)]^+$ complex shows the largest out of plane distortions of individual porphyrin core atoms, likely due to steric reasons discussed above (Fig.

3.9). Unlike the neutral analogues, the Ru atoms of the cationic complexes are coincident or nearly coincident with the porphyrin plane. As depicted in Figure 3.9d, the HIm ligand in the cationic complex bisects the porphyrin's nitrogen core at 29.0(8)º, which is similar to the angles at which the imidazolate ligands in the neutral complexes bisected the mean plane. The cationic 5(4)-MeHIm complex, however, bisects the nitrogen core of the porphyrin at 36.75(17)° which otherwise increases the distance between the methyl group of the 4-MeHIm ligand and the nitrogens of the porphyrin core and further relieves steric strain caused by the close proximity of the methyl group of the 4-MeHIm isomer and the porphyrin plane (Fig. 3.9d).

Conclusion

We have prepared a series of ruthenium porphyrin complexes containing axial imidazolate, 5-methylimidazolate, imidazole, 1-methylimidazole, and an isomeric mixture of the 4-methylimidazole and 5-methylimidazole ligand *trans* to nitric oxide. The infrared and ^{1}H NMR spectroscopic characteristics of these complexes are typical of diamagnetic $\{MNO\}^{6}$ metalloporphyrin complexes with linear metal nitrosyl groups. The aryl *meso*-substituted porphyrins displayed higher nitrosyl stretches in the IR than the electron rich octaethyl β-substituted porphyrins due to decreased metal-nitrosyl π back-bonding to NO.

The addition of 4-methylimidazole to $[(OEP)Ru(NO)]^{+}$ afforded an interesting isomeric mixture of $[(OEP)Ru(NO)(5\text{-MeHIm})]^{+}$ and $[(OEP)Ru(NO)(4\text{-MeHIm})]^{+}$ complexes. We were able to determine that the sterically unstable 4-MeHIm isomer undergoes a first order dissociation of the 4-MeHIm ligand from the Ru center with

the rate constant, $k = 1.44 \times 10^{-5}\ s^{-1}$ and the half-life, $t_{1/2} = 4.81 \times 10^{4}$ s. Subsequently, the release of the 4-MeHIm ligand and subsequent binding of the tautomeric 5-MeHIm ligand to form the more stable $[(OEP)Ru(NO)(5\text{-}MeHIm)]^{+}$ isomer appears to have a more intricate mechanism preventing the determination of the rate-law using the methods employed in this work.

Solid-state structures were obtained for the (OEP)Ru(NO)(Im), $[(OEP)Ru(NO)(HIm)]SbF_6$, (OEP)Ru(NO)(5-MeIm) complexes. Additionally, the crystal structure for an isomeric mixture of the $[(OEP)Ru(NO)(5\text{-}MeHIm)]SbF_6$ and $[(OEP)Ru(NO)(4\text{-}MeHIm)]SbF_6$ complexes was solved. All solid-state structures display characteristics typical of linear metal-nitrosyl linkages. The complexes containing an imidazolate ligand displayed Ru-NO and $Ru\text{-}N_{ligand}$ bond lengths and angles similar to their imidazole analogues. The Ru-atoms in the imidazolate (OEP)Ru(NO)(Im) and (OEP)Ru(NO)(5-MeIm) complexes, however, show a larger displacement from the 24-atom porphyrin plane than their imidazole analogues and may reflect the greater degree of π-backbonding in the imidazolate complexes that was suggested by the IR studies.

The structures reported here are the first such structures reported for nitrosyl-ruthenium porphyrin imidazole/imidazolate complexes and the neutral imidazole and 5-methylimidazole complexes compose two of only three structures containing a ruthenium-imidazolate linkage that can be found in the literature to date. Of particular interest are the close structural similarities of these complexes to the previously reported $[(OEP)Fe(1\text{-}MeIm)(NO)]ClO_4$ structure reported by Ellison et al.[10] Where this putative iron-nitrosyl model of the biological heme prosthetic groups

showed poor stability requiring specially developed crystallization techniques in order to obtain the molecular structure, the related *Group 8* ruthenium complexes have the advantage of relatively high stability in inert atmospheres and show similar structural features. Hence, these derivatives provide an attractive alternative to iron containing models of nitrosyl proteins with metal bound histidine.

References

(1) Mason, M. G.; Nicholls, P.; Wilson, M. T.; Cooper, C. E. *Proc. Natl. Acad. Sci. U.S.A.* **2006**, *103*, 708-713.
(2) Suzuki, S.; Yoshimura, T.; Nakahara, A.; Iwasaki, H.; Shidara, S.; Matsubara, T. *Inorg. Chem.* **1987**, *26*, 1006-1008.
(3) Andrew, C. R.; George, S. J.; Lawson, D. M.; Eady, R. R. *Biochemistry* **2002**, *41*, 2353-2360.
(4) Sjogren, T.; Hajdu, J. *J. Biol. Chem.* **2001**, *276*, 13072-13076.
(5) Jafferji, A.; Allen, J. W. A.; Ferguson, S. J.; Fulop, V. *J. Biol. Chem.* **2000**, *275*, 25089-25094.
(6) Sjogren, T.; Hajdu, J. *J. Biol. Chem.* **2001**, *276*, 29450-29455.
(7) Sono, M.; Eble, K. S.; Dawson, J. H.; Hager, L. P. *J. Biol. Chem.* **1985**, *260*, 15530-15535.
(8) Jensen, K. P.; Ryde, U. *Mol. Phys.* **2003**, *101*, 2003-2018.
(9) Bohle, D. S.; Hung, C.-H.; Smith, B. D. *Inorg. Chem.* **1998**, *37*, 5798-5806.
(10) Ellison, M. K.; Scheidt, W. R. *J. Amer. Chem. Soc.* **1999**, *121*, 5210-5219.
(11) Yi, G.-B.; Khan, M. A.; Richter-Addo, G. B. *Chem. Commun.* **1996**, 2045-2046.
(12) Yi, G.-B.; Khan, M. A.; Richter-Addo, G. B. *Inorg. Chem.* **1996**, *35*, 3453-3454.
(13) Yi, G.-B.; Khan, M. A.; Powell, D. R.; Richter-Addo, G. B. *Inorg. Chem.* **1998**, *37*, 208-214.
(14) Andreasen, L. V.; Lorkovic, I. M.; Richter-Addo, G. B.; Ford, P. C. *Nitric Oxide* **2002**, *6*, 228-235.
(15) Lee, J.; Yi, G.-B.; Powell, D. R.; Khan, M. A.; Richter-Addo, G. B. *Can. J. Chem.* **2001**, *79*, 830-840.
(16) Lee, J.; Yi, G.-B.; Khan, M. A.; Richter-Addo, G. B. *Inorg. Chem.* **1999**, *38*, 4578-4584.
(17) Formitchev, D. V.; Coppens, P.; Li, T.; Bagley, K. A.; Chen, L.; Richter-Addo, G. B. *Chem. Commun.* **1999**, 2013-2014.

(18) Cheng, L.; Powell, D. R.; Khan, M. A.; Richter-Addo, G. B. *Inorg. Chem.* **2001**, *40*, 125-133.
(19) Yi, G.-B.; Chen, L.; Khan, M. A.; Richter-Addo, G. B. *Inorg. Chem.* **1997**, *36*, 3876-3885.
(20) Chen, L.; Khan, M. A.; Richter-Addo, G. B. *Inorg. Chem.* **1998**, *37*, 533-540.
(21) Carter, S. M.; Lee, J.; Hixson, C. A.; Powell, D. R.; Wheeler, R. A.; Shaw, M. J.; Richter-Addo, G. B. *Dalton Transactions* **2006**, *10*, 1338-1346.
(22) Rillema, D. P.; Nagle, J. K.; L.F. Barringer, J.; Meyer, T. J. *J. Amer. Chem. Soc.* **1981**, *103*, 56-62.
(23) Baird, I. R.; Rettig, S. J.; James, B. R.; Skov, K. A. *Can. J. Chem.* **1998**, *76*, 1379-1388.
(24) Senge, M. O. *J. Porph. Phtahlo.* **1998**, *2*, 107-121.
(25) Clarke, M. J.; Baily, V. M.; Doan, P. E.; Hiller, C. D.; LaChance-Galang, K. J.; Daghlian, H.; Mandal, S.; Bastos, C. M.; Lang, D. *Inorg. Chem.* **1996**, *35*, 4896-4903.
(26) Cheng, L.; Richter-Addo, G. B. In *The Porphyrin Handbook*; Guilard, R., Smith, K., Kadish, K. M., Eds.; Academic Press: New York, 2000; Vol. 4, p Ch. 33.
(27) All reports of Ruthenium nitrosyl porphyrin complexes to date have exhibited spectroscopic characteristics that are commonly attributed with Ru(II) compounds that are low-spin and diamagnetic .
(28) Toyama, A.; Ono, K.; Hashimoto, S.; Takeuchi, H. *J. Phys. Chem., A* **2002**, *106*, 3403-3412.
(29) Pyman, F. L. *J. Chem. Soc.* **1922**, *121*, 2616-2626.
(30) Bohle, D. S.; Goodson, P.; Smith, B. *Polyhedron* **1996**, *15*, 3147-3150.
(31) Reddy, K. B.; Cho, M.-o. P.; Wishart, J. F.; Emge, T. J.; Isied, S. S. *Inorg. Chem.* **1996**, *35*, 7241-7245.
(32) Faham, S.; Day, M. W.; Connick, W. B.; Crane, B. R.; Di Bilio, A. J.; Schaefer, W. P.; Rees, D. C.; Gray, H. B. *Acta Crystallog, Sect. D* **1999**, *D55*, 379-385.
(33) Alessio, E.; Balucci, G.; Lutman, A.; Mestroni, G.; Calligaris, M.; Attia, W. M. *Inorg. Chim. Acta* **1993**, *203*, 205-217.
(34) Anderson, C.; Beauchamp, A. L. *Inorg. Chim. Acta* **1995**, *233*, 33-41.
(35) Yang, X.-J.; Drepper, F.; Wu, B.; Sun, W.-H.; Haehnel, W.; Janiak, C. *Dalton Transactions* **2005**, 256-267.
(36) Anderson, C.; Beauchamp, A. L. *Inorg. Chem.* **1995**, *34*, 6065-6073.
(37) LaChance-Galang, K. J.; Doan, P. E.; Clarke, M. J.; Rao, U.; Yamano, A.; Hoffman, B. M. *J. Amer. Chem. Soc.* **1995**, *117*, 3529-3538.
(38) Clarke, M. J.; Bailey, V. M.; Doan, P. E.; Hiller, C. D.; LaChance-Galang, K. J.; Daghlian, H.; Mandal, S.; Bastos, C. M.; Lang, D. *Inorg. Chem.* **1996**, *35*, 4896-4903.
(39) Wishart, J. F.; Zhang, X.; Isied, S. S.; Potenza, J. A.; Schugar, H. J. *Inorg. Chem.* **1992**, *31*, 3179-3181.
(40) Anderson, C.; Beauchamp, A. L. *Can. J. Chem.* **1995**, *73*, 471-482.

(41) Keppler, B. K.; Wehe, D.; Endres, H.; Rupp, W. *Inorg. Chem.* **1987**, *26*, 844-846.
(42) Keppler, B. K.; Rupp, W.; Juhl, U. M.; Niebl, R.; Balzer, W. *Inorg. Chem.* **1987**, *26*, 4366-4370.
(43) Serli, B.; Zangrando, E.; Iengo, E.; Mestroni, G.; Yellowlees, L.; Alessio, E. *Inorg. Chem.* **2002**, *41*, 4033-4043.
(44) Sudha, C.; Mandal, S. K.; Chakravarty, A. R. *Inorg. Chem.* **1998**, *37*, 270-278.

Chapter 4. Fiber-optic infrared reflectance spectroelectrochemical studies of ruthenium-nitrosyl porphyrins containing imidazolate and imidazole ligands

Introduction

Nitric oxide (NO), the biologically ubiquitous free radical, is a key signaling molecule in numerous biological events including vasodilation. Many of these processes occur when NO interacts with the iron center of heme enzymes.[1] Of these enzymes, cytochromes have an imidazole containing histidine (His) residue attached to the iron center and are generally considered to exhibit electron transfers closely associated with proton or hydrogen-atom exchanges. Cytochromes play an important role in the terminal steps of the oxidative respiration chain.

Cytochrome *c* oxidase (C*c*O), specifically, reduces molecular oxygen to water through a series of electron transfers which in-turn provides energy to pump protons across the mitochondrial membrane in eukaryotic cells.[2,3] C*c*O is composed of two hemes (heme *a* and a_3) a dimeric copper center (Cu_A) and a mononuclear Cu_B center. Reduction of dioxygen occurs at the heme-copper binuclear site, where heme a_3 and Cu_B are in close proximity. The structural features of various C*c*O enzymes have been extensively explored.[2] The heme a_3 contains an Fe center axially linked with a His, whereas the Cu_B site is linked to three His residues, one of which is covalently bound to a tyrosine (Tyr) residue. The cross-linked His-Tyr unit has been suggested to play important roles in the reduction of oxygen by either the concerted or coupled electron transfer from the Cu bound imidazole to the Tyr resulting in a proton or

hydrogen-atom transfer from the Tyr to the Fe bound dioxygen. Among, the many factors that govern this process, it is believed that the protonation state of the covalently bound His may be important.[4]

Evidence showing that NO reversibly binds to the iron center of C*c*O competitively with oxygen has been presented. It is believed that the binding of NO to the heme center plays a role in oxygen sensing and the cells response to hypoxia.[5] Additionally, interaction of a NO molecule with the Cu_B site induces limited inhibition of the dioxygen reduction.[6] The mechanism by which NO interacts with the heme-copper binuclear center is not well understood and is an active area of research.

Our previous research explored the structure and chemistry of the heme related ruthenium-porphyrin model complexes containing *trans* axial linked nitric oxide and imidazole(ate) ligands (Chapter 3). The importance detailed above of the electron/proton transfers in the native cytochrome *c* oxidase in the reduction of molecular oxygen and the inhibition of this process in the presence of nitric oxide under certain cell condition has led us to explore the electrochemical reactions of the (OEP)Ru(NO)(RIm), where OEP is the dianion of octaethylporphyrin and R is either a vacant $N_{imidazole}$ position, or occupied by H or a methyl group. We were interested in examining how the protonation state of an imidazole ligand affects the redox properties of metalloporphyrin complexes as well as detailing the possibility of proton or atomic-hydrogen transfers from the ruthenium-bound imidazole(ate) upon oxidation and reduction. Herein, we report the first infrared spectroelectrochemical

studies of a set of (OEP)Ru(NO)-containing complexes with an imidazolate, imidazole, or 1-methylimidazole ligand *trans* to the nitrosyl.

Experimental Section

Chemicals. The compounds (OEP)Ru(NO)(Im), [(OEP)Ru(NO)(HIm)]BF_4 and [(OEP)Ru(NO)(1-MeIm)]BF_4 were prepared as previously reported in Chapter 3. Methylene chloride for use in the spectroelectrochemistry experiments was purified just prior to use by passing it though an Innovative Technologies Solvent Purification system. Ferrocene (Cp_2Fe; Cp = η^5-cyclopentadienyl anion) was sublimed prior to use. NBu_4PF_6 was recrystallized from hot ethanol and dried prior to use.

Instrumentation. Electrochemical measurements were recorded using a BAS CV50W instrument (Bioanalytical Systems, West Lafayette, IN, USA). For all electrochemical experiments, a 3.0 mm diameter Pt disk electrode was used as the working electrode, a silver wire coated with silver chloride acted as the reference electrode, and a platinum wire served as the auxiliary electrode. Experiments were performed at room temperature unless otherwise noted, and were performed under an atmosphere of pre-purified nitrogen in a solution of the analyte in CH_2Cl_2 containing 0.5 - 1.0 M NBu_4PF_6 as supporting electrolyte. Ferrocene served as an internal standard, and potentials are referenced to the $Cp_2Fe^{0/+}$ couple set at 0.00 V (+0.44 V vs. Ag/AgCl).[7] Typical solvent system windows with our configuration were +1.2-1.5 V for the oxidation limit, and –1.8 to –2.1 V for the reduction limit (vs. the $Cp_2Fe^{0/+}$ couple).

Infrared spectroscopic measurements were performed using a Bruker Vector 22 FTIR spectrometer equipped with a mid-IR fiber-optic dip probe and liquid nitrogen cooled MCT detector (RemSpec Corporation, Sturbridge, MA, USA) as described previously.[8] The same electrode configuration was used for both cyclic voltammetry and infrared spectroelectrochemical experiments. The fiber-optic infrared reflectance spectroelectrochemical experiments were performed in a specially designed cell and in a manner that was previously reported.[8] For the low-temperature work, we jacketed the cell with a dry ice/acetone bath as described in our complementary studies on manganese nitrosyl porphyrins.[9]

Extended Hückel Calculations. Extended Hückel calculations, as implemented in the YAeHMOP suite of programs,[10] were performed on the six-coordinate ruthenium nitrosyl complexes (OEP)Ru(NO)(Im) and $[(OEP)Ru(NO)(HIm)]^+$ using geometries obtained from the crystal structures included in Chapter 3 of this work. Calculations on the theoretical five-coordinate complex $[(OEP)Ru(NO)]^+$ were also performed using a geometry derived from the crystal structure of (OEP)Ru(NO)(Im) by removing the imidazolate ligand. Initial images of the molecular orbitals were produced using the viewkel application distributed in the YAeHMOP suite.[10] Adobe Photoshop® was used to add color to the figures.

Results and Discussion

Our previous studies of the ruthenium-nitrosyl porphyrin complexes containing imidazole (HIm) and imidazolate (Im) ligands examined the synthesis, and

structural/ spectroscopic characteristics of this class of compounds (Chapter 3). We demonstrated that the neutral complexes could be prepared through the reaction of a ruthenium-nitrosyl porphyrin alkoxide with imidazole, while cationic complexes could be prepared through the reaction of a cationic ruthenium-nitrosyl porphyrin with imidazole (Eqs. 4.1 and 4.2, respectively).

$$(por)Ru(NO)(O\text{-}i\text{-}C_5H_{11}) + HIm \rightarrow (por)Ru(NO)(Im) + HO\text{-}i\text{-}C_5H_{11} \quad (4.1)$$

$$[(por)Ru(NO)]^+ + HIm \rightarrow [(por)Ru(NO)(HIm)]^+ \quad (4.2)$$

Both the cationic Ru-HIm and neutral Ru-Im complexes exhibit linear metal-nitrosyl linkages and have characteristic infrared nitrosyl stretches between 1845 and 1855 cm^{-1} for the neutral complexes and 1866 to 1868 cm^{-1} for the cationic complexes (in CH_2Cl_2).

In the current studies, we compare the infrared (IR) spectroelectrochemistry of the imidazolate complex (OEP)Ru(NO)(Im) with that of the imidazole $[(OEP)Ru(NO)(HIm)]^+$ complex and the structurally related $[(OEP)Ru(NO)(1\text{-}MeIm)]^+$ analogue. Extended Hückel calculations were performed and the obtained data complement the results of the electrochemical and spectroelectrochemical experiments.

Table 4.1. Electrochemical data for the $[(OEP)Ru(NO)(RIm)]^{n+}$ (R = nothing and n = 0; X = H or 1-Me and n = 1) compounds in CH_2Cl_2.[a]

	Oxidation	Reduction		
Compound	$E^{\circ\prime}_1$	E_{pc1}	E_{pc2}	$E^{\circ\prime}_3$
(OEP)Ru(NO)(Im)	0.73 (203)	-0.83[b]	-1.24[b]	
$[(OEP)Ru(NO)(HIm)]^+$	0.71 (90)			-1.09 (105)
$[(OEP)Ru(NO)(1\text{-}MeIm)]^+$	0.72 (130)			-1.10 (224)

[a] Potentials are in volts, and are referenced to the ferrocene-ferrocenium couple set at 0.00 V. Conditions: 0.5 - 1 mM analyte, 200 mV/s, 0.1 M NBu_4PF_6. The numbers are in brackets represent the ΔE values (in mV) for the redox couples.
[b] These peaks represent irreversible processes.

Cyclic Voltammetry and Infrared Spectroelectrochemistry

The redox properties of the three compounds (OEP)Ru(NO)(RIm) were examined by cyclic voltammetry, and the electrochemical data are summarized in Table 4.1. We will consider the neutral imidazolate followed by the cationic imidazole and then 1-methylimidazole complexes.

Neutral Ru-Imidazolate Complex. The response features of the cyclic voltammogram of (OEP)Ru(NO)(Im) are shown in Fig. 4.1c. A major oxidation couple occurs at $E^{\circ\prime}_1$ = 0.73 V, which is partially reversible (i_{pa}/i_{pc} = 0.71, ΔE = 203 mV). The $|E_p\text{-}E_{p/2}|$ value of 80 mV (at 200 mV s^{-1}) and the linear plot of i_{pa} *vs*. (scan rate)$^{1/2}$ suggests a reversible diffusion controlled second oxidation followed by a chemical reaction. Indeed, the appearance of two daughter peaks at -0.83 and -1.24 V upon the negative return scan is consistent with the proposed EC mechanism.

Interestingly, in addition to $E^{\circ\prime}_1$ there was a reversible oxidation at 0.47 V that measured ~1/3 the intensity of the major oxidation couple. Exhaustive purification of

the complex showed no evidence of free imidazole or other impurities via ^{1}H NMR spectroscopy, suggesting that this small pre-wave is not due to a ^{1}H NMR active impurity. Previous studies of metalloporphyrins containing N-bound imidazole linkages have shown the existence of an equilibrium between the complexes containing bound imidazole and free imidazole. [11] The absence of this pre-wave at low temperatures scans (dry ice/acetone bath) of the voltammogram suggest that an equilibrium is established between a five- and six-coordinate complex and is shifted to the six-coordinate complex at lower temperatures.[12] Since the electrochemical response of the (OEP)Ru(NO)(Im) complex was maintained in the cyclic voltammogram at low temperatures minus the pre-wave, the complex responsible for the pre-wave does not seem to interfere with the electrochemical response of the imidazolate complex. Hence, the identity of the minor component in the redox reaction will not be further explored at this time.

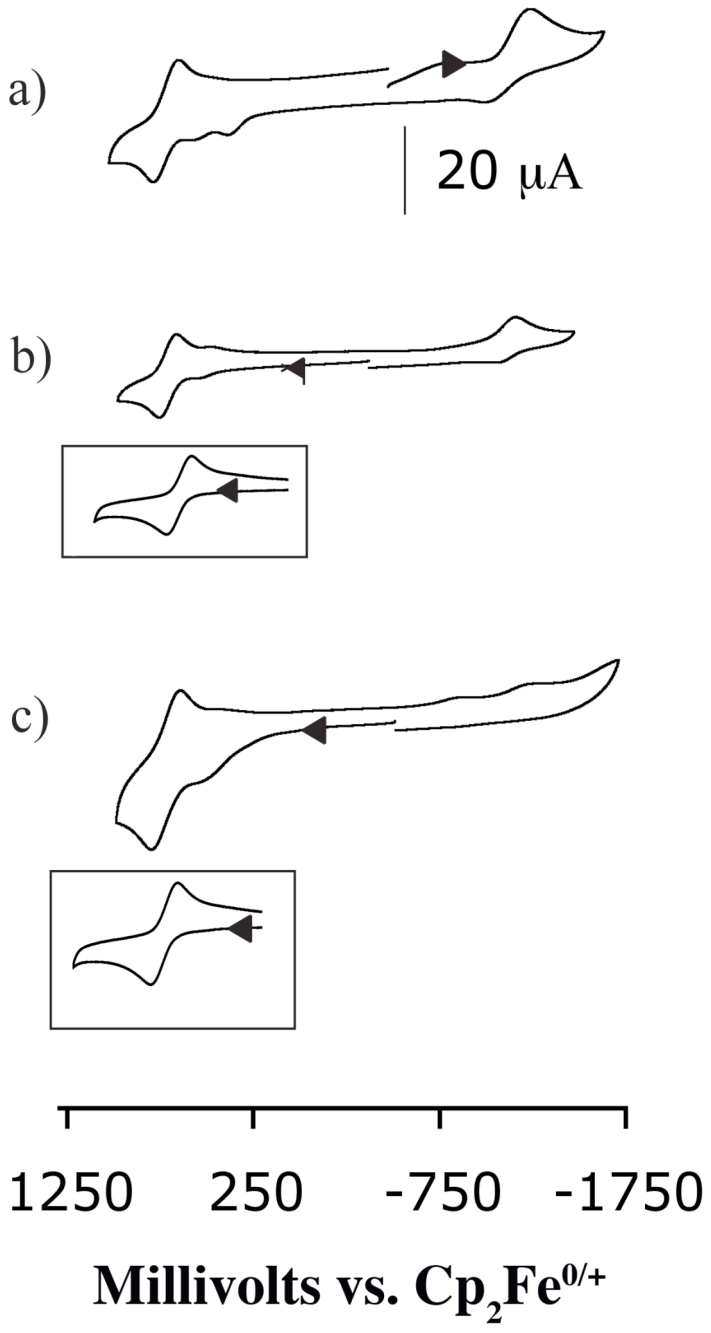

Figure 4.1. Cyclic voltammogram of (**a**) $[(OEP)Ru(NO)(1\text{-}MeIm)]^+$, (**b**) $[(OEP)Ru(NO)(HIm)]^+$, and (**c**) (OEP)Ru(NO)(Im) in CH_2Cl_2 containing 0.1 mM NBu_4PF_6. The insets are the low temperature cyclic voltammograms of the respective complexes. Potentials are referenced to the $Cp_2Fe^{+/0}$ couple (at 0.00 V). Scan rates are 200 mV s^{-1}.

The IR difference spectrum which shows product formation after the second oxidation of (OEP)Ru(NO)(Im) is presented in Fig. 4.2c. The electrogenerated product of the oxidation has a ν_{NO} band at 1870 cm^{-1}, which is shifted by +23 cm^{-1} from the starting compound. Such a relatively small shift in ν_{NO} is attributed to an oxidation site that is somewhat remote from the RuNO fragment. Indeed, evidence for a porphyrin-centered oxidation is provided by the appearance in the spectrum of a new band at 1527 cm^{-1} assigned to an OEP-containing π-radical cation. Bands between 1520 and 1570 cm^{-1} have been previously reported as characteristic of OEP-containing π-radical cations[13] and were also present in the porphyrin-centered oxidations reported in our earlier study (Chapter 2) of the complexes (OEP)M(NO)(XEt) (where M = Os, Ru; X = O, S).[14] The extra NO peaks that follow the oxidation product peak in the difference IR spectrum could arise due to the potential being held close to the solvent potential limit, giving rise to significant side reactions.

It is interesting that the product of oxidation shows a ν_{NO} band that is similar to the band for the cationic $[(OEP)Ru(NO)(HIm)]^+$ complex (*vide infra*). Indeed, the electrochemical and IR spectroelectrochemical data suggests that the net partially reversible first oxidation of (OEP)Ru(NO)(Im) can be described as consisting of a reversible oxidation process centered on the porphyrin followed by H-atom extraction by the imidazolate ligand from the solvent (Eqs 4.3 and 4.4).

$$(OEP)Ru(NO)(Im) \rightleftharpoons [(OEP^{\bullet})Ru(NO)(Im)]^+ + e^- \quad (4.3)$$

$$[(OEP^{\bullet})Ru(NO)(Im)]^+ + H^{\bullet}_{solv} \rightarrow [(OEP)Ru(NO)(HIm)]^+ \quad (4.4)$$

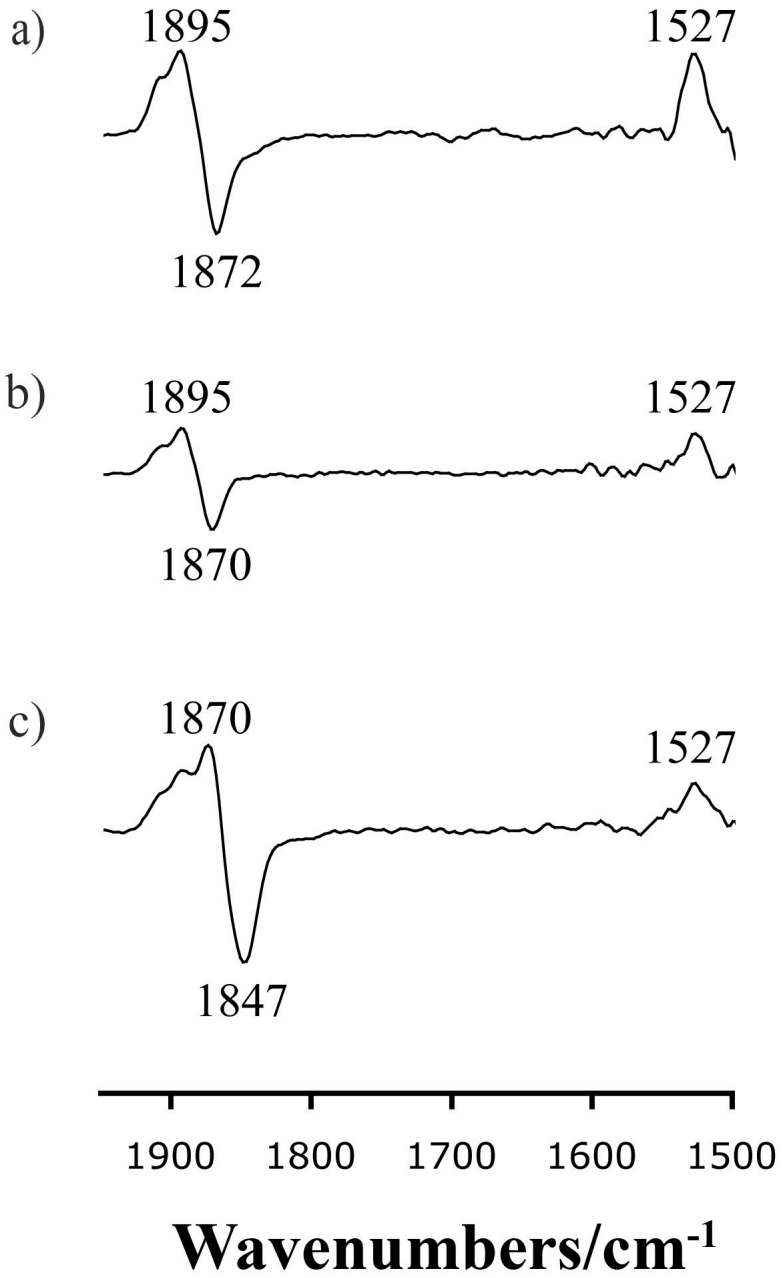

Figure 4.2. Difference FTIR spectra showing the formation of products from the first oxidations of (**a**) $[(OEP)Ru(NO)(1\text{-}MeIm)]^+$, (**b**) $[(OEP)Ru(NO)(HIm)]^+$, and (**c**) (OEP)Ru(NO)(Im) in CH_2Cl_2 containing 0.1 M NBu_4PF_6.

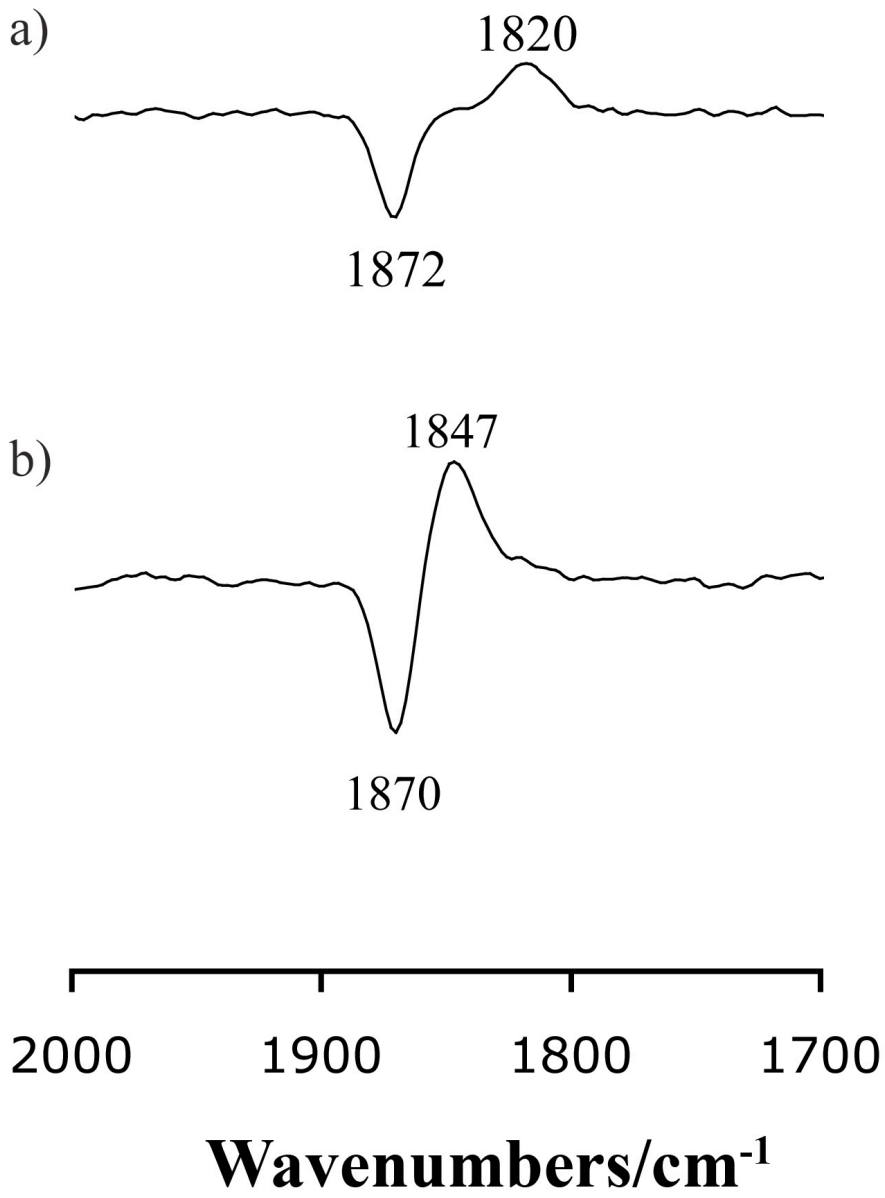

Figure 4.3. Difference FTIR spectrum showing the formation of product from the reduction of (**a**) $[(OEP)Ru(NO)(1\text{-}MeIm)]^+$ and (**b**) $[(OEP)Ru(NO)(HIm)]^+$ in CH_2Cl_2 containing 0.1 M NBu_4PF_6.

Holding the potential at 620 mV, just prior to the major first oxidation, resulted in difference IR spectra that were devoid of ν_{NO} bands. The relatively small amount of material responsible for the cyclic voltammogram response wave may have been insufficient for producing enough of the oxidized species on the electrode for detection with infrared spectroscopy under our conditions.

Cationic Ru-Imidazole Complex. The cyclic voltammogram of the cationic imidazole complex $[(OEP)Ru(NO)(HIm)]^+$ is shown in Fig. 4.1b. The redox behavior is characterized by two oxidations and a reduction. Similar to the electrochemical response of the imidazolate complex, the initial oxidation at 0.52 V (ΔE = 65 mV) is relatively small, only ca. 1/3 the intensity of the other redox waves and is absent from the voltammogram at low temperatures (Fig. 4.1b inset). The room-temperature ^1H NMR spectrum of the imidazole complex in $CDCl_3$ exhibits no peaks associated with the unbound imidazole ligand or any other impurities, suggesting that the response may be due to a 5-coordinate equilibrium product that does not contain the imidazole ligand.

A well-defined oxidation is evident at 0.71 V *versus* the ferrocene-ferricenium couple. The ΔE_p for this redox couple is 90 mV at 200 mV s^{-1}. The cathodic to anodic peak current ration (i_{pc}/i_{pa}) is 0.9 at 200 mV s^{-1}, and approaches unity at higher scan rates, suggesting that the oxidation is chemically reversible. The plot of i_{pa} *vs.* (scan rate)$^{1/2}$ is linear and indicative of diffusion-controlled reversible one-electron transfer process (Eq. 4.5) site of oxidation not specified).

$$[(OEP)Ru(NO)(HIm)]^+ \rightleftharpoons [(OEP)Ru(NO)(HIm)]^{2+} + e^- \qquad (4.5)$$

A partially reversible reduction peak for $[(OEP)Ru(NO)(HIm)]^+$ is observed at $E^{\circ\prime} = -1.09$ V ($\Delta E = 105$ mV). The i_{pa}/i_{pc} for this redox couple was between 0.5 and 0.6 at scan speeds between 50 mV s^{-1} and 1.0 V s^{-1}, indicating high reactivity of the reduction product. This is consistent with the observation of a daughter peak at 0.39 V upon the return scan after the reduction. The $|E_p - E_{p/2}|$ value of 78 mV is similar to the value for the ferrocene/ferrocenium couple (68 mV) under the same conditions and suggests a fast reversible electron transfer followed by a chemical change.

The IR spectroelectrochemistry results obtained for the well-defined oxidation of $[(OEP)Ru(NO)(HIm)]^+$ are shown in Fig. 4.2b and display a new ν_{NO} at 1895 cm^{-1} ($\Delta\nu_{NO} = 25$ cm^{-1}) and a small band at 1527 cm^{-1} in the IR difference spectrum. Similar to what was observed for the neutral imidazolate analogue, this minor shift of ν_{NO} with the appearance of the diagnostic OEP-containing π-radical cation band suggests, along with the electrochemical evidence, a reversible porphyrin centered electron transfer (Eq. 4.6)

$$[(OEP)Ru(NO)(HIm)]^+ \rightleftharpoons [(OEP^{\bullet})Ru(NO)(HIm)]^{2+} + e^- \qquad (4.6)$$

Porphyrin centered oxidations have been observed for a number of (por)Ru(NO)-containing complexes[15-17] including those reported by us for OEP porphyrins (Chapter 2).[14,18] Similar to the oxidation of the imidazolate analogue, a series of small peaks is evident in the difference IR spectrum and likely arise from the

potential being held close to the oxidation potential limit of the solvent, resulting in a number of labile species.

As is evident in Fig. 4.3b, a new ν_{NO} band was observed at 1847 cm^{-1} ($\Delta\nu_{NO}$ = 23 cm^{-1}) when the potential was held slightly negative of the $E^{\circ\prime}$ for the reduction. As previously discussed, the electrochemical data suggests that the reduction of the $[(OEP)Ru(NO)(Im)]^+$ proceeds through an initial reversible electron transfer (and is likely centered on the porphyrin as evidenced by the small shift in the nitrosyl stretch), followed by an irreversible chemical change. The similarity of the frequency of this nitrosyl band at 1847 cm^{-1} to the ν_{NO} of the neutral imidazolate (OEP)Ru(NO)(Im) complex (at 1847 cm^{-1}) suggests that H-atom abstraction from neutral (OEP)Ru(NO)(HIm) to the solvent system to form the neutral complex (OEP)Ru(NO)(Im) (Eqs 4.7 and 4.8) could have occurred. Similar types of radical hydrogen extractions have been observed when photo generated t-butoxyl radicals react with amine-boryl complexes to give the corresponding iminyl radical through $H^{\bullet}$ extraction from the amine portion of the complex; additionally, a recent publication has shown that a covalently linked phenoxy-imidazole complex exchanges radical hydrogen between the O of a phenoxyl group and the N of the imidazole upon oxidation and reduction.[19,20] The complimentary process, where by $H^{\bullet}$ was extracted from the solvent by the bound imidazolate ligand in the (OEP)Ru(NO)(Im) complex to form the cationic analogue, was previously discussed.

$$[(OEP)Ru(NO)(HIm)]^+ + e^- \rightleftharpoons (OEP)Ru(NO)(HIm) \quad (4.7)$$

$$(OEP)Ru(NO)(HIm) \rightarrow (OEP)Ru(NO)(Im) + H^{\bullet}_{solv} \quad (4.8)$$

Comparison of the oxidation potentials of the imidazolate and the imidazole complexes shows a difference of 20 mV, suggesting that the state of protonation of the imidazole derivative has little effect on the oxidation potentials of ruthenium-nitrosyl complexes. However, it appears to have a significant effect on the reduction potentials of the complexes. It is interesting that the reduction potential of the imidazolate complex (reduction of the imidazolate complex was not observed under our conditions) is presumably more negative than the reduction potential of the imidazole complex. Similar observations were made for the protonation states of imidazole/imidazolate containing His residues attached to the ferric heme centers of Rieske clusters upon reduction.[21] Hirst and co-workers demonstrated that the reduction potential is lowered when histidines attached to their ferric heme centers of Rieske clusters are deprotonated because the negatively charged "deprotonated" imidazolates contained in the His residue are easier to oxidize than the imidazoles in neutral His residues. The authors propose that this is due to neutral imidazoles in ferric bound His being more electron withdrawing than the "deprotonated" analogue and favor reduction.

$[$(OEP)Ru(NO)(1-MeIm)$]^+$ compound. The results obtained from the cyclic voltammetry of $[$(OEP)Ru(NO)(1-MeIm)$]^+$ were quite similar to those of the cationic imidazole analogue, as can be seen in Fig. 4.1a The redox behavior of this complex shows a well-defined reversible oxidation at $E^{\circ\prime} = 0.72$ V ($i_{pc}/i_{pa} = 1.0$, $\Delta E_p = 130$ mV). Additionally, reduction of the 1-MeIm complex is evident at $E^{\circ\prime} = -1.10$ V ($\Delta E_p = 224$ mV) and $i_{pa}/i_{pc} = 0.6$ at 200 mV s^{-1} and approaches unity at higher scan rates. The $|E_p - E_{p/2}|$ value of 73 mV is similar to the value for the ferrocene/ferrocenium

couple of 75 mV under the same conditions. An additional minor reduction peak at -0.80 V was observed on forward and reverse scans. The reduction wave showed strong similarities to the redox response of 1-methylimidazole and was attributed to the presence of the free ligand. Further characterization of this reduction wave was not explored. The electrochemical data suggests that the $[(OEP)Ru(NO)(1\text{-}MeIm)]^+$ complex undergoes a fast electron transfer upon reduction followed by a chemical change. The appearance of two daughter peaks at 0.39 V and 0.58 V after the reduction upon the forward scan of the potential further supports the proposed EC mechanism. The electrochemical response of the $[(OEP)Ru(NO)(1\text{-}MeIm)]^+$ complex is remarkably similar to the analogous $[(OEP)Ru(NO)(HIm)]^+$ complex minus the pre-wave that plagued both the cationic imidazole and neutral imidazolate complexes (vide supra). This is particularly of interest since the ca. 1% of the unbound 1-methyl imidazole ligand was evident in the ^1H NMR despite exhaustive purification of the $[(OEP)Ru(NO)(1\text{-}MeIm)]^+$ complex. As noted in chapter 3, (OEP)Ru(NO) complexes containing imidazole and analogues of imidazole can form an equilibrium between the six-coordinate imidazole containing complexes and the five-coordinate imidazole free complexes (Eq. 4.9). Equilibria between five- and six-coordinate complexes have also been observed in similar imidazole containing porphyrin complexes.[11]

$$[(OEP)Ru(NO)(1\text{-}MeIm)]^+ \rightleftharpoons [(OEP)Ru(NO)]^+ + 1\text{-}MeIm \qquad (4.9)$$

Absence of the pre-wave in the 1-methyl imidazole complex highlights the probable formation of the five-coordinate complexes in the imidazole and imidazolate complexes. The excess unbound 1-MeIm ligand in solution drives the equilibrium to the formation of the six-coordinate $[(OEP)Ru(NO)(1\text{-}MeIm)]^+$ complex leaving no five-coordinate complex in solution; hence, the cyclic voltammogram response displayed no pre-wave. In previous electrochemical studies, excess imidazole was used to prepare a single $[(por)Fe(Im)_2]^+$ complex and prevent the formation of equilibrium products.[22]

As mentioned previously, the electrochemical responses of $[(OEP)Ru(NO)(HIm)]^+$ and $[(OEP)Ru(NO)(1\text{-}MeIm)]^+$ are very similar. Structurally, the complexes differ only at the unbound N-position, which is protected by a methyl group in the 1-MeIm complex. The lack of an N-H bond on the imidazole in the $[(OEP)Ru(NO)(1\text{-}MeIm)]^+$ complex and the similarities of the redox responses displayed in the voltammagrams by the two complexes suggests that oxidation and reduction waves in the $[(OEP)Ru(NO)(HIm)]^+$ are not due to the formation of hydrogen bonds between the N-H of the ligand and the electrolyte solution.

The IR spectroelectrochemical results for the oxidation of the $[(OEP)Ru(NO)(1\text{-}MeIm)]^+$ can be seen in Fig. 4.2a, while those for the reduction can be seen in Fig. 4.3a. A new ν_{NO} at 1895 results from holding the potential just past the oxidation response of the complex. Similar to what was observed with the electrogenerated oxidation product of the cationic imidazole complex, a reversible porphyrin based electron transfer upon oxidation is evident by cyclic voltammetry data and the relatively small shift in ν_{NO} from the starting complex and the

electogenerated product ($\Delta\nu_{NO}$ = 23 cm^{-1}) with the formation of a small peak at 1527 cm^{-1} (Eq. 4.10).

$$[(OEP)Ru(NO)(1\text{-}MeIm)]^{+} \rightleftharpoons [(OEP^{\bullet})Ru(NO)(1\text{-}MeIm)]^{2+} \qquad (4.10)$$

The series of small peaks just subsequent to the ν_{NO} band in the difference IR that were noted earlier for both the imidazolate and imidazole complexes, were also visible in the spectrum for the 1-methyl imidazole complex.

The electrogenerated product that resulted from the reduction of the $[(OEP)Ru(NO)(1\text{-}MeIm)]^{+}$ complex displayed a ν_{NO} at 1820 cm^{-1} ($\Delta\nu_{NO}$ = 52 cm^{-1}) in the difference IR spectrum. This shift of the NO stretching frequency is similar to the magnitude of what we previously reported for the reduction of the (OEP)Ru(NO)(SEt) complex and suggests a porphyrin based reduction. Considered with the cyclic voltammetry data, the IR spectroelectrochemical indicates that the reduction of the $[(OEP)Ru(NO)(1\text{-}MeIm)]^{+}$ complex proceeds via a reversible electron transfer based on the porphyrin ring followed by a chemical change which likely involves the loss of the 1-MeIm ligand (Eqs. 4.11 and 4.12)

$$[(OEP)Ru(NO)(1\text{-}MeIm)]^{+} + e^{-} \rightleftharpoons (OEP^{\bullet})Ru(NO)(1\text{-}MeIm) \qquad (4.11)$$

$$(OEP^{\bullet})Ru(NO)(1\text{-}MeIm) \rightarrow (OEP^{\bullet})Ru(NO) + 1\text{-}MeIm \qquad (4.12)$$

Extended Hückel calculations

The net oxidation of the (OEP)Ru(NO)(Im) complex resulted in the neutral formation of the cationic $[(OEP)Ru(NO)(HIm)]^+$ complex; similarly, reduction of the cationic ("protonated") complex produced the neutral ("deprotonated") complex. Extended Hückel calculations on both the "deprotonated" imidazolate and "protonated" imidazole complexes of (OEP)Ru(NO) and the corresponding theoretical five-coordinate nitrosyl complex were obtained in order to better understand the complimentary but opposite redox chemistry exhibited by these complexes.

The highest occupied molecular orbitals (HOMOs) of (OEP)Ru(NO)(Im), $[(OEP)Ru(NO)(HIm)]^+$, and $[(OEP)Ru(NO)]^+$ are shown in Fig. 4.4. The HOMO of (OEP)Ru(NO)(Im) is porphyrin centered with all of the charge concentrated on the porphyrin ring. The infrared spectroelectrochemical results for the oxidation of (OEP)Ru(NO)(Im), described earlier, reveal a net formation of a porphyrin-based π-radical cation as the primary observable product. The axial ligands display little effect by the oxidation of (OEP)Ru(NO)(Im), consistent with the HOMO of (OEP)Ru(NO)(Im) having no axial contributions. The lowest unoccupied molecular orbital (LUMO) of (OEP)Ru(NO)(Im) (Fig. 4.5b) involves antibonding interactions between the metal d_{xz} orbital and the π^* orbital of NO. In the reduction of (OEP)Ru(NO)(Im), however, the LUMO was not accessible due to the reduction potential falling outside the solvent limit.

The HOMO of $[(OEP)Ru(NO)(HIm)]^+$ is shown in Fig. 4.4a. Similar to the imidazolate HOMO, it is porphyrin-centered showing no charge on the axial position

of the complex. The similarities between the imidazolate and imidazole HOMOs are not surprising. The two compounds vary only in the nitrogen atom of the imidazole ring in the cationic $[(OEP)Ru(NO)(HIm)]^+$ complex is bound to a proton, making them isoelectronic. The infrared spectroelectrochemical results, discussed previously, for the oxidation of $[(OEP)Ru(NO)(HIm)]^+$ revealed a small change in the nitrosyl stretch in addition to a new peak that is associated with a porphyrin-based π-radical cation peak. The observation of the porphyrin-based π radical cation peak with little affect on the axial ligands is consistent with the nature of the HOMO of the $[(OEP)Ru(NO)(HIm)]^+$ complex.

The LUMO of $[(OEP)Ru(NO)(HIm)]^+$ (Fig. 4.5a) involves antibonding interactions between the metal d_{xz} orbital and a π^* orbital on the NO. Thus, it would be expected that reduction of $[(OEP)Ru(NO)(HIm)]^+$ would result in a weakening in the Ru-NO bond and increase in the antibonding character in the N-O bond. The increased charge on the metal nitrosyl would lead to a bent metal-nitrosyl geometry. With the exception of a few organometallic ruthenium-nitrosyl porphyrin complexes,[23,24], ruthenium-nitrosyl porphyrin complexes prefer to have linear metal-nitrosyl linkages.[14,15,25-33] Nan Xu, in our lab, is currently examining the spectroelectrochemistry of a series of novel organometallic ruthenium-nitrosyl porphyrins containing bent metal-nitrosyl linkages. In order to relieve the strain placed on the molecule by the bending of the metal-NO fragment, the charge on the LUMO could be redistributed away from being mostly metal-nitrosyl based, thereby, allowing for a linear Ru-NO bond. The electrochemical and spectroelectrochemical results obtained from the reduction of the cationic imidazole complex

$[(OEP)Ru(NO)(HIm)]^+$, discussed previously, suggested a reversible electron transfer followed by an irreversible chemical change involving a small shift of the ν_{NO} to a new nitrosyl stretch at 1847 cm^{-1} ($\Delta\nu_{NO}$ = 23 cm^{-1}), characteristic of the neutral (OEP)Ru(NO)(Im) complex. This is consistent with the LUMO where the initial site of electron transfer is on the ruthenium-nitrosyl fragment followed by a rearrangement of the charge to relieve the bent metal-nitrosyl linkage, allowing for the extraction of $H^{\bullet}$ from the imidazole ligand by the solvent to form the neutral analogue (OEP)Ru(NO)(Im) (Eqs. 4.13 and 4.14).

$$[(OEP)Ru(NO)(HIm)]^+ + e^- \rightleftharpoons (OEP)Ru(NO^{\bullet})(HIm) \quad (4.13)$$

$$(OEP)Ru(NO^{\bullet})(HIm) \rightarrow (OEP)Ru(NO)(Im) + H^{\bullet}_{solv} \quad (4.14)$$

The (OEP)Os(NO)(SEt) complex, previously discussed in Chapter 2, showed nearly identical electrochemical and spectroelectrochemical responses to the ruthenium analogue (OEP)Ru(NO)(SEt). The LUMO of the osmium complex also displayed antibonding character between metal d_{xz} and the π^* orbital on NO. Additionally, there was significant antibonding character between the metal d_{xz} and the S-atom orbital. The reduction of the (OEP)Os(NO)(SEt) complex resulted in an axial centered electron transfer followed by the loss of the NO fragment, likely due of the formation of an unfavorable bent metal-nitrosyl geometry.

As seen in Fig. 4.4b, the HOMO of the five-coordinate $[(OEP)Ru(NO)]^+$ complex is porphyrin centered, similar to the HOMOs for the six-coordinate (OEP)Ru(NO)(Im) and $[(OEP)Ru(NO)(HIm)]^+$ complexes. This similarity is

expected due to the lack of any charge contribution from the metal-nitrosyl or the imidazolate or imidazole ligands in the structurally related six-coordinate complexes. Though the six-coordinate complexes are in principle more electron-rich than the five-coordinate complexes, oxidation may be easier for the five-coordinate depending on interactions between the metal center of the five-coordinate complex and the solvent or the supporting electrolyte that composes the system used for the electrochemical and spectroelectrochemical studies. The identity of the resulting species may explain the lower oxidation potentials observed for the five-coordinate complexes in the equilibrium that is established with the imidazolate and imidazole complexes of (OEP)Ru(NO)(Im) and $[(OEP)Ru(NO)(HIm)]^+$.

Comparison of the oxidation potentials of (OEP)Ru(NO) imidazole(ate) complexes to those of the (OEP)Ru(NO) alkoxide/thiolate complexes (detailed in Chapter 2) show a ease of reduction that is 280 – 360 mV lower for the alkoxide and thiolate complexes as a group. This is not surprising when considering the HOMOs of the alkoxide exhibited charge contribution from the O- and S-bound ligands. The HOMOs of the imidazole/imidazolate complexes had no such features. The increased bonding contribution from the alkoxide and thiolate ligands leads to relatively more electron donation to the (OEP)Ru(NO) fragment resulting in easier reduction when compared to the imidazole(ate) analogues.

Conclusion

We have shown that the complexes (OEP)Ru(NO)(Im) and $[(OEP)Ru(NO)(HIm)]^+$ can undergo electrochemical oxidation and reduction,

respectively. The redox behaviors and identities of the electrochemical products can be readily explained by extended Hückel calculations as well as by infrared spectroelectrochemistry analyses.

Both the (OEP)Ru(NO)(Im) and the $[(OEP)Ru(NO)(HIm)]^+$ complexes exhibit equilibria between their six-coordinate and five-coordinate ruthenium-nitrosyl porphyrin forms, which are apparent from the cyclic voltammagrams of the complexes. Electrochemical oxidation of the (OEP)Ru(NO)(Im) complex in CH_2Cl_2 displayed a partially reversible single electron transfer centered on the porphyrin followed by radical hydrogen extraction from the solvent by the nitrogen atom of the imidazolate ring to form the cationic $[(OEP)Ru(NO)(HIm)]^+$ derivative. The $[(OEP)Ru(NO)(HIm)]^+$ complex, however, exhibits a porphyrin based reversible (diffusion controlled) single electron transfer upon oxidation. The calculated HOMOs for both the (OEP)Ru(NO)(Im) complex and $[(OEP)Ru(NO)(HIm)]^+$ complexes show charge distribution on the porphyrin, providing supporting evidence for the generation of a porphyrin-centered π-radical cations upon oxidation.

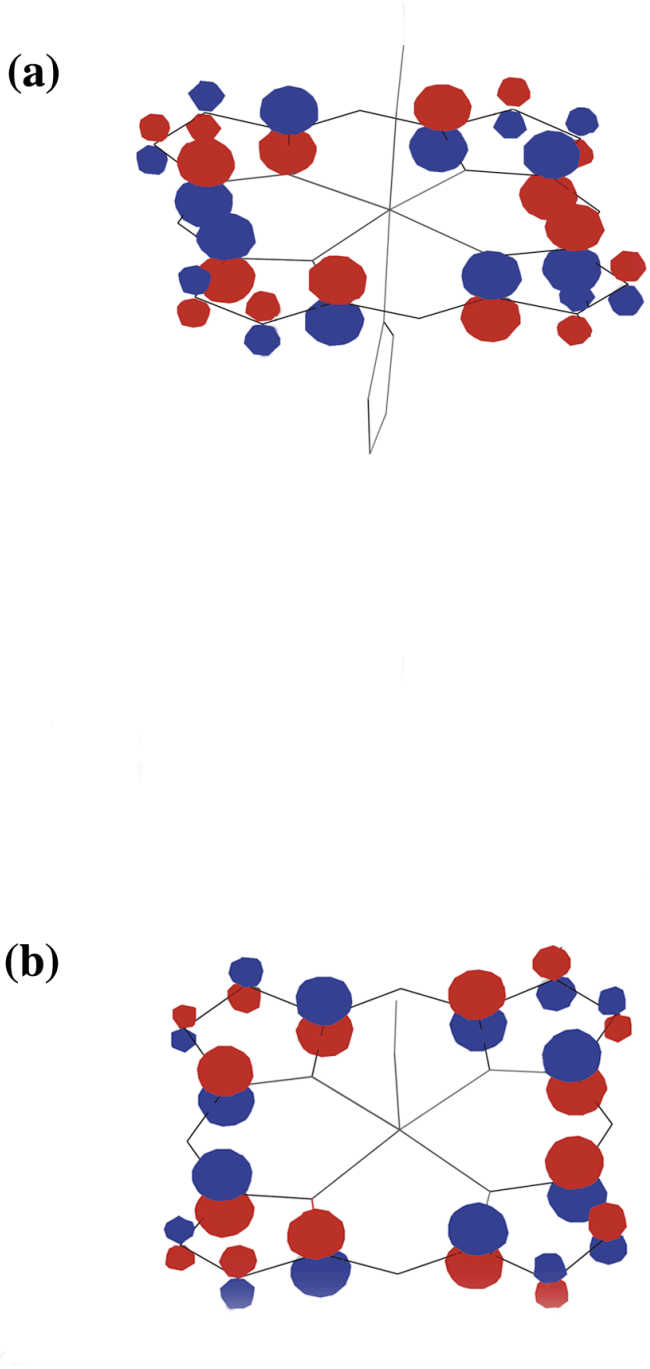

Figure 4.4. Highest molecular orbitals of (**a**) $[(OEP)Ru(NO)(HIm)]^+$ and (OEP)Ru(NO)(Im) (these complexes are isoelectronic and calculations result in identical HOMOs), and (**b)** model compound $[(OEP)Ru(NO)]^+$ as determined by Extended Hückel calculations. The eight ethyl groups on the porphyrin and the hydrogens were included in the calculation but are not shown for clarity.

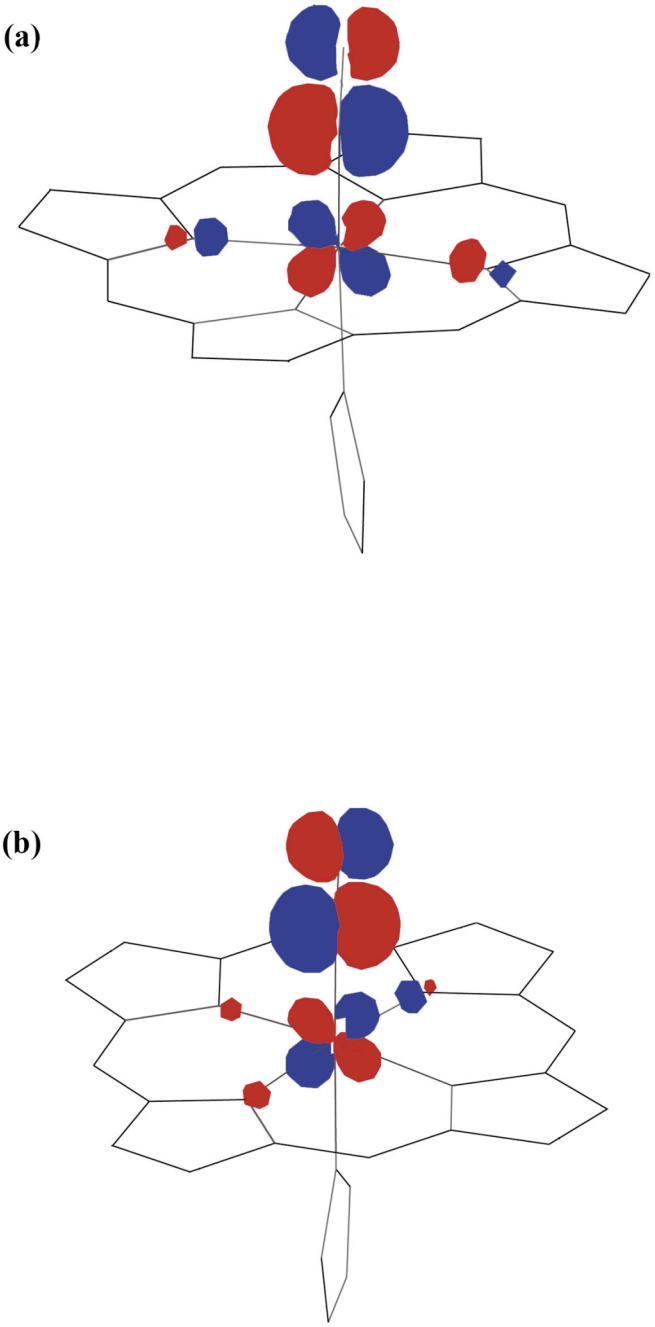

Figure 4.5. Lowest molecular orbitals of (**a**) $[(OEP)Ru(NO)(HIm)]^{+}$ and (**b**) (OEP)Ru(NO)(Im) as determined by Extended Hückel calculations. The eight ethyl groups on the porphyrin and the hydrogens were included in the calculation but are not shown for clarity.

Reduction of the $[(OEP)Ru(NO)(HIm)]^+$ complex proceeds through a partially reversible single electron transfer followed by a $H^\bullet$ extraction from the nitrogen of the imidazole by the solvent system to form the neutral (OEP)Ru(NO)(Im) derivative. The calculated LUMO suggests that reduction occurs first on the metal-nitrosyl fragment of the $[(OEP)Ru(NO)(HIm)]^+$ increasing the antibonding interaction between the metal d_{xz} and the π^* orbital on NO. Presumably, the resulting unfavorable bent Ru-NO^- like geometry is relieved by an electronic rearrangement that leads to the extraction of $H^\bullet$ from the nitrogen of the imidazole by the solvent system. The similarities in the electrochemical responses of the $[(OEP)Ru(NO)(HIm)]^+$ and the $[(OEP)Ru(NO)(1\text{-}MeIm)]^+$ suggest that the redox properties of the cationic $[(OEP)Ru(NO)(HIm)]^+$ cannot be attributed to the formation of hydrogen bonding in solution. This research suggests that conversion between the imidazole and imidazolate forms of (OEP)Ru(NO) can be achieved through redox reactions.

References

(1) Cheng, L.; Richter-Addo, G. B. In *The Porphyrin Handbook*; Guilard, R., Smith, K., Kadish, K. M., Eds.; Academic Press: New York, 2000; Vol. 4, p Ch. 33.
(2) Namslauer, A.; Brzezinski, P. *FEBS Letters* **2004**, *567*, 103-110 and references therein.
(3) Popović, D. M.; Quenneville, J.; Stuchebrukhov, A. A. *J. Phys. Chem., B* **2005**, *109*, 3616-3626.
(4) Bu, Y.; Cukier, R. I. *J. Phys. Chem., B* **2005**, *109*, 22013-22026.
(5) Clementi, E.; Nisoli, E. *Comp. Biochem. Physiol., A* **2005**, *142*, 102-110.

(6) Mason, M. G.; Nicholls, P.; Wilson, M. T.; Cooper, C. E. *Proc. Natl. Acad. Sci. U.S.A.* **2006**, *103*, 708-713.
(7) Connelly, N. G.; Geiger, W. E. *Chem. Rev.* **1996**, *96*, 877-910.
(8) Shaw, M. J.; Henson, R.; Houk, S. E.; Westhoff, J. W.; Jones, M. W.; Richter-Addo, G. B. *J. Electroanal. Chem* **2002**, *534*, 47-53.
(9) Zahran, Z. N.; Shaw, M. J.; Khan, M. A.; Richter-Addo, G. B. *Inorg. Chem.* **2006**, *45*, 2661-2668.
(10) Landrum, G. A.; Glassey, W. V. 2004.
(11) Yoshimura, T. *Inorg. Chim. Acta* **1980**, *46*, 69-76.
(12) There have been no reports of the formation of five-coordinate ruthenium-nitrosyl porphyrin complexes in the literature. It is likely, in our case, that the fifth coordination sphere is occupied by solvent or supporting electrolyte, however, for simplicity we will refer to this complex as the five-coordinate complex.
(13) Shimomura, E. T.; Phllippi, M. A.; Goff, H. M. *J. Amer. Chem. Soc.* **1981**, *103*, 6778-6780.
(14) Carter, S. M.; Lee, J.; Hixson, C. A.; Powell, D. R.; Wheeler, R. A.; Shaw, M. J.; Richter-Addo, G. B. *Dalton Transactions* **2006**, *10*, 1338-1346.
(15) Kadish, K. M.; Adamian, V. A.; Caemelbecke, E. V.; Tan, Z.; Tagliatesta, P.; Bianco, P.; Boschi, T.; Yi, G.-B.; Khan, M. A.; Richter-Addo, G. B. *Inorg. Chem.* **1996**, *35*, 1343-1348.
(16) Bohle, D. S.; Hung, C.-H.; Smith, B. D. *Inorg. Chem.* **1998**, *37*, 5798-5806.
(17) Leung, W.-H.; Chim, J. L. C.; Lai, W.; Lam, L.; Wong, W.-T.; Chan, W. H.; Yeung, C. H. *Inorg. Chim. Acta* **1999**, *290*, 28-35.
(18) Xu, N.; Lee, J.; Powell, D. R.; Richter-Addo, G. B. *Inorg. Chim. Acta* **2005**, *358*, 2855-2860.
(19) Kirwan, J. N.; Roberts, B. P. *J. Chem. Soc., Faraday Trans. 2* **1989**, *7*, 1125-1132.
(20) Bensivy, L.; Bittl, R.; McMaster, J.; Ross, S.; Teutloff, C.; Nesse, F. *Angew., Int. Ed. Engl.* **2005**, *44*, 5314-5317.
(21) Zu, Y.; Couture, M. M.-J.; Kolling, D. R. J.; Croft, A. R.; Eltis, L. D.; Fee, J. A.; Hist, J. *Biochemistry* **2003**, *42*, 12400-12408.
(22) Brown, G. M.; Hopf, F. R.; Meyer, T. J.; Whitten, D. G. *J. Amer. Chem. Soc.* **1975**, *97*, 5385-5390.
(23) Richter-Addo, G. B.; Wheeler, R. A.; Hixson, C. A.; Chen, L.; Khan, M. A.; Ellison, M. K.; Schulz, C. E.; Sheidt, W. R. *J. Amer. Chem. Soc.* **2001**, *123*, 6314-6326.
(24) Hodge, S. J.; Wang, L.-S.; Khan, M. A.; Young, V. G.; Richter-Addo, G. B. *Chem. Commun.* **1996**, 2283-2284.
(25) Lorkovic, I. M.; Miranda, K. M.; Lee, B.; Bernhard, S.; Schoonover, J. R.; Ford, P. C. *J. Amer. Chem. Soc.* **1998**, *120*, 11674-11683.
(26) Formitchev, D. V.; Coppens, P.; Li, T.; Bagley, K. A.; Chen, L.; Richter-Addo, G. B. *Chem. Commun.* **1999**, 2013-2014.
(27) Yi, G.-B.; Chen, L.; Khan, M. A.; Richter-Addo, G. B. *Inorg. Chem.* **1997**, *36*, 3876-3885.

(28) Miranda, K. M.; Bu, X.; Lorkovic, I.; Ford, P. C. *Inorg. Chem.* **1997**, *36*, 4838-4848.
(29) Kurtikyan, T. S.; Marirosyan, G. G.; Lorkovic, I. M.; Ford, P. C. *J. Amer. Chem. Soc.* **2002**, *124*, 10124-10129.
(30) Lee, J.; Yi, G.-B.; Khan, M. A.; Richter-Addo, G. B. *Inorg. Chem.* **1999**, *38*, 4578-4584.
(31) Yi, G.-B.; Khan, M. A.; Richter-Addo, G. B. *Inorg. Chem.* **1996**, *35*, 3453-3454.
(32) Yi, G.-B.; Khan, M. A.; Powell, D. R.; Richter-Addo, G. B. *Inorg. Chem.* **1998**, *37*, 208-214.
(33) Serli, B.; Zangrando, E.; Iengo, E.; Mestroni, G.; Yellowlees, L.; Alessio, E. *Inorg. Chem.* **2002**, *41*, 4033-4043.

Appendix

Table 2.5. Bond lengths [Å] for (OEP)Os(NO)(OEt).

Os(1)-O(2)#1	1.849(7)	C(3)-C(13)	1.494(8)
Os(1)-O(2)	1.849(7)	C(4)-C(5)	1.391(6)
Os(1)-N(3)#1	1.880(7)	C(5)-C(6)	1.381(7)
Os(1)-N(3)	1.880(7)	C(6)-C(7)	1.456(6)
Os(1)-N(1)#1	2.059(4)	C(7)-C(8)	1.354(8)
Os(1)-N(1)	2.059(4)	C(7)-C(15)	1.501(8)
Os(1)-N(2)	2.066(4)	C(8)-C(9)	1.436(8)
Os(1)-N(2)#1	2.066(4)	C(8)-C(17)	1.534(8)
N(1)-C(4)	1.364(7)	C(8)-C(17')	1.535(9)
N(1)-C(1)	1.372(6)	C(9)-C(10)	1.388(8)
N(2)-C(6)	1.361(7)	C(10)-C(1)#1	1.385(8)
N(2)-C(9)	1.380(6)	C(11)-C(12)	1.515(8)
N(3)-O(1)	1.165(9)	C(13)-C(14)	1.529(7)
C(1)-C(10)#1	1.385(8)	C(15)-C(16)	1.521(8)
C(1)-C(2)	1.454(8)	C(17)-C(18)	1.532(11)
C(2)-C(3)	1.353(8)	C(17')-C(18')	1.531(12)
C(2)-C(11)	1.508(7)	O(2)-C(19)	1.351(12)
C(3)-C(4)	1.453(7)	C(19)-C(20)	1.475(16)

Table 2.6. Bond angles [°] for (OEP)Os(NO)(OEt).

O(2)#1-Os(1)-O(2)	180.000(1)	C(9)-N(2)-Os(1)	126.0(4)
O(2)#1-Os(1)-N(3)#1	168.4(6)	O(1)-N(3)-Os(1)	172.4(10)
O(2)-Os(1)-N(3)#1	11.6(6)	N(1)-C(1)-C(10)#1	125.0(5)
O(2)#1-Os(1)-N(3)	11.6(6)	N(1)-C(1)-C(2)	108.5(5)
O(2)-Os(1)-N(3)	168.4(6)	C(10)#1-C(1)-C(2)	126.6(4)
N(3)#1-Os(1)-N(3)	180.000(1)	C(3)-C(2)-C(1)	107.6(4)
O(2)#1-Os(1)-N(1)#1	85.2(3)	C(3)-C(2)-C(11)	128.0(5)
O(2)-Os(1)-N(1)#1	94.8(3)	C(1)-C(2)-C(11)	124.4(5)
N(3)#1-Os(1)-N(1)#1	84.1(3)	C(2)-C(3)-C(4)	106.8(5)
N(3)-Os(1)-N(1)#1	95.9(3)	C(2)-C(3)-C(13)	128.7(5)
O(2)#1-Os(1)-N(1)	94.8(3)	C(4)-C(3)-C(13)	124.4(5)
O(2)-Os(1)-N(1)	85.2(3)	N(1)-C(4)-C(5)	125.3(4)
N(3)#1-Os(1)-N(1)	95.9(3)	N(1)-C(4)-C(3)	109.2(4)
N(3)-Os(1)-N(1)	84.1(3)	C(5)-C(4)-C(3)	125.5(5)
N(1)#1-Os(1)-N(1)	180.000(1)	C(6)-C(5)-C(4)	128.0(5)
O(2)#1-Os(1)-N(2)	90.8(3)	N(2)-C(6)-C(5)	124.8(4)
O(2)-Os(1)-N(2)	89.2(3)	N(2)-C(6)-C(7)	108.7(4)
N(3)#1-Os(1)-N(2)	93.7(4)	C(5)-C(6)-C(7)	126.5(5)
N(3)-Os(1)-N(2)	86.3(4)	C(8)-C(7)-C(6)	107.1(5)
N(1)#1-Os(1)-N(2)	89.89(16)	C(8)-C(7)-C(15)	129.1(5)
N(1)-Os(1)-N(2)	90.11(16)	C(6)-C(7)-C(15)	123.8(5)
O(2)#1-Os(1)-N(2)#1	89.2(3)	C(7)-C(8)-C(9)	107.5(4)
O(2)-Os(1)-N(2)#1	90.8(3)	C(7)-C(8)-C(17)	122.0(7)
N(3)#1-Os(1)-N(2)#1	86.3(4)	C(9)-C(8)-C(17)	130.4(7)
N(3)-Os(1)-N(2)#1	93.7(4)	C(7)-C(8)-C(17')	134.8(9)
N(1)#1-Os(1)-N(2)#1	90.11(16)	C(9)-C(8)-C(17')	117.2(9)
N(1)-Os(1)-N(2)#1	89.89(16)	C(17)-C(8)-C(17')	15.8(9)
N(2)-Os(1)-N(2)#1	180.000(1)	N(2)-C(9)-C(10)	124.7(5)
C(4)-N(1)-C(1)	107.9(4)	N(2)-C(9)-C(8)	108.9(5)
C(4)-N(1)-Os(1)	125.6(3)	C(10)-C(9)-C(8)	126.4(4)
C(1)-N(1)-Os(1)	126.4(4)	C(1)#1-C(10)-C(9)	127.9(4)
C(6)-N(2)-C(9)	107.7(4)	C(2)-C(11)-C(12)	113.9(5)
C(6)-N(2)-Os(1)	126.2(3)	C(3)-C(13)-C(14)	112.5(4)

C(7)-C(15)-C(16)	112.2(4)	C(19)-O(2)-Os(1)	128.0(8)
C(18)-C(17)-C(8)	111.3(6)	O(2)-C(19)-C(20)	109.8(10)
C(18')-C(17')-C(8)	112.0(7)		

Table 2.7. Bond lengths [Å] for (OEP)Os(NO)(SEt).0.5(CH_2Cl_2).

Os(1)-N(3)	1.944(10)	C(11)-C(12)	1.517(4)
Os(1)-N(1)	2.048(3)	C(11)-H(11A)	0.9900
Os(1)-N(1)#1	2.048(3)	C(11)-H(11B)	0.9900
Os(1)-N(2)#1	2.054(2)	C(12)-H(12A)	0.9800
Os(1)-N(2)	2.054(2)	C(12)-H(12B)	0.9800
Os(1)-S(1)	2.227(2)	C(12)-H(12C)	0.9800
S(1)-C(19)	1.768(10)	C(13)-C(14)	1.525(5)
N(1)-C(1)	1.366(4)	C(13)-H(13A)	0.9900
N(1)-C(4)	1.369(4)	C(13)-H(13B)	0.9900
N(2)-C(6)	1.363(4)	C(14)-H(14A)	0.9800
N(2)-C(9)	1.369(4)	C(14)-H(14B)	0.9800
N(3)-O(1)	1.136(11)	C(14)-H(14C)	0.9800
C(1)-C(10)#1	1.389(4)	C(15)-C(16)	1.525(5)
C(1)-C(2)	1.443(5)	C(15)-H(15A)	0.9900
C(2)-C(3)	1.365(4)	C(15)-H(15B)	0.9900
C(2)-C(11)	1.497(4)	C(16)-H(16A)	0.9800
C(3)-C(4)	1.440(5)	C(16)-H(16B)	0.9800
C(3)-C(13)	1.486(5)	C(16)-H(16C)	0.9800
C(4)-C(5)	1.385(4)	C(17)-C(18)	1.518(5)
C(5)-C(6)	1.379(5)	C(17)-H(17A)	0.9900
C(5)-H(5)	0.9500	C(17)-H(17B)	0.9900
C(6)-C(7)	1.446(4)	C(18)-H(18A)	0.9800
C(7)-C(8)	1.362(5)	C(18)-H(18B)	0.9800
C(7)-C(15)	1.491(4)	C(18)-H(18C)	0.9800
C(8)-C(9)	1.451(4)	C(19)-C(20)	1.559(16)
C(8)-C(17)	1.493(4)	C(19)-H(19A)	0.9900
C(9)-C(10)	1.378(5)	C(19)-H(19B)	0.9900
C(10)-C(1)#1	1.389(4)	C(20)-H(20A)	0.9800
C(10)-H(10)	0.9500	C(20)-H(20B)	0.9800

C(20)-H(20C)	0.9800	Cl(1T)-C(1T)	1.721(3)
Cl(1S)-C(1S)	1.719(3)	C(1T)-Cl(2T)	1.720(3)
C(1S)-Cl(2S)	1.720(3)	C(1T)-H(1T1)	0.9900
C(1S)-H(1S1)	0.9900	C(1T)-H(1T2)	0.9900
C(1S)-H(1S2)	0.9900		

Table 2.8. Bond angles [°] for (OEP)Os(NO)(SEt).0.5(CH_2Cl_2).

N(3)-Os(1)-N(1)	82.9(3)	C(2)-C(3)-C(4)	106.9(3)
N(3)-Os(1)-N(1)#1	97.1(3)	C(2)-C(3)-C(13)	128.2(3)
N(1)-Os(1)-N(1)#1	180.000(1)	C(4)-C(3)-C(13)	124.8(3)
N(3)-Os(1)-N(2)#1	92.7(3)	N(1)-C(4)-C(5)	124.9(3)
N(1)-Os(1)-N(2)#1	90.18(10)	N(1)-C(4)-C(3)	109.3(3)
N(1)#1-Os(1)-N(2)#1	89.82(10)	C(5)-C(4)-C(3)	125.7(3)
N(3)-Os(1)-N(2)	87.3(3)	C(6)-C(5)-C(4)	127.5(3)
N(1)-Os(1)-N(2)	89.82(10)	C(6)-C(5)-H(5)	116.3
N(1)#1-Os(1)-N(2)	90.18(10)	C(4)-C(5)-H(5)	116.3
N(2)#1-Os(1)-N(2)	180.00(12)	N(2)-C(6)-C(5)	125.2(3)
N(3)-Os(1)-S(1)	172.0(3)	N(2)-C(6)-C(7)	109.3(3)
N(1)-Os(1)-S(1)	89.58(10)	C(5)-C(6)-C(7)	125.5(3)
N(1)#1-Os(1)-S(1)	90.42(10)	C(8)-C(7)-C(6)	107.0(3)
N(2)#1-Os(1)-S(1)	90.02(10)	C(8)-C(7)-C(15)	128.5(3)
N(2)-Os(1)-S(1)	89.98(10)	C(6)-C(7)-C(15)	124.5(3)
C(19)-S(1)-Os(1)	112.8(4)	C(7)-C(8)-C(9)	107.0(3)
C(1)-N(1)-C(4)	107.5(3)	C(7)-C(8)-C(17)	127.6(3)
C(1)-N(1)-Os(1)	126.2(2)	C(9)-C(8)-C(17)	125.4(3)
C(4)-N(1)-Os(1)	126.3(2)	N(2)-C(9)-C(10)	125.1(3)
C(6)-N(2)-C(9)	107.8(3)	N(2)-C(9)-C(8)	108.9(3)
C(6)-N(2)-Os(1)	126.2(2)	C(10)-C(9)-C(8)	126.0(3)
C(9)-N(2)-Os(1)	125.9(2)	C(9)-C(10)-C(1)#1	127.7(3)
O(1)-N(3)-Os(1)	172.7(8)	C(9)-C(10)-H(10)	116.1
N(1)-C(1)-C(10)#1	124.9(3)	C(1)#1-C(10)-H(10)	116.1
N(1)-C(1)-C(2)	109.3(3)	C(2)-C(11)-C(12)	113.3(3)
C(10)#1-C(1)-C(2)	125.8(3)	C(2)-C(11)-H(11A)	108.9
C(3)-C(2)-C(1)	106.9(3)	C(12)-C(11)-H(11A)	108.9
C(3)-C(2)-C(11)	127.6(3)	C(2)-C(11)-H(11B)	108.9
C(1)-C(2)-C(11)	125.5(3)	C(12)-C(11)-H(11B)	108.9

H(11A)-C(11)-H(11B)	107.7	C(8)-C(17)-C(18)	112.8(3)
C(11)-C(12)-H(12A)	109.5	C(8)-C(17)-H(17A)	109.0
C(11)-C(12)-H(12B)	109.5	C(18)-C(17)-H(17A)	109.0
H(12A)-C(12)-H(12B)	109.5	C(8)-C(17)-H(17B)	109.0
C(11)-C(12)-H(12C)	109.5	C(18)-C(17)-H(17B)	109.0
H(12A)-C(12)-H(12C)	109.5	H(17A)-C(17)-H(17B)	107.8
H(12B)-C(12)-H(12C)	109.5	C(17)-C(18)-H(18A)	109.5
C(3)-C(13)-C(14)	112.9(3)	C(17)-C(18)-H(18B)	109.5
C(3)-C(13)-H(13A)	109.0	H(18A)-C(18)-H(18B)	109.5
C(14)-C(13)-H(13A)	109.0	C(17)-C(18)-H(18C)	109.5
C(3)-C(13)-H(13B)	109.0	H(18A)-C(18)-H(18C)	109.5
C(14)-C(13)-H(13B)	109.0	H(18B)-C(18)-H(18C)	109.5
H(13A)-C(13)-H(13B)	107.8	C(20)-C(19)-S(1)	114.9(8)
C(13)-C(14)-H(14A)	109.5	C(20)-C(19)-H(19A)	108.5
C(13)-C(14)-H(14B)	109.5	S(1)-C(19)-H(19A)	108.5
H(14A)-C(14)-H(14B)	109.5		
C(13)-C(14)-H(14C)	109.5		
H(14A)-C(14)-H(14C)	109.5		
H(14B)-C(14)-H(14C)	109.5		
C(7)-C(15)-C(16)	112.3(3)		
C(7)-C(15)-H(15A)	109.1		
C(16)-C(15)-H(15A)	109.1		
C(7)-C(15)-H(15B)	109.1		
C(16)-C(15)-H(15B)	109.1		
H(15A)-C(15)-H(15B)	107.9		
C(15)-C(16)-H(16A)	109.5		
C(15)-C(16)-H(16B)	109.4		
H(16A)-C(16)-H(16B)	109.5		
C(15)-C(16)-H(16C)	109.5		
H(16A)-C(16)-H(16C)	109.5		
H(16B)-C(16)-H(16C)	109.5		

C(20)-C(19)-H(19B)	108.5
S(1)-C(19)-H(19B)	108.5
H(19A)-C(19)-H(19B)	107.5
C(19)-C(20)-H(20A)	111.6
C(19)-C(20)-H(20B)	107.7
H(20A)-C(20)-H(20B)	109.5
C(19)-C(20)-H(20C)	109.1
H(20A)-C(20)-H(20C)	109.5
H(20B)-C(20)-H(20C)	109.5
Cl(1S)-C(1S)-Cl(2S)	112.2(17)
Cl(1S)-C(1S)-H(1S1)	109.2
Cl(2S)-C(1S)-H(1S1)	109.2
Cl(1S)-C(1S)-H(1S2)	109.2
Cl(2S)-C(1S)-H(1S2)	109.2
H(1S1)-C(1S)-H(1S2)	107.9
Cl(2T)-C(1T)-Cl(1T)	115.7(6)
Cl(2T)-C(1T)-H(1T1)	108.4
Cl(1T)-C(1T)-H(1T1)	108.4
Cl(2T)-C(1T)-H(1T2)	108.3
Cl(1T)-C(1T)-H(1T2)	108.3
H(1T1)-C(1T)-H(1T2)	107

Table 3.4. Bond lengths (Å) for (T(*p*-OMe)PP)Ru(NO)(O-*i*-C_5H_{11}).

Ru(1)-N(5)	1.754(4)	C(3)-C(4)	1.441(6)
Ru(1)-O(2)	1.932(3)	C(3)-H(3)	0.9500
Ru(1)-N(2)	2.053(4)	C(4)-C(5)	1.403(6)
Ru(1)-N(4)	2.055(4)	C(5)-C(6)	1.397(6)
Ru(1)-N(1)	2.058(4)	C(5)-C(21)	1.500(6)
Ru(1)-N(3)	2.061(4)	C(6)-C(7)	1.441(6)
O(1)-N(5)	1.172(5)	C(7)-C(8)	1.344(7)
O(2)-C(49")	1.293(8)	C(7)-H(7)	0.9500
O(2)-C(49)	1.294(8)	C(8)-C(9)	1.440(6)
O(2)-C(49')	1.295(8)	C(8)-H(8)	0.9500
O(3)-C(24)	1.369(5)	C(9)-C(10)	1.394(6)
O(3)-C(27)	1.421(6)	C(10)-C(11)	1.406(6)
O(4)-C(31)	1.367(6)	C(10)-C(28)	1.501(6)
O(4)-C(34)	1.420(9)	C(11)-C(12)	1.430(6)
O(5)-C(38)	1.373(5)	C(12)-C(13)	1.364(6)
O(5)-C(41)	1.423(7)	C(12)-H(12)	0.9500
O(6)-C(45)	1.366(6)	C(13)-C(14)	1.440(6)
O(6)-C(48)	1.444(8)	C(13)-H(13)	0.9500
N(1)-C(4)	1.370(5)	C(14)-C(15)	1.391(6)
N(1)-C(1)	1.373(6)	C(15)-C(16)	1.401(6)
N(2)-C(6)	1.378(6)	C(15)-C(35)	1.508(6)
N(2)-C(9)	1.379(6)	C(16)-C(17)	1.432(6)
N(3)-C(11)	1.359(6)	C(17)-C(18)	1.346(7)
N(3)-C(14)	1.375(5)	C(17)-H(17)	0.9500
N(4)-C(16)	1.367(6)	C(18)-C(19)	1.439(6)
N(4)-C(19)	1.369(6)	C(18)-H(18)	0.9500
C(1)-C(20)	1.402(6)	C(19)-C(20)	1.399(6)
C(1)-C(2)	1.436(6)	C(20)-C(42)	1.504(6)
C(2)-C(3)	1.343(6)	C(21)-C(26)	1.373(6)
C(2)-H(2)	0.9500	C(21)-C(22)	1.385(6)

C(22)-C(23)	1.387(6)	C(39)-C(40)	1.386(7)
C(22)-H(22)	0.9500	C(39)-H(39)	0.9500
C(23)-C(24)	1.370(7)	C(40)-H(40)	0.9500
C(23)-H(23)	0.9500	C(41)-H(41A)	0.9800
C(24)-C(25)	1.391(7)	C(41)-H(41B)	0.9800
C(25)-C(26)	1.393(6)	C(41)-H(41C)	0.9800
C(25)-H(25)	0.9500	C(42)-C(47)	1.383(7)
C(26)-H(26)	0.9500	C(42)-C(43)	1.385(7)
C(27)-H(27A)	0.9800	C(43)-C(44)	1.393(7)
C(27)-H(27B)	0.9800	C(43)-H(43)	0.9500
C(27)-H(27C)	0.9800	C(44)-C(45)	1.370(8)
C(28)-C(33)	1.356(7)	C(44)-H(44)	0.9500
C(28)-C(29)	1.393(7)	C(45)-C(46)	1.376(8)
C(29)-C(30)	1.384(7)	C(46)-C(47)	1.386(7)
C(29)-H(29)	0.9500	C(46)-H(46)	0.9500
C(30)-C(31)	1.377(8)	C(47)-H(47)	0.9500
C(30)-H(30)	0.9500	C(48)-H(48A)	0.9800
C(31)-C(32)	1.369(7)	C(48)-H(48B)	0.9800
C(32)-C(33)	1.395(6)	C(48)-H(48C)	0.9800
C(32)-H(32)	0.9500	C(49)-C(50)	1.575(7)
C(33)-H(33)	0.9500	C(49)-H(49A)	0.9900
C(34)-H(34A)	0.9800	C(49)-H(49B)	0.9900
C(34)-H(34B)	0.9800	C(50)-C(51)	1.573(7)
C(34)-H(34C)	0.9800	C(50)-H(50A)	0.9900
C(35)-C(36)	1.367(7)	C(50)-H(50B)	0.9900
C(35)-C(40)	1.380(7)	C(51)-C(53)	1.569(6)
C(36)-C(37)	1.382(7)	C(51)-C(52)	1.570(6)
C(36)-H(36)	0.9500	C(51)-H(51)	1.0000
C(37)-C(38)	1.365(7)	C(52)-H(52A)	0.9800
C(37)-H(37)	0.9500	C(52)-H(52B)	0.9800
C(38)-C(39)	1.385(7)	C(52)-H(52C)	0.9800

C(53)-H(53A)	0.9800	C(53')-H(53F)	0.9800
C(53)-H(53B)	0.9800	C(49")-C(50")	1.570(7)
C(53)-H(53C)	0.9800	C(49")-H(49E)	0.9900
C(49')-C(50')	1.567(7)	C(49")-H(49F)	0.9900
C(49')-H(49C)	0.9900	C(50")-C(51")	1.573(7)
C(49')-H(49D)	0.9900	C(50")-H(50E)	0.9900
C(50')-C(51')	1.568(7)	C(50")-H(50F)	0.9900
C(50')-H(50C)	0.9900	C(51")-C(53")	1.569(7)
C(50')-H(50D)	0.9900	C(51")-C(52")	1.571(7)
C(51')-C(52')	1.569(7)	C(51")-H(51")	1.0000
C(51')-C(53')	1.573(7)	C(52")-H(52G)	0.9800
C(51')-H(51')	1.0000	C(52")-H(52H)	0.9800
C(52')-H(52D)	0.9800	C(52")-H(52I)	0.9800
C(52')-H(52E)	0.9800	C(53")-H(53G)	0.9800
C(52')-H(52F)	0.9800	C(53")-H(53H)	0.9800
C(53')-H(53D)	0.9800	C(53")-H(53I)	0.9800
C(53')-H(53E)	0.9800		

Table 3.5. Bond angles (°) for (T(*p*-OMe)PP)Ru(NO)(O-*i*-C_5H_{11}).

N(5)-Ru(1)-O(2)	178.39(14)	C(11)-N(3)-Ru(1)	127.3(3)
N(5)-Ru(1)-N(2)	91.17(15)	C(14)-N(3)-Ru(1)	125.0(3)
O(2)-Ru(1)-N(2)	90.40(14)	C(16)-N(4)-C(19)	107.2(4)
N(5)-Ru(1)-N(4)	92.72(15)	C(16)-N(4)-Ru(1)	125.9(3)
O(2)-Ru(1)-N(4)	85.71(14)	C(19)-N(4)-Ru(1)	126.9(3)
N(2)-Ru(1)-N(4)	176.11(15)	O(1)-N(5)-Ru(1)	176.9(3)
N(5)-Ru(1)-N(1)	92.40(15)	N(1)-C(1)-C(20)	126.1(4)
O(2)-Ru(1)-N(1)	87.93(14)	N(1)-C(1)-C(2)	108.4(4)
N(2)-Ru(1)-N(1)	90.36(15)	C(20)-C(1)-C(2)	125.5(4)
N(4)-Ru(1)-N(1)	89.44(14)	C(3)-C(2)-C(1)	107.7(4)
N(5)-Ru(1)-N(3)	92.03(15)	C(3)-C(2)-H(2)	126.1
O(2)-Ru(1)-N(3)	87.66(14)	C(1)-C(2)-H(2)	126.1
N(2)-Ru(1)-N(3)	89.16(15)	C(2)-C(3)-C(4)	107.6(4)
N(4)-Ru(1)-N(3)	90.74(15)	C(2)-C(3)-H(3)	126.2
N(1)-Ru(1)-N(3)	175.56(15)	C(4)-C(3)-H(3)	126.2
C(49")-O(2)-Ru(1)	129.1(9)	N(1)-C(4)-C(5)	126.4(4)
C(49)-O(2)-Ru(1)	128.0(8)	N(1)-C(4)-C(3)	108.3(4)
C(49')-O(2)-Ru(1)	161.1(12)	C(5)-C(4)-C(3)	125.2(4)
C(24)-O(3)-C(27)	116.8(4)	C(6)-C(5)-C(4)	125.2(4)
C(31)-O(4)-C(34)	114.3(5)	C(6)-C(5)-C(21)	117.5(4)
C(38)-O(5)-C(41)	116.2(4)	C(4)-C(5)-C(21)	117.4(4)
C(45)-O(6)-C(48)	115.3(5)	N(2)-C(6)-C(5)	126.3(4)
C(4)-N(1)-C(1)	107.8(4)	N(2)-C(6)-C(7)	108.4(4)
C(4)-N(1)-Ru(1)	125.7(3)	C(5)-C(6)-C(7)	125.3(4)
C(1)-N(1)-Ru(1)	126.2(3)	C(8)-C(7)-C(6)	107.4(4)
C(6)-N(2)-C(9)	108.0(4)	C(8)-C(7)-H(7)	126.3
C(6)-N(2)-Ru(1)	125.8(3)	C(6)-C(7)-H(7)	126.3
C(9)-N(2)-Ru(1)	126.2(3)	C(7)-C(8)-C(9)	108.4(4)
C(11)-N(3)-C(14)	107.7(4)	C(7)-C(8)-H(8)	125.8

C(9)-C(8)-H(8)	125.8	N(4)-C(19)-C(20)	125.8(4)
N(2)-C(9)-C(10)	126.8(4)	N(4)-C(19)-C(18)	108.7(4)
N(2)-C(9)-C(8)	107.8(4)	C(20)-C(19)-C(18)	125.6(4)
C(10)-C(9)-C(8)	125.4(4)	C(19)-C(20)-C(1)	125.1(4)
C(9)-C(10)-C(11)	124.5(4)	C(19)-C(20)-C(42)	117.3(4)
C(9)-C(10)-C(28)	118.1(4)	C(1)-C(20)-C(42)	117.5(4)
C(11)-C(10)-C(28)	117.3(4)	C(26)-C(21)-C(22)	118.1(4)
N(3)-C(11)-C(10)	125.9(4)	C(26)-C(21)-C(5)	120.7(4)
N(3)-C(11)-C(12)	109.5(4)	C(22)-C(21)-C(5)	121.2(4)
C(10)-C(11)-C(12)	124.6(4)	C(21)-C(22)-C(23)	120.8(4)
C(13)-C(12)-C(11)	107.2(4)	C(21)-C(22)-H(22)	119.6
C(13)-C(12)-H(12)	126.4	C(23)-C(22)-H(22)	119.6
C(11)-C(12)-H(12)	126.4	C(24)-C(23)-C(22)	120.5(4)
C(12)-C(13)-C(14)	107.0(4)	C(24)-C(23)-H(23)	119.8
C(12)-C(13)-H(13)	126.5	C(22)-C(23)-H(23)	119.8
C(14)-C(13)-H(13)	126.5	O(3)-C(24)-C(23)	116.3(4)
N(3)-C(14)-C(15)	126.4(4)	O(3)-C(24)-C(25)	124.0(4)
N(3)-C(14)-C(13)	108.6(4)	C(23)-C(24)-C(25)	119.7(4)
C(15)-C(14)-C(13)	125.0(4)	C(24)-C(25)-C(26)	118.8(4)
C(14)-C(15)-C(16)	126.3(4)	C(24)-C(25)-H(25)	120.6
C(14)-C(15)-C(35)	116.9(4)	C(26)-C(25)-H(25)	120.6
C(16)-C(15)-C(35)	116.8(4)	C(21)-C(26)-C(25)	122.0(4)
N(4)-C(16)-C(15)	125.7(4)	C(21)-C(26)-H(26)	119.0
N(4)-C(16)-C(17)	109.4(4)	C(25)-C(26)-H(26)	119.0
C(15)-C(16)-C(17)	124.9(4)	O(3)-C(27)-H(27A)	109.5
C(18)-C(17)-C(16)	107.1(4)	O(3)-C(27)-H(27B)	109.5
C(18)-C(17)-H(17)	126.4	H(27A)-C(27)-H(27B)	109.5
C(16)-C(17)-H(17)	126.4	O(3)-C(27)-H(27C)	109.5
C(17)-C(18)-C(19)	107.6(4)	H(27A)-C(27)-H(27C)	109.5
C(17)-C(18)-H(18)	126.2	H(27B)-C(27)-H(27C)	109.5
C(19)-C(18)-H(18)	126.2	C(33)-C(28)-C(29)	118.0(4)

C(33)-C(28)-C(10)	121.2(4)	C(36)-C(37)-H(37)	120.0
C(29)-C(28)-C(10)	120.8(4)	C(37)-C(38)-O(5)	124.1(5)
C(30)-C(29)-C(28)	120.8(5)	C(37)-C(38)-C(39)	119.6(5)
C(30)-C(29)-H(29)	119.6	O(5)-C(38)-C(39)	116.3(4)
C(28)-C(29)-H(29)	119.6	C(38)-C(39)-C(40)	119.7(5)
C(31)-C(30)-C(29)	120.0(5)	C(38)-C(39)-H(39)	120.2
C(31)-C(30)-H(30)	120.0	C(40)-C(39)-H(39)	120.2
C(29)-C(30)-H(30)	120.0	C(35)-C(40)-C(39)	120.8(5)
O(4)-C(31)-C(32)	125.1(5)	C(35)-C(40)-H(40)	119.6
O(4)-C(31)-C(30)	115.2(5)	C(39)-C(40)-H(40)	119.6
C(32)-C(31)-C(30)	119.7(5)	O(5)-C(41)-H(41A)	109.5
C(31)-C(32)-C(33)	119.6(5)	O(5)-C(41)-H(41B)	109.5
C(31)-C(32)-H(32)	120.2	H(41A)-C(41)-H(41B)	109.5
C(33)-C(32)-H(32)	120.2	O(5)-C(41)-H(41C)	109.5
C(28)-C(33)-C(32)	121.9(5)	H(41A)-C(41)-H(41C)	109.5
C(28)-C(33)-H(33)	119.1	H(41B)-C(41)-H(41C)	109.5
C(32)-C(33)-H(33)	119.1	C(47)-C(42)-C(43)	118.3(4)
O(4)-C(34)-H(34A)	109.5	C(47)-C(42)-C(20)	121.5(4)
O(4)-C(34)-H(34B)	109.5	C(43)-C(42)-C(20)	120.1(4)
H(34A)-C(34)-H(34B)	109.5	C(42)-C(43)-C(44)	121.0(5)
O(4)-C(34)-H(34C)	109.4	C(42)-C(43)-H(43)	119.5
H(34A)-C(34)-H(34C)	109.5	C(44)-C(43)-H(43)	119.5
H(34B)-C(34)-H(34C)	109.5	C(45)-C(44)-C(43)	119.7(5)
C(36)-C(35)-C(40)	118.5(4)	C(45)-C(44)-H(44)	120.1
C(36)-C(35)-C(15)	119.9(4)	C(43)-C(44)-H(44)	120.1
C(40)-C(35)-C(15)	121.7(4)	O(6)-C(45)-C(44)	124.4(5)
C(35)-C(36)-C(37)	121.4(5)	O(6)-C(45)-C(46)	115.7(5)
C(35)-C(36)-H(36)	119.3	C(44)-C(45)-C(46)	119.9(5)
C(37)-C(36)-H(36)	119.3	C(45)-C(46)-C(47)	120.3(5)
C(38)-C(37)-C(36)	120.1(5)	C(45)-C(46)-H(46)	119.9
C(38)-C(37)-H(37)	120.0	C(47)-C(46)-H(46)	119.9

C(42)-C(47)-C(46)	120.7(5)	H(52A)-C(52)-H(52C)	109.5
C(42)-C(47)-H(47)	119.7	H(52B)-C(52)-H(52C)	109.5
C(46)-C(47)-H(47)	119.7	C(51)-C(53)-H(53A)	109.7
O(6)-C(48)-H(48A)	109.5	C(51)-C(53)-H(53B)	109.3
O(6)-C(48)-H(48B)	109.5	H(53A)-C(53)-H(53B)	109.5
H(48A)-C(48)-H(48B)	109.5	C(51)-C(53)-H(53C)	109.4
O(6)-C(48)-H(48C)	109.5	H(53A)-C(53)-H(53C)	109.5
H(48A)-C(48)-H(48C)	109.5	H(53B)-C(53)-H(53C)	109.5
H(48B)-C(48)-H(48C)	109.5	O(2)-C(49')-C(50')	104.4(8)
O(2)-C(49)-C(50)	101.5(8)	O(2)-C(49')-H(49C)	110.9
O(2)-C(49)-H(49A)	111.5	C(50')-C(49')-H(49C)	110.9
C(50)-C(49)-H(49A)	111.5	O(2)-C(49')-H(49D)	110.9
O(2)-C(49)-H(49B)	111.5	C(50')-C(49')-H(49D)	110.9
C(50)-C(49)-H(49B)	111.5	H(49C)-C(49')-H(49D)	108.9
H(49A)-C(49)-H(49B)	109.3	C(49')-C(50')-C(51')	109.9(6)
C(51)-C(50)-C(49)	107.5(6)	C(49')-C(50')-H(50C)	109.7
C(51)-C(50)-H(50A)	110.2	C(51')-C(50')-H(50C)	109.7
C(49)-C(50)-H(50A)	110.2	C(49')-C(50')-H(50D)	109.7
C(51)-C(50)-H(50B)	110.2	C(51')-C(50')-H(50D)	109.7
C(49)-C(50)-H(50B)	110.2	H(50C)-C(50')-H(50D)	108.2
H(50A)-C(50)-H(50B)	108.5	C(50')-C(51')-C(52')	108.8(5)
C(53)-C(51)-C(52)	109.8(6)	C(50')-C(51')-C(53')	108.7(6)
C(53)-C(51)-C(50)	108.6(6)	C(52')-C(51')-C(53')	108.6(6)
C(52)-C(51)-C(50)	106.4(6)	C(50')-C(51')-H(51')	110.3
C(53)-C(51)-H(51)	110.6	C(52')-C(51')-H(51')	110.3
C(52)-C(51)-H(51)	110.6	C(53')-C(51')-H(51')	110.3
C(50)-C(51)-H(51)	110.6	C(51')-C(52')-H(52D)	109.4
C(51)-C(52)-H(52A)	109.4	C(51')-C(52')-H(52E)	109.4
C(51)-C(52)-H(52B)	109.6	H(52D)-C(52')-H(52E)	109.5
H(52A)-C(52)-H(52B)	109.5	C(51')-C(52')-H(52F)	109.6
C(51)-C(52)-H(52C)	109.4	H(52D)-C(52')-H(52F)	109.5

H(52E)-C(52')-H(52F)	109.5	C(53")-C(51")-C(52")	108.3(6)
C(51')-C(53')-H(53D)	109.4	C(53")-C(51")-C(50")	108.6(6)
C(51')-C(53')-H(53E)	109.2	C(52")-C(51")-C(50")	108.2(6)
H(53D)-C(53')-H(53E)	109.5	C(53")-C(51")-H(51")	110.5
C(51')-C(53')-H(53F)	109.8	C(52")-C(51")-H(51")	110.5
H(53D)-C(53')-H(53F)	109.5	C(50")-C(51")-H(51")	110.5
H(53E)-C(53')-H(53F)	109.5	C(51")-C(52")-H(52G)	109.5
O(2)-C(49")-C(50")	104.2(8)	C(51")-C(52")-H(52H)	109.5
O(2)-C(49")-H(49E)	110.9	H(52G)-C(52")-H(52H)	109.5
C(50")-C(49")-H(49E)	110.9	C(51")-C(52")-H(52I)	109.5
O(2)-C(49")-H(49F)	110.9	H(52G)-C(52")-H(52I)	109.5
C(50")-C(49")-H(49F)	110.9	H(52H)-C(52")-H(52I)	109.5
H(49E)-C(49")-H(49F)	108.9	C(51")-C(53")-H(53G)	109.5
C(49")-C(50")-C(51")	108.5(6)	C(51")-C(53")-H(53H)	109.5
C(49")-C(50")-H(50E)	110.0	H(53G)-C(53")-H(53H)	109.5
C(51")-C(50")-H(50E)	110.0	C(51")-C(53")-H(53I)	109.5
C(49")-C(50")-H(50F)	110.0	H(53G)-C(53")-H(53I)	109.5
C(51")-C(50")-H(50F)	110.0	H(53H)-C(53")-H(53I)	109.5
H(50E)-C(50")-H(50F)	108.4		

Table 3.6. Bond lengths (Å) for (OEP)Ru(NO)(Im).

Ru(1)-N(5)	1.748(3)	C(7)-C(25)	1.499(4)
Ru(1)-N(4)	2.046(2)	C(8)-C(9)	1.448(4)
Ru(1)-N(2)	2.049(2)	C(8)-C(27)	1.500(4)
Ru(1)-N(3)	2.054(2)	C(9)-C(10)	1.383(4)
Ru(1)-N(1)	2.058(3)	C(10)-C(11)	1.388(4)
Ru(1)-N(6)	2.063(3)	C(11)-C(12)	1.448(4)
O(1)-N(5)	1.148(4)	C(12)-C(13)	1.362(4)
N(1)-C(1)	1.364(4)	C(12)-C(29)	1.502(4)
N(1)-C(4)	1.372(4)	C(13)-C(14)	1.449(4)
N(2)-C(6)	1.367(4)	C(13)-C(31)	1.501(4)
N(2)-C(9)	1.369(4)	C(14)-C(15)	1.383(4)
N(3)-C(11)	1.369(4)	C(15)-C(16)	1.380(4)
N(3)-C(14)	1.370(4)	C(16)-C(17)	1.451(4)
N(4)-C(16)	1.372(4)	C(17)-C(18)	1.359(5)
N(4)-C(19)	1.373(4)	C(17)-C(33)	1.494(4)
N(6)-C(39)	1.348(4)	C(18)-C(19)	1.455(4)
N(6)-C(37)	1.379(4)	C(18)-C(35)	1.486(7)
N(7)-C(39)	1.322(4)	C(18)-C(35')	1.530(13)
N(7)-C(38)	1.372(4)	C(19)-C(20)	1.380(5)
C(1)-C(20)	1.381(4)	C(21)-C(22)	1.521(5)
C(1)-C(2)	1.453(4)	C(23)-C(24)	1.521(5)
C(2)-C(3)	1.361(5)	C(25)-C(26)	1.522(4)
C(2)-C(21)	1.495(4)	C(27)-C(28)	1.524(5)
C(3)-C(4)	1.449(4)	C(29)-C(30)	1.528(5)
C(3)-C(23)	1.502(4)	C(31)-C(32)	1.516(5)
C(4)-C(5)	1.387(4)	C(33)-C(34)	1.524(5)
C(5)-C(6)	1.388(4)	C(35)-C(36)	1.535(9)
C(6)-C(7)	1.438(4)	C(35')-C(36')	1.539(13)
C(7)-C(8)	1.360(5)	C(37)-C(38)	1.354(5)

N(8)-C(42)	1.338(5)	C(40)-C(41)	1.350(8)
N(8)-C(40)	1.344(5)	Cl(1)-C(43)	1.743(6)
N(9)-C(42)	1.287(7)	C(43)-Cl(2)	1.756(5)
N(9)-C(41)	1.374(9)		

Table 3.7. Bond angles (°) for (OEP)Ru(NO)(Im).

N(5)-Ru(1)-N(4)	90.08(11)	C(39)-N(6)-Ru(1)	127.9(2)
N(5)-Ru(1)-N(2)	95.56(11)	C(37)-N(6)-Ru(1)	128.0(2)
N(4)-Ru(1)-N(2)	174.36(10)	C(39)-N(7)-C(38)	104.1(3)
N(5)-Ru(1)-N(3)	94.02(11)	N(1)-C(1)-C(20)	125.2(3)
N(4)-Ru(1)-N(3)	89.97(10)	N(1)-C(1)-C(2)	109.1(3)
N(2)-Ru(1)-N(3)	89.76(10)	C(20)-C(1)-C(2)	125.7(3)
N(5)-Ru(1)-N(1)	91.62(11)	C(3)-C(2)-C(1)	107.0(3)
N(4)-Ru(1)-N(1)	89.67(10)	C(3)-C(2)-C(21)	128.6(3)
N(2)-Ru(1)-N(1)	90.05(10)	C(1)-C(2)-C(21)	124.3(3)
N(3)-Ru(1)-N(1)	174.35(10)	C(2)-C(3)-C(4)	107.0(3)
N(5)-Ru(1)-N(6)	176.95(10)	C(2)-C(3)-C(23)	128.4(3)
N(4)-Ru(1)-N(6)	87.05(10)	C(4)-C(3)-C(23)	124.5(3)
N(2)-Ru(1)-N(6)	87.31(10)	N(1)-C(4)-C(5)	125.3(3)
N(3)-Ru(1)-N(6)	87.02(10)	N(1)-C(4)-C(3)	109.1(3)
N(1)-Ru(1)-N(6)	87.33(10)	C(5)-C(4)-C(3)	125.7(3)
C(1)-N(1)-C(4)	107.8(3)	C(4)-C(5)-C(6)	127.0(3)
C(1)-N(1)-Ru(1)	126.1(2)	N(2)-C(6)-C(5)	125.5(3)
C(4)-N(1)-Ru(1)	125.9(2)	N(2)-C(6)-C(7)	109.5(3)
C(6)-N(2)-C(9)	107.4(2)	C(5)-C(6)-C(7)	125.0(3)
C(6)-N(2)-Ru(1)	126.2(2)	C(8)-C(7)-C(6)	107.1(3)
C(9)-N(2)-Ru(1)	126.4(2)	C(8)-C(7)-C(25)	128.0(3)
C(11)-N(3)-C(14)	107.7(2)	C(6)-C(7)-C(25)	124.8(3)
C(11)-N(3)-Ru(1)	126.1(2)	C(7)-C(8)-C(9)	106.9(3)
C(14)-N(3)-Ru(1)	126.1(2)	C(7)-C(8)-C(27)	127.9(3)
C(16)-N(4)-C(19)	107.8(2)	C(9)-C(8)-C(27)	125.1(3)
C(16)-N(4)-Ru(1)	126.0(2)	N(2)-C(9)-C(10)	125.3(3)
C(19)-N(4)-Ru(1)	126.0(2)	N(2)-C(9)-C(8)	109.0(3)
O(1)-N(5)-Ru(1)	174.9(3)	C(10)-C(9)-C(8)	125.7(3)
C(39)-N(6)-C(37)	104.0(3)	C(9)-C(10)-C(11)	126.9(3)

N(3)-C(11)-C(10)	125.3(3)	C(35)-C(18)-C(35')	7.0(7)
N(3)-C(11)-C(12)	109.0(3)	N(4)-C(19)-C(20)	125.3(3)
C(10)-C(11)-C(12)	125.8(3)	N(4)-C(19)-C(18)	108.7(3)
C(13)-C(12)-C(11)	107.3(3)	C(20)-C(19)-C(18)	126.0(3)
C(13)-C(12)-C(29)	128.3(3)	C(19)-C(20)-C(1)	127.2(3)
C(11)-C(12)-C(29)	124.3(3)	C(2)-C(21)-C(22)	112.5(3)
C(12)-C(13)-C(14)	106.8(3)	C(3)-C(23)-C(24)	112.1(3)
C(12)-C(13)-C(31)	128.0(3)	C(7)-C(25)-C(26)	112.2(3)
C(14)-C(13)-C(31)	125.2(3)	C(8)-C(27)-C(28)	113.1(3)
N(3)-C(14)-C(15)	125.0(3)	C(12)-C(29)-C(30)	113.6(3)
N(3)-C(14)-C(13)	109.2(2)	C(13)-C(31)-C(32)	114.0(3)
C(15)-C(14)-C(13)	125.8(3)	C(17)-C(33)-C(34)	110.3(3)
C(16)-C(15)-C(14)	127.3(3)	C(18)-C(35)-C(36)	114.2(5)
N(4)-C(16)-C(15)	125.4(3)	C(18)-C(35')-C(36')	110.7(10)
N(4)-C(16)-C(17)	109.0(3)	C(38)-C(37)-N(6)	108.0(3)
C(15)-C(16)-C(17)	125.5(3)	C(37)-C(38)-N(7)	109.7(3)
C(18)-C(17)-C(16)	107.1(3)	N(7)-C(39)-N(6)	114.2(3)
C(18)-C(17)-C(33)	127.5(3)	C(42)-N(8)-C(40)	106.4(4)
C(16)-C(17)-C(33)	125.2(3)	C(42)-N(9)-C(41)	104.8(4)
C(17)-C(18)-C(19)	107.3(3)	N(8)-C(40)-C(41)	106.7(5)
C(17)-C(18)-C(35)	126.7(4)	C(40)-C(41)-N(9)	109.2(4)
C(19)-C(18)-C(35)	125.9(4)	N(9)-C(42)-N(8)	112.9(5)
C(17)-C(18)-C(35')	129.6(7)	Cl(1)-C(43)-Cl(2)	109.0(4)
C(19)-C(18)-C(35')	122.9(7)		

Table 3.8. Bond lengths (Å) for [(OEP)Ru(NO)(HIm)]SbF_6.

Ru(1)-N(7)	1.695(9)	C(7)-C(25)	1.520(3)
Ru(1)-N(2)	2.007(7)	C(8)-C(9)	1.440(11)
Ru(1)-N(3)	2.033(7)	C(8)-C(27)	1.513(10)
Ru(1)-N(4)	2.037(7)	C(9)-C(10)	1.412(13)
Ru(1)-N(1)	2.047(7)	C(10)-C(11)	1.354(12)
Ru(1)-N(5)	2.069(8)	C(11)-C(12)	1.446(12)
O(1)-N(7)	1.131(12)	C(12)-C(13)	1.371(12)
N(1)-C(4)	1.368(12)	C(12)-C(29)	1.493(11)
N(1)-C(1)	1.396(11)	C(13)-C(14)	1.468(13)
N(2)-C(6)	1.394(12)	C(13)-C(31)	1.485(15)
N(2)-C(9)	1.420(10)	C(14)-C(15)	1.362(12)
N(3)-C(14)	1.355(12)	C(15)-C(16)	1.381(12)
N(3)-C(11)	1.393(9)	C(16)-C(17)	1.434(11)
N(4)-C(16)	1.363(12)	C(17)-C(18)	1.384(13)
N(4)-C(19)	1.387(10)	C(17)-C(33)	1.493(14)
N(5)-C(39)	1.274(12)	C(18)-C(19)	1.447(13)
N(5)-C(37)	1.368(13)	C(18)-C(35)	1.499(12)
N(6)-C(38)	1.297(14)	C(19)-C(20)	1.364(13)
N(6)-C(39)	1.337(15)	C(21)-C(22)	1.517(4)
C(1)-C(20)	1.358(13)	C(23)-C(24)	1.520(3)
C(1)-C(2)	1.379(14)	C(25)-C(26)	1.519(3)
C(2)-C(3)	1.329(9)	C(27)-C(28)	1.495(11)
C(2)-C(21)	1.523(3)	C(29)-C(30)	1.471(13)
C(3)-C(4)	1.391(11)	C(31)-C(32)	1.465(17)
C(3)-C(23)	1.523(3)	C(33)-C(34)	1.514(16)
C(4)-C(5)	1.383(13)	C(35)-C(36)	1.458(15)
C(5)-C(6)	1.381(13)	C(37)-C(38)	1.319(14)
C(6)-C(7)	1.426(9)	Sb(1)-F(6)	1.789(8)
C(7)-C(8)	1.313(7)	Sb(1)-F(4)	1.803(7)

Sb(1)-F(5)	1.804(8)	Sb(1)-F(3)	1.819(7)
Sb(1)-F(2)	1.803(7)		
Sb(1)-F(1)	1.815(7)		

Table 3.9. Bond Angles (°) for [(OEP)Ru(NO)(HIm)]SbF_6.

N(7)-Ru(1)-N(2)	93.1(3)	C(39)-N(5)-Ru(1)	128.2(8)
N(7)-Ru(1)-N(3)	93.5(4)	C(37)-N(5)-Ru(1)	128.9(6)
N(2)-Ru(1)-N(3)	90.7(3)	C(38)-N(6)-C(39)	104.8(9)
N(7)-Ru(1)-N(4)	92.7(3)	O(1)-N(7)-Ru(1)	175.3(7)
N(2)-Ru(1)-N(4)	174.2(3)	C(20)-C(1)-C(2)	133.1(9)
N(3)-Ru(1)-N(4)	89.5(3)	C(20)-C(1)-N(1)	124.3(9)
N(7)-Ru(1)-N(1)	91.6(4)	C(2)-C(1)-N(1)	102.6(8)
N(2)-Ru(1)-N(1)	89.4(3)	C(3)-C(2)-C(1)	115.7(4)
N(3)-Ru(1)-N(1)	174.8(3)	C(3)-C(2)-C(21)	124.0(7)
N(4)-Ru(1)-N(1)	89.8(3)	C(1)-C(2)-C(21)	120.3(8)
N(7)-Ru(1)-N(5)	177.8(3)	C(2)-C(3)-C(4)	102.5(5)
N(2)-Ru(1)-N(5)	88.1(3)	C(2)-C(3)-C(23)	129.0(4)
N(3)-Ru(1)-N(5)	88.3(3)	C(4)-C(3)-C(23)	128.1(5)
N(4)-Ru(1)-N(5)	86.1(3)	N(1)-C(4)-C(5)	124.7(10)
N(1)-Ru(1)-N(5)	86.5(3)	N(1)-C(4)-C(3)	110.4(7)
C(4)-N(1)-C(1)	107.9(8)	C(5)-C(4)-C(3)	124.3(10)
C(4)-N(1)-Ru(1)	125.7(5)	C(6)-C(5)-C(4)	129.6(11)
C(1)-N(1)-Ru(1)	126.2(6)	C(5)-C(6)-N(2)	120.4(8)
C(6)-N(2)-C(9)	103.6(6)	C(5)-C(6)-C(7)	130.1(9)
C(6)-N(2)-Ru(1)	129.4(5)	N(2)-C(6)-C(7)	109.5(7)
C(9)-N(2)-Ru(1)	126.4(6)	C(8)-C(7)-C(6)	110.2(5)
C(14)-N(3)-C(11)	107.0(7)	C(8)-C(7)-C(25)	126.6(4)
C(14)-N(3)-Ru(1)	126.3(5)	C(6)-C(7)-C(25)	123.1(5)
C(11)-N(3)-Ru(1)	126.2(6)	C(7)-C(8)-C(9)	106.3(5)
C(16)-N(4)-C(19)	107.0(7)	C(7)-C(8)-C(27)	129.5(7)
C(16)-N(4)-Ru(1)	126.6(5)	C(9)-C(8)-C(27)	123.9(7)
C(19)-N(4)-Ru(1)	125.8(6)	C(10)-C(9)-N(2)	123.8(7)
C(39)-N(5)-C(37)	102.8(9)	C(10)-C(9)-C(8)	125.9(7)

N(2)-C(9)-C(8)	110.2(7)	C(1)-C(20)-C(19)	128.4(8)
C(11)-C(10)-C(9)	126.9(8)	C(22)-C(21)-C(2)	112.5(3)
C(10)-C(11)-N(3)	125.5(8)	C(24)-C(23)-C(3)	112.2(3)
C(10)-C(11)-C(12)	124.7(7)	C(26)-C(25)-C(7)	112.6(2)
N(3)-C(11)-C(12)	109.8(7)	C(28)-C(27)-C(8)	114.4(8)
C(13)-C(12)-C(11)	106.6(7)	C(30)-C(29)-C(12)	112.0(8)
C(13)-C(12)-C(29)	128.7(9)	C(32)-C(31)-C(13)	111.7(9)
C(11)-C(12)-C(29)	124.6(8)	C(17)-C(33)-C(34)	110.8(8)
C(12)-C(13)-C(14)	106.9(8)	C(36)-C(35)-C(18)	112.1(7)
C(12)-C(13)-C(31)	128.2(9)	C(38)-C(37)-N(5)	109.3(9)
C(14)-C(13)-C(31)	124.7(8)	N(6)-C(38)-C(37)	108.9(11)
N(3)-C(14)-C(15)	125.1(9)	N(5)-C(39)-N(6)	114.1(11)
N(3)-C(14)-C(13)	109.6(7)	F(6)-Sb(1)-F(4)	89.7(4)
C(15)-C(14)-C(13)	125.2(9)	F(6)-Sb(1)-F(5)	178.9(4)
C(14)-C(15)-C(16)	128.0(10)	F(4)-Sb(1)-F(5)	89.4(3)
N(4)-C(16)-C(15)	123.8(8)	F(6)-Sb(1)-F(2)	93.0(4)
N(4)-C(16)-C(17)	110.8(8)	F(4)-Sb(1)-F(2)	91.0(3)
C(15)-C(16)-C(17)	125.4(9)	F(5)-Sb(1)-F(2)	87.6(4)
C(18)-C(17)-C(16)	106.0(8)	F(6)-Sb(1)-F(1)	90.5(4)
C(18)-C(17)-C(33)	126.9(8)	F(4)-Sb(1)-F(1)	179.2(3)
C(16)-C(17)-C(33)	126.9(9)	F(5)-Sb(1)-F(1)	90.4(3)
C(17)-C(18)-C(19)	107.3(8)	F(2)-Sb(1)-F(1)	89.8(3)
C(17)-C(18)-C(35)	127.9(9)	F(6)-Sb(1)-F(3)	87.6(4)
C(19)-C(18)-C(35)	124.8(9)	F(4)-Sb(1)-F(3)	89.1(3)
C(20)-C(19)-N(4)	125.2(8)	F(5)-Sb(1)-F(3)	91.8(4)
C(20)-C(19)-C(18)	126.1(8)	F(2)-Sb(1)-F(3)	179.4(4)
N(4)-C(19)-C(18)	108.7(8)	F(1)-Sb(1)-F(3)	90.1(3)

Table 3.10. Bond lengths (Å) for (OEP)Ru(NO)(5-MeIm).

Ru(1)-N(7)	1.740(4)	C(7)-C(8)	1.369(7)
Ru(1)-N(4)	2.042(4)	C(7)-C(25)	1.497(7)
Ru(1)-N(3)	2.051(4)	C(8)-C(9)	1.449(7)
Ru(1)-N(2)	2.054(4)	C(8)-C(27)	1.491(7)
Ru(1)-N(1)	2.057(4)	C(9)-C(10)	1.396(7)
Ru(1)-N(5)	2.059(4)	C(10)-C(11)	1.379(7)
O(1)-N(7)	1.145(5)	C(10)-H(10A)	0.9500
N(1)-C(4)	1.365(6)	C(11)-C(12)	1.440(7)
N(1)-C(1)	1.379(7)	C(12)-C(13)	1.360(7)
N(2)-C(9)	1.372(7)	C(12)-C(29)	1.506(7)
N(2)-C(6)	1.375(6)	C(13)-C(14)	1.450(7)
N(3)-C(14)	1.379(6)	C(13)-C(31)	1.494(7)
N(3)-C(11)	1.383(6)	C(14)-C(15)	1.384(7)
N(4)-C(19)	1.378(7)	C(15)-C(16)	1.392(7)
N(4)-C(16)	1.389(6)	C(15)-H(15A)	0.9500
N(5)-C(37)	1.359(6)	C(16)-C(17)	1.438(7)
N(5)-C(39)	1.366(6)	C(17)-C(18)	1.377(7)
N(6)-C(37)	1.332(6)	C(17)-C(33)	1.493(7)
N(6)-C(38)	1.383(7)	C(18)-C(19)	1.450(7)
C(1)-C(20)	1.385(7)	C(18)-C(35)	1.486(7)
C(1)-C(2)	1.459(7)	C(19)-C(20)	1.397(7)
C(2)-C(3)	1.363(7)	C(20)-H(20A)	0.9500
C(2)-C(21)	1.505(7)	C(21)-C(22)	1.523(8)
C(3)-C(4)	1.452(7)	C(21)-H(21A)	0.9900
C(3)-C(23)	1.512(7)	C(21)-H(21B)	0.9900
C(4)-C(5)	1.396(7)	C(22)-H(22A)	0.9800
C(5)-C(6)	1.385(7)	C(22)-H(22B)	0.9800
C(5)-H(5A)	0.9500	C(22)-H(22C)	0.9800
C(6)-C(7)	1.451(7)	C(23)-C(24)	1.535(7)

C(23)-H(23A)	0.9900	C(33)-H(33A)	0.9900
C(23)-H(23B)	0.9900	C(33)-H(33B)	0.9900
C(24)-H(24A)	0.9800	C(34)-H(34A)	0.9800
C(24)-H(24B)	0.9800	C(34)-H(34B)	0.9800
C(24)-H(24C)	0.9800	C(34)-H(34C)	0.9800
C(25)-C(26)	1.511(7)	C(35)-C(36)	1.519(7)
C(25)-H(25A)	0.9900	C(35)-H(35A)	0.9900
C(25)-H(25B)	0.9900	C(35)-H(35B)	0.9900
C(26)-H(26A)	0.9800	C(36)-H(36A)	0.9800
C(26)-H(26B)	0.9800	C(36)-H(36B)	0.9800
C(26)-H(26C)	0.9800	C(36)-H(36C)	0.9800
C(27)-C(28)	1.527(7)	C(37)-H(37A)	0.9500
C(27)-H(27A)	0.9900	C(38)-C(39)	1.353(7)
C(27)-H(27B)	0.9900	C(38)-C(40)	1.486(8)
C(28)-H(28A)	0.9800	C(39)-H(39A)	0.9500
C(28)-H(28B)	0.9800	C(40)-H(40A)	0.9800
C(28)-H(28C)	0.9800	C(40)-H(40B)	0.9800
C(29)-C(30)	1.523(7)	C(40)-H(40C)	0.9800
C(29)-H(29A)	0.9900	N(8)-C(43)	1.329(8)
C(29)-H(29B)	0.9900	N(8)-C(41)	1.384(7)
C(30)-H(30A)	0.9800	N(8)-H(8N)	0.8800
C(30)-H(30B)	0.9800	N(9)-C(43)	1.299(8)
C(30)-H(30C)	0.9800	N(9)-C(42)	1.366(9)
C(31)-C(32)	1.523(7)	C(41)-C(42)	1.385(9)
C(31)-H(31A)	0.9900	C(41)-H(41A)	0.9500
C(31)-H(31B)	0.9900	C(42)-C(44)	1.467(9)
C(32)-H(32A)	0.9800	C(44)-H(44A)	0.9800
C(32)-H(32B)	0.9800	C(44)-H(44B)	0.9800
C(32)-H(32C)	0.9800	C(44)-H(44C)	0.9800
C(33)-C(34)	1.543(7)	C(43)-H(43A)	0.9500

Table 3.11. Bond angles (°) for (OEP)Ru(NO)(5-MeIm).

N(7)-Ru(1)-N(4)	88.60(18)	C(39)-N(5)-Ru(1)	127.9(3)
N(7)-Ru(1)-N(3)	91.46(18)	C(37)-N(6)-C(38)	104.3(4)
N(4)-Ru(1)-N(3)	90.12(17)	O(1)-N(7)-Ru(1)	171.2(4)
N(7)-Ru(1)-N(2)	97.05(18)	N(1)-C(1)-C(20)	124.6(5)
N(4)-Ru(1)-N(2)	174.35(17)	N(1)-C(1)-C(2)	109.5(5)
N(3)-Ru(1)-N(2)	89.91(17)	C(20)-C(1)-C(2)	125.9(5)
N(7)-Ru(1)-N(1)	94.15(18)	C(3)-C(2)-C(1)	106.3(5)
N(4)-Ru(1)-N(1)	89.99(17)	C(3)-C(2)-C(21)	127.4(5)
N(3)-Ru(1)-N(1)	174.39(15)	C(1)-C(2)-C(21)	126.3(5)
N(2)-Ru(1)-N(1)	89.44(17)	C(2)-C(3)-C(4)	107.6(5)
N(7)-Ru(1)-N(5)	174.60(19)	C(2)-C(3)-C(23)	127.2(5)
N(4)-Ru(1)-N(5)	86.25(16)	C(4)-C(3)-C(23)	125.3(5)
N(3)-Ru(1)-N(5)	86.94(16)	N(1)-C(4)-C(5)	125.6(5)
N(2)-Ru(1)-N(5)	88.11(16)	N(1)-C(4)-C(3)	109.4(5)
N(1)-Ru(1)-N(5)	87.48(15)	C(5)-C(4)-C(3)	124.9(5)
C(4)-N(1)-C(1)	107.2(4)	C(6)-C(5)-C(4)	126.3(5)
C(4)-N(1)-Ru(1)	126.3(4)	C(6)-C(5)-H(5A)	116.8
C(1)-N(1)-Ru(1)	126.4(3)	C(4)-C(5)-H(5A)	116.8
C(9)-N(2)-C(6)	107.0(4)	N(2)-C(6)-C(5)	125.3(5)
C(9)-N(2)-Ru(1)	126.4(4)	N(2)-C(6)-C(7)	109.5(5)
C(6)-N(2)-Ru(1)	126.6(4)	C(5)-C(6)-C(7)	125.3(5)
C(14)-N(3)-C(11)	107.2(4)	C(8)-C(7)-C(6)	107.0(5)
C(14)-N(3)-Ru(1)	126.1(4)	C(8)-C(7)-C(25)	127.5(5)
C(11)-N(3)-Ru(1)	126.5(3)	C(6)-C(7)-C(25)	125.5(5)
C(19)-N(4)-C(16)	106.9(4)	C(7)-C(8)-C(9)	106.6(5)
C(19)-N(4)-Ru(1)	126.9(3)	C(7)-C(8)-C(27)	128.8(5)
C(16)-N(4)-Ru(1)	126.1(3)	C(9)-C(8)-C(27)	124.5(5)
C(37)-N(5)-C(39)	104.0(4)	N(2)-C(9)-C(10)	124.8(5)
C(37)-N(5)-Ru(1)	128.1(4)	N(2)-C(9)-C(8)	110.0(5)

C(10)-C(9)-C(8)	125.2(5)	C(1)-C(20)-C(19)	127.8(5)
C(11)-C(10)-C(9)	127.7(5)	C(1)-C(20)-H(20A)	116.1
C(11)-C(10)-H(10A)	116.2	C(19)-C(20)-H(20A)	116.1
C(9)-C(10)-H(10A)	116.2	C(2)-C(21)-C(22)	113.3(4)
C(10)-C(11)-N(3)	124.6(5)	C(2)-C(21)-H(21A)	108.9
C(10)-C(11)-C(12)	126.7(5)	C(22)-C(21)-H(21A)	108.9
N(3)-C(11)-C(12)	108.7(5)	C(2)-C(21)-H(21B)	108.9
C(13)-C(12)-C(11)	108.1(5)	C(22)-C(21)-H(21B)	108.9
C(13)-C(12)-C(29)	127.2(5)	H(21A)-C(21)-H(21B)	107.7
C(11)-C(12)-C(29)	124.5(5)	C(21)-C(22)-H(22A)	109.5
C(12)-C(13)-C(14)	106.7(5)	C(21)-C(22)-H(22B)	109.5
C(12)-C(13)-C(31)	128.2(5)	H(22A)-C(22)-H(22B)	109.5
C(14)-C(13)-C(31)	125.2(5)	C(21)-C(22)-H(22C)	109.5
N(3)-C(14)-C(15)	125.2(5)	H(22A)-C(22)-H(22C)	109.5
N(3)-C(14)-C(13)	109.3(5)	H(22B)-C(22)-H(22C)	109.5
C(15)-C(14)-C(13)	125.5(5)	C(3)-C(23)-C(24)	114.3(5)
C(14)-C(15)-C(16)	126.9(5)	C(3)-C(23)-H(23A)	108.7
C(14)-C(15)-H(15A)	116.5	C(24)-C(23)-H(23A)	108.7
C(16)-C(15)-H(15A)	116.5	C(3)-C(23)-H(23B)	108.7
N(4)-C(16)-C(15)	125.0(5)	C(24)-C(23)-H(23B)	108.7
N(4)-C(16)-C(17)	109.2(5)	H(23A)-C(23)-H(23B)	107.6
C(15)-C(16)-C(17)	125.8(5)	C(23)-C(24)-H(24A)	109.5
C(18)-C(17)-C(16)	107.8(5)	C(23)-C(24)-H(24B)	109.5
C(18)-C(17)-C(33)	127.2(5)	H(24A)-C(24)-H(24B)	109.5
C(16)-C(17)-C(33)	125.0(5)	C(23)-C(24)-H(24C)	109.5
C(17)-C(18)-C(19)	106.3(5)	H(24A)-C(24)-H(24C)	109.5
C(17)-C(18)-C(35)	127.7(5)	H(24B)-C(24)-H(24C)	109.5
C(19)-C(18)-C(35)	125.8(5)	C(7)-C(25)-C(26)	114.3(5)
N(4)-C(19)-C(20)	124.2(5)	C(7)-C(25)-H(25A)	108.7
N(4)-C(19)-C(18)	109.8(5)	C(26)-C(25)-H(25A)	108.7
C(20)-C(19)-C(18)	126.0(5)	C(7)-C(25)-H(25B)	108.7

C(26)-C(25)-H(25B)	108.7	H(30B)-C(30)-H(30C)	109.5
H(25A)-C(25)-H(25B)	107.6	C(13)-C(31)-C(32)	113.1(5)
C(25)-C(26)-H(26A)	109.5	C(13)-C(31)-H(31A)	109.0
C(25)-C(26)-H(26B)	109.5	C(32)-C(31)-H(31A)	109.0
H(26A)-C(26)-H(26B)	109.5	C(13)-C(31)-H(31B)	109.0
C(25)-C(26)-H(26C)	109.5	C(32)-C(31)-H(31B)	109.0
H(26A)-C(26)-H(26C)	109.5	H(31A)-C(31)-H(31B)	107.8
H(26B)-C(26)-H(26C)	109.5	C(31)-C(32)-H(32A)	109.5
C(8)-C(27)-C(28)	113.2(4)	C(31)-C(32)-H(32B)	109.5
C(8)-C(27)-H(27A)	108.9	H(32A)-C(32)-H(32B)	109.5
C(28)-C(27)-H(27A)	108.9	C(31)-C(32)-H(32C)	109.5
C(8)-C(27)-H(27B)	108.9	H(32A)-C(32)-H(32C)	109.5
C(28)-C(27)-H(27B)	108.9	H(32B)-C(32)-H(32C)	109.5
H(27A)-C(27)-H(27B)	107.8	C(17)-C(33)-C(34)	112.8(4)
C(27)-C(28)-H(28A)	109.5	C(17)-C(33)-H(33A)	109.0
C(27)-C(28)-H(28B)	109.5	C(34)-C(33)-H(33A)	109.0
H(28A)-C(28)-H(28B)	109.5	C(17)-C(33)-H(33B)	109.0
C(27)-C(28)-H(28C)	109.5	C(34)-C(33)-H(33B)	109.0
H(28A)-C(28)-H(28C)	109.5	H(33A)-C(33)-H(33B)	107.8
H(28B)-C(28)-H(28C)	109.5	C(33)-C(34)-H(34A)	109.5
C(12)-C(29)-C(30)	111.2(4)	C(33)-C(34)-H(34B)	109.5
C(12)-C(29)-H(29A)	109.4	H(34A)-C(34)-H(34B)	109.5
C(30)-C(29)-H(29A)	109.4	C(33)-C(34)-H(34C)	109.5
C(12)-C(29)-H(29B)	109.4	H(34A)-C(34)-H(34C)	109.5
C(30)-C(29)-H(29B)	109.4	H(34B)-C(34)-H(34C)	109.5
H(29A)-C(29)-H(29B)	108.0	C(18)-C(35)-C(36)	111.1(4)
C(29)-C(30)-H(30A)	109.5	C(18)-C(35)-H(35A)	109.4
C(29)-C(30)-H(30B)	109.5	C(36)-C(35)-H(35A)	109.4
H(30A)-C(30)-H(30B)	109.5	C(18)-C(35)-H(35B)	109.4
C(29)-C(30)-H(30C)	109.5	C(36)-C(35)-H(35B)	109.4
H(30A)-C(30)-H(30C)	109.5	H(35A)-C(35)-H(35B)	108.0

C(35)-C(36)-H(36A)	109.5	H(40B)-C(40)-H(40C)	109.5
C(35)-C(36)-H(36B)	109.5	C(43)-N(8)-C(41)	106.2(6)
H(36A)-C(36)-H(36B)	109.5	C(43)-N(8)-H(8N)	126.9
C(35)-C(36)-H(36C)	109.5	C(41)-N(8)-H(8N)	126.9
H(36A)-C(36)-H(36C)	109.5	C(43)-N(9)-C(42)	105.0(6)
H(36B)-C(36)-H(36C)	109.5	N(8)-C(41)-C(42)	105.1(6)
N(6)-C(37)-N(5)	113.6(5)	N(8)-C(41)-H(41A)	127.5
N(6)-C(37)-H(37A)	123.2	C(42)-C(41)-H(41A)	127.5
N(5)-C(37)-H(37A)	123.2	N(9)-C(42)-C(41)	109.6(6)
C(39)-C(38)-N(6)	108.8(5)	N(9)-C(42)-C(44)	121.5(7)
C(39)-C(38)-C(40)	130.5(6)	C(41)-C(42)-C(44)	128.9(7)
N(6)-C(38)-C(40)	120.8(5)	C(42)-C(44)-H(44A)	109.5
C(38)-C(39)-N(5)	109.4(5)	C(42)-C(44)-H(44B)	109.5
C(38)-C(39)-H(39A)	125.3	H(44A)-C(44)-H(44B)	109.5
N(5)-C(39)-H(39A)	125.3	C(42)-C(44)-H(44C)	109.5
C(38)-C(40)-H(40A)	109.5	H(44A)-C(44)-H(44C)	109.5
C(38)-C(40)-H(40B)	109.5	H(44B)-C(44)-H(44C)	109.5
H(40A)-C(40)-H(40B)	109.5	N(9)-C(43)-N(8)	114.1(6)
C(38)-C(40)-H(40C)	109.5	N(9)-C(43)-H(43A)	123.0
H(40A)-C(40)-H(40C)	109.5	N(8)-C(43)-H(43A)	123.0

Table 3.12. Bond lengths (Å) for [(OEP)Ru(NO)(5(4)-MeHIm)]SbF_6.

Ru(1)-N(5)	1.7305(17)	C(8)-C(27)	1.495(3)
Ru(1)-N(3)	2.0542(17)	C(9)-C(10)	1.390(3)
Ru(1)-N(1)	2.0549(17)	C(10)-C(11)	1.401(3)
Ru(1)-N(2)	2.0568(15)	C(10)-H(10A)	0.9500
Ru(1)-N(4)	2.0580(15)	C(11)-C(12)	1.438(3)
Ru(1)-N(6)	2.1036(17)	C(12)-C(13)	1.373(3)
O(1)-N(5)	1.144(2)	C(12)-C(29)	1.502(3)
N(1)-C(4)	1.373(3)	C(13)-C(14)	1.443(3)
N(1)-C(1)	1.377(2)	C(13)-C(31)	1.499(3)
N(2)-C(9)	1.370(2)	C(14)-C(15)	1.393(3)
N(2)-C(6)	1.375(3)	C(15)-C(16)	1.387(3)
N(3)-C(11)	1.375(2)	C(15)-H(15A)	0.9500
N(3)-C(14)	1.375(3)	C(16)-C(17)	1.450(3)
N(4)-C(19)	1.372(2)	C(17)-C(18)	1.363(3)
N(4)-C(16)	1.376(3)	C(17)-C(33)	1.501(3)
C(1)-C(20)	1.389(3)	C(18)-C(19)	1.451(3)
C(1)-C(2)	1.446(3)	C(18)-C(35)	1.501(3)
C(2)-C(3)	1.367(3)	C(19)-C(20)	1.387(3)
C(2)-C(21)	1.500(3)	C(20)-H(20A)	0.9500
C(3)-C(4)	1.446(3)	C(21)-C(22)	1.502(3)
C(3)-C(23)	1.499(3)	C(21)-H(21A)	0.9900
C(4)-C(5)	1.388(3)	C(21)-H(21B)	0.9900
C(5)-C(6)	1.388(3)	C(22)-H(22A)	0.9800
C(5)-H(5A)	0.9500	C(22)-H(22B)	0.9800
C(6)-C(7)	1.445(2)	C(22)-H(22C)	0.9800
C(7)-C(8)	1.363(3)	C(23)-C(24)	1.539(3)
C(7)-C(25)	1.504(3)	C(23)-H(23A)	0.9900
C(8)-C(9)	1.456(3)	C(23)-H(23B)	0.9900

C(24)-H(24A)	0.9800	C(32)-H(32B)	0.9800
C(24)-H(24B)	0.9800	C(32)-H(32C)	0.9800
C(24)-H(24C)	0.9800	C(33)-C(34)	1.522(4)
C(25)-C(26)	1.526(4)	C(33)-H(33A)	0.9900
C(25)-H(25A)	0.9900	C(33)-H(33B)	0.9900
C(25)-H(25B)	0.9900	C(34)-H(34A)	0.9800
C(26)-H(26A)	0.9800	C(34)-H(34B)	0.9800
C(26)-H(26B)	0.9800	C(34)-H(34C)	0.9800
C(26)-H(26C)	0.9800	C(35)-C(36)	1.536(3)
C(27)-C(28)	1.533(3)	C(35)-H(35A)	0.9900
C(27)-H(27A)	0.9900	C(35)-H(35B)	0.9900
C(27)-H(27B)	0.9900	C(36)-H(36A)	0.9800
C(28)-H(28A)	0.9800	C(36)-H(36B)	0.9800
C(28)-H(28B)	0.9800	C(36)-H(36C)	0.9800
C(28)-H(28C)	0.9800	N(6)-C(37)	1.320(3)
C(29)-C(30')	1.494(3)	N(6)-C(39)	1.367(3)
C(29)-C(30)	1.494(3)	N(7)-C(37)	1.335(3)
C(29)-H(29A)	0.9900	N(7)-C(38)	1.379(4)
C(29)-H(29B)	0.9900	N(7)-H(7A)	0.8800
C(29)-H(29C)	0.9900	C(37)-H(37A)	0.9500
C(29)-H(29D)	0.9900	C(38)-C(39)	1.350(3)
C(30)-H(30A)	0.9800	C(38)-C(40)	1.489(4)
C(30)-H(30B)	0.9800	C(38)-H(38A)	0.9500
C(30)-H(30C)	0.9800	C(39)-C(40')	1.478(4)
C(30')-H(30D)	0.9800	C(39)-H(39A)	0.9500
C(30')-H(30E)	0.9800	C(40)-H(40A)	0.9800
C(30')-H(30F)	0.9800	C(40)-H(40B)	0.9800
C(31)-C(32)	1.525(4)	C(40)-H(40C)	0.9800
C(31)-H(31A)	0.9900	C(40')-H(40D)	0.9800
C(31)-H(31B)	0.9900	C(40')-H(40E)	0.9800
C(32)-H(32A)	0.9800	C(40')-H(40F)	0.9800

Sb(1)-F(2)	1.8473(16)	Sb(1)-F(4)	1.8678(19)
Sb(1)-F(3)	1.8525(18)	Sb(1)-F(1)	1.8725(17)
Sb(1)-F(6)	1.8639(15)	Sb(1)-F(5)	1.8790(14)

Table 3.13. Bond angles (°) for [(OEP)Ru(NO)(5(4)-MeHIm)]SbF_6.

N(5)-Ru(1)-N(3)	92.94(8)	N(1)-C(1)-C(2)	109.28(17)
N(5)-Ru(1)-N(1)	92.06(8)	C(20)-C(1)-C(2)	125.92(17)
N(3)-Ru(1)-N(1)	174.99(7)	C(3)-C(2)-C(1)	106.99(17)
N(5)-Ru(1)-N(2)	91.50(7)	C(3)-C(2)-C(21)	127.2(2)
N(3)-Ru(1)-N(2)	89.83(6)	C(1)-C(2)-C(21)	125.34(19)
N(1)-Ru(1)-N(2)	90.07(6)	C(2)-C(3)-C(4)	107.09(19)
N(5)-Ru(1)-N(4)	94.00(7)	C(2)-C(3)-C(23)	128.78(19)
N(3)-Ru(1)-N(4)	89.89(6)	C(4)-C(3)-C(23)	123.88(18)
N(1)-Ru(1)-N(4)	89.73(6)	N(1)-C(4)-C(5)	125.15(19)
N(2)-Ru(1)-N(4)	174.49(7)	N(1)-C(4)-C(3)	109.34(16)
N(5)-Ru(1)-N(6)	177.32(7)	C(5)-C(4)-C(3)	125.5(2)
N(3)-Ru(1)-N(6)	88.56(6)	C(4)-C(5)-C(6)	127.4(2)
N(1)-Ru(1)-N(6)	86.44(7)	C(4)-C(5)-H(5A)	116.3
N(2)-Ru(1)-N(6)	86.28(6)	C(6)-C(5)-H(5A)	116.3
N(4)-Ru(1)-N(6)	88.22(6)	N(2)-C(6)-C(5)	124.97(17)
C(4)-N(1)-C(1)	107.28(17)	N(2)-C(6)-C(7)	109.37(17)
C(4)-N(1)-Ru(1)	125.53(12)	C(5)-C(6)-C(7)	125.65(19)
C(1)-N(1)-Ru(1)	126.34(14)	C(8)-C(7)-C(6)	107.25(17)
C(9)-N(2)-C(6)	107.31(15)	C(8)-C(7)-C(25)	128.56(17)
C(9)-N(2)-Ru(1)	126.51(13)	C(6)-C(7)-C(25)	124.17(18)
C(6)-N(2)-Ru(1)	125.98(12)	C(7)-C(8)-C(9)	106.71(16)
C(11)-N(3)-C(14)	106.76(16)	C(7)-C(8)-C(27)	128.42(18)
C(11)-N(3)-Ru(1)	126.41(14)	C(9)-C(8)-C(27)	124.73(18)
C(14)-N(3)-Ru(1)	125.84(12)	N(2)-C(9)-C(10)	125.13(17)
C(19)-N(4)-C(16)	107.43(15)	N(2)-C(9)-C(8)	109.34(17)
C(19)-N(4)-Ru(1)	126.12(14)	C(10)-C(9)-C(8)	125.51(17)
C(16)-N(4)-Ru(1)	125.51(12)	C(9)-C(10)-C(11)	127.05(17)
O(1)-N(5)-Ru(1)	176.94(18)	C(9)-C(10)-H(10A)	116.5
N(1)-C(1)-C(20)	124.76(19)	C(11)-C(10)-H(10A)	116.5

N(3)-C(11)-C(10)	124.71(19)	C(22)-C(21)-H(21A)	109.2
N(3)-C(11)-C(12)	109.75(17)	C(2)-C(21)-H(21A)	109.2
C(10)-C(11)-C(12)	125.45(17)	C(22)-C(21)-H(21B)	109.2
C(13)-C(12)-C(11)	107.08(18)	C(2)-C(21)-H(21B)	109.2
C(13)-C(12)-C(29)	127.4(2)	H(21A)-C(21)-H(21B)	107.9
C(11)-C(12)-C(29)	125.47(18)	C(21)-C(22)-H(22A)	109.5
C(12)-C(13)-C(14)	106.60(19)	C(21)-C(22)-H(22B)	109.5
C(12)-C(13)-C(31)	127.95(19)	H(22A)-C(22)-H(22B)	109.5
C(14)-C(13)-C(31)	125.44(17)	C(21)-C(22)-H(22C)	109.5
N(3)-C(14)-C(15)	124.64(19)	H(22A)-C(22)-H(22C)	109.5
N(3)-C(14)-C(13)	109.79(16)	H(22B)-C(22)-H(22C)	109.5
C(15)-C(14)-C(13)	125.55(19)	C(3)-C(23)-C(24)	111.77(18)
C(16)-C(15)-C(14)	127.64(19)	C(3)-C(23)-H(23A)	109.3
C(16)-C(15)-H(15A)	116.2	C(24)-C(23)-H(23A)	109.3
C(14)-C(15)-H(15A)	116.2	C(3)-C(23)-H(23B)	109.3
N(4)-C(16)-C(15)	124.90(17)	C(24)-C(23)-H(23B)	109.3
N(4)-C(16)-C(17)	109.21(17)	H(23A)-C(23)-H(23B)	107.9
C(15)-C(16)-C(17)	125.90(19)	C(23)-C(24)-H(24A)	109.5
C(18)-C(17)-C(16)	107.02(18)	C(23)-C(24)-H(24B)	109.5
C(18)-C(17)-C(33)	127.86(18)	H(24A)-C(24)-H(24B)	109.5
C(16)-C(17)-C(33)	125.12(19)	C(23)-C(24)-H(24C)	109.5
C(17)-C(18)-C(19)	107.13(16)	H(24A)-C(24)-H(24C)	109.5
C(17)-C(18)-C(35)	127.56(18)	H(24B)-C(24)-H(24C)	109.5
C(19)-C(18)-C(35)	125.0(2)	C(7)-C(25)-C(26)	112.98(17)
N(4)-C(19)-C(20)	125.42(17)	C(7)-C(25)-H(25A)	109.0
N(4)-C(19)-C(18)	109.19(18)	C(26)-C(25)-H(25A)	109.0
C(20)-C(19)-C(18)	125.19(17)	C(7)-C(25)-H(25B)	109.0
C(1)-C(20)-C(19)	127.01(18)	C(26)-C(25)-H(25B)	109.0
C(1)-C(20)-H(20A)	116.5	H(25A)-C(25)-H(25B)	107.8
C(19)-C(20)-H(20A)	116.5	C(25)-C(26)-H(26A)	109.5
C(22)-C(21)-C(2)	111.86(17)	C(25)-C(26)-H(26B)	109.5

H(26A)-C(26)-H(26B)	109.5	C(30')-C(29)-H(29D)	107.0
C(25)-C(26)-H(26C)	109.5	C(30)-C(29)-H(29D)	49.7
H(26A)-C(26)-H(26C)	109.5	C(12)-C(29)-H(29D)	107.0
H(26B)-C(26)-H(26C)	109.5	H(29A)-C(29)-H(29D)	65.5
C(8)-C(27)-C(28)	111.43(16)	H(29B)-C(29)-H(29D)	144.5
C(8)-C(27)-H(27A)	109.3	H(29C)-C(29)-H(29D)	106.8
C(28)-C(27)-H(27A)	109.3	C(29)-C(30)-H(30A)	109.5
C(8)-C(27)-H(27B)	109.3	C(29)-C(30)-H(30B)	109.5
C(28)-C(27)-H(27B)	109.3	C(29)-C(30)-H(30C)	109.5
H(27A)-C(27)-H(27B)	108.0	C(29)-C(30')-H(30D)	109.5
C(27)-C(28)-H(28A)	109.5	C(29)-C(30')-H(30E)	109.5
C(27)-C(28)-H(28B)	109.5	H(30D)-C(30')-H(30E)	109.5
H(28A)-C(28)-H(28B)	109.5	C(29)-C(30')-H(30F)	109.5
C(27)-C(28)-H(28C)	109.5	H(30D)-C(30')-H(30F)	109.5
H(28A)-C(28)-H(28C)	109.5	H(30E)-C(30')-H(30F)	109.5
H(28B)-C(28)-H(28C)	109.5	C(13)-C(31)-C(32)	113.7(2)
C(30')-C(29)-C(30)	122.2(5)	C(13)-C(31)-H(31A)	108.8
C(30')-C(29)-C(12)	121.2(5)	C(32)-C(31)-H(31A)	108.8
C(30)-C(29)-C(12)	116.53(19)	C(13)-C(31)-H(31B)	108.8
C(30')-C(29)-H(29A)	50.1	C(32)-C(31)-H(31B)	108.8
C(30)-C(29)-H(29A)	108.2	H(31A)-C(31)-H(31B)	107.7
C(12)-C(29)-H(29A)	108.2	C(31)-C(32)-H(32A)	109.5
C(30')-C(29)-H(29B)	57.3	C(31)-C(32)-H(32B)	109.5
C(30)-C(29)-H(29B)	108.2	H(32A)-C(32)-H(32B)	109.5
C(12)-C(29)-H(29B)	108.2	C(31)-C(32)-H(32C)	109.5
H(29A)-C(29)-H(29B)	107.3	H(32A)-C(32)-H(32C)	109.5
C(30')-C(29)-H(29C)	107.0	H(32B)-C(32)-H(32C)	109.5
C(30)-C(29)-H(29C)	57.2	C(17)-C(33)-C(34)	112.83(18)
C(12)-C(29)-H(29C)	107.0	C(17)-C(33)-H(33A)	109.0
H(29A)-C(29)-H(29C)	144.7	C(34)-C(33)-H(33A)	109.0
H(29B)-C(29)-H(29C)	57.6	C(17)-C(33)-H(33B)	109.0

C(34)-C(33)-H(33B)	109.0	N(7)-C(38)-C(40)	127.7(2)
H(33A)-C(33)-H(33B)	107.8	C(39)-C(38)-H(38A)	128.0
C(33)-C(34)-H(34A)	109.5	N(7)-C(38)-H(38A)	128.0
C(33)-C(34)-H(34B)	109.5	C(40)-C(38)-H(38A)	1.9
H(34A)-C(34)-H(34B)	109.5	C(38)-C(39)-N(6)	110.61(18)
C(33)-C(34)-H(34C)	109.5	C(38)-C(39)-C(40')	113.9(3)
H(34A)-C(34)-H(34C)	109.5	N(6)-C(39)-C(40')	132.4(4)
H(34B)-C(34)-H(34C)	109.5	C(38)-C(39)-H(39A)	124.7
C(18)-C(35)-C(36)	111.66(18)	N(6)-C(39)-H(39A)	124.7
C(18)-C(35)-H(35A)	109.3	C(40')-C(39)-H(39A)	18.5
C(36)-C(35)-H(35A)	109.3	C(38)-C(40)-H(40A)	109.5
C(18)-C(35)-H(35B)	109.3	C(38)-C(40)-H(40B)	109.5
C(36)-C(35)-H(35B)	109.3	C(38)-C(40)-H(40C)	109.5
H(35A)-C(35)-H(35B)	108.0	C(39)-C(40')-H(40D)	109.5
C(35)-C(36)-H(36A)	109.5	C(39)-C(40')-H(40E)	109.5
C(35)-C(36)-H(36B)	109.5	H(40D)-C(40')-H(40E)	109.5
H(36A)-C(36)-H(36B)	109.5	C(39)-C(40')-H(40F)	109.5
C(35)-C(36)-H(36C)	109.5	H(40D)-C(40')-H(40F)	109.5
H(36A)-C(36)-H(36C)	109.5	H(40E)-C(40')-H(40F)	109.5
H(36B)-C(36)-H(36C)	109.5	F(2)-Sb(1)-F(3)	91.06(9)
C(37)-N(6)-C(39)	106.56(18)	F(2)-Sb(1)-F(6)	90.72(7)
C(37)-N(6)-Ru(1)	122.49(16)	F(3)-Sb(1)-F(6)	89.88(8)
C(39)-N(6)-Ru(1)	130.93(13)	F(2)-Sb(1)-F(4)	90.65(9)
C(37)-N(7)-C(38)	109.69(19)	F(3)-Sb(1)-F(4)	177.87(9)
C(37)-N(7)-H(7A)	125.2	F(6)-Sb(1)-F(4)	91.37(8)
C(38)-N(7)-H(7A)	125.2	F(2)-Sb(1)-F(1)	177.45(8)
N(6)-C(37)-N(7)	109.2(2)	F(3)-Sb(1)-F(1)	89.13(9)
N(6)-C(37)-H(37A)	125.4	F(6)-Sb(1)-F(1)	91.82(8)
N(7)-C(37)-H(37A)	125.4	F(4)-Sb(1)-F(1)	89.11(9)
C(39)-C(38)-N(7)	103.9(2)	F(2)-Sb(1)-F(5)	89.18(7)
C(39)-C(38)-C(40)	128.3(2)	F(3)-Sb(1)-F(5)	91.20(8)

F(6)-Sb(1)-F(5)	178.91(7)
F(4)-Sb(1)-F(5)	87.54(8)
F(1)-Sb(1)-F(5)	88.28(7)